A QUANTIFICATION OF CHEMICAL AND PHYSICAL FACTORS ON SO_2 OXIDATION CATALYSTS

B. Von M. HARMSE
B.Ing.(Chem) PU FOR CHE

A thesis submitted in partial fulfilment of the requirements for the degree
Magister Scientiae in the Department of Chemical Engineering,
Potchefstroom University for Christian Higher Education, Potchefstroom, South Africa

January, 1989

DECLARATION

I hereby certify that, unless specific indication to the contrary is made in the text, everything contained in this thesis is my own original work. This work has not been accepted in substance, or submitted in candidature for a degree at any university other than the Potchefstroom University for Christian Higher Education of Potchefstroom, South Africa.

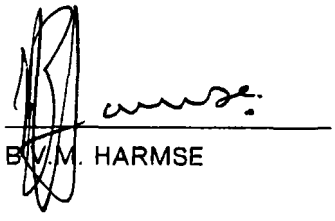

B.V.M. HARMSE

6 Sept 1989

DATE

ACKNOWLEDGEMENTS

Special thanks to Dr. John Davidtz who provided the main stimulation, guidance, encouragement and support, throughout this work.

Thanks to H. van Zyl for his willingness to help and assist in setting up the equipment.

Thanks to Dr. W.D. Basson of Prochem for encouragment and financial support.

I am grateful to SASTECK and Provon Chemicals for the use of their facilities.

Finally, thanks to Mrs. M. Scott for typing this thesis and her patience with me.

NOTES TO THE EXAMINER

Some parts of this work are scientifically new or have led to new concepts, and should not be released for proprietary reasons. Provon Chemicals has the property rights and responsibility of releasing:

- All experimental data.
- Conclusions drawn.

To facilitate reading a separate loose insert is included that contains all the equations and symbols.

Due to the nature of Statgraphics used to generate graphs the size of the script on the axes could not be changed.

ABSTRACT

This study entailed the design and optimization of the the supported liquid phase V_2O_5 catalyst system for SO_2 oxidation.

The active melt consisted of V_2O_5 dissolved in alkali metal pyrosulphates. The activity increased with increasing ionic radii of the alkaline metal cation. Replacement of *K* by *Na* decreases activity. There is an optimum vanadium to alkaline promoter ratio. An optimum active constituent loading exists at $0{,}3cm^3$ melt $/cm^3$ pore and this is determined by product of the gas- and liquid phase effectiveness factors.

Studies on pellet size and geometry on reaction rate, pressure drop and mechanical strength indicated that a high activity can be maintained by the use of exotic shapes with a substantial reduction in bed pressure drop. The effect of geometry, amount of carrier matrix sintering and liquid loading on mechanical strength was quantified at room- and operating temperature.

TABLE OF CONTENTS

LIST OF FIGURES

LIST OF TABLES

LIST OF PRINCIPAL SYMBOLS

a_1; a_2; a_i	Defined in Eqs. (48a), (48b), (48c).
A_{EL}	Coefficient in K_{EL}, Eq. (42).
A_L	Coefficient in k_L, table 7.
B_{EL}	Coefficient in K_{EL}, Eq. (42).
B_L	Coefficient in k_L, table 7.
C_i	Concentration of component i [$mole/cm^3$].
C_s	Concentration on the surface of a pellet [$mole/cm^3$].
C_v	Mass concentration of V_2O_5 in the melt [gV_2O_5/cm^3 melt].
D_i	Diffusivity of component i [cm^2/s].
$D_{i,eff}$	Effective diffusivity of component i [cm^2/s].
d_p	Effective diameter of the pellet.
ESR	Electron spin resonance measurements.
F_k	Pellet external surface area [cm^2].
g_c	Gravitation constant.
G_v	V_2O_5 content [g V_2O_5/g support].
$\Delta H°$	Standard heat of reaction [$kJ/mole$].
H_{O_2}	Hendry's coefficient for O_2[$cm^3kPa/mole$].
H	Height measured from the top of the bed to a certain point in the catalyst bed.
ID	Internal diameter of reactor.
k_i	Rate constant [units defined by equation form].
K_{EL}	Arrhenius type constant defined in Eq. (42).
K_c	Equilibrium constant for Eq. (14a).
k_n	Rate constant for n-th order reaction.
Kp	Equilibrium constant for Eq. (8) [$kPa^{-1/2}$].
L	Total height of catalyst bed
	or
L	Characteristic length [cm].
LFR	Liquid filled region.
M	*Li*, *Na*, *K*, *Cs*
n_i	Orders of reaction.
P_i	Partial pressure of component i [kPa].
P_i^o	Partial pressure of component i in the feed [kPa].
ΔP	Pressure drop across a fixed bed.
Pt	Total pressure.
q	P_{SO_2}/P_{SO_3} ratio defined by Eq. (21).
r	Effective reaction rate.
R	Gas constant.
r'	Intrinsic reaction rate.

Re_p	Particle Reynolds number as defined in Eq. (60).
r'_L	Intrinsic net reaction rate in the liquid phase [*mole* SO_3/cm^3 *melt* . *s*].
r'_{Lf}	Intrinsic forward reaction rate in the liquid phase not including reverse reaction [*mole* $SO_3/cm^3 melt.s$].
r_p	Average pore radius of support [*cm*].
RPS	Residual pore system.
r_s	Reaction rate based on catalyst bed volume [*mole* SO_2/cm^2bed vol .*s*].
r'_v	Intrinsic reaction rate on surface of liquid, based on pellet volume [$moleSO_3/cm^3$. pellet .*s*].
S	Kinetic parameter defined in Eq. (19).
s	Constant defined in Eq. (5) [*cm*].
SLP	Supported liquid phase systems.
T	Temperature [*K*].
U	SO_2 conversion.
U_{eq}	SO_2 equilibrium conversion.
U_{di}	Defined in Eq. (49).
u_o	Superficial gas velocity (measured on an empty tube basis) through a catalyst bed [*m/s*].
V_k	Pellet volume [cm^3].
V_p	Pore volume of support per unit mass support [cm^3/g].
x_i	Mole fraction of component *i*.
z_i	Parameters consisting of catalyst data.
α	Volume of liquid catalyst as a fraction of support pore volume [cm^3 melt /cm^3 pores].
δ	Equivalent slab thickness of the liquid film [*cm*].
ε	Void fraction of the catalyst bed.
ε_o	Initial clean void fraction of the catalyst bed.
η	Effectiveness factor.
η_L	Liquid phase effectiveness factor.
η_G	Gas phase effectiveness factor.
Θ	Porosity, total pore volume as a fraction of the pellet volume [cm^3 pores /cm^3 pellet].
λ_{eff}	Effective thermal conductivity of the pellet [*J/m.s.K*].
μ	Viscosity of the gas.
ξ	Equilibrium approach coefficient defined by Eq. (20).
ρ_g	Density of the gas.
ρ_K	Apparent density of the catalyst pellet [g/cm^3].
ρ_s	Skeletal density of solid support material [g/cm^3].
ρ_{Tr}	Density of support [g/cm^3].

τ_G Gas phase tortuosity factor.

τ_L Liquid phase tortuosity factor.

ϕ_L Thiele modulus for liquid phase.

ϕ_G Thiele modulus for gas phase.

ϕ_s Sphericity of a particle defined by Eq. (58).

ω Accumulated dust per bed cross section [kg/m^2 bed cross section].

ω_i Defined in Eq. (31a) and (31b).

CHAPTER 1

INTRODUCTION

Catalyst development in South Africa is in its infancy. Most of the catalysts used in our chemical industries are imported or finished products, and in remote cases they are locally manufactured under licence. This is the case with one of the only local manufacturers Provon Chemicals.

Provon Chemical currently manufacture vanadium based sulphur dioxide oxidation catalysts in joint venture, and under license with ISC of Bristol, UK.

Because of the lack of catalyst development in South Africa very little local expertise exists in the field of catalyst design and development.

When the thought arises that local South African raw materials, such as: Vanadium, Platinum, Nickel and many other noble metal and, noble metal combinations, are technologically exploited beyond the local manufacturing infrastructure, and in particular, in catalytic processes, then it may be significant to appreciate the value of revenue lost by a lack of local industrial competition on international markets.

With the advent of local V_2O_5-catalysed SO_2 oxidation catalyst production, a new era in catalysis within South Africa has been entered. Bearing in mind the quantities of local raw materials and exothermic energy involved, one can imagine that small improvements in catalyst design and composition could imply sigficant value to the local infrastructure.

Voluminous literature exits on experimentally based studies on SO_2 oxidation. but, most of the work has been based on measurements where diffusional mass transfer dominated. The conventional kinetic data and mechanisms presented therefore are questionable. It has recently, been proved that a molten catalyst state exists under operating conditions which places doubt on the validity of former literature.

Since the catalytic system involves a metal oxide one of the (V_2O_5), alkali- metal oxides and sulphates, supported on an acid resistant silicious carrier, that supports the liquid phase melt under operating conditions, the reaction becomes a multi-phase, multi-component system. It is in fact a three phase system; the solid silica carrier, the catalytically active liquid melt and the reactive gas in the pores. Throughout this network, the reactant molecules and products migrate and reach reaction equilibrium.

To model this system, reaction kinetics has to take into account the simultaneous diffusion effects in both the liquid and gas phases.

Factors such as phase compositions of the melt, and in particular melt viscosities and the concomitant effects on diffusion in the liquid phase are affected by reactant conditions such as $SO_2/O_2/SO_3$ ratios.

This thesis is an attempt to optimise those factors that apply to the design and engineering of this catalytic system. It considers only a specific support with a specific pore size distribution.

The results of this investigation follow.

CHAPTER 2

LITERATURE SURVEY AND AN OVERVIEW

2.1 INTRODUCTION

The first few sections in this chapter are devoted to the physical interactions between the catalyst melt and the support material. Thereafter the chemical nature of the active liquid constituents, thermodynamics, reaction mechanism and the intrinsic kinetic equations are discussed. Next the important section dealing with the transport restrictions that decreases the reaction rate in industrial SO_2 oxidation catalysts are dealt with. In the last few sections a number of isolated topics like catalyst shape and pressure drop, catalyst manufacturing and catalyst deactivation are covered.

2.2 SUPPORT MATERIAL AND LIQUID DISPERSION

Investigation of the SO_2 catalyst has shown unequivocally that the oxidation takes place as a homogeneous reaction in the liquid phase, but due to liquid diffusion resistance only a thin surface layer is effective during reaction. Thus the SO_2 oxidation catalyst falls into a unique group of catalysts, i.e. supported liquid phase catalysts (SLP system).

2.2.1 Distribution of the liquid phase in the pores

According to Livbjerg, Sorensen & Villadsen (1974: 293) SLP systems are gas/liquid contact systems where the liquid phase is dispersed in a porous support material. Because the pore system used in SLP systems is finely dispersed, the forces governing the liquid distribution in the pore system will be surface forces acting at the solid-liquid and gas-liquid interfaces - i.e., capillary-, surface tension- and adsorption forces. The influence of gravity on the geometry of the liquid is negligible. The liquid will be distributed under the influence of surface forces so that the thermodynamic free energy of the system attains a minimum. For liquids with a contact angle $< 90°$ (i.e., with a positive affinity to the solid surface), which implies a tendency to minimize the area of high energy gas/liquid surface and at the same time maximize the area of low energy liquid/solid surface. Thus, the liquid is drawn into the smaller pores, and if the

liquid loading in the SLP system is increased, larger and larger pores will be filled with liquid. This phenomenon is extensively used to analyze pore structures by measuring capillary condensation of vapors. Topsoe and Nielsen, (1948: 1) proved the mobility of the nonvolatile liquid phase in an SLP catalyst, which is necessary for redistributing the liquid in the pores. They showed that a catalyst melt initially non-uniformly distributed in a support pellet, would be uniformly distributed after some time at reaction conditions. The resulting liquid distribution is shown schematically in figure (1).

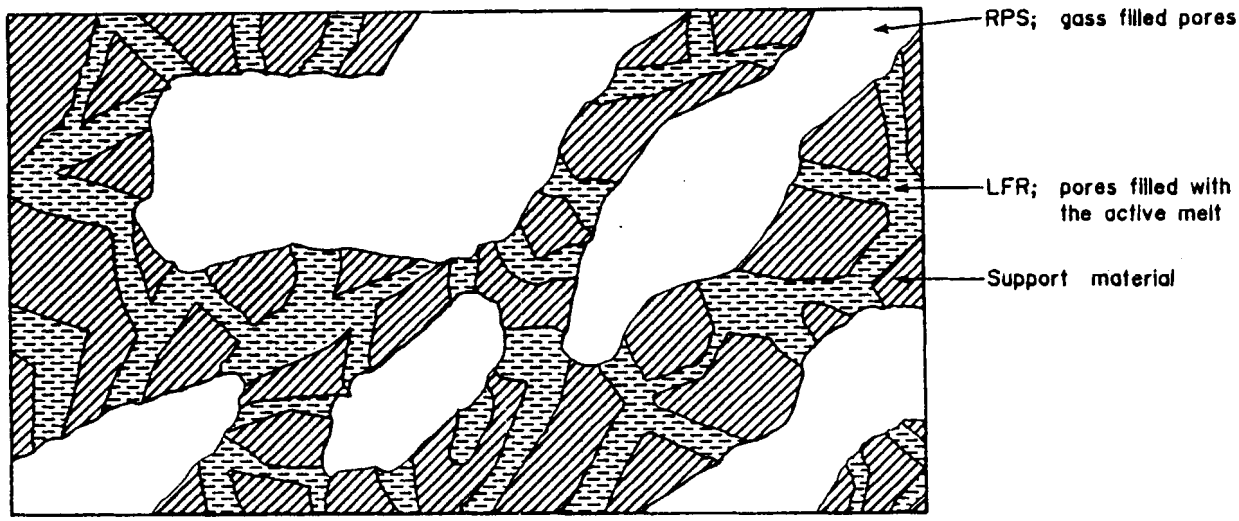

Figure 1. : Liquid contained in smaller pores of support pore system.

The SLP system is divided into two regions:

- One is the pore system of larger gas-filled pores which is called the residual pore system (RPS).
- The other is a two phase area consisting of a solid phase permeated by a pore system of liquid-filled smaller pores - i.e., liquid-filled region (LFR).

The geometry of the residual pore system (RPS) - i.e., pore size distribution and porosity - is important for the rate at which reaction components diffuse through it. The geometry of the LFR is important in determining the lengths of the liquid phase diffusion paths from the residual pores into the liquid-filled pores. These geometric characteristics can be derived from the pore volume distribution of the support material.

In principle it is possible to design an optimal SLP support pore structure and liquid loading by proper balancing of the mass transfer resistances in the liquid phase and in the residual pore system. Theoretical work on this is reported by Rony (1969: 142) and Livbjerg **et al.** (1976: 216).

Very little is known about the physical interaction between the catalyst melt and the support that disperses the liquid phase. Kakinoki **et al.** (1962: 113) observed that the melt migrated from particle to particle in a mixture of impregnated and non-impregnated particles. By porosimeter measurements on impregnated and activated SO_2 oxidation catalysts Tarasova **et al.** (1968: 1111) found that the reduction in pore volume is much larger for the small pores in a given support than for the large ones, especially for bidisperse pore structures where the macropore volume is almost unchanged.

These observations give little insight into the actual dispersion of the liquid phase, but verify the liquid nature of the catalyst and also suggest that surface forces are active in determining the final degree of liquid dispersion.

The degree of liquid dispersion can be characterized by a single length parameter, δ, which denotes the average maximum distance that the reactants must penetrate into the liquid from the gas/liquid surface in order to utilize the whole liquid volume for the chemical reaction. According to Livbjerg **et al.** (1976: 218) the liquid dispersion (or δ) is strongly influenced by the average support pore radius r_p and by the fraction α of the pore volume which is filled with liquid. This fraction α is known as the liquid loading factor and can be calculated by the method of Neth **et al.** (1980: 45). The directly measured V_2O_5 content, G_v, gV_2O_5/g support is first transformed to fractional liquid loading α, the parameter which appears in most liquid distribution models:

$$\alpha = \frac{G_v}{C_v V_p} \tag{1}$$

where C_v is the mass concentration of vanadium (as equivalent amount of V_2O_5) in the melt. C_v could in principle be derived from the molar composition of the melt, but this can lead to uncertain values since the melt may for example absorb largely unknown amounts of gaseous reactants at different temperatures. On the assumption that 1 mole SO_3 is consumed per mole K_2SO_4 and an estimated melt density of 2 g/cm^3 a value for C_v can be estimated (this value however is very uncertain). In order to calculate the V_2O_5 content in the melt, the value of $C_v = 0.28$ g V_2O_5/cm^3 melt, according to Livbjerg **et al.** (1976: 225), was used as a reference value at a promotor/vanadium ratio, $M/V = 3.5{:}1$, and the following expression

$$C_V = 0.28 \frac{4.5}{1 + M/V} \tag{2}$$

can thus be employed to calculate other C_v values corresponding to the actual M/V ratios.

Livbjerg **et al.** (1976: 218) discussed various possible patterns of liquid distribution. It is expedient to arrange such patterns in accordance with their degree of segregation of the liquid phase. In figure (2) the different types of liquid distribution are shown schematically.

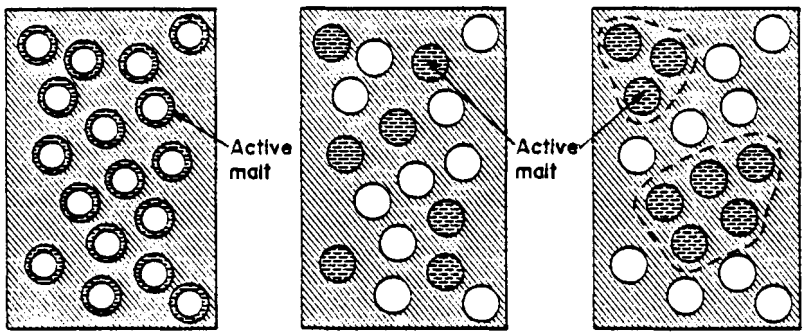

Figure 2. : Schematic representation of different types of liquid distribution in a porous solid. The hatched areas are the solid phase. Circles represent pore cores sections.

a. **Uniform liquid film**

Assuming long cylindrical pores and taking δ to be the equivalent slab thickness of the liquid phase (i.e., liquid volume divided by gas/liquid surface area) δ is obtained from:

$$\delta = \frac{\frac{1}{2} r_p \alpha}{(1-\alpha)^{\frac{1}{2}}} \tag{3}$$

b. **Dispersed liquid plugs**

As discussed by Livbjerg **et al.** (1974: 243) the surface forces tend to reduce the gas/liquid surface area by forming plugs in the pores so that the cross section of some pores is completely filled with liquid while other pores are empty. If the plugs are evenly distributed throughout the solid one can visualize the combined solid and liquid phases as one porous structure. This liquid-filled region is accessible from the gas phase anywhere along the interior surface of the residual pore system. Diffusion in the liquid-filled region is assumed to be equivalent to the liquid phase diffusion in a completely liquid-filled porous body. Hence δ can be estimated as the equivalent slab thickness of the liquid-filled region (i.e., the combined solid and liquid volumes divided by the residual pore surface area):

$$\delta = \frac{\frac{1}{2}r_p\left[\frac{1}{V_p\rho_s} + \alpha\right]}{(1-\alpha)} \tag{4}$$

c. **Cluster models**

The liquid can reduce the gas/liquid surface area further by coalescence to clusters which form continuous liquid regions that are larger than the pore dimensions. Rony (1969: 142), by measurements of hydroformylation rate, produced evidence in support of cluster formation and this was incorporated in his model of liquid distribution. There is no available knowledge of the mechanisms leading to cluster formation or of the stability of cluster distributions. Hence a δ value for clusters can at present only be found from experiments.

d. **Simplified model**

In a more simplified form of the correlation equation, obtained by the authors, the mean thickness of the melt, δ, is directly proportional to the liquid leading factor α:

$$\delta = s\alpha \tag{5}$$

with the constant s being of the order of 10^{-4} and slightly dependent on the mean pore radius. This simplified method of Livbjerg **et al.** (1974: 242) was used to calculate the liquid effectiveness factor.

2.2.2 Support material characteristics

A number of factors need consideration when choosing a support; the most important of which are:

- Inertness,
- Influence on the properties of the catalytic material and promoters,
- Surface area, which can be in macropores or micropores or both,
- Porosity (the amount of open volume in the pellet), which is related to surface area (average pore size and pore-size distribution are important variables),
- Adsorptive properties related to the catalytic material, reactants and products, poisons etc.,
- Thermal resistance to pore collapse, sintering and other structural degradation,
- Chemical stability,

- Catalyst pellet size and configuration,
- Compressive strength, hardness and resistance to attrition,
- Stability under anticipated operating conditions,
- Cost.

A wide range of supports have been used including zeolites, carborundum, pumice, titanium dioxide, aluminium oxide, aluminium silicates, silica gel, marshalite and several other forms of silica. Investigations on the properties of the abovementioned support materials by Urbanek & Trela (1980: 77) have shown that the highest catalytic activities are obtained with the supports prepared from suitably pretreated kieselguhr or diatomaceous earth. These supports exhibit bimodal pore distribution, but the relationship between the properties of their surface and catalytic activity is difficult to describe because of the coinciding effects of pore structure and degree of development of the active liquid surface. Boreskov **et al.** (1973: 626) demonstrated that SiO_2 supports are inert to oxidative catalytic processes.

Catalytic activity appears to depend on the degree of liquid phase dispersion and also on the accessibility of reactants to the liquid phase within the porous pellet matrix. Any chemical or thermal deactivation involving the support should be assumed to consist of a modification of the active surface, which changes the degree of liquid dispersion, the shape of the liquid droplets in capillaries, pore size distribution and interstitial volume.

2.2.3 Diatomite (Kieselguhr)

Silica in the form of diatomaceous earth is a widely used support material. Geologically, diatomite is a sedimentary rock of marine or lacustrine deposition. It consists mainly of accumulated shells or frustules of hydrous silica secreted by diatoms, which are microscopic, one-celled, flowerless plants of the class Bacillarieae.

Chemically, diatomite primarily consists of silicon dioxide, and is catalytically inert. It is reactive to strong alkalies and hydrofluoric acid, but is inert to other acids. Because of the variable structures of the diatom skeletons the silicon dioxide has variable physical and chemical properties; some of these are:

1. **High porosity**
   Up to 85% of the volume of diatomite is made up of tiny interconnected pores or voids. This porosity lends itself to catalyst carrier material.

2. **High Absorption**
   Diatomite can generally absorb up to 1½ times their own weight of liquid and still exhibit the properties of a dry powder. The absorption characteristics are important physical characteristic and are affected by:

   a. **Particle size:** This is an obvious relationship and can to a large extent be controlled by air classification techniques used by the producers to separate the various grades.

   b. **Internal structure of the particles:** This depends on the types of diatom skeletons present and varies throughout the deposits.

3. **Unique Particle Structure/High Surface Area**
   Diatomite particles are characterized by their highly irregular shapes, generally spiny structures and pitted surfaces on an average only 5 to 50 microns in diameter, with a surface area of $\pm 20 m^2/g$.

4. **Great Bulk per Unit Weight**
   Because of their structure, diatomite particles do not readily pack together and they resist compression because contact is limited to the outer points of individual particles.

Weight loss on ignition varies between 2 and 10 percent. Impurities are other aquatic fossils such as sponge residues, sand, clay, volcanic ash, calcium carbonate, magnesium carbonate, soluble salts and organic matter.

The types and amounts of impurities are highly variable and variations exist among deposits as well as among parts of the same deposit. A typical chemical analysis of diatomite is given in table (1).

The true specific gravity of diatomite is 2.1 - 2.2, the same as for opaline silica or opal. Thermal conductivity is fairly low and the fusion point depends on the purity but averages about 1590°C for pure material (slightly less than pure silica). The addition of certain chemical agents can reduce the fusion point.

Table 1: Chemical analysis of typical diatomite.

Grade	% Chemical Analysis								
	Ignition Loss %	SiO_2	Al_2O_3	Fe_2O_3	P_2O_3	TiO_2	CaO	MgO	Na_2O $+K_2O$
Uncalcined (Natural)	3.6	85.8	3.8	1.2	0.2	0.2	0.5	0.6	1.1
Calcined	0.5	91.1	4.0	1.3	0.2	0.2	0.5	0.6	1.1
Flux Calcined	0.2	89.6	4.0	1.5	0.2	0.2	0.5	0.6	3.3

2.3 CHEMICAL NATURE OF THE MELT AND ITS PHYSICAL PROPERTIES

Commercial SO_2 oxidation catalysts usually contain 6 – 8 *wt* % vanadium (based on V_2O_5), and are promoted by alkali-metal sulphates (usually K_2SO_4 with K/V mole ratio of 2 – 4.). As far back as 1940 Frazer and Kirkpatrick (1940: 1659) reported that the promoting action of the alkali metals in vanadium catalyst formulations was due to the formation of higher sulphates. These materials, pyrosulphates, have lower melting points than the corresponding sulphates and may also form eutectic mixtures with sulphates. Furthermore, it has been shown that the pyrosulphates have the ability to dissolve appreciable quantities of vanadium oxides.

2.3.1 Effect of the type of alkaline promoter

Tandy (1956: 68) examined systems of alkali-metal sulphates in equilibrium with SO_2/SO_3/air mixtures. His experiments covered a temperature range of 380 – 600°C with V_2O_5 and metal sulphates (Na, K, Rb, Cs). In the range between 440 and 600°C a liquid is produced that is a vanadium compound dissolved in alkali pyrosulphate-sulphate melt, with the melting point of the mixture increasing with increasing atomic weight of the alkali metal.

According to Gay **et al.** (1983: 114) the melting point of the alkali metal sulphates (no pyrosulphate present) reached a maximum melting point with Rb_2SO_4. See table (2).

Table 2: Melting temperatures and thermal stabilities for some metal sulphates

Sulphate	Melting temperature (K)
Li_2SO_4	1132
Na_2SO_4	1157
K_2SO_4	1342
Rb_2SO_4	1347
Cs_2SO_4	1277

The higher atomic weight alkali elements, i.e. potassium, rubidium, or cesium are preferred. Tandy (1956: 68) found with a metal/vanadia mole ratio of 2.5, that the normal pyrosulphate, $M_2S_2O_7$, and probably vanadyl sulphate, $VOSO_4$, are formed (M = alkali metal). With Rb_2SO_4 and Cs_2SO_4 there was evidence of partial formation of higher sulphates, $M_2S_3O_{10}$. The extent of reduction of vanadium pentoxide was less with the alkali-metal sulphates of higher atomic weight. Thus the ability to stabilize vanadium in the pentavalent state is greatest with rubidium, and decreases in the order $Rb > Cs > K > Na$. The technical advantages of rubidium and cesium are apparently insufficient to provide commercial justification for their use.

2.3.2 Mixtures of Alkaline promoters

Mixtures of alkaline promoters generally enhance the activity of vanadium catalysis at low temperatures (low bite characteristics) due to the formation of eutectic mixtures with lower melting points.

The composition and melting points for some eutectic mixtures are given in table (3) (Gay **et al.**, 1983: 115).

The substitution of 30-50% potassium promoter by sodium in vanadium catalysts for SO_2 oxidation is shown to increase their activity at low temperatures (Simonova, 1982: 59). ESR studies indicate that the presence of sodium inhibits the evolution of inactive V^{4+} compounds. Jiru (1960: 2113) agreed with earlier work by Topsoe and Nielsen (1948: 1) that increased activity can be obtained by exchanging 10% of K_2SO_4 for Cs_2SO_4. It has been questioned by Simicek (1970: 83) whether this is correct, although it is likely that the ignition temperature may be lowered. Simicek also reported that small additions of sodium to a potassium-based catalyst increase activity at low temperatures.

Table 3: The composition and melting temperatures of some sulphate eutectic mixtures

System	Composition (mol %)	Melting temperature (K)
Li_2SO_4:K_2SO_4	80:20	808
Li_2SO_4:Na_2SO_4:K_2SO_4	7:8.5:13.5	785
K_2SO_4:$MgSO_4$	60:40	1023
K_2SO_4:$CaSO_4$	60:40	1140
Na_2SO_4:$ZnSO_4$	45:55	745

More recently, studies on the effects of changing the ratio of different alkali-metal sulphates as well as the M/V ratio (M/V ratio of 1.4 to 1.7) have been made. Mokhlenov (1976: 226) has shown that the conversion of SO_2 increased with increasing atomic weight of the alkali metal added to the K_2SO_4. The optimum reaction temperature increased with decreasing promoter atomic weight. Also the viscosity of the melt decreased as the atomic weight of the added metal was increased and greater wetting of the pore walls was observed.

2.3.3 Degree of vanadium oxidation and composition colour relationships

Oxides corresponding to different vanadium valences have different colours. To test the possibility that the change in catalyst activity might be attributable to the valence of vanadium in the catalyst, the colour of the catalyst was observed under different reaction conditions (Tamura, 1975: 122).

The widespread use of potassium oxide promoted vanadium catalysts has resulted in extensive investigation of the $(V_2O_5)_m(K_2SO_4)_n(SO_3)_p$ system.

Most commercial catalysts are obtained from the manufacturers as greenish yellow pellets. On crushing, the greenish yellow colour is retained. Tamura (1975: 124) made the following observations:

- The colour persists when a typical commercial catalyst is brought to a temperature of 400°C in a stream of pure nitrogen.
- When a SO_2-air mixture is introduced the colour changes to a yellowish green within minutes and no further change in colour is observed in the first 10 hr.

- When the sample treated with SO_2-air at 400°C for 10 hr. is cooled to ambient temperature in a stream of nitrogen, the colour becomes greyish green.
- For a sample brought to 400°C in a stream of air the colour changes to brown.

Tables (4) and (5) summarise the colour and melting point observations in the literature.

Table 4: Composition-color relationships

System	Color	Vanadium valence
V_2O_5	Reddish-yellow	+5
$K_2SO_4.V_2O_5$	Brown-olive	95% +5
$2.5K_2S_2O_7.V_2O_5$	Dark brown	+5
Alkali promoted vanadia catalysts	Brown	+5
V_2O_4	Bright blue	+4
$K_2O - V_2O_5 - SO_3$ melt	Green	+4
Alkali promoted vanadia catalysts on silica support	Bluish green	Between +4 and +5
Alkali promoted vanadia catalysts on silica support in presence of SO_3	Yellow	Between +4 and +5
V_2O_3	Black	+3

The brown color observed when the catalysts are exposed to air at high temperatures corresponds to V^{5+}. The greenish yellow color found when commercial catalysts are exposed to SO_2 is more difficult to interpret. The greenish yellow color appears to correspond to mixtures of V^{4+} and V^{5+} compounds.

The free energy change for the reduction of V_2O_5 to V_2O_4 by SO_2 is +58.4 kJ/mole of pentoxide at 400°C. Potasssium and sulphate will influence this increase in free energy; however thermodynamic data to calculate the actual change are simply not available.

Reduction of V_2O_4 to V_2O_3 by SO_2 is even less favorable; the free energy change at 400°C is positive and +125 kJ/mole. Mars & Maessen (1964: 266) also suggest V^{3+} is not formed in the $SO_2/O_2/V_2O_5$ systems.

Topsoe & Nielsen (1948: 2) associated the green color in potassium-promoted vanadia catalysts with a vanadium valence between +4 and +5, but claim a yellow color appears in the presence of high SO_3, levels, that is, when the potassium pyrosulphate would be found.

Table 5: Melting point-composition relationships

System	Melting point (°C)
$2.5K_2S_2O_7.V_2O_5$	ca. 400
$K_2SO_4.V_2O_5$ (equimolar)	478
$K_2SO_4 - V_2O_5$	mp-composition diagram determined [a]
$K_2S_2O_7 - V_2O_5$	mp-composition diagram determined [b]
Alkali promoted vanadia	ca. 450
$K_2O - V_2O_5 - SO_3$	440
$K_2S_2O_7 - V_2O_5$	mp-composition diagram determined [c]

[a]Eutectic mp at 430°C at ca. 70% K_2SO_4; mp of K_2SO_4 is 585°C.
[b]Eutectic mp at 230°C at ca. 55% $K_2S_2O_7$.
[c]Compounds corresponding to $1.25K_2S_2O_7.V_2O_5$ detected melting at 380°C and to $6\,K_2S_2O_7$. V_2O_5 melting at 330°C; $K_2S_2O_7$ melts at 415°C.

Commercial catalysts (greenish yellow) are therefore supplied as a sulphate compound containing both V^{4+} and V^{5+}, and potassium as a mixture of $K_2S_2O_7$ and K_2SO_4. On exposure to the reaction mixture some reduction occurs. The change of color to greyish green when the catalyst is purged with nitrogen and cooled suggests that SO_3 may be stripped from the catalyst. It probably comes from decomposition of $K_2S_2O_7$.

Tamura (1975: 129) suggests that the catalyst may be more active as V^{4+} than as V^{5+}. There is some evidence (Mars & Maessen, 1964: 266) that the overall rate of oxidation of SO_2 may be controlled by a step involving either the adsorption of oxygen on a V^{4+} site or a complex group of surface steps resulting in the oxidation of the +4 site. The reduced form of the catalyst might then provide a greater number of reduced sites and therefore a higher intrinsic activity.

Alternatively, increased activity may also be associated with the increase in sulphur in the catalyst as will be discussed in the next section.

2.3.4 Thermochemical nature of pyrosulphate formation

The solubility of SO_3 in molten sulphates is dominated by the chemical equilibrium for the formation of the pyrosulphate ion described by the equation

$$S_2O_7^{2-} \rightleftarrows SO_4^{2-} + SO_3 \qquad (6)$$

with the equilibrium constant

$$K = \frac{[SO_4^{2-}]P_{SO_3}}{[S_2O_7^{2-}]} \qquad (7)$$

a function of temperature and the partial pressure of SO_3 (Gale, 1983: 123). The equilibrium constants for the reaction are summarised in table (6).

Table 6: Equilibrium constants for the reaction

$$S_2O_7^{2-} \rightleftarrows SO_4^{2-} + SO_3$$

$$K = \frac{[SO_4^{2-}]P_{SO_3}}{[S_2O_7^{2-}]}$$

$$\log_{10}K = a - \frac{b \times 10^3}{T(K)}$$

Sulphate	a	b	Range (K)
Li_2SO_4	8.42	6.76	644-700
Na_2SO_4	8.09	7.93	828-928
K_2SO_4	7.07	8.56	926-1000

The formation of SO_3 shifts the potassium sulphate in the catalyst towards the pyrosulphate $S_2O_7^{2-}$. There is evidence that the mixed vanadium potassium salts of the pyrosulphate have melting points well below those of the sulphates. Increasing SO_3 content therefore lowers the melting point of the catalyst phase. The pyrosulphate serves as a flux lowering the melting point or at least causes a vitreous rather than a crystalline catalyst phase.

If, as Topsoe & Nielsen (1948: 2) and Holroyd (1971: 1964) suggest, the rate of reaction is associated with the viscosity of the catalyst phase, the increasing $K_2S_2O_7$ should raise the rate by reducing the catalyst phase viscosity. Most authors suggest that a transport step in the catalyst phase is rate controlling in SO_2 oxidation. Lower viscosity could increase this rate by raising mobility of species in the liquid phase.

Table (5) indicates the existence of potassium vanadium sulphates and pyrosulphates melting between 230 and 500°C. Holroyd's (1971: 1964) data suggest that a pyrosulphate $(S_2O_7)^{2-}$ may be formed as a compound $K_2V(S_2O_7)_3$ with a melting point of 230°C.

According to Tamura (1976: 129) fresh commercial catalyst has the nominal composition $2K_2O.V_2O_5.3SO_3$. In view of its colour, its actual composition is $K_2SO_4.K_2S_2O_7.V_2O_4$ assuming vanadium is primarily present as V^{4+}. A sulfovanadia compound $VOSO_4$ is a possible form according to Glueck & Kenny (1968: 1257) and Boreskov **et al.** (1973: 626). Tamura suggested an approximate composition of $\pm 0.7K_2SO_4.1.4K_2S_2O_7.V_2O_5$ for commercial catalysts.

Bazarova **et al.** (1968: 1132) noted that the pyrosulphate is unstable in air above 420°C. Boreskov **et al.** (1973: 626) and Holroyd (1971: 1964) also reported $K_2S_2O_7$ decomposition in the absence of SO_3 at temperatures above 300°C. Tamura (1976: 129) noted that heating the catalyst at 400°C for 10 hr in air appears to decompose some of the pyrosulphate $K_2S_2O_7$ to K_2SO_4. According to him adsorbed SO_3 and SO_2 on vanadium catalysts between 400 and 500°C are rapidly desorbed in a nitrogen purge, thus it is unlikely that the increase in total sulphur in a catalyst at operating conditions arises from adsorption of SO_2 and SO_3 alone.

The ability of the catalyst to change its activity depending upon its exposure to different reactant (SO_2, O_2) concentrations as discussed above suggests a potentially valuable means of exploitation of this catalyst through cycling of feed concentrations (Tamura **et al.**, 1975: 130).

The question of whether the running-in or proper activation of a catalyst to enhance pyrosulphates formation could provide higher **permanent** catalyst activity must be negative according to Tamura. The strike temperature of fresh new catalyst might however be temporarily lowered to ease startup of plants (low strike temperature). Careful shutdown procedures by cooling the catalyst under high SO_3 partial pressures could lead to a much easier startup due to the low strike temperature characteristics endowed to the catalyst during the shutdown.

These abovementioned possibilities might be of vital importance not only for the catalyst manufacturer, but also for the plant design companies and plant operators.

2.4 THERMODYNAMICS

The reaction of sulphur dioxide with oxygen to form sulphur trioxide is a highly exothermic, reversible reaction, associated with a reduction in volume.

$$SO_2 + \tfrac{1}{2}\, O_2 \rightleftarrows SO_3 \quad \Delta H^\circ = -99 kJ/mole. \tag{8}$$

The sulphur trioxide is absorbed in sulphuric acid and reacts with added water to form more sulphuric acid.

$$SO_{3(g)} + H_2O_{(\ell)} \rightleftarrows H_2SO_{4(\ell)} \quad \Delta H^\circ = -132.5 kJ/mole. \tag{9}$$

The position of the equilibrium in the exothermic oxidation of sulphur trioxide in the gas phase depends on the prevailing temperature, total pressure and concentrations (partial pressures) of the reactants. The thermodynamic equilibrium is determined by the equilibrium constant Kp according to the Law of Mass Action:

$$Kp = \frac{P_{SO_3}}{P_{SO_2} \cdot P_{O_2}^{0.5}} \tag{10}$$

Due to the negative reaction enthalpy of sulphur dioxide oxidation, both Kp and the SO_2 equilibrium conversion decrease with rising temperature. The classical relation between Kp (in atm $^{-0.5}$) and temperature was correlated by numerous authors:

$$\log\ Kp = \frac{5186.5}{T} + 0.611\ \log\ T - 6.75 \tag{11}$$

(T = absolute temperature in K)

An increase in the overall pressure will increase the equilibrium conversion, as the reaction involves a reduction of volume as shown in figure (3).

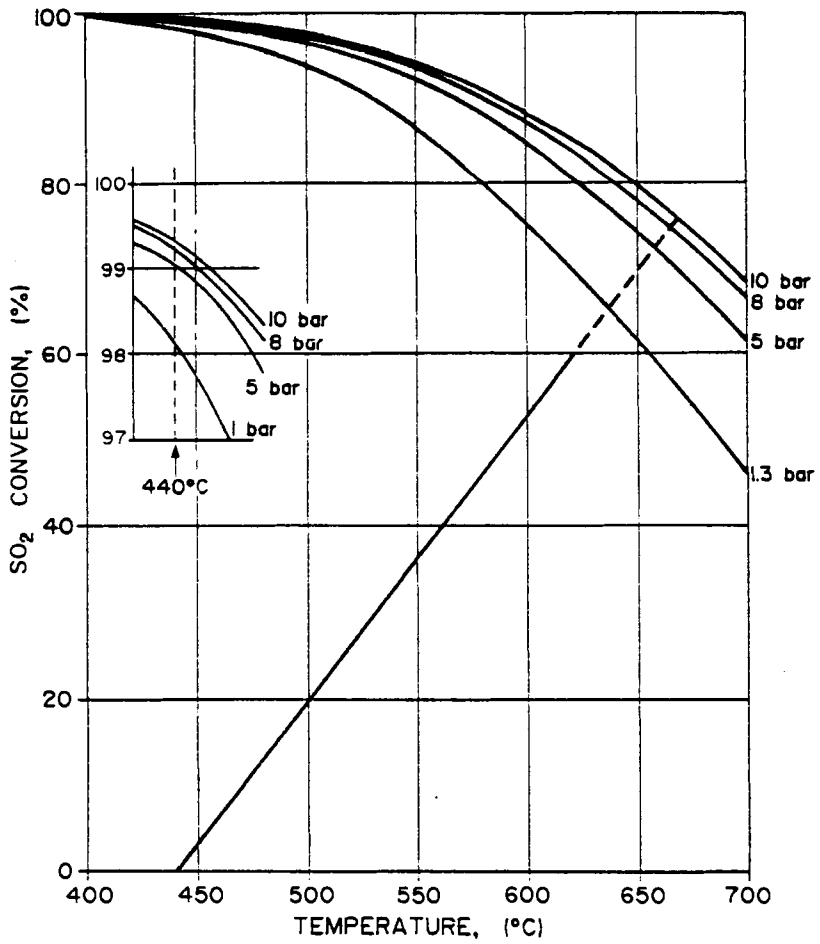

Figure 3. : Theoretical conversion equilibrium in the oxidation of SO_2 to SO_3 as a function of temperature and pressure (feed gas composition 10% vol SO_2, 10,9% vol O_2.)

The possible equilibrium sulphur dioxide conversion at a defined temperature, T, and a defined total pressure, Pt, is dependent on the SO_2 and O_2 concentrations of the reactant gases (figure 4).

If the sulphur dioxide concentration is $2a$ vol - % and the oxygen concentration b vol - %, the fraction, x, of the sulphur dioxide oxidized to sulphur trioxide at equilibrium can be calculated from the following equation according to the Law of Mass Action:

$$Kp = \frac{1}{Pt} \quad \frac{x}{1-x} \quad \frac{100-ax}{b-ax} \tag{12}$$

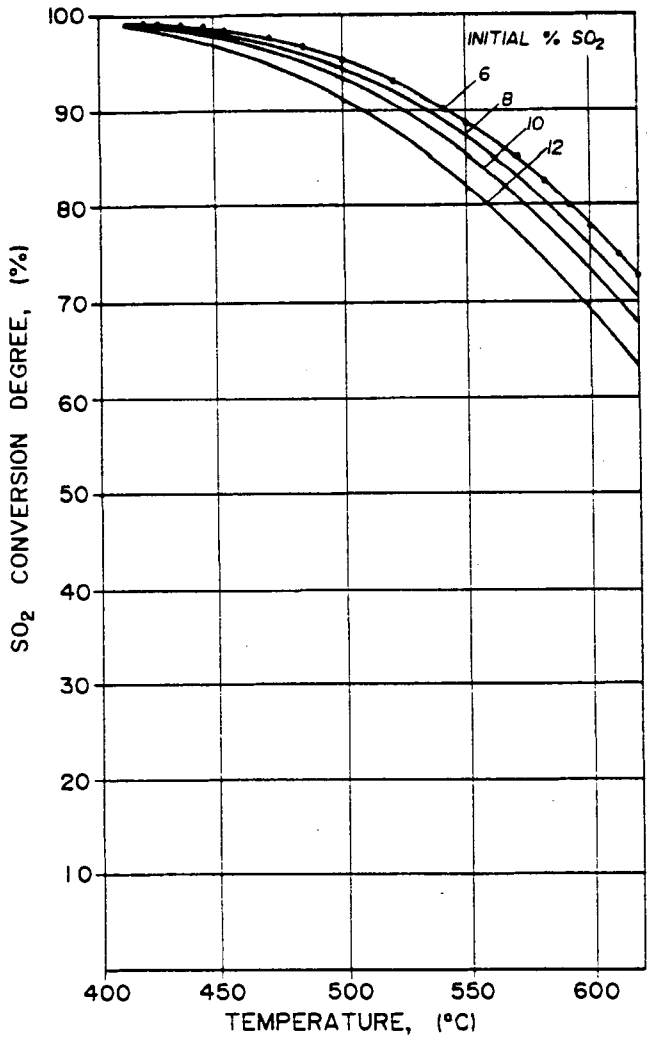

Figure 4. : Effect of the initial SO_2 on the SO_2 conversion degree as a function of temperature. Urbanek & Trela (1980: 75).

The appropriate value of Kp is determined from the equation of Sander **et al.** (1981: 281). In accordance with the Law of Mass Action, increasing the oxygen partial pressure will also increase the degree of conversion. However, when air alone is used as the source of oxygen, as is the usual practice in sulphur dioxide oxidation, the oxygen and sulphur dioxide concentrations are in inverse proportion, as the greater the oxygen concentration in the combustion gases, the lower the sulphur dioxide content will be. The essential factor determining the attainable SO_2 conversion is thus the volumetric O_2/SO_2 ratio in the feed gases. Whereas sulphur dioxide oxidation requires a stoichiometric O_2/SO_2 ratio of only 0.5:1, it is normal practice to use a ratio of at least 1:1 in industry. The presence of the surplus oxygen not only raises the SO_2 equilibrium conversion but is also an essential prerequisite for maintaining the activity of the vanadium contact catalyst. There are, however, practical limits on the amount of extra air that can be added, as the nitrogen present in the air dilutes the

sulphur dioxide to the point where the economics of the process is impaired. Although it would be technically possible to avoid nitrogen dilution by using oxygen instead of air, as is sometimes done in pyrometallurgical processes which produce high-strength by-product sulphur dioxide gas streams, it is usually difficult to justify in a sulphur burning installation.

The actual sulphur dioxide conversion does not attain the theoretical equilibrium value in an industrial plant. Gas-phase oxidation of sulphur dioxide is kinetically inhibited and virtually impossible without a catalyst at any temperature. The reaction is so slow at ordinary temperatures that, in practical terms, it does not occur at all. Increasing the temperature increases the rate of reaction, but simultaneously the position of the equilibrium shifts unfavourably; away from sulphur trioxide and towards sulphur dioxide and oxygen.

The actual sulphur dioxide conversion is lower than the theoretical (equilibrium) conversion as shown in the following figure:

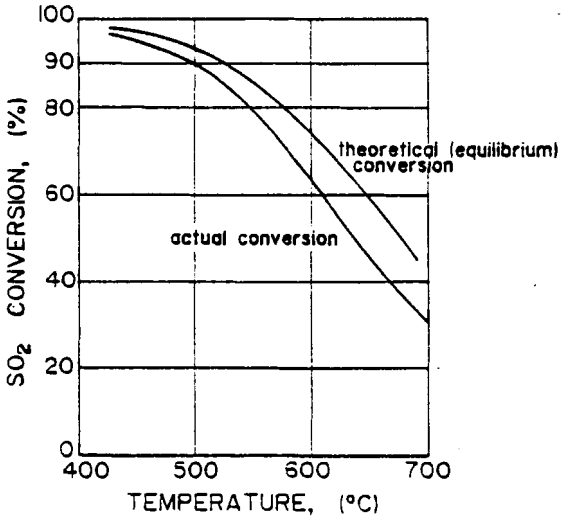

Figure 5. : Comparison of theoretical equilibrium SO_2 conversion (10 SO_2, 10.9 O_2) with actual SO_2 conversion attained over a specific catalyst.

The actual conversion characteristics are substantially influenced by the specific catalyst activity, which has to be determined for each individual catalyst by measurement.

Thus it would be thermodynamically favourable for high conversions of SO_2 to develop a process that:

- Operates under elevated pressures (figure 3) because of the volume decrease accompanying the reaction. The main problem is to design a suitable tail gas expansion turbine for power recovery, since sulphuric acid mist in the tail gas is very corrosive.

- Improves the conversion of sulphur dioxide to sulphur trioxide by removing, at an intermediate stage in the process, the sulphur trioxide already formed. In the double-absorption type of sulphuric acid plant, this is done by routing the reaction gasses after two or three stages of catalytic conversion through an intermediate absorption stage and then through one or two subsequent catalytic conversion stages. Because of the large (100%) stoichiometric oxygen excess in the original feed gas and the diminished sulphur dioxide concentration, the O_2/SO_2 ratio at this point is about six times more thermodynamically favourable than at the start (figure 6).

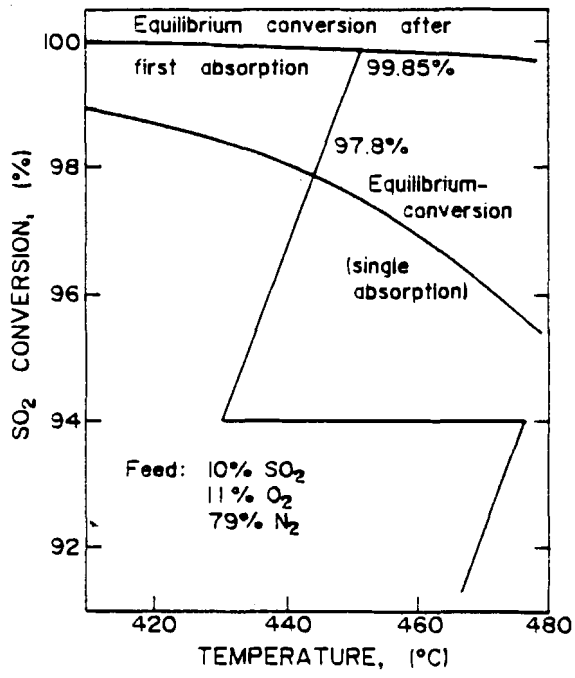

Figure 6. : Improvement in equilibrium conversion through interstage absorption after the third catalyst bed.

- Incorporates a catalyst that is very active at substantially lower temperatures, permitting, for example, an ignition temperature of 340°C instead of 420°C. Then it would be possible to achieve high conversions without intermediate adsorption, even at high SO_2 concentrations in the feed gas (figure 5).

2.5 REACTION MECHANISM

Details of the SO_2/SO_3 reaction mechanism and the overall kinetics are not fully understood or quantified. There is little agreement on this subject and a generally accepted model or equation cannot be found in the literature. Reviews by Kenney (1975: 197-224) and by Urbanek & Trela (1980: 73-133) discuss this topic in detail.

The fact that the catalytically active constituents occur in the liquid state under reaction conditions was often disregarded, and numerous studies, especially those on reaction mechanism, are of disputable value. Only those proposed mechanisms in which the active phase was treated as a liquid under reaction conditions will be mentioned here.

From the majority of kinetic measurements it is concluded that the reaction:

$$SO_2 + \tfrac{1}{2}O_2 \rightleftarrows SO_3 \qquad (13)$$

is of first order with respect to oxygen. However, there are different interpretations of the roles that SO_2 and SO_3 play in the reaction mechanism.

Mars and Maessen (1964: 266) proposed the following scheme

$$SO_2 + 2V^{5+} + O^{2-} \rightleftarrows 2V^{4+} + SO_3 \qquad (14a)$$

$$\tfrac{1}{2}O_2 + 2V^{4+} \rightarrow 2V^{5+} + O^{2-} \qquad (14b)$$

where (14a) is the reaction at equilibrium, and the re-oxidation of V^{4+} represented by (14b) is the rate determining step. This particular mechanism has been used most frequently.

Regner and Simecek (1968: 2540) suggested that gaseous oxygen reacts with V^{4+} ions in three steps:

$$SO_2 + 2V^{5+} + O^{2-} \rightleftarrows SO_3 + 2V^{4+} \qquad (15a)$$

$$\tfrac{1}{2}\left[O_2 + V^{4+} \rightleftarrows V^{5+} + O_2^- \right] \qquad (15b)$$

$$\tfrac{1}{2}\left[O_2 + V^{4+} \rightleftarrows V^{5+} + 2O^- \right] \qquad (15c)$$

$$O^- + V^{4+} \rightleftarrows V^{5+} + O^{2-} \qquad (15d)$$

Using finely divided catalyst, for which the effectiveness factor is unity, it was concluded that the rate equation based on (15c) was the rate controlling step. With conversions above 30%, the equilibrium reactions (15a), (15b) and (15d) fit the data best.

Glueck and Kenney (1968: 1257) studied the overall kinetics of SO_2 oxidation at temperatures between 277°C and 377°C. It was concluded that unsupported $V_2O_5/K_2S_2O_7$ melts may be used for kinetic measurements, thereby eliminating problems of heat and mass transfer to a porous catalyst pellet. A three-step mechanism involving no rate-controlling step was proposed:

$$V_2O_5 \cdot SO_3 + SO_2 \rightleftarrows (VOSO_4)_2 \qquad (16a)$$

$$(VOSO_4)_2 \rightleftarrows V_2O_4 \cdot SO_2 + SO_3 + \tfrac{1}{2}O_2 \qquad (16b)$$

$$V_2O_4 \cdot SO_2 + \tfrac{1}{2}O_2 \rightleftarrows V_2O_4 \cdot SO_3 \qquad (16c)$$

First V^{5+} reacts with sulfur dioxide and next V^{4+} is oxidized by the oxygen dissolved in the liquid or chemisorbed at the gas-liquid interface.

Grydgaard et al. (1978: 582-595) imposed restrictions with respect to the V^{4+} concentration in the Mars and Maessen (1964: 266) model. According to him a part of V^{4+} can exist in an inactive state. Grydgaard **et al.** (1978: 582) have taken this uncertainty in the Mars and Maessen mechanism into consideration by introducing a maximum solubility of V^{4+} as a factor into the vanadium balance. The following scheme was proposed:

$$
\begin{array}{c}
+\ \tfrac{1}{2}\ O_2 \\
\overset{a}{\Big\downarrow} \\
SO_2 + mV^{5+} \underset{b}{\rightleftarrows} nV^{4+}_{(s)} + SO_3 \\
\uparrow\downarrow c \\
V^{4+}_{(s)}
\end{array}
\qquad (17)
$$

where (17a) is the rate determining step.

Hansen (1979) studied the chemistry of the molten salt by electrochemical and other techniques. He studied the $K_2S_2O_7/K_2SO_4/V_2O_5$ system and suggested the following equilibrium:

$$VO(SO_4)_3^{3-} + SO_4^{2-} \rightleftarrows VO_2(SO_4)_2^{3-} + S_2O_7 \qquad (18)$$

where only $VO_2(SO_4)_2^{3-}$ is catalytically active. Whether the Lux (1939: 303) and Flood (1947: 592) acid-base concepts advocated by Hansen are useful or not in this system, the proposed active species seems chemically more reasonable than the ones in Equations (16a, b, c).

Other useful reviews of various reaction mechanisms are given by Neth (1980: 44), Boreskov (1967: 126), Weychert (1969: 396) and Livbjerg (1972: 21).

2.6 INTRINSIC KINETIC EQUATIONS

With specified initial SO_2 and O_2 concentrations, the dependence of the oxidation rate on the degree of SO_2 conversion and temperature follows a course imposed by the exothermicity and reversibility of the reaction (figure 7).

Most of the rate expressions found in the literature can be put in the form:

$$r'_L = r'_{Lf}(1 - \xi^{1/S}) \qquad (19)$$

where ξ is defined by:

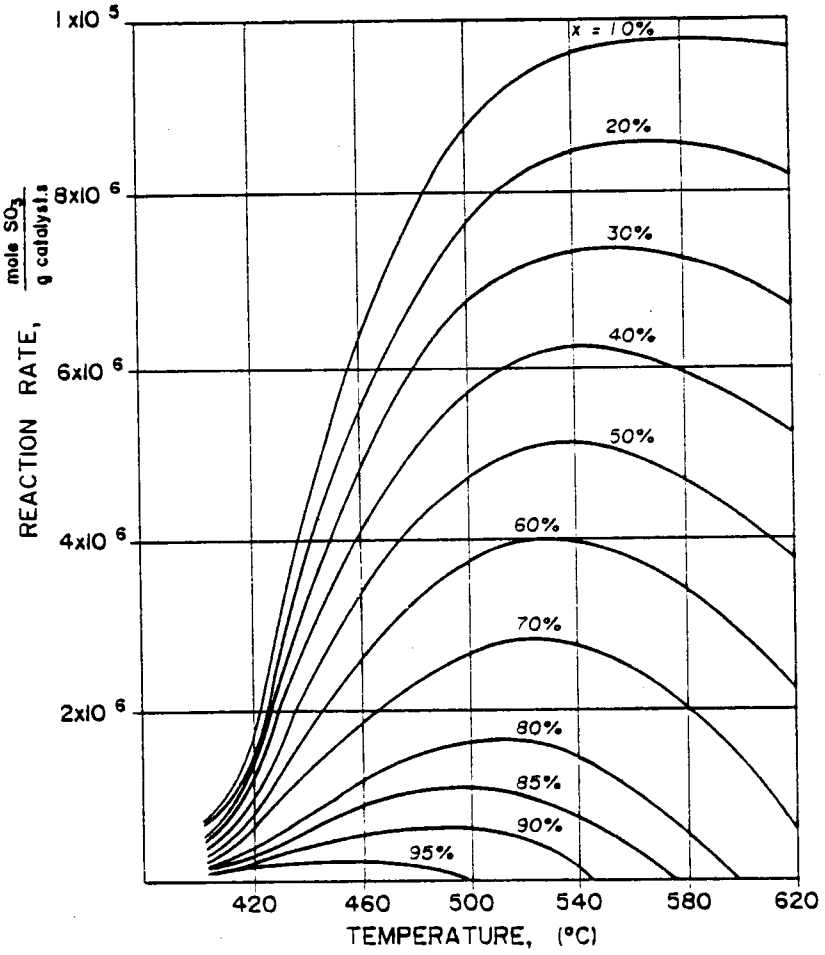

Figure 7. : Typical dependence of the oxidation rate on the degree of SO_2 conversion and temperature (Urbanek, 1980: 81).

$$\xi = \frac{1}{q\sqrt{PO_2}\,Kp} \tag{20}$$

$$q = \frac{P_{SO_2}}{P_{SO_3}} \tag{21}$$

and r'_{Lf} is the forward reaction rate. The majority of forward reaction rate expressions r'_{Lf} found in the literature are of the form:

$$r'_{Lf} = kP^{\ell}_{SO_2}P^{m}_{O_2}P^{n}_{SO_3} \tag{22}$$

or

$$r'_{Lf} = \frac{kP^{\ell}_{SO_2} P^{m}_{O_2} P^{n}_{SO_3}}{1 + AP^{d}_{SO_2} + BP^{e}_{O_2} + CP^{f}_{SO_3}} \tag{23}$$

where equations (22) and (23) are the power law and the Langmuir-Hinshelwood form, respectively.

There is no agreement on the parameters in equations (22) and (23) except that in the majority of studies ℓ and m are between 0.5 and 1.0 and n is usually 0 to -1. In equation (23) d, e, and f are usually 1.0 and the parameters A, B and C may or may not be temperature dependent. The parameters A, B and C are functions of temperature rather than sorption equilibrium constants of suitable reactants. Any interpretation of the parameters in terms of adsorption constants is wholly unjustified since the catalyst is a liquid state at the reaction conditions.

The temperature dependence of the rate constant k is very complicated, and in commercial catalysts the apparent activation energy can vary from as much as 67 kJ/mol to 272 kJ/mol in the range 416 – 484°C. Breaks in Arrhenius plots of reaction rate logarithm versus $1/T$ are found in most studies if the experiment covers a large temperature range.

Most of the earlier equations and even some of the more recent kinetic equations beyond any doubt reflects the results of the experiments carried out in the diffusional region. According to Urbanek & Trela (1980: 93) who evaluated the different equations found in the literature critically, the differences revealed are considered to be so great as to render any of these equations inapplicable as a general rate expression. Urbanek evaluated these expressions by comparing the forms of the concentration-dependent function in the various equations. At the lower temperatures the average error involved in the rate constant ranges from 8 to 80% and, at the higher temperatures, from 3 to 30%.

The Mars & Maessen (1964: 266) equation deviates the least from the mean value while the Boreskov (1970: 181) is fairly close to the Mars & Maessen equation but it results in slightly lower reaction rates at lower temperatures. Only the Mars & Maessen and the Boreskov equations will be discussed in more detail because they are the most widely used equations.

Mars & Maessen (1964: 226) were the first to relate the reaction rate to the composition of the active liquid by assuming the reaction $\frac{1}{2}O_2 + 2V^{4+} \rightarrow 2V^{5+} + O^{2-}$ as the rate-determining step, and the V^{4+} concentration is given by the established equilibrium according to equation (14a), expressed by:

$$C^2_{V^{4+}} = \frac{C^2_V K_c q}{(1 + \sqrt{K_c q})^2} \tag{24}$$

Equation (24) contains the vanadium balance

$$C_V = C_{V^{4+}} + C_{V^{5+}} \tag{25}$$

The equilibrium constant K_c related to equation (14a) was found to be:

$$K_c = 2.3 \times 10^{-8} e^{13700/T} \tag{26}$$

from the equilibrium measurements in which the V^{4+}/V^{5+} ratio was determined in the cooled solidified melt. The P_{SO_2}/P_{SO_3} ratio is denoted by q.

In accordance with most empirical results, the reaction can be regarded as first order with respect to oxygen, the rate equation being given by:

$$r'_L = -\frac{dC_{SO_2}}{dt} = -2\frac{dC_{O_2}}{dt} = k_L P_{O_2} \frac{K_c q}{(1+\sqrt{K_c q})^2}(1-\xi^{1/S}) \tag{27}$$

where

$$\xi = \frac{1}{q\sqrt{P_{O_2} K_p}} \tag{28}$$

and

$$K_p = 10^{(4956/T)-4678} \tag{29}$$

Equation (27) is frequently employed for the chemical reaction in the melt, but it is clear from the results of numerous investigations that restrictions have to be imposed with respect to the V^{4+} concentration achieved with equation (24). According to Holroyd and Kenney (1971: 1963) part of V^{4+} can exist in an inactive state. It is assumed that V^{4+} is only partly soluble in the melt and that at lower temperatures some V^{4+} precipitates out. The existence of two different V^{4+} species has been confirmed by Boreskov **et al.** (1973: 626) using ESR methods. This has not been taken into account by the vanadium balance contained in equation (24), so that in this case the total V^{4+} yield is calculated.

Grydgaard (1978: 582) modified the Mars & Maessen model equation by introducing a maximum solubility of V^{4+} as a factor into the vanadium balance. The solubility function is a function of temperature and the melt composition was determined by regression analysis using experimental data from kinetic measurements. This procedure did not appear practicable in the present work where the measured reaction rates are assumed to be significantly affected by mass transfer limitations, and as a result, if additional solubility parameters are taken into account, they would become too uncertain.

Consequently, another rate equation was tested as an alternative to equation (27), which though formally similar to equation (27), results in lower reaction rates at lower temperatures. The following equation has been found empirically by Boreskov **et al.** (1970: 181)

$$r'_L = k_L P_{O_2} \frac{P_{SO_2}}{P_{SO_2} + 0.8P_{SO_3}} (1 - \xi^{1/S}) \tag{30}$$

from kinetic measurement, and consequently no attention need be paid to inactive V^{4+}. Equations (28) and (30) differ only with regard to the forms defined by:

$$\omega_1 = \frac{K_c q}{(1 + \sqrt{K_c q})^2} \tag{31a}$$

and

$$\omega_2 = \frac{P_{SO_2}}{P_{SO_2} + 0.8P_{SO_3}} = \frac{1.25q}{1 + 1.25q} \tag{31b}$$

where

$$\omega_1 = C_{V^{4+}}^2.$$

ω_1 practically coincides with ω_2 at about 535°C but depending on $K_c(T)$, the ω_1/ω_2 ratio increases with decreasing temperature. Hence, ω_2 can be considered as an approximated expression of ω_1 which reflects the influence of inactive V^{4+} by employing a specific value for K_c instead of using $K_c(T)$, whereby the specific value can be regarded as a quasi temperature independent equilibrium constant for a modified equation (14a) (that is equation (17)) which includes only the active V^{4+} species.

The effect of the total V_2O_5 concentration on the reaction rate is incorporated into the rate constant as equation (27) of:

$$k_L = k'_L C_V^2 \tag{32}$$

whereas no corresponding relation was quoted by Boreskov (1970: 181). However, in view of the fact that the two equations are assumed to be analogous, the same correlation should apply to both of them.

In the study that follows, both these equations will be tested and the final rate equation can be expressed in a general form as:

$$r'_L = k_L P_{O_2} \omega_i (1 - \xi^{1/S}) \tag{33}$$

Under certain conditions a physical interpretation may be given to the parameter $1/S$ in equation (33). If one single elementary reaction mechanism step is rate determining for the overall reaction, $1/S$ will be the stoichiometric number for this step assuming that the rate of the forward reaction, $k_L P_{O_2} \omega_i$, is described correctly even close to equilibrium. It is plausible that a rate determining step may involve one of the following:

a) One oxygen molecule
b) one oxygen atom
c) one sulphur dioxide molecule or
d) one sulphur trioxide molecule.

In the first case $S = ½$ while $S = 1$ for $(b) - (d)$. These two values are consistent with the S-values proposed by the different kinetic models. There is no agreement on the correct value of S and it is doubtful that one value is best for all cases.

2.7 TRANSPORT PHENOMENA

Livbjerg & Villadsen (1971: 21) and numerous other investigations indicate that transport restrictions may considerably decrease the reaction rate in industrial SO_2 oxidation reactors.

The first step in the engineering of a catalyst is to quantify the phenomena that govern its performance. These fall into two broad categories:

1. Transport Phenomena (i.e. mass and heat transport)
2. Reaction kinetics.

According to Kovenklioglu **et al.** (1978: 841) the transport phenomena, especially mass transport inside the pellet, plays a far more important role than the form of the intrinsic kinetic equations in the case of commercial SO_2 oxidation catalysts. The behavior of a gas-phase supported liquid phase heterogeneous catalyst in an operating reactor is influenced by three transport phenomena depicted in figure (8).

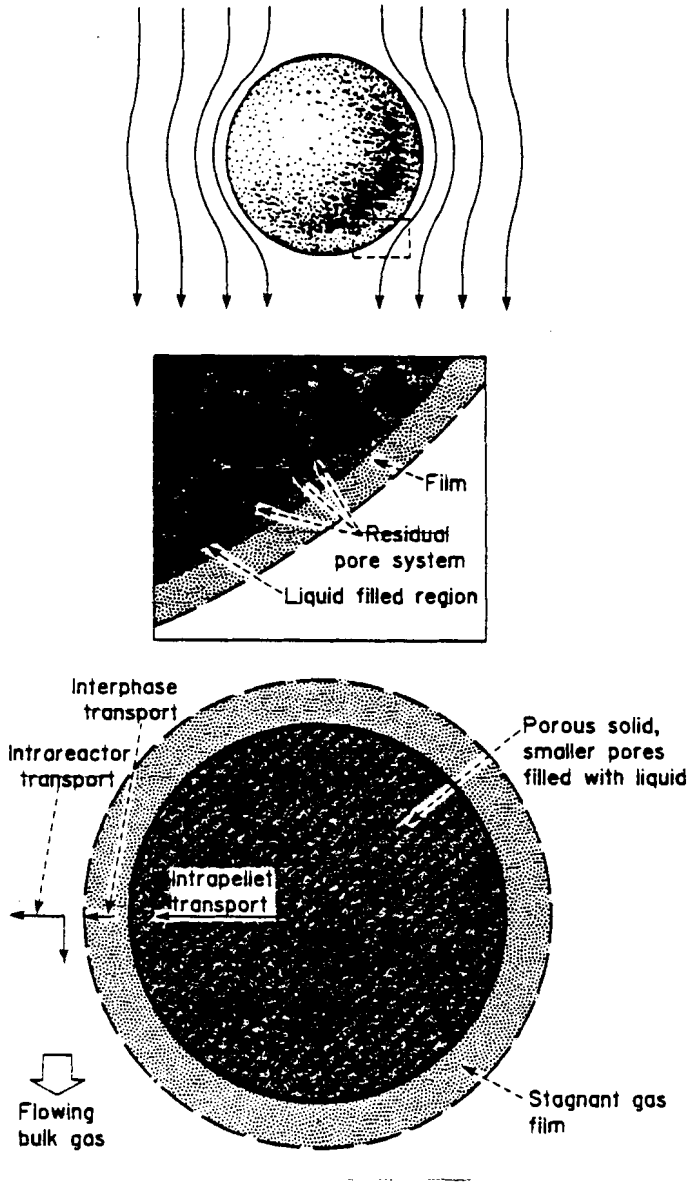

Figure 8. : Mass and heat transfer take place in a reactor as a result of intrareactor, interphase and intrapellet transport.

As the gas passes through the interstices of the catalyst bed, it flows around the exterior of the catalyst pellet. If a reaction ensues, a concentration gradient (and, possibly, a temperature gradient) will develop between the inlet and outlet of the reactor. These are called axial gradients. Also, concentration and temperature gradients can arise between the center of the reactor and its wall. These are known as radial gradients. These gradients will, in turn, ge-

nerate conductive and diffusive heat and mass transfer, which phenomena are referred to as *intrareactor* transport.

Because the flowrate at the surface of the catalyst pellet is zero, a thin stagnant film surrounds the pellet. If a chemical reaction takes place within the pellet, there are concentration and possibly temperature gradients between the pellet and the flowing gas. These gradients cross the boundary layer between the pellet and the gas bulk. Heat and mass transfer across this boundary layer is called *interphase* transport.

When chemical reactions occur, heat and mass transfer take place inside the porous pellet. This is known as *intrapellet* transport. This intrapellet transport can be divided into two regions i.e. transport in the residual pore system (RPS) and transport in the liquid filled region (LFR).

The experimental evidence presented by Urbanek (1980: 100) allows one to rank diffusional effects in the descending order : intrapellet mass transport > interphase mass and heat transport > intrapellet heat transport. However current tendencies to prepare increasingly active catalysts will give rise to transport processes becoming more and more frequently the rate-controlling step in the oxidation of SO_2, and the above ranking may well undergo modification. Therefore, a search for new potent catalysts should be run parallel to transport process studies, especially as improvement of e.g. intrapellet diffusion condition (expanded or ring-shaped pellets) can result in a greatly enhanced process rate.

2.7.1 Effectiveness factors

Effectiveness factor concepts are basic to catalyst design and are used as a basis to describe the performance of the V_2O_5 SLP system.

The effectiveness factor is the amount by which the intrinsic reaction rate has been reduced due to diffusional mass transfer restrictions. Signified by η, it can be defined as the actual reaction rate divided by the reaction rate that would occur if all the active constituents throughout the inside of the pellet were exposed to a reactant of the same concentration and temperature as that on the outside of the pellet. Multiplying the intrinsic reaction rate by this factor yields the actual reaction rate

$$\eta = \frac{r_{\text{actual reaction rate with diffusion}}}{r_{\text{intrinsic reaction rate without diffusion}}} \tag{34}$$

where

r' = intrinsic reaction rate, r = effective reaction rate

The progressive drop in concentration on moving into a catalyst pore is shown in figure 9 and this is seen to be dependent on the dimensionless quantity ϕ, called the Thiele modulus (Levenspiel, 1972: 460).

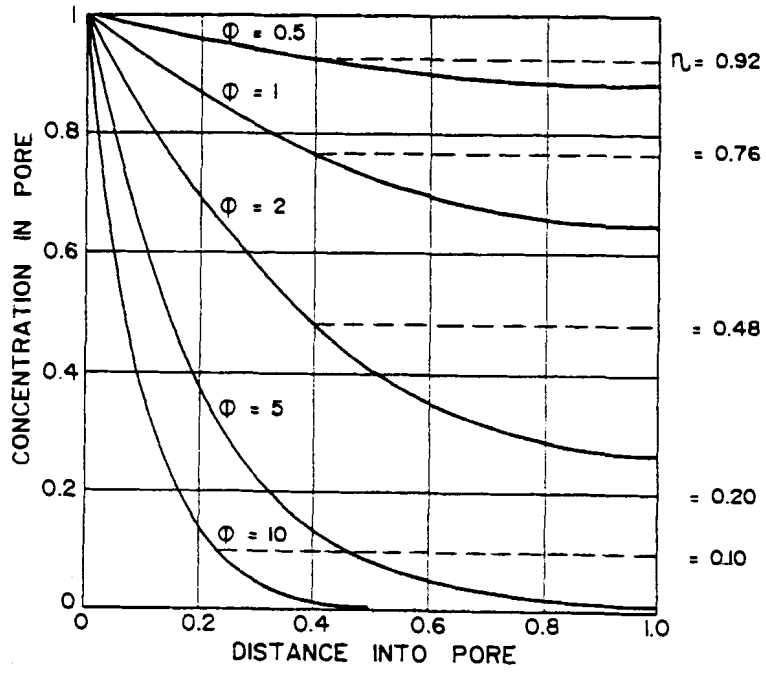

Figure 9. : Progressive drop in reactant concentration within a catalyst pore as a function of ϕ

The Thiele modulus is a function of:

1. Diffusional path length, which is typically the thickness and dispersion of the melt in the case of the liquid effectiveness factor (LFR), or it can be the particle size in the case of the gas effectiveness factor (RPS).
2. Intrinsic reaction kinetic constant, k.
3. The effective diffusion coefficient in the pores (RPS) or in the melt (LFR).
4. The reaction order in the case of higher n-th order reactions.
5. The Thiele modulus also depends on the shape of the pellet.

For a first order reaction for example

$$r' = kC_s \tag{35}$$

the Thiele modulus is given by

$$\phi = L\sqrt{\frac{k}{D_{eff}}} \tag{36}$$

The η vs ϕ relationship for various shapes, orders and volume changes during reaction is graphically represented in figure (10).

For a flat plate the relationship between the effectiveness factor and Thiele modulus is given by

$$\eta = \frac{\tanh \phi}{\phi} \tag{37}$$

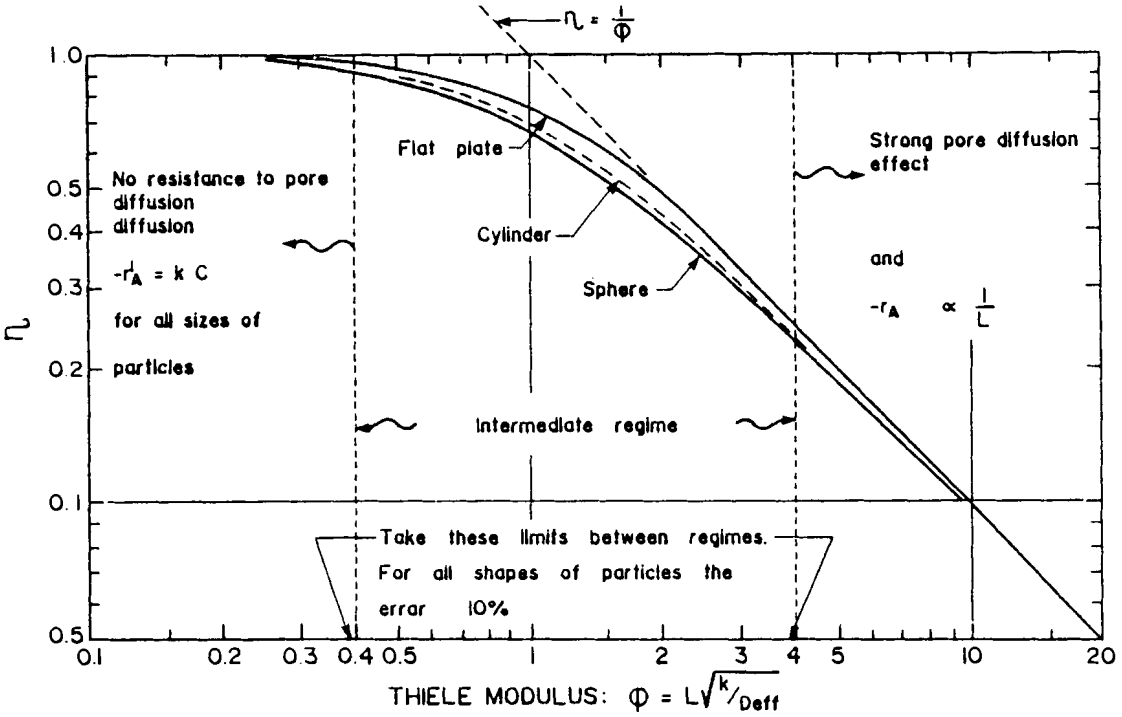

Figure 10. : The Thiele modulus versus effectiveness factor relationship for an isothermal pellet.

This flat plate expression is a good approximation for all particle shapes as seen in figure (10). From figure (10) it can be concluded that:

1. There is negligible diffusion resistance to reaction when

$$\phi < 0.4 \quad \text{or} \quad \eta \simeq 1$$

2. We have strong diffusion effects when

$$\phi > 4 \quad \text{and} \quad \eta \simeq 1/\phi.$$

The resistance due to diffusion does not act in series with the intrinsic reaction resistance and hence cannot be treated independently of it. The pore diffusion resistance can therefore only be accounted for by a separate, multiplicative correction term, η, to the kinetic equations. This is true; however η involves not only a diffusion term but also a surface reaction term in the form of the rate constant. Thus pore diffusion can never become controlling in the sense that it alone will determine the overall rate of reaction mechanism.

Numerous reports are available on this topic, see for example Aris (1975: vol 1 & 2).

2.7.2 Interphase transport

Urbanek & Trela (1980: 93) pointed out that although both the investigations on vanadium catalysts and the commercial process involve linear velocities varying over a broad range (0.05 to 1.5 m/s STP), little attention has been devoted to the effect of interphase mass and heat transport upon the catalyzed reaction. By virtue of the general laws at a given degree of conversion, this effect should be highest at a temperature closely approaching optimum, i.e., when the process rate attains a maximum.

This supposition was confirmed by the calculations, first performed by Boreskov (1970: 181), for commercial catalyst pellets and a linear velocity of 1.5 m/s (Re = 150). The interphase transport has been shown to reduce the process rate by 1 to 20% depending on the point in the conversion degree versus temperature diagram (figure 7). The difference between the turbulent stream temperature and the particle temperature (the particle was assumed to have an identical temperature at all points) did not exceed 11°C(T = 500 to 600°C).

Eklund (1956: 201) reported temperature differences between the turbulent stream and the exterior particle surface lower than 0.06°C at a temperature of 437°C (linear velocity of 0.27 m/s, STP, Re = 6.0). This agrees with the majority of workers who agree that interphase heat transport has no significant effect upon process rate. Experimental data obtained in mass and heat transport studies appear to be more reliable than calculated data.

Goldman **et al.** (1957: 274) were the first to point out that interphase mass transport has an effect upon the SO_2 oxidation rate in integral flow measurements. The more accurate data due to Schytil and Schwalb (1961: 367) show that, at a degree of conversion x = 85%, an increase in linear velocity from 0.3 to 0.6 m/s (STP) has no effect upon the process rate (

$r = 5 \times 10^{-6} moleSO_3/cm^2$ sec.). However, at x = 74% and $r = 1 \times 10^{-5} moleSO_3/cm^2$. sec, a similar increase in linear velocity has resulted in a change in r of about 10%. Urbanek (1980: 95) has found that, at $r = 0.5 \times 10^{-6}$ mole SO_3/cm^2 . sec and x = 80%, the effect of interphase transport becomes eliminated at a linear velocity as low as 0.05 m/s (STP.). At lower conversions, x = 20% to x = 50% ($0.5 \times 10^{-6} < r < 4 \times 10^{-6} moleSO_3/cm^2$. sec), and at temperatures usually applied in commercial catalyst reactors, the limiting linear velocity has been found to be 0.15 m/s (STP).

The experimental data of Schytil and Schwalb (1961: 367) are consistent with those of Urbanek. It is evident from their results that with more active catalysts (higher reaction rates per unit exterior particle surface area), the linear velocities required to eliminate the effect of interphase diffusion will be higher than the hitherto reported values established experimentally.

According to Urbanek & Trela (1980: 95) preliminary studies on local transport conditions outside the vanadium catalyst particle have shown that *particle shape and particle arrangement* in the bed have a significant effect upon process rate, primarily on account of the varying transport conditions outside the particle. This factor is of consequence for processes occurring within the particle and for the methodology of experimental determination of reaction rates in differential reactors.

2.7.3 Intrapellet transport

The ratio of internal to external surface area for commercial catalysts is typically 10^4. Therefore, the overwhelming portion of the active liquid phase is distributed within catalyst particles, and the reactants and the heat released are transported through the porous particle.

The existence of an optimal liquid loading for a given pore structure has been verified by Rony (1969: 142) and is explained by the gradual disappearance of the residual pore system (RPS) at high liquid loading. The existence of an optimal pore size is an important consequence of his liquid distribution model. Poor liquid dispersion (large δ) and therefore low catalyst activity result from large mean pore sizes. Below a given pore size, however, any further reduction of pore size to increase the local liquid effectiveness factor is overcompensated by an increasing Knudsen pore diffusion restriction in the RPS. Activity should be lower for very large and very small pore sizes. Livbjerg **et al.** (1974: 255) noted from experiments with three mean pore sizes that a shift from pore diffusion controlled reaction to liquid phase diffusion reaction is possible. For *optimal* liquid loading and pore size the diffusion resistance is almost evenly divided between liquid phase diffusion and pore diffusion. Hence the necessity of

including both factors in the SLP model is accentuated: The intrapellet effectiveness factor is divided into the liquid phase effectiveness factor and the residual gas filled pore effectiveness factor. These two intrapellet transport resistance are treated in the next two sections.

The mathematical model of Neth **et al.** (1980: 44) will be used to describe the transport restrictions in the LFR and RPS.

Unlike mass transport, heat transport within the particle has been consistently regarded as having a minor effect due to the relatively high effective thermal conductivity of the catalyst pellet.

$$\lambda_{eff} = 0.32 \text{ J/msK}$$

Fulton (1986: 118) also confirmed that there is no significant temperature gradient inside the sulphuric acid catalyst, even for reactor inlet conditions at which the gradient would be the largest.

2.7.4 Liquid phase effectiveness factor

The "cluster model" of Livbjerg **et al.** (1976: 216) appears to be the most suitable distribution model for the melt in the porous solid for the system under consideration. However any one of the liquid distribution models may be used in the effectiveness factor model presented by Neth (1980: 46). Thus δ may be calculated from equations (3), (4) and (5).

The reaction in the melt is assumed to be pseudo first order with respect to oxygen; the assumption being based on the relatively low solubility of oxygen compared to that of SO_2 and SO_3 in the melt. Provided the temperature gradient in the melt exerts no significant influence on the reaction rate, the Thiele modulus for a first order reaction can be applied, resulting in:

$$\phi_L = \delta \frac{\sqrt{k_L \omega_i H_{O_2}}}{D_{O_2,\,eff}} \tag{38}$$

and the liquid effectiveness factor η_L can be calculated from:

$$\eta_L = \frac{\tanh \phi_L}{\phi_L} \tag{39}$$

According to Neth (1980: 46) the effective diffusivity of oxygen in the melt is:

$$D_{O_2,\,eff} = \frac{D_{O_2} \Theta \alpha}{\tau_L} \tag{40}$$

where D_{O_2} is the diffusivity of oxygen in the unsupported melt and τ_L is the tortuosity factor. Using δ calculated from equations (3) or (4) or (5) and equations (38) and (40), the Thiele modulus can be written as:

$$\Phi_L = K_{EL}\sqrt{\frac{\alpha}{\Theta}}\sqrt{k_L \omega_I} \tag{41}$$

where K_{EL} can be expressed in an Arrhenius-type equation as:

$$K_{EL} = A_{EL}\, e^{B_{EL}/T} \tag{42}$$

A_{EL} and B_{EL} being defined by:

$$A_{EL}\, e^{B_{EL}/T} = s\sqrt{\frac{H_{O_2}\tau_L}{D_{O_2}}} \tag{43}$$

if the simplified liquid distribution model, equation (4) is used. The ratio α/Θ depends on the catalyst properties. The effective reaction rate per unit volume of melt is determined by:

$$r_L = r'_L \eta_L \tag{44}$$

and the reaction rate per unit volume of catalyst particles can be obtained by multiplying r_L by the density of the support ρ_{Tr}, the pore volume V_p and the liquid loading factor α:

$$r'_v = \rho_{Tr} V_p \alpha k_L P_{O_2} \omega_I \eta_L (1 - \xi^{1/S}) \tag{45}$$

2.7.5 Gas phase effectiveness factor

The model of Neth **et al.** (1980: 47) will be presented. It is known from experimental results that in the range of particle sizes used in industry, a considerable pore diffusion resistance has to be taken into account. To allow for this effect in a gas phase effectiveness factor η_G, the reaction rate according to equation (45) was considered to be the intrinsic rate occurring on the surface of the solid, comparable to the intrinsic rate in other heterogeneous gas-solid reaction systems.

This is in contrast to the model presented by Rony (1969: 142) who regarded the diffusion resistance in the gas phase as part of the total diffusion resistance in the gas and liquid phases, with respect to the reaction rate in the liquid phase. However, in the present work it has been assumed that the diffusion resistances in the liquid and gas phases can be calculated independently of each other. Whereas in the liquid phase the oxygen gradient is largest on account of the lower solubility of oxygen in the melt, the oxygen gradient in the gas

phase is assumed to be negligible, since in most practical cases, there is an excess of oxygen in the gas phase.

Based on this assumption, the rate equation, Equation (45) can be regarded as applying to a pseudo n-th order reaction with respect to SO_2 when the following assumptions are made:

a) $\omega_1\eta_L$ and $\omega_2\eta_L$ can be approximated by power functions of P_{SO_2}, and
b) The reversible nature of the reaction can be taken into account by replacing the actual partial pressure P_{SO_2} by the driving concentration difference:

$$P_{SO_2} - P_{SO_2,\,eq}$$

This is possible when

$$D_{SO_2} \simeq D_{SO_3}$$

which is nearly satisfied by

$$\frac{D_{SO_2,\,eff}}{D_{SO_3,\,eff}} = 0.9 \qquad \text{(Livbjerg } \textbf{et al.}\text{)},$$

When it is further assumed that:

c) The temperature gradient inside the catalyst pellet does not significantly affect the reaction rate, a general Thiele modulus can be employed for an n-th order reaction:

$$\phi_G = \sqrt{\frac{n+1}{2}}\,\frac{V_K}{F_K}\sqrt{\frac{k_n(C - C_{eq})^{n-1}}{D_{eff}}} \tag{46}$$

and the effectiveness factor η_G can be calculated from:

$$\eta_G = \frac{\tanh \phi_G}{\phi_G} \tag{47}$$

Finding approximate power functions of P_{SO_2} for $\omega_i\eta_L$, two limiting cases were considered

a) $\eta_L \simeq 1$: $\omega_i\eta_L \simeq \omega_i$,
b) $\eta_L < 0.4$: $\omega_i\eta_L \simeq \omega_i/\phi_L$

In case a), the following function for ω_1 was found:

$$\omega_1 \simeq 0.4(K_c)^{0.4}(1-U)^{(1+K_c)^{-0.25}}$$

which agrees fairly with the original function sufficiently, as seen in figure (11). A good approximation for ω_2 was:

$$\omega_2 \simeq (1-U)^{0.9}$$

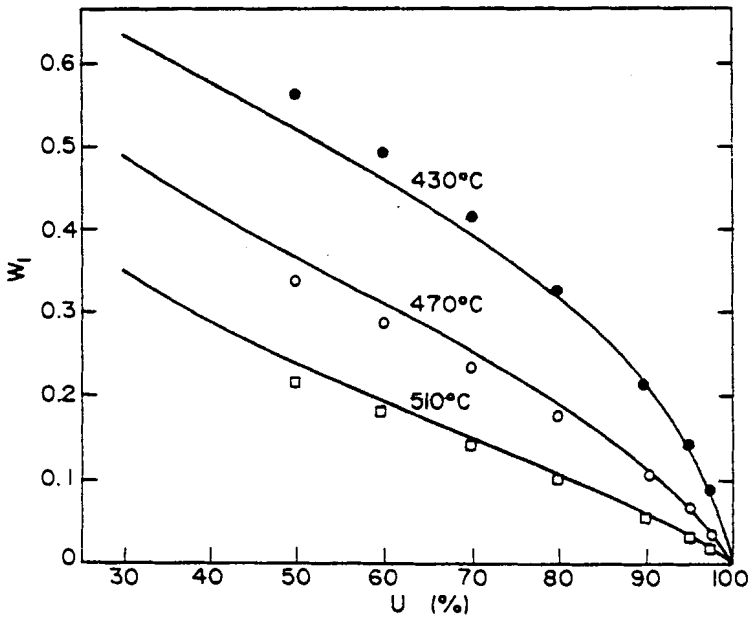

Figure 11. : Comparison between ω_1 (drawn out curves, Equation (31a) and the approximation according to Equation (48a) (points).

When $1-U$ is assumed to be approximately equal to

$$\frac{P_{SO_2}}{P^o_{SO_2}},$$

ω_1 and ω_2 can be expressed by:

$$\omega_1 \approx 0.4(K_c)^{0.4}(P_{SO_2}/P^o_{SO_2})^{(1+K_c)^{-0.25}} = a_1(P_{SO_2})^{n_1}, \tag{48a}$$

$$\omega_2 \approx (P_{SO_2}/P^o_{SO_2})^{0.9} = a_2(P_{SO_2})^{n_2} \tag{48b}$$

or in a general form by:

$$\omega_i \approx a_i(P_{SO_2})^{n_i} \tag{48c}$$

At 535°C, $n_1 = n_2 = 0.9$, and $\omega_1(U)$ is close to $\omega_2(U)/a_1$, as shown in figure (12) and mentioned in section 2.6.

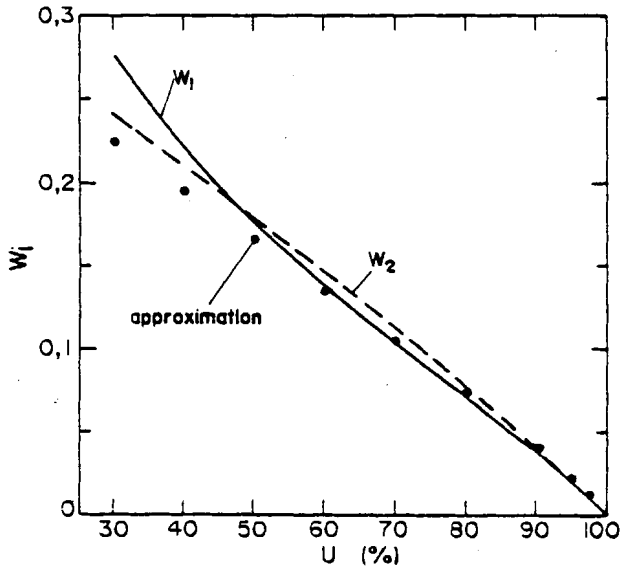

Figure 12. : Comparison between ω_1 (continuous line) and ω_2/a_1 (broken line) corresponding to Eqs.(31a) and (31b) at 535°C, where a_1 is defined by Eq.(48a). The points were calculated by Eq.(49a).

On substitution of P_{SO_2} by

$$\Delta P_{SO_2} = P_{SO_2} - P_{SO_2,\,eq},$$

it follows from:

$$\Delta P_{SO_2} = \frac{P^o_{SO_2}(1-U)}{1-0.5x^o_{SO_2}U} - \frac{P^o_{SO_2}(1-U_{eq})}{1-0.5x^o_{SO_2}U_{eq}},$$

using the approximation:

$$1-0.5x^o_{SO_2}U \simeq 1-0.5x^o_{SO_2}U_{eq},$$

that ΔP_{SO_2} can be written as:

$$\Delta P_{SO_2} \simeq P_{SO_2}\left(1-\frac{1-U_{eq}}{1-U}\right)$$

since ΔP_{SO_2} deviates significantly from P_{SO_2} only in the vicinity of equilibrium.

By defining U_{di} as:

$$U_{di} = 1 - \frac{1 - U_{eq.}}{1 - U}$$

ΔP_{SO_2} can ultimately be expressed by:

$$\Delta P_{SO_2} \simeq P_{SO_2} U_{di} \tag{49}$$

Taking into account Equation (48c), introduction of ΔP_{SO_2} into Equation (45) gives the intrinsic rate equation in the following form:

$$r'_v \simeq r_n = \rho_{Tr} V_p \alpha k_L P_{O_2} a_i (P_{SO_2} U_{di})^{n_i} \tag{50}$$

when $\eta_L \simeq 1$

In Equation (50), the product

$$\rho_{Tr} V_p \alpha K_L P_{O_2} a_i$$

is assumed to be constant inside the catalyst pellet and hence can be regarded as the rate constant of the pseudo n-th order reaction with respect to SO_2, the expression being comparable to k_n in the Thiele modulus (Equation (46)). Thus, when $\eta_L \simeq 1$, the Thiele modulus can be calculated by means of the following equation:

$$\phi_{G,a} = \frac{V_k}{F_K} \sqrt{\frac{n_i + 1}{2}} \sqrt{\frac{\rho_{Tr} V_p \alpha k_L P_{O_2} RT (U_{di})^{n_i - 1}}{D_{SO_2, eff} P_{SO_2}}} \tag{51}$$

where instead of $k_n(\Delta c)^{n-1}$ the term $r_n RT/\Delta P_{SO_2}$ is used. Moreover, in Equation (51), $a_i P_{Sb_2}^{n_i}$ is again expressed by ω_i, since in this case only the exponents n_i have to be taken from the approximations Equations (18a) and (18b), while the original equations (Equations (31a) and (31b)) can be employed for ω_i.

The effective diffusivity $D_{SO_2, eff}$ can be calculated from:

$$D_{SO_2, eff} = \frac{D_{SO_2} \Theta (1 - \alpha)}{\tau_G} \tag{52}$$

where D_{SO_2} is computed from the binary gas diffusivity $D_{SO_2, g}$, and the Knudsen diffusivity $D_{SO_2, K}$:

$$D_{SO_2} = \left(\frac{1}{D_{SO_2, g}} + \frac{1}{D_{SO_2, K}} \right)^{-1}$$

as well as from the tortuosity factor τ_G of the gas phase. $D_{SO_2,K}$ was obtained from:

$$D_{SO_2,K} = 9700\sqrt{\frac{T}{64}}\,r_p$$

and $D_{SO_2,g}$ from the equation which correlates the results of Livbjerg **et al.** (1976: 216) :

$$D_{SO_2,g} = 0.655\left(\frac{T}{758}\right)^{1.75}.$$

In accordance with the equation for the liquid phase Thiele modulus (Equation (41)), Equation (51) can be rearranged as follows:

$$\phi_{G,b} = A_{EG}\frac{V_k}{F_k}\sqrt{\frac{\alpha}{1-\alpha}}\sqrt{\frac{n_i+1}{2}} \times \times \frac{\sqrt{k_L P_{O_2}\omega_i T(U_{di})^{n_i-1}}}{D_{SO_2}P_{SO_2}} \tag{53}$$

where the coefficient $A_{EG} = \sqrt{R\tau_G}$ and a parameter $\frac{V_K}{F_K}\sqrt{\frac{\alpha}{(1-\alpha)}}$, depending on the catalyst properties, occur separately. The square root term in the catalyst parameter has been simplified by substituting

$$\rho_{Tr}V_p = \Theta.$$

For the limiting case $\eta_L \simeq \frac{1}{\phi_L}$, the procedure employed to obtain Equation (51) results in:

$$\phi_{G,b} = \phi_{G,a}\sqrt{\frac{n_i/2+1}{n_i+1}}\sqrt{\frac{1}{\phi_L}}(U_{di})^{-0.25}n_i \tag{54}$$

Here, the reaction order becomes $n_i/2$ since η_L is a function of $\sqrt{\omega_i}$.

For the intermediate regime ($1 < \eta_L < \frac{1}{\phi_L}$), ϕ_G was determined in the form of the weighted mean of $\phi_{G,a}$ and $\phi_{G,b}$ as a function of η_L. This method has no theoretical foundation and in fact, can only be checked, together with the other assumptions made previously, by numerical calculation, applying the method of orthogonal collocation.

The *mean* Thiele modulus was obtained from:

$$\phi_G = \phi_{G,b} + (\phi_{G,a} - \phi_{G,b})F_{EG} \tag{55}$$

where

$$F_{EG} = \eta_L^4 e^{\sqrt{1-\eta_L}}$$

which nearly satisfies the conditions:

$$F_{EG}(\eta_L \rightarrow 1) \simeq 1 \quad \text{and} \quad F_{EG}(\eta_L \rightarrow 0.4) \simeq 0.$$

The gas phase effectiveness factor η_G can be obtained using Equation (47), (51), (53) and (55) and the effective reaction rate in the catalyst pellet is given by:

$$r_v = \rho_{Tr} V_p \alpha k_L P_{O_2} \omega_i \eta_L \eta_G (1 - \xi^{1/S}) \tag{56}$$

2.7.6 Conclusions

The rate equation for the overall reaction, i.e. Equation (56), and the functions which are involved in the rate equation can be represented as shown in Table (8), where the parameters constituting the catalyst data are designated by z_1 to z_5. Table (7) lists these parameters which could almost completely characterize each type of catalyst.

Neth **et al.** (1980: 49), checked this model against experimental results obtained from three different catalysts. The following observations and ranges of coefficients can be extracted from his results:

- When the Mars & Maessen equation was used ($\omega_i = \omega_1$ and $n_i = n_1$) , a comparison between the calculated and the measured $r = f(U)$-profiles revealed the occurrence of a systematic error, whereas no such error was observed when the Boreskov equation ($\omega_i = \omega_2$ and $n_i = n_2$) was employed and, in addition, the mean error for the three catalysts tested by Neth **et al.** was found to be considerably smaller.

- A $K_{EL}(470°C) = 111$ and $\tau_G = 5.6$ were found to be suitable for all three catalysts tested by Neth **et al.** (1980: 49) provided that the different catalysts were chatacterized with enough accuracy by the parameters z_i.

- When adopting the same values for τ_L and D_{O_2}/H_{O_2} as used by Livbjerg **et al.** (1976: 216), i.e. $\tau_L = 2$ and $D_{O_2}/H_{O_2} = 2 \times 10^{-13}$, the coefficient s of Equation (5) resulted in $s = 3.51 \times 10^{-5}$ cm when $K_{EL}(470°C) = 111$ and the mean thickness δ was 1350Å when $\alpha = 0.385$.

- Compared to the mean pore radius of about 3300Å, of the catalyst tested the obtained mean thickness of the melt can be seen to agree with the *cluster model* rather than characterising thin layers of melt covering the pore walls.

- Due to the fact that the coefficient, s, in Equation (5) is affected by the nature of the rate equation applied to the reaction in the melt, the absolute value of s is still uncertain and

the difference in values compared to the results in Livbjerg **et al.** (1976: 216) can be explained by the use of different rate equations.

Table 7: Catalyst parameters

Type of Catalyst

	Type 1	Type 2	Type 3
α	0.385	0.380	0.253
c_v	0.288	0.354	0.293
$z_1 = \rho_{Tr} V_p \alpha$	0.206	0.208	0.147
$z_2 = C_v^2$	0.0829	0.125	0.0858
$z_3 = \sqrt{\alpha}/\Theta$	0.850	0.833	0.660
$z_4 = V_K/F_K\sqrt{\alpha/(1-\alpha)}$	7.12×10^{-2}	7.05×10^{-2}	4.13×10^{-2}
$z_5 = 9{,}700 r_p$	0.317	0.457	0.063

- The difference obtained in $K_{EL}(470°C)$ for different types of catalysts tested by Neth **et al.** (1980: 50) can be explained by the dependence of the mean melt thickness δ on the mean pore radius, as has also been found by Livbjerg. The melt is utilized to a greater extent in the case of larger catalyst pores for a certain liquid loading.

- The different values of τ_G remain within a narrow range and also appear to be slightly dependent on the pore radius ($4.0 < \tau_G < 6.0$).

- The evaluated apparent activation energy of about 105 kJ/mol is seen to be still in agreement with the value of about 84 kJ/mol given by Livbjerg **et al.** (1976: 216).

- The dependence of the rate constant

$$k_L = C_v^2 A_L e^{-B_L/T}$$

on C_v^2 was confirmed by Neth; comparing several runs in which C_v was changed. This is in line with the view that the Boreskov equation can be regarded as a modified Mars and Maessen equation, as discussed in section 2.6.

Table 8: Rate equations

$$r_v = z_1 k_L P_{O_2} \omega_i \eta_L \eta_G (1 - \xi^{1/S}),$$

$$k_L = z_2 A_L e^{-B_L/T},$$

$$\omega_1 = \frac{K_c q}{(1 + \sqrt{K_c}\, q)^2},$$

$$\omega_2 = \frac{1.25q}{1 + 1.25q},$$

$$q = \frac{P_{SO_2}}{P_{SO_3}}$$

$$\eta_L = \frac{\tanh \phi_L}{\phi_L}$$

$$\phi_L = z_3 K_{EL} \sqrt{k_L \omega_i},$$

$$\eta_G = \frac{\tanh \phi_G}{\phi_G}.$$

$$\phi_G = \phi_{G,b} + (\phi_{G,a} - \phi_{G,b}) \eta_L^4 e^{\sqrt{1-\eta_L}}.$$

$$\phi_{G,a} = A_{EG} z_4 \sqrt{\frac{n_i + 1}{2}} \sqrt{\frac{k_L P_{O_2} \omega_i T (U_{ab})^{n_i - 1}}{D_{SO_2} P_{SO_2}}},$$

$$\phi_{G,b} = \phi_{G,a} \sqrt{\frac{n_i/2 + 1}{n_i + 1}} \sqrt{\frac{1}{\phi_L}} (U_{ab})^{-0.25 n_i},$$

$$D_{SO_2} = (1/(0.655(T/758)^{1.75}) + 1/(z_5\sqrt{T/64}))^{-1},$$

$$n_1 = (1 + K_c)^{-0.25},$$

$$n_2 = 0.9,$$

$$U_{di} = 1 - \frac{1 - U_{eq}}{1 - U},$$

$$\xi = 1/(q\sqrt{P_{O_2}}\, K_p),$$

$$K_c = 2.3 \times 10^{-8} e^{13700/T},$$

$$K_p = 10^{(4956/T) - 4.678}$$

- For practical purposes the rate r_s, based on catalyst bed volume, is more informative than the rate r_v, based on the pellet volume; r_s can be obtained from r_v on multiplication by $\frac{\rho_s}{\rho_k}$.

- In industrial catalysts α is in the range of about 0.3 to 0.4. At temperatures from just under 500°C, the above range can be regarded as practically optimal, while at lower

temperatures an increased liquid loading can improve the catalyst activity. This is confirmed by practical experience in as far as, during the past few years, the application of higher liquid loadings has allowed the ignition temperature to be lowered and the catalyst activity to be improved at lower temperatures (Neth **et al.**, 1980: 52).

- The different types of catalyst could be almost completely characterized in the rate equation by means of the parameters z_i consisting of the catalyst data.

Finally it can be concluded from the results of Neth **et al.** that this rate equation is suitable for the interpretation of measured reaction rates obtained with industrial catalysts.

2.8 CATALYST DEACTIVATION

Relative to other catalytic materials, vanadia catalysts exhibit remarkably long lifetimes. Some installations have operated on the same catalyst load for a decade. Catalyst activity changes little over periods of years and it appears that it is mechanical deterioration of the catalyst that eventually leads to its replacement (Tamura **et al.**, 1975: 122).

2.8.1 General considerations

Donovan **et al.** (1983: 271) reported that the catalyst life can be shortened significantly whenever the catalyst is misused either during storage or in use. Water vapour is the biggest problem during storage. The free SO_3 absorbed in the melt may be hydrated to sulfuric acid in the presence of moisture. This in turn forms brown or reddish crystals at the pellet surface that can cause local decrepitation and material losses during handelling (Donovan, 1983: 271). In addition, water will also be absorbed by the hygroscopic active constituents, and this will impair the mechanical strength of the pellets (Sander, 1981: 286).

The average service life usually quoted by catalyst producers is about ten years, but the catalyst's performance gradually deteriorates in high temperature or dusty operating locations. Catalyst life is generally considered long when compared with other catalysts, although there are significant differences in aging behaviour and life between different commercial catalysts.

The dust accumulating on the catalyst eventually increases the gas pressure drop through the catalyst bed and will consequently reduce the gas throughput as well as decrease the SO_2 conversion efficiency. The general practice is to screen the catalyst annually (the first pass is

always screened plus, occasionally, one of the other passes on a rotating basis) to remove most of the dust and scale on the catalyst. The volume of material lost during screening is replaced with fresh catalyst which is always placed at the top layer because its ignition temperature is lowest when new.

Donovan (1983: 272) classified the deactivation process of the catalyst in three mechanisms that acted simultaneously:

1. Thermal deactivation,
2. Mechanical deactivation,
3. Chemical deactivation.

2.8.2 Thermal deactivation

The upper operating temperature limit is usually determined by the thermal stability of the catalyst. Above 600 – 650°C, catalyst activity may be lost irreversibly because of damage to the structure of the carrier and reduction of its internal surface area.

Donovan (1983: 272) observed that at high temperatures, fine globules of silica appear to be dissolved in the melt. As a result, the thickness of the melt film increases and possibly blocks part of the pore structure. The role of silicon dioxide is not fully understood because it can reportedly react with vanadium species to form vanadium silicate ($V_2Si_2O_7$), which in turn can react with the active constituents in the melt (Glueck, 1968: 1257). Thermal deactivation is also dependant on the expertise of the catalyst manufacturer and the choice of the support material. Poor quality support material may sinter at operating temperatures, closes the smallest pores first, resulting in a reduction of the total surface area. The reduction in surface area is correlated with a reduction in catalyst activity (Donovan **et al.**, 1983: 272).

According to Donovan, high temperatures can also cause phase transitions of the silica support. These transitions may cause softening of the catalyst matrix via expansion or contraction. Most workers who studied the ageing process reported a gradual transformation of SiO_2 to α -cristobalite. The increase in crystallinity was found to be proportional to the time of industrial use. Because cristobalite forms at a lower temperature in the presence of vanadium compared with SiO_2 alone, suggests that a chemical interaction of SiO_2 occurs with the molten salt (Donovan **et al.**, 1983: 273). It was reported that the crystalline transition is accelerated by higher temperature, but is reduced with increasing K / V ratio and increasing concentration of SO_3 in the gas. Donovan noted that because some samples contained

α-cristobalite and still had high thermal stability, it can be concluded that the role of phase conversion in the support may not be critical in the ageing process.

Catalysts activated by sodium are apparently thermally less stable than catalysts activated by potassium. Donovan also concluded that the main cause of thermal deactivation in catalysts promoted by potassium is a combination of potassium and V_2O_5 with SiO_2 and as a result, formation of an inert vanadium phase.

Thermal deactivation generally proceeds rather slowly, and it has been found by plant experience that good quality catalysts can be exposed to abnormally high temperatures ($700 - 800°C$) for short periods of time without causing drastic deactivation (Donovan **et al.**, 1983: 273).

2.8.3 Mechanical deactivation

The most common source of mechanical deactivation is attrition losses in the catalyst bed due to vibration between the layers of catalyst. Attrition losses and crushing of pellets during the regular screening intervals can also be responsible for as much as $\pm$ 5% screening losses for hand screening methods and $\pm$ 10% losses using pneumatic screening equipment.

Dust accumulation also mechanically deactivate the pellet by plugging the voids between catalyst pellets to differing degrees and thus partially isolates the pellets from the reactants. The molten salts in the catalyst can also migrate into the dust (depending mainly on the dust particle size distribution), which causes an overall loss of vanadium salts from the catalyst (Donovan **et al.**, 1983: 274).

2.8.4 Chemical deactivation

A number of substances react chemically with the catalyst either to reduce activity, cause gradual losses of vanadium, or alter pellet physical strength. Even the major reactant SO_2, causes some loss of activity when present in high concentrations at low temperatures (Donovan **et al.**, 1983: 274). However, this decrease in activity is limited in extent and is reversible; full activity is restored by exposing the catalyst to relatively high oxygen (or $SO_3 + O_2$) concentrations and/or raising its temperature.

Most of the information to quantify the effects of various poisons has been obtained from plant experience and for this reason the available information in many cases is only semiquantitative.

Arsenic is probably the most feared catalyst poison in sulphuric acid plants. Other undesirable contaminants include carbon monoxide, fluorides, lead, mercury and selenium, however small amounts can be tolerated.

Table (9), derived from Donovan **et al.** (1983: 275) outlines the effects of contaminants in feed gases on the catalyst.

Table 9 Effect of contaminants in feed gases on the catalyst

Contaminant	**Effect on vanadium catalysts**
H_2O	Does not have an effect at temperatures above typical dew points for sulfuric acid (150 – 200°C). At lower temperatures, there may be degradation of the catalyst with loss of activity and mechanical strength, depending on the extent of condensation. Catalyst can usually be regenerated by careful heating.
As_2O_3	At temperatures significantly below 600°C, the catalyst is saturated with arsenic and a reduced plateau of catalytic activity is reached, which apparently does not change appreciably with further exposure. The decrease of activity appears to be connected with blocking of the catalyst surface by arsenic trioxide (As_2O_3). At temperatures near 600°C the volatile compound $V_2O_3.As_2O_3$ can be formed, and some long-term loss of activity may be noted because of vanadium losses.
AsH_3	Because of its easy oxidizability it has the same effect as As_2O_3.
Se	Harmful effect only at temperatures below 400°C; initial activity is restored after heating.
C_nH_m (hydrocarbons)	Harmless in small concentrations. In individual cases there has been catalyst activity loss as a result of surface deposition of carbon formed by incomplete oxidation of hydrocarbons. The amount of carbon produced is dependent on properties and concentration of the hydrocarbon, the concentration of oxygen, and temperature. In large amounts, heat release from oxidation can be a serious problem.
SiF_4, HF	Sharply reduces activity, but extremely low levels act relatively slowly. HF reacts with silica supports forming volatile SiF_4, and

	deposition of silica gel on the catalyst surface has also been noted.
$FeSO_4$	Mechanically covers the surface of the catalyst and causes a loss of activity and pressure drop increase. When catalyst beds contaminated with iron are observed in a cold condition, hard crusts between pellets are noted. The crusts contain appreciable potassium plus vanadium and it is evident that substantial migration of molten-salt actives occurs.
S, CS_2, H_2S	Are not objectionable in small amounts if there is sufficient oxygen to permit oxidation. Large amounts can produce harmful heat release or block the catalyst surface with sulfur deposits.
H_2	May cause loss of catalyst activity by reducing vanadium pentoxide to a lower oxidation state. Heat release may be a problem.
NH_3	Harmless in reasonable quantities. Can be oxidized with objectionable heat release when present in large amounts.
NO, CO_2	Are not objectionable at reasonably low concentrations. (Note that NO may be troublesome in acid plants because it can contaminate product acids and/or cause formation of submicrometer acidic mists.)
CO	According to most workers, does not harm catalyst, but in the presence of large quantities of CO it is theoretically possible for the reaction to be inhibited owing to reduction of SO_3. $SO_3 + CO \rightleftarrows SO_2 + CO_2$. Heat release from oxidation can be troublesome and there is some evidence of vanadium reduction at low temperatures (below approximately 450 to 475°C) .
Cl_2, HCl	Do not cause significant problems in low concentrations. If there is extended exposure, losses of vanadium from the catalyst occur as a result of volatile $VOCl_3$ formation.
Pb, Hg	Information is limited, but analyses of spent catalysts from a number of acid plants indicate that compounds of these elements are readily deposited from very low concentrations in gases. Significant catalyst activity loss then occurs. Where elemental mercury is present in small concentrations, its volatility is apparently sufficient to prevent deposition on catalyst at operating temperatures.

2.9 CATALYST SHAPE AND PRESSURE DROP

Pressure drop in sulphuric acid plants is becoming an increasingly important consideration, not only because efforts are being made to save energy, but also because it affects the sizing of equipment items in the plant. The pressure drop occurs mostly in the catalyst beds of the converter, and it increases during operation as dust from the feed gas accumulates in the first bed. Catalyst manufacturers are therefore faced with the problem of designing a catalyst shape or form which not only presents a low resistance to gas flow, but can also absorb the largest possible amount of dust for the minimum pressure drop without compromising on any of the other attributes - activity, abrasion resistance, crush strength and fabrication cost.

2.9.1 Economic implications

Gas pressure drop across the multiple catalyst beds in a sulphuric acid plant represents between one-quarter and one-third of the total resistance to gas flow under clean plant conditions (Donovan **et al.**, 1977: 46).

The power consumed in circulating the gas is dependent on the resistance to flow. Based on empirical information of Donovan, a typical acid plant centrifugal compressor consumes 1.08 kw of electricity per 10 000 m^3/h gas circulated for each 25 mm H_2O pressure drop across the bed. For a 1000 t.p.d. sulphuric acid plant operating on 7.5% sulphur dioxide pyrite rooster gas with a 98% conversion efficiency, each 25mm H_2O increase in pressure drop consumes 335 kWh/day. Assuming an electricity price of R0,064/kWh and a plant on-stream factor of 90%, the extra cost is about R7830/year/25mm H_2O. Therefore, it is important to lower the pressure drop to reduce costs and conserve energy.

Dust accumulation on the catalyst causes a gradual increase in pressure drop and the additional costs and limitations on blower capacity makes it necessary to clean the catalyst from time to time. Plant downtime and handling cost for the cleaning operation and the make-up of about 10% to compensate for screening costs also contribute to the running costs of the plant.

2.9.2 Effects of size and shape

A catalyst pellet shape and dimensions should promote catalytic activity, strengthen the pellet's resistance to crushing and abrasion, minimize bed pressure drop, lessen fabrication cost, and distribute dust buildup uniformly. Unfortunately, these objectives are not easily achieved. Indeed, several are mutually exclusive. For example, a smaller size will enhance activity but also increase bed pressure drop (Fulton, 1986: 97).

The greater activity found with smaller particle sizes is due to the more favourable ratio of the geometric surface to the volume, which, by allowing better access, makes more efficient use of the active mass. In principle, this advantage can be maintained at a lower pressure drop when some more exotic shapes or profiles for the catalyst particles are chosen. But the need for high mechanical strength to withstand the repeated unloading, screening and reloading operations does not favour this approach. Carefully planned shapes can alter the nature of fines deposition in the reactive bed and the voids can influence dust distribution and the eventual screening frequency. Shapes can also influence heat transfer characteristics (Donovan, 1977: 46).

The hollow cylinder requires the least amount of material, affords the maximum strength and abrasion resistance and is easily extruded. Therefore an obvious choice of pellet shape is the hollow cylinder (Fulton, 1986: 98). Hollow cylinder catalysts are widely employed; as well as improving pressure drop characteristics, such catalysts offer improved tolerance to dust.

Although some shapes appear attractive from the point of view of initial pressure drop or dirt holding, there are some potential long-term problems which must be investigated in depth before any can be recommended (Donovan, 1978: 39).

- Will interior orifices or pockets become coated or plugged with dust which cannot be removed by normal catalyst screening procedures? This is a critical question for ring or dimpled pellet shapes.

- Will reduced physical strength, in comparison with solid cylinders of the same composition, result in increased attrition or crushing losses? Here again, hollow rings or ribbed shapes face a major test.

- Will increased surface and reduced solids volume result in accelerated depletion of the active molten salt through migration into surface dust and thus reduce the catalyst life?

- At what point will dust cease to be collected in the first catalyst pass and start to foul the second catalyst pass, requiring two passes to be screened instead of one and thus extending shutdowns and making them more expensive?

2.9.3 Origin and effect of dust

The alkali-promoted catalyst acts as a very effective dust filter owing to the "fly paper" effect of the vanadium pyrosulphate melt. The chemical composition of each catalyst affects its "stickiness" and may be almost as important a variable as pellet shape and size (Donovan, 1978: 40). The general trend appears to be that catalytic activity and "stickiness" for dust vary together; more active catalysts have a greater tendency to pick up dust. This raises the question: What is the optimum economic balance between catalyst activity, pressure drop and dirt holding capacity?

Chemical analysis of the dust usually reveals Fe, Zn, Cu and Si and may give an indication of the origin of the dust. Donovan observed that iron compounds appear to promote catalyst crusting or caking.

The active molten salt can migrate from the support material to the dust layer by capillary action. This migration depends on surface tension, as well as on the relative sizes of particles and pores in the pelleted catalyst support and in adjacent dust. This migration action will drain the support from active material and will deactivate the catalyst (Donovan, 1978: 40).

The sensitivity to plugging and pressure drop build-up in a catalyst bed by dust-loaded gas depends on the bed void fraction, ε, and how the dust is distributed (Schoubye, 1978: 34). Pressure buildup rates can be greatly reduced by larger pellets with more uniform dust distribution (figure 13).

When using a 6mm diameter pellet, a large fraction of the dirt in the gas is deposited in the first few inches at the top of the bed. Donovan (1977: 49) reported that the top 20% of a bed containing 6mm diameter catalyst collected 62% of the dirt; this forms a barrier which rapidly causes an increase in pressure drop. In a bed with 8mm diameter catalyst, the dirt is distributed more uniformly and the top 20% of this bed collected only 28% of the dirt, consequently the pressure drop increased at a proportionately lower rate, which means that the amount of dirt that can be deposited in the bed before the pressure drop becomes intolerable, is greater. With the larger pellet it is important that a good balance between dirt holding and filtering ability is achieved; in other words the dirt must move farther into the bed without passing through it to any great extent (Donovan, 1977: 49).

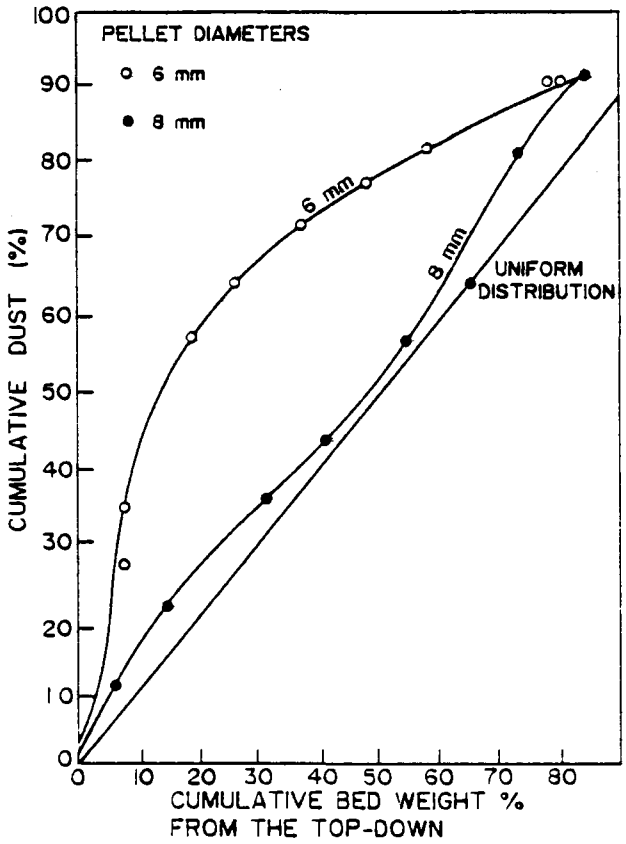

Figure 13. : Comparison of dust distribution in 6 and 8mm diameter catalyst located in first-pass after 12 months service.

Based on the initial results of Donovan, it is estimated that a bed of 8mm catalyst would be in service 50% longer than a bed of 6mm catalyst before screening is required, which would reduce the annual screening costs proportionately. Alternatively, if the catalyst is screened each year, the pressure drop will be reduced significantly (figure 14), thus reducing energy consumption or allowing a greater production rate.

2.9.4 Pressure drop correlations

Before the Ergun correlation for pressure drop through fixed beds of uniformly sized solids will be presented a few shape and size related parameters must first be defined.

For non-spherical particles, the effective diameter, d_p, may be defined as:

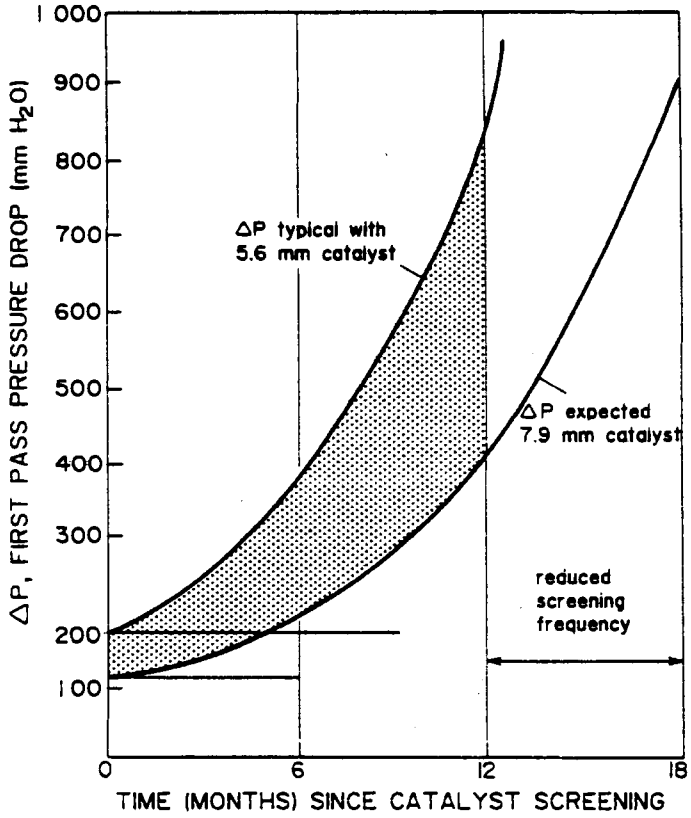

Figure 14. : Relation of rate of increase in pressure drop to catalyst particle and screening frequency.

$$d_p = \left(\begin{array}{l} \text{diameter of sphere} \\ \text{having the volume} \\ \text{of the particle} \end{array} \right) \tag{57}$$

A variety of measures of non-sphericity can be used for non-spherical particles; however, for our purpose the following is most useful (Kunii, 1977: 64). We define sphericity ϕ_s as:

$$\phi_s = \left(\frac{\text{surface of sphere}}{\text{surface of particle}} \right)_{\text{both of same volume}} \tag{58}$$

With this definition, $\phi_s = 1$ for spheres, and $0 < \phi_s < 1$ for all other particle shapes.

According to Kunii the fraction voids, ε, in a packed bed are related to the sphericity of the particles, as shown in figure (15).

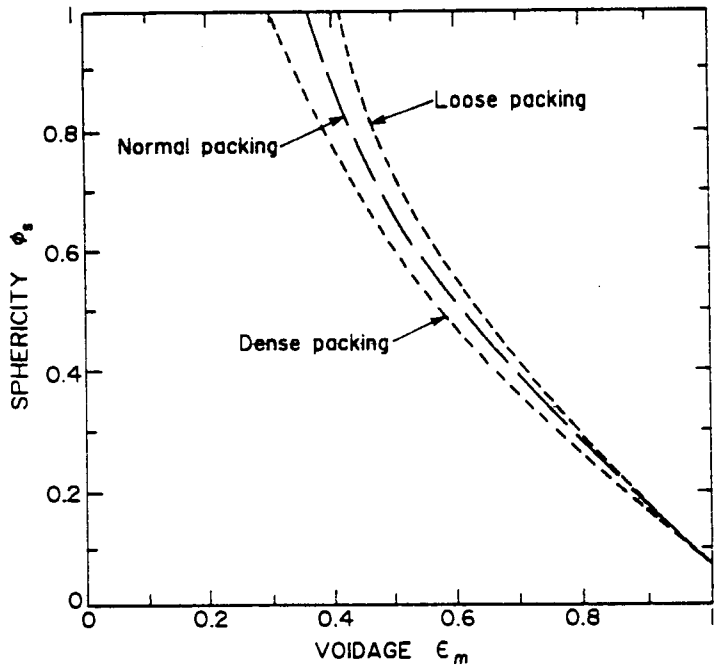

Figure 15. : Voidage in uniformly sized, randomly packed beds.

The pressure drop through a packed bed of pellets can be correlated by the Ergun equation:

$$\frac{\Delta P}{L} g_c = 150 \frac{(1-\varepsilon)^2}{\varepsilon^3} \frac{\mu u_o}{(\phi_s d_p)^2} + 1.75 \frac{1-\varepsilon}{\varepsilon^3} \frac{\rho_g u_o^2}{\phi_s d_p} \tag{59}$$

For a randomly packed beds this expression is expected to represent the data within $\pm$ 25%, however it may not be expected to extend to beds of solids of abnormal void content.

The pressure drop in Equation (59) represents two factors, the viscous and the kinetic energy losses. The viscous losses predominate at low Reynolds numbers and Equation (59) simplifies to:

$$\frac{\Delta P}{L} g_c = 150 \frac{(1-\varepsilon)^2}{\varepsilon^3} \frac{\mu u_o}{(\phi_s d_p)^2}$$

$$Re_p = \frac{d_p \rho_g u_o}{\mu} < 20 \tag{60}$$

Only the kinetic energy losses need be considered at high Reynolds numbers; thus Equation (59) simplifies to:

$$\frac{\Delta P}{L} g_c = 1.75 \frac{1-\varepsilon}{\varepsilon^3} \frac{\rho_g u_o^2}{\phi_s d_p} \qquad Re_p > 1000. \tag{61}$$

Both terms must be used in the intermediate region.

Figure (16), extracted from Schoubye (1978: 35) shows calculated pressure drops across a typical first bed of a sulphuric acid converter operating on dust-loaded feed gas at a linear velocity of 1600 m^3 feed gas per hour per m^2 bed cross section.

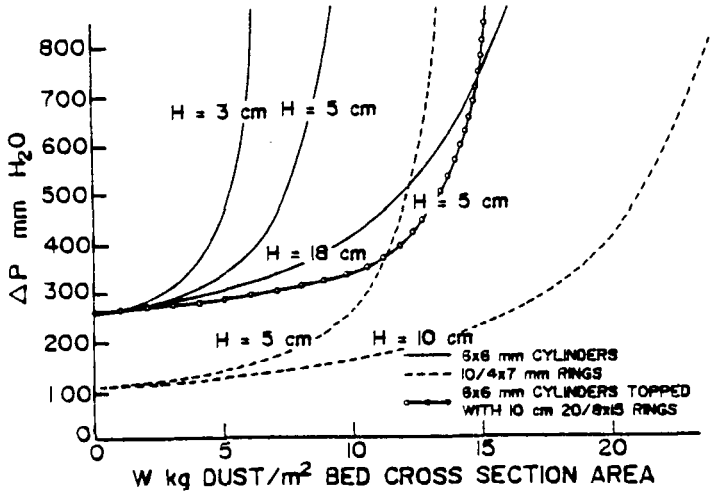

Figure 16. : Calculated pressure drop across the first bed according to dust loading.

The bed height is taken as 0.5m; the inlet and outlet temperatures are 410°C and 600°C respectively.

The curves are based on the assumption that the total amount of dust accumulated in kg/m^2 of bed cross section, ω, is evenly distributed over a certain height, H, measured from the top of the bed. The bulk density of the dust is taken as $800kg/m^3$, so that ω kg dust/m^2 distributed evenly in a layer of H meters thickness will reduce the void fraction from ε_o in the clean catalyst to (Schoubye, 1978: 35)

$$\varepsilon = \varepsilon_o - \frac{\omega}{800} H \tag{62}$$

ε_o is 0.35 - 0.4 in beds of cylinders or spheres. For the $6 \times 6mm$ cylinders $\varepsilon_o = 0.36$, for $10/4 \times 7mm$ rings $\varepsilon_o \leq 0.46$ and for the 20mm rings $\varepsilon_o = 0.50$.

The decrease in void fraction in the top layer of the catalyst bed can be calculated by substituting ε in the Ergun correlation (Equation (3)).

These calculations of Schoubye (1978: 35) reproduce typical accelerating pressure drop curves found in practice and may be used to evaluate catalyst shapes relative to each other.

2.10 MAKING THE CATALYST

SO_2 oxidation catalysts are chiefly produced by one of three general techniques:

- mixing
- impregnation
- precipitation (not common)

All three processes are similar, the major differences being in the order in which the manufacturing steps are conducted. The unit operations involved include solution mixing, solids blending, precipitation, impregnation, washing, filtration, drying, calcination, tableting, extrusion and sizing.

2.10.1 The mixing process

The components are mixed either in liquid or solid state (or a combination) to form a "paste-like" mass. When the active ingredients are added to the mix it becomes a complex physical system whose behaviour depends on composition, handling and time. Controlling this to give a consistent product is important.

Sodium or potassium silicate or colloidal silica is frequently added as a binder to increase the mechanical strength of the pellets. Raw materials generally include V_2O_5 or another vanadium salt (NH_4VO_3 or $VOSO_4$) and potassium (and sodium) as hydroxides, carbonates, or sulphates (Donovan, 1983: 259).

When the catalyst salts are in solution, capillary forces of several hundred bar (depending on the pore sizes) will draw the solution into the pores of the support particles. At this point, the catalyst salts may be precipitated (Fulton, 1986: 59).

Pellets of desired sizes and shapes are then formed by extrusion at ambient temperature. Gum Arabic is often added to the mix as an extrusion lubricant and to increase the void

fraction after activation. Other methods of compacting powders or pastes such as disk granulators or tablet machines have been used.

Figure (17) (Fulton, 1986:59) shows how the pressure applied to form the pellet affects pore-size distribution

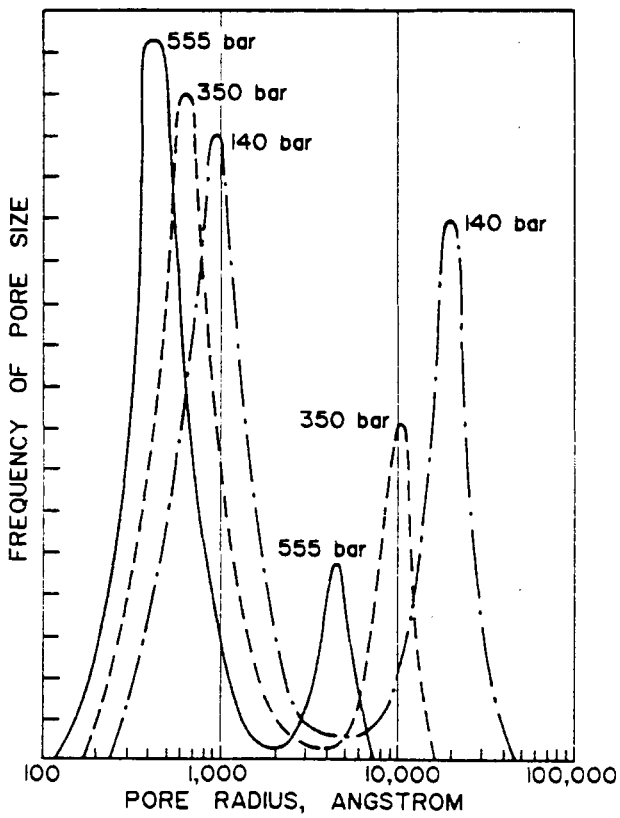

Figure 17. : The pressure applied in forming the catalyst pellet will affect its pore-size distribution.

Due to their high production costs the other processes such as the impregnation and precipitation processes are not frequently used.

2.10.2 Drying operations

The method of drying pellets during manufacture can strongly influence the performance of a catalyst in the plant reactor (Fulton, 1986: 60). In general, drying at lower temperatures and higher humidities produces the best catalyst. These conditions, however, require excessively long drying times and large, expensive dryers. Some strategy, therefore, must be sought to

attain the best catalyst at reasonable cost - i.e., to optimize the dryer design and operating conditions of a new dryer, or to redesign and modify the operating conditions of an existing dryer.

The phenomena involved in drying can be characterized by figure (18).

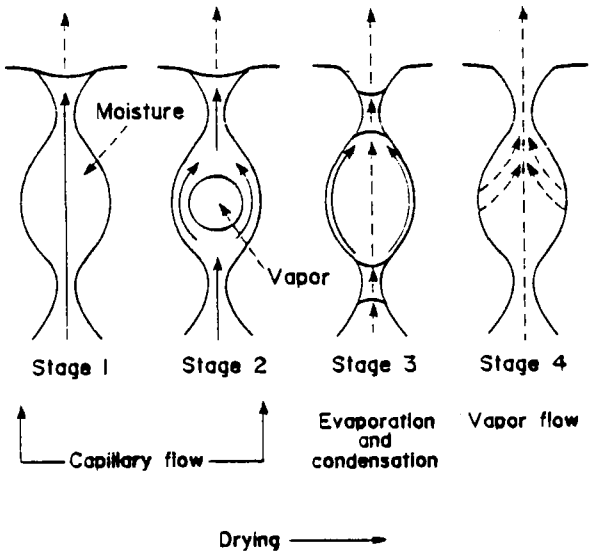

Figure 18. : The removal of moisture within a pellet pore during drying operation occurs in four primary stages.

Initially, the porous material is saturated with liquid so that a thin film covers the external surface. Drying first evaporates the surface liquid (Stage 1), then the liquid in the pores. Vapor generated in the pores forces the evaporating liquid out (Stage 2). If the drying rate is excessive vapor will be generated faster within the pellets than moisture can be forced out of the pores, and the catalyst pellets will break, or in more moderate conditions damage internally. Internally damaged pellets will crush easily in service. As drying continues, the free liquid in the pores will vaporize, and only adsorbed and bound water will remain in the pores (Stage 3). This water will ultimately be removed by drying to the desired final moisture level (Stage 4).

2.10.3 Activation

After drying the catalyst is activated (calcined) in a SO_2 or SO_3 air mixture to convert the alkali materials into pyrosulfates while simultaneously increasing the mechanical strength substantially by the process of sintering. The following reaction is the most important reaction during activation:

$$K_2SO_4 + SO_3 \rightleftarrows K_2S_2O_7$$

$$\Delta H°(298°C) = -159kJ/mole$$

This reaction releases a lot of heat and good temperature control is necessary (Fulton, 1986: 63). The catalyst's chemical and physical properties are affected by the activation conditions. Not only the pore size but also pore-size distribution can be changed by the calcination and/or activation temperature. In figure (19), the mean pore diameter of the macro pores was not changed, but the diameter of the micropores was altered by an order of magnitude after activation (Fulton, 1986: 63). This, in turn, reduced the total pore volume and surface area for reaction by an order of magnitude.

Activation needs to be carefully defined and controlled, and it influences the catalyst in the following ways:

- It removes the lubricants, binding agents and other materials not wanted in the finished catalyst.
- It results in a small amount of sintering, which increases the strength of the catalyst (too much sintering would degrade the pore volume).
- It converts the alkali metal oxides and sulfates to pyrosulfates, and thus lowers the initial **activation temperature** while increasing the activity.

In conclusion, the final properties are sensitive to the preparative procedure.

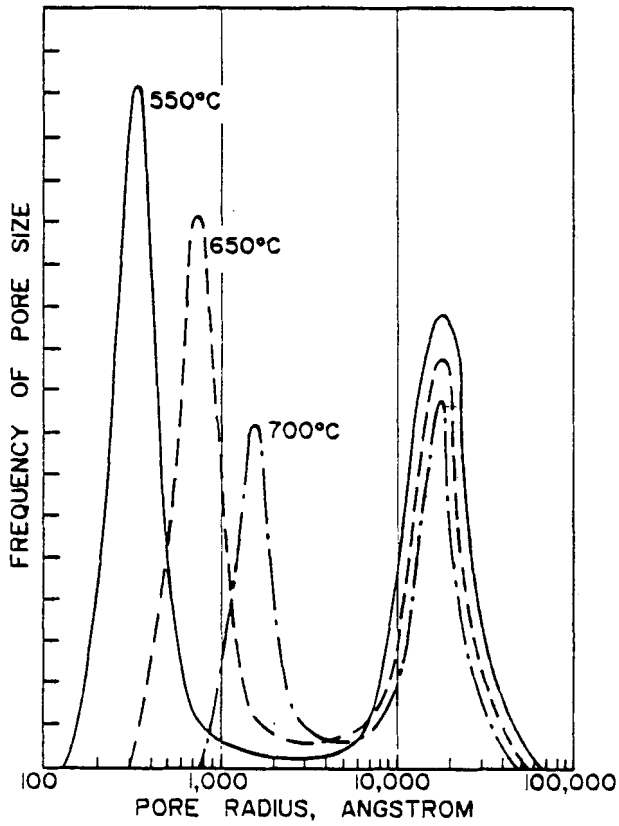

Figure 19. : A catalyst pellet's pore size and pore size distribution can be changed by the temperature of activation.

CHAPTER 3

EXPERIMENTAL APPARATUS, PROCEDURE AND STRATEGY

3.1 EXPERIMENTAL DESIGN AND STRATEGY

In the design of sulphur dioxide oxidation catalysts, the primary objectives are catalytic activity, stability and pressure drop during plant operating conditions. Pivotal to laboratory scale investigations that are aimed at achieving the necessary catalyst design are: intrinsic reaction limitations, mass transfer effects as affected by interparticle- and intraparticle diffusion, pressure drop and both chemical and mechanical stability. The physical and chemical factors are interrelated as given in the following diagram (figure 20).

To ensure statistical validity of experimental data, the design of experiments was based on two-level, full factorial matrices, with two compositional and/or configurational variables, the rest being kept constant. The compositional, configuration and operating ranges were selected in such a way that the overlapping matrices containing the variables could be optimised. To analyse the results of these experiments multiple regression procedures were used to quantify the relationships between variables.

3.1.1 Subdivision of Experiments

The experimental outlay is given in figure (21). The objectives were to

- Optimise the experimental conditions to extract intrinsic rates from the data;
- Quantify the effect of catalyst composition on reaction rates;
- Determine the effect of mass transfer on kinetics;
- Evaluate particle geometry effects on global reaction rates and
- Define the physical parameters that influence pressure drop, mechanical strength, porosity and surface area.

1) Time to reach steady state conditions:

2) Space velocity:

Composition

1) Different M & M2O/V2O5 mole ratio's:

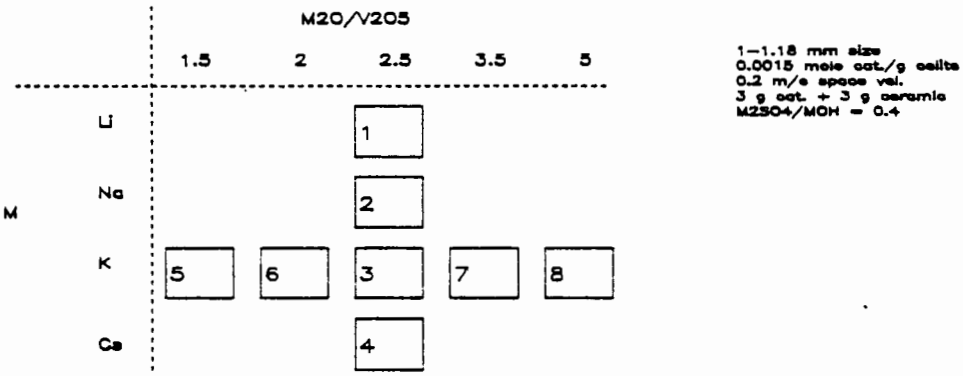

2) Different Na/K & M2O/V2O5 mole ratio's:

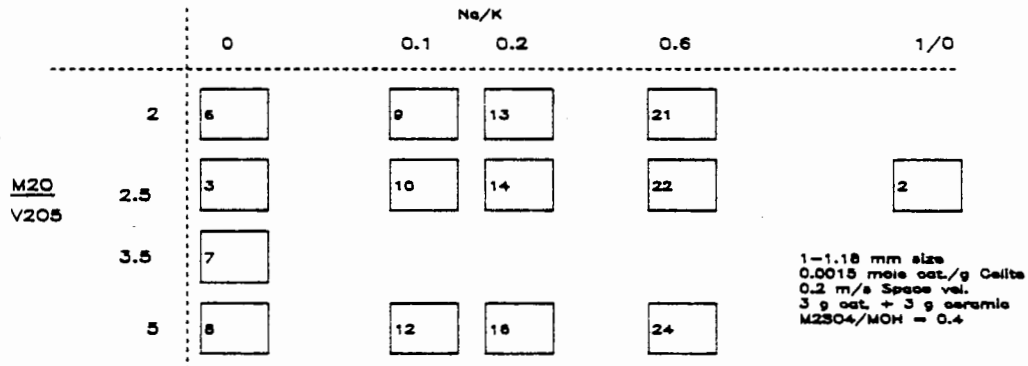

3) Different M2SO4/MOH mole ratio's:

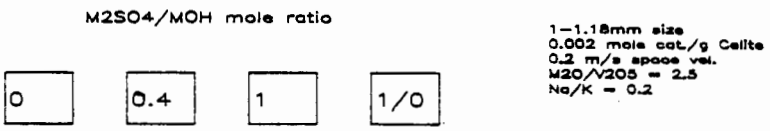

Figure 20. : Catalyst compositional variations to evaluate kinetic effects on SO_2 oxidation. A square represents 5 experimental runs at different temperature levels.

Mass transport experiments

1) Different liquid loadings:

mole catalyst / g Celite

0.0005	0.001	0.0015	0.002	0.004	0.008	0.01

1–1.18 mm size
0.2 m/s space vel.
3g cat. + 3g ceramic
Na/K = 0.2
M2O/V2O5 = 2.5
M2SO4/MOH = 0.4

2) Liquid loadings, effect on gas diffusion:

mole cat./ g Celite

0.0005	0.001	0.0015	0.002	0.004	0.008	0.01

6 mm extrudates
0.2 m/s space vel.
+— 20 g catalyst, no diluting
Na/K = 0.2
M2O/V2O5 = 2.5
M2SO4/MOH = 0.4

3) Different pellet geometry:

S1	S4	S7	S10
S2	S5	S8	S11
S3	S6	S9	S12

0.2 m/s space vel.
LB formulation
+— 20 g catalyst

Physical & Mechanical

1) Pressure drop experiments:

All shapes
Room temperature
Linear superficial vel.= 0.05–0.8 m/s
Void fraction, bulk dencity, equil. length ect.

2) Mechanical crush strenght:

Effect of MOH on crush strength
Effect of catalyst shape on crush strength
Effect of temperature on the catalyst crush st.

3) Attrition resistance:

Effect of geometry on attrition

4) Surface area & porosity:

Effect of liquid loading on surface area
Effect of liquid loading on pore volume
Effect of liquid loading on porosity
EDAX scans & electron microscope studies

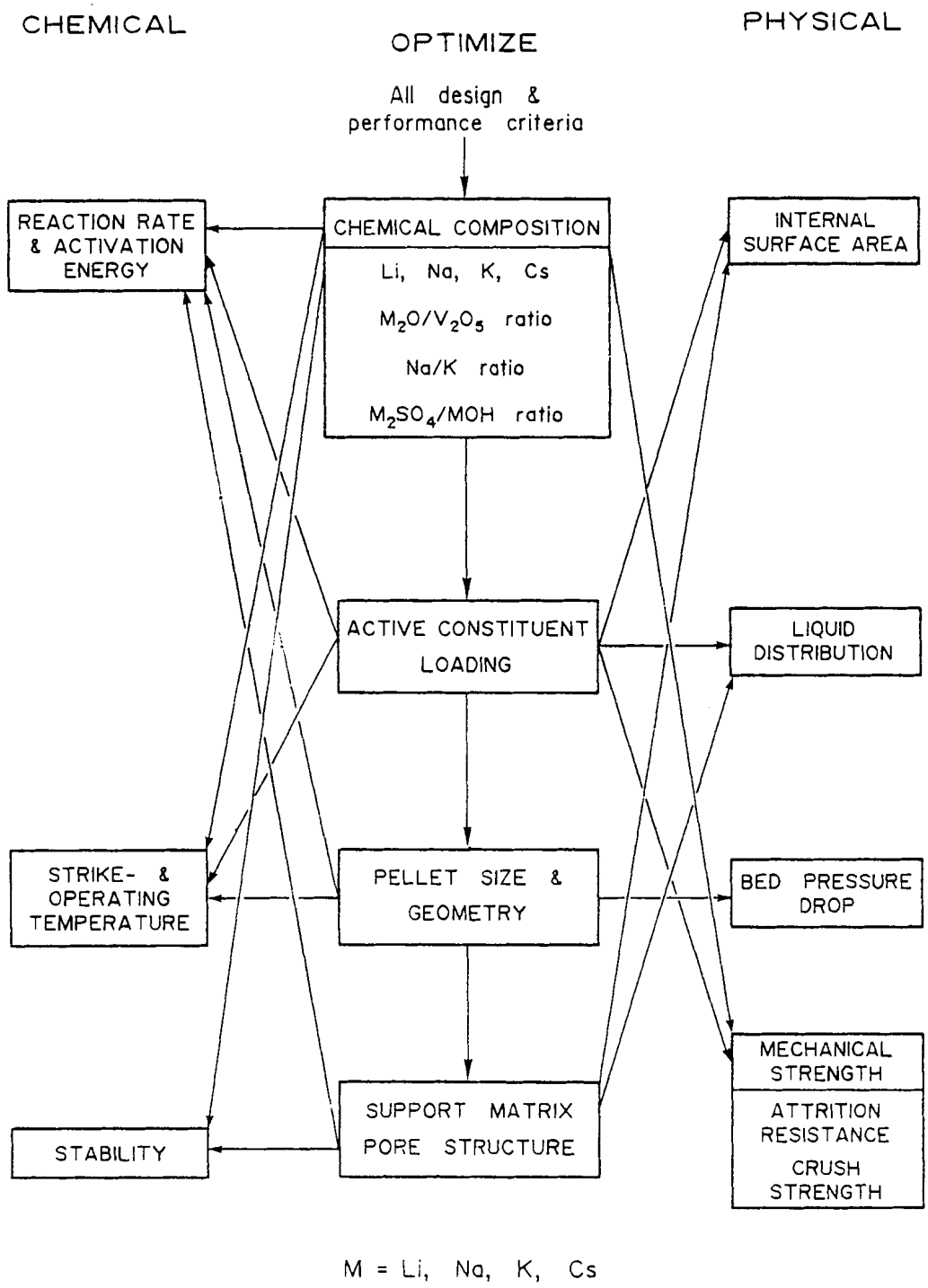

Figure 21. : Physical and chemical factors that influence the catalyst design.

3.2 EXPERIMENTAL REACTOR SYSTEM

3.2.1 Description of the reactor system

Figure (22) is a schematic flow sheet of the reactor system used in this investigation.

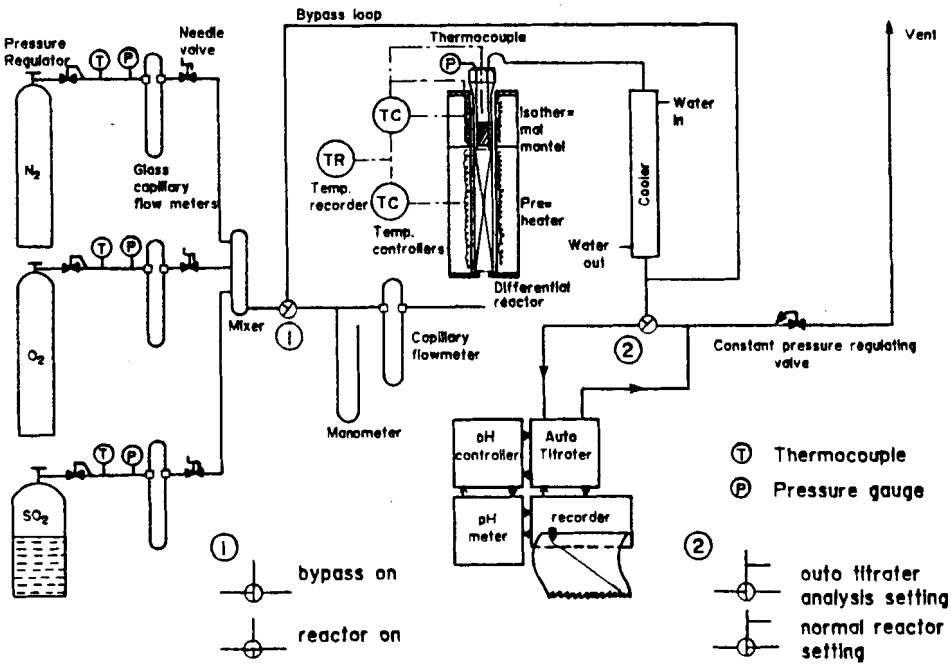

Figure 22. : Flow sheet of reactor system.

A single pass differential reactor was used. This enable the extraction of intrinsic catalytic data from the compositions of matter studied.

Three precalibrated capillary flowmeters with streams of dried N_2, SO_2 and O_2 produced a mixture of 82% N_2, 8% SO_2 and 10% O_2. These compositions were typically that of the first bed of an industrial reactor.

The reactor tube was constructed from a 316 stainless steel tube and consisted of two separate sections. The bottom section within the reactor tube was packed with ceramic saddles and served as a preheater. The differential reactor section, removable with an internal diameter of 32mm, large enough to eliminate excessive wall effects, was located in the top

controlled preheater and was heated within 2% of the reactor temperature. The reactor section was finally controlled to an accuracy of $\pm 0.2°C$ of the setpoint using a fast response thermocouple within the catalyst bed. A datalogger was used to record all temperature readings to obtain a history of each run.

The effluent was cooled and vented through a pressure control valve that controlled the reactor pressure at 10 *kPag.* The effluent gas was analysed via a three-way valve to the analysis section. The analytical equipment consisted of an autotitrator, pH meter, pH controller and a recorder. The bypass loop was used to calibrate the equilibrium pH-setpoint of the autotitrator.

3.2.3 Analysis

From a precision point of view the standard starch method of SO_2 analysis was found to be unsatisfactory. This is primarily due to high SO_2 concentrations from the differential reactor. Improved accuracy was obtained by directly measuring SO_3.

In the **novel method** developed here, the effluent was bubbled through distilled water containing a few drops of glycerol to inhibit the oxidation of dissolved sulphur dioxide. Both sulphur dioxide and - trioxide dissolve in the water forming H_2SO_3 and H_2SO_4 respectively. The following reactions occur:

$$SO_{2_{(g)}} + H_2O \rightleftarrows \quad H_2SO_{3_{(aq)}} \rightleftarrows H^+ + HSO_3^- \tag{63a}$$

$$SO_{2_{(g)}} + H_2O \rightleftarrows \quad H_2SO_{4_{(aq)}} \rightarrow H^+ + HSO_4^- \rightleftarrows H^+ + SO_4^{2-} \tag{63b}$$

Further ionization of HSO_3^- occurs at high pH values (pKa $\simeq$ 7.26 @ 25 °C) and can therefore be ignored. The second ionization step for HSO_4^- occurs at lower pH values (pKa $\simeq$ 1.92 @ 25 °C.)

If a gas stream containing only $SO_{2_{(g)}}$ is bubbled through distilled water containing a few drops of glycerol, an equilibrium pH value of 1.77 is reached.

$$SO_{2_{(g)}} + H_2O \rightleftarrows H^+ + HSO_3^- \qquad pKa = 1.77 \tag{64}$$

Equilibrium is not affected by the presence of dissolved O_2 and N_2 and was found to be only slightly dependent on the SO_2 partial pressure. This equilibrium pH value was determined

regularly by means of the bypass circuit. The values varied between pH = 1.76 and 1.78. When SO_3 is present, the pH drops to zero since the first proton in H_2SO_4 is fully dissociated in water.

$$SO_{3_{(g)}} + H_2O \rightarrow H^+ + HSO_4^- \quad pKa \simeq 0 \tag{65}$$

The second ionization of HSO_4^- occurs at pKa $\simeq$ 1.92 which is above the equilibrium value.

The pH controller connected to the autotitrator was used to maintain a constant pH value at the SO_2 equilibrium level (pH = 1.77). Standardized *NaOH* was automatically titrated the moment SO_3 ($H_2SO_{4_{(aq)}}$) was present and the pH dropped below 1.77. The amount of standardized *NaOH* titrated is directly proportional to the SO_3 content and thus the catalytic conversion. The slope of this constant pH titration curve on the recorder is the SO_2 converted to SO_3 per time. The cell construction is shown in figure (23).

Precautions were taken to eliminate the escape and/or condensation of any SO_3. The product gas stream entering the cell was dispersed by means of a sintered Pyrex bubbler and swing-out magnetic stirrer. Any sulphuric acid mist that might have formed during absorption was trapped by a sintered Pyrex filter. Care was taken to ensure that SO_3 remained in the vapour phase from the reactor system until it was neutralized by the caustic.

This analytical method was checked for validity on a sulphur trioxide-free basis. Sulphuric acid of known strength was added to the analysis cell while it was at equilibrium conditions with a $SO_2/N_2/O_2$ gas mixture bubbling through it. The analysis system responded rapidly and the amount of *NaOH* (1N solution) added to keep the pH at 1.77 corresponded to the stoichiometric quantities of *NaOH* necessary to neutralise the sulphuric acid added. A small correction factor was necessary to account for effects of the second ionization stop of HSO_4^- and possible mass transfer limitations. Those effects were found to be insignificant and constant over a wide range of SO_2 concentrations. The maximum error associated with the product analysis was estimated to be less than 5% of high conversions.

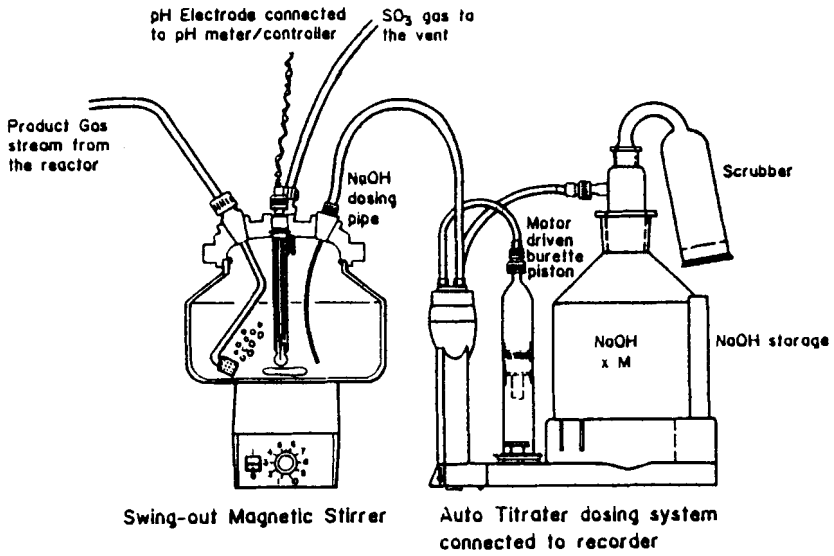

Figure 23. : Schematic of the analytic system.

3.2.4 Experimental conditions

3.2.4.1 Temperature range

The experiments were carried out in the temperature range of 400°C to 600°C with 50°C increments. These experiments were conducted with increasing temperature sequences because of the dynamic hysteresis effect that occurs with decreasing temperature sequences (Jensen-Holm, 1978).

3.2.4.2 Feed gas composition

The inlet gas composition chosen corresponds to the conditions of a typical first bed in an industrial converter. Inlet gas compositions given below were kept constant during all experimental runs:

8% SO_2
10% O_2
82% N_2

therefor O_2/SO_2 ratio $= 1.25$

3.2.4.3 Tests to eliminate transport limitations

The rate data required can be divided into two parts:

- Intrinsic kinetic data necessary to evaluate melt chemical composition effects on catalyst activity.
- Rate data with selective mass transfer limitations to evaluate these transfer effects seperately (i.e. effect of liquid loading and particle geometry).

• Intrapellet transport

A series of runs with progressively smaller catalyst pellets was performed to determine at what size intrapellet effects were eliminated. The particle size range selected where no intrapellet transfer effects occur was 1-1.18 mm crushed pellets. This is in agreement with the work of Livbjerg (1971:21), Urbanek (1980:97) and Eklund (1956:100) who found the effectiveness factor η to be unity for 0.8 to 1.25 mm particles. A minimum liquid loading of 0.0015 mole catalyst/g celite produced a liquid phase effectiveness factor of unity.

• Interphase transport

The effect of interphase transport was determined by measuring the effect of flowrate on conversion (figure 24). Based on the results below a linear gas velocity U_o of $0.2m/$ sec was selected and kept constant at all temperature levels.

• Intrareactor transport

The intrareactor radial and axial heat and mass transfer effects were minimized by using a differential reactor with low conversions. Heat transport effects were minimized by diluting the catalyst with inert ceramic particles of the same particle size (50% mass ceramic particles were added. This technique increases the reactor wall heat transfer area with respect to the heat generated in the catalyst bed. In addition the relatively small reactor diameter reduces radial heat transfer effects. High linear velocities (0.2 m/s) ensured that the axial diffusion rate was negligible compared to the bulk flowrate.

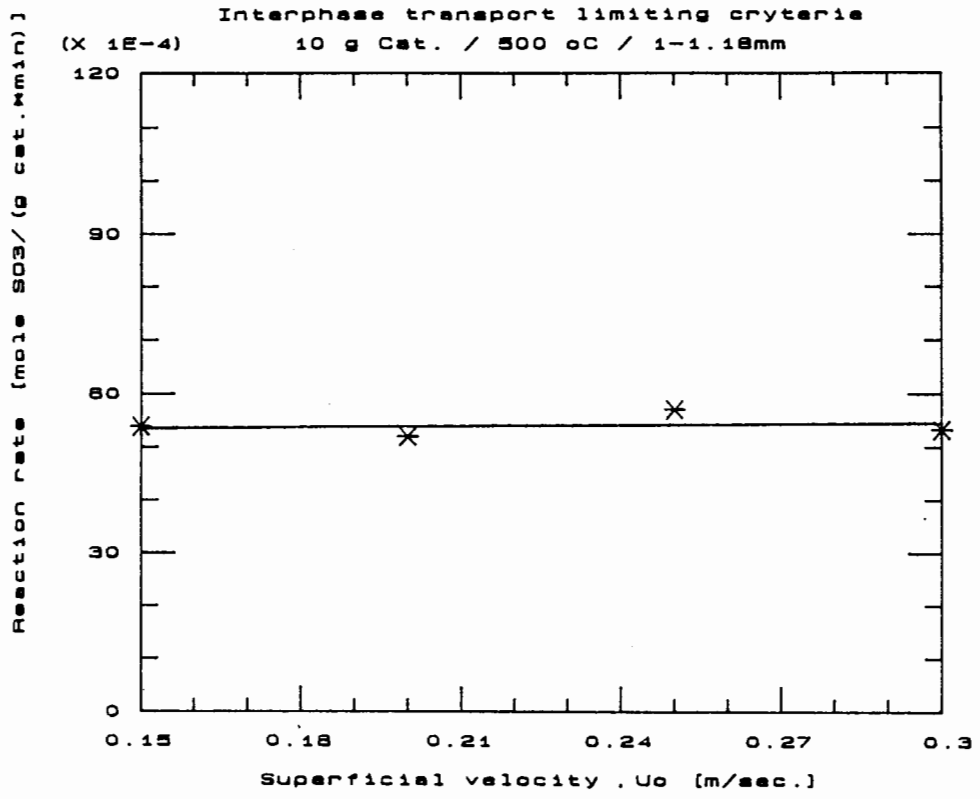

Figure 24. : The effect of interphase transport at different superficial velocities

- **Empty reactor activity**

Compounds present at a stainless steel surface such as Fe_2O_3 and Cr_2O_3 are known to be catalytically active in sulphur dioxide reaction. The catalytic activity of the empty reactor and preheater were measured at all tempereature levels (400°C – 600°C). It has been found that the empty reactor activity expressed in terms of an equivalent weight of standard V_2O_5 catalyst was about 0.02g. This quantity is neglegible.

- **Steady state conditions**

To determine the time necessary to reach steady state conditions, conversion versus time experiments at 500°C were conducted. From figure (25) it is concluded that steady state conditions were rapidly attained. A time interval of one hour was allowed between temperature changes to ensure steady state conditions.

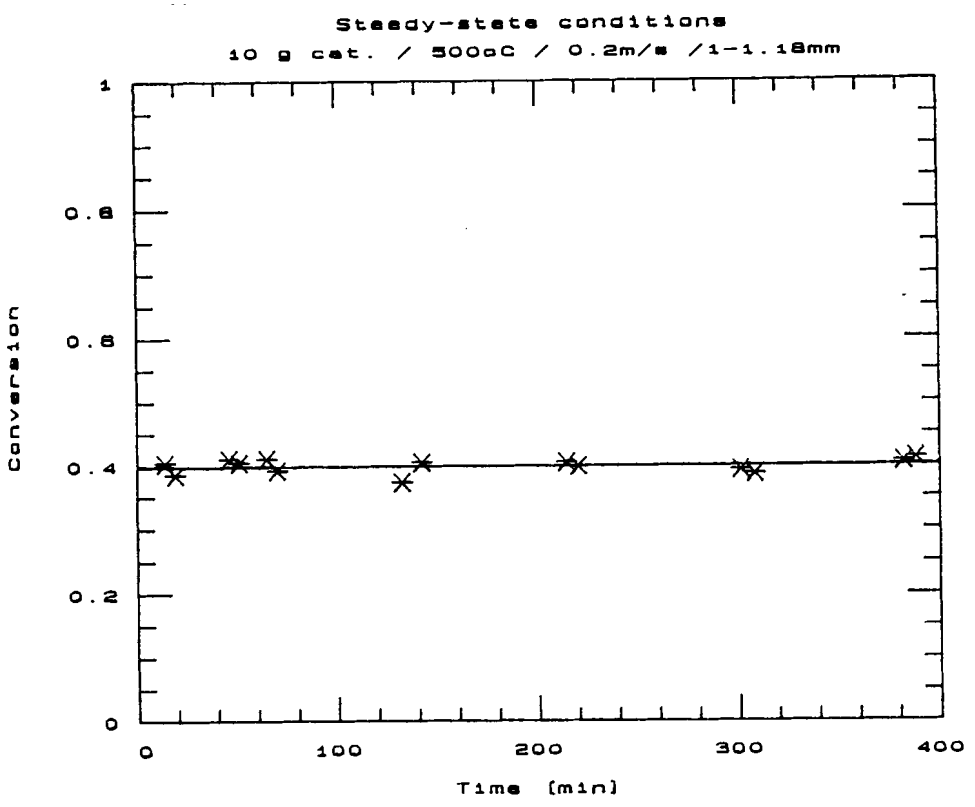

Figure 25. : Time to reach steady state conditions.

3.3 PHYSICAL AND MECHANICAL EXPERIMENTS

3.3.1 Pressure Drop

A large sample was used for accuracy. The packed bed was vibrated to ensure an acceptable reproducibility by minimizing variations in catalyst bulk density (or void fraction). A large bed-to-catalyst diameter ratio was used to reduce wall effects (figure 26).

The pressure drop was measured with a manometer using air at room temperature and atmospheric pressure with superficial velocities in the range 0,05 m/s to 0.8 m/s.

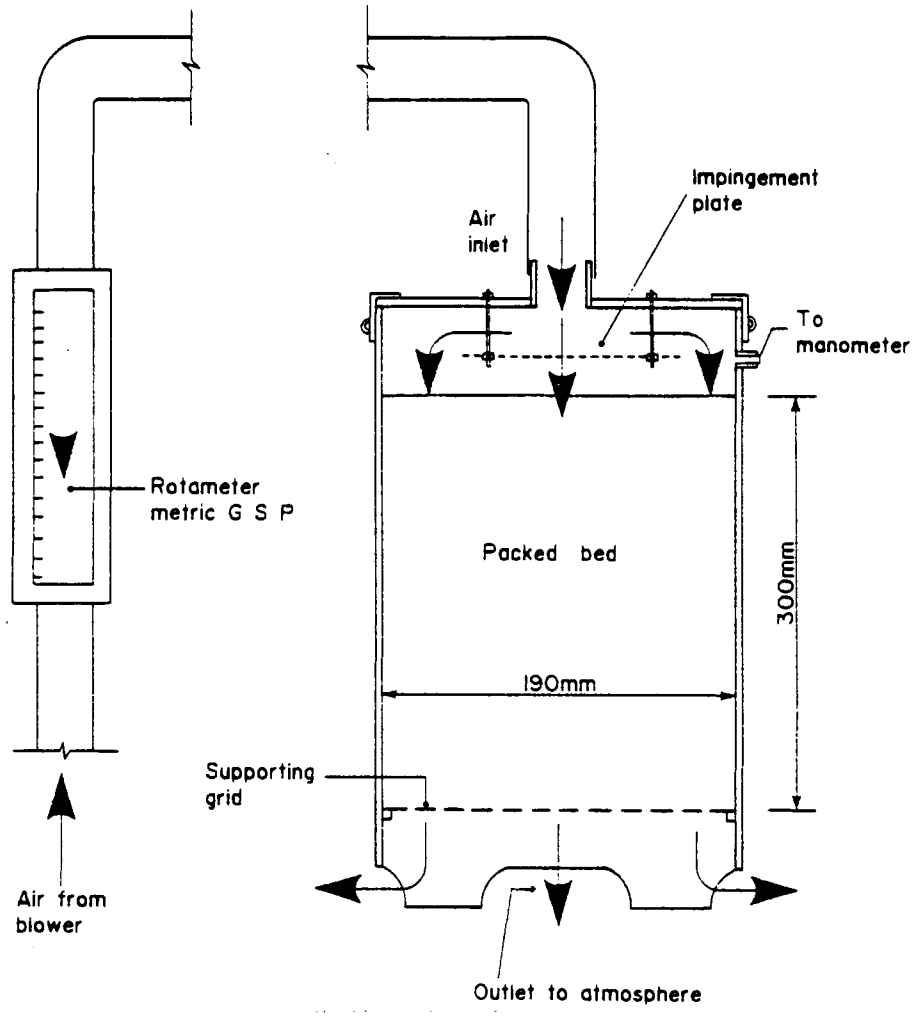

Figure 26. : Pressure drop cell.

3.3.2 Crush strength

Crush strengths measured with hand-operated equipment depend on the rate of force application and thus by the operator doing the testing. Hand operator equipment is used for obtaining the average crush strengths. The problem is that catalysts with similar average values, but broader distributions can behave differently under plant operation conditions.

A recent development within Monsanto Polymers & Petrochemicals Company is a bulk catalyst tester. A slightly modified version was developed and is shown in figure (27).

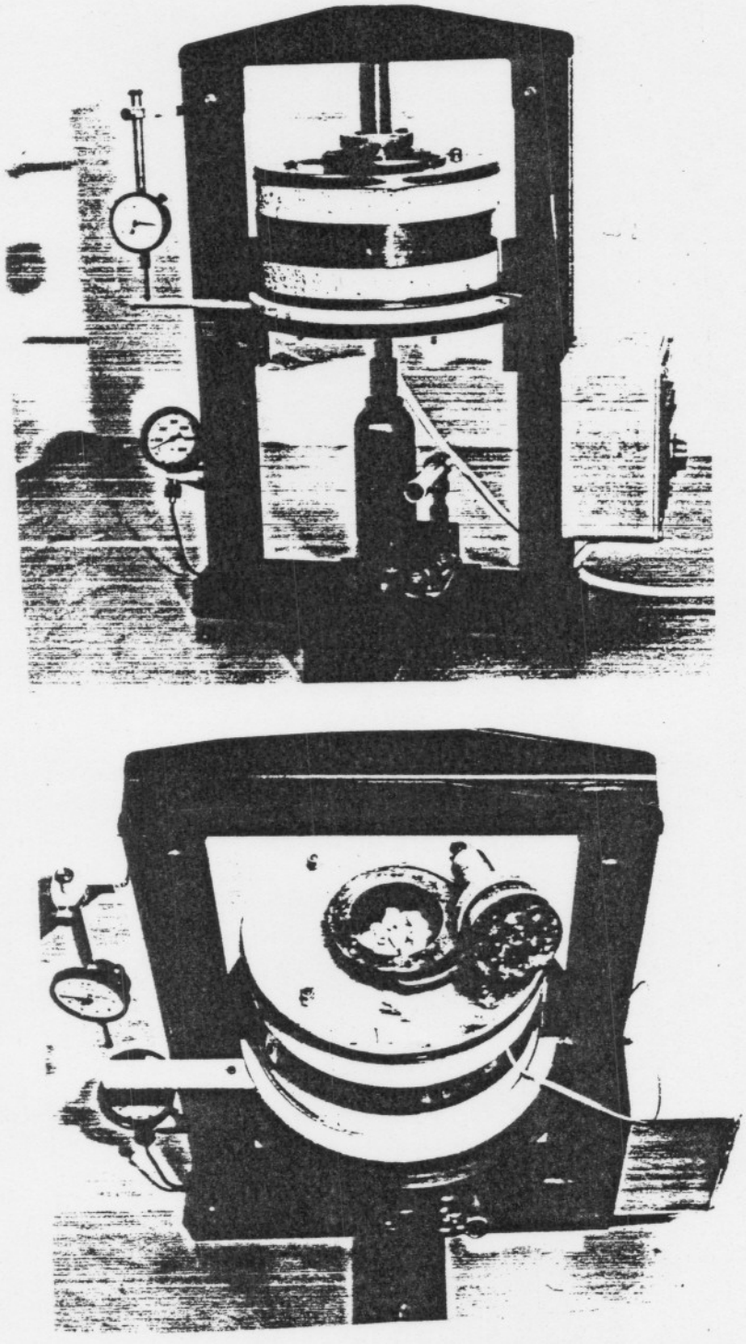

Figure 27. : Photographs of the bulk tester to measure the crush strength at temperatures up to 600°C.

This device allows testing of a 300cm^3 sample of catalyst sample at reactor temperatures. The crushing piston, 69 mm diameter, is forced into the catalyst bed by a hydraulic system. The force applied versus displacement represents the differential crush strength of the catalyst. Smaller piston displacement at a given pressure indicates greater strengths.

3.3.3 Attrition resistance

Attrition tests are based on principles of milling kinetics. In this study the equipment consists of a 300 mm diameter and 250 mm long stainless steel drum, mounted horizontally with a single 50 mm wide baffel. The drum, containing a 100 g sample, is rotated at 60 rev./min for 1500 revolutions (figure 28).

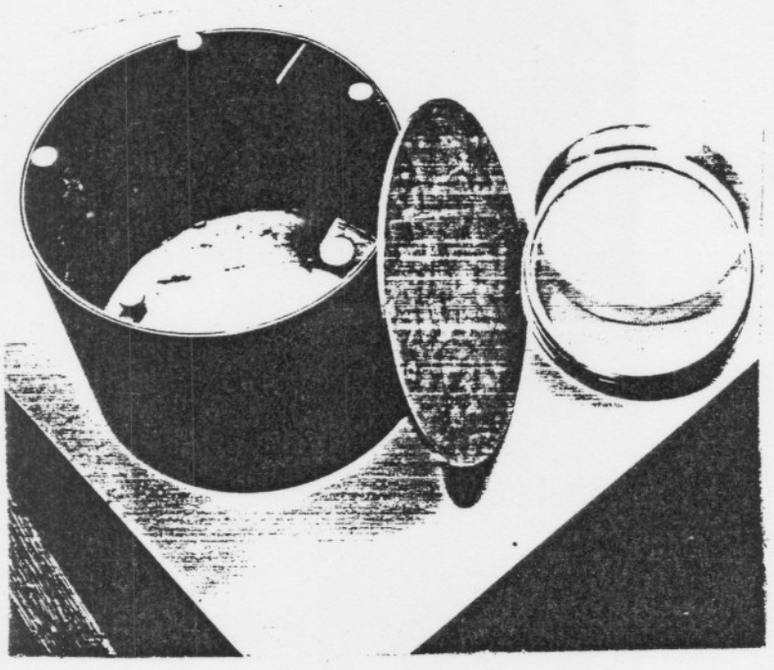

Figuur 28. : Attrition mill.

As the drum rotates the catalyst is caught by the baffel, brought to the top, and dropped back to the bottom where it is gathered again and the process repeated. The final weight was obtained by screening. The attrition loss was calculated as follows:

$$\text{Attrition loss} = \text{Initial weight (100 g)} - \text{Final weight} \qquad (66)$$

3.3.4 Other physical property measurements

3.3.4.1 Pore volume and pore size distribution

Pore volumes and pore size distributions were measured by mercury intrusion. The calculations were based on a 130° contact angle. The pore sizes were measured up to 30Å. The actual testing was conducted by SASTECK.

3.3.4.2 Surface area

The specific surface area in m^2/g was determined using low temperature adsorption of nitrogen, measured by a standard BET method. Complete adsorption isotherms at −195°C were determined from which the specific surface areas were calculated.

3.3.4.3 SEM Examination

Scanning electron micrographs were made of the catalyst to study the morphology and the microstructure. The SEM used was a Cambridge stereo scanner 250 with a Link System EDAX analyser connected to it. Pinpoint chemical compositions were determined using the EDAX scanner.

3.4 CATALYST PREPARATION

Formulations were calculated by an itterative procedure within the boundaries determined by fixed constraints. They were (See Appendix A for more detail):

- Water/Celite ratio
- M_2O/V_2O_5 mole ratios
- Na/K mole ratios
- M_2SO_4/MOH mole ratios
- Mass of dry sample required
- Purities of the chemicals used
- Liquid loading

All soluble chemicals (MOH; M_2SO_4; $M = Li, Na, K, Cs$) were weighed and dissolved in an amount of water necessary to produce an extrudable product. The dry insoluble solids (NH_4VO_3 and Gum arabic) were thoroughly dry mixed with Celite 209 using a large kitchen mixer. Water (96°C) containing the dissolved chemicals was carefully sprayed onto the dry solid with rapid mixing. Some ammonia was evolved during hot water addition. The mix was extruded using a laboratory pneumatically-operated extruder with a single 6mm die. Extrudates were cut with a rotating wire spoke cutter. The feed rate was kept constant to ensure uniform die pressure for all catalyst formulations. (Fluctuating die pressures can lead to variable pore size distributions.) After extrusion pellets of green mass, containing 40 to 45% water, were dried in a muffle furnace at 200°C for 2 hours. Residual moisture content of the pellets leaving the oven was less than 1%. All catalyst samples were activated in the Provon activator in stainless steel baskets. These baskets were concentrically placed in the top section of the activation bed to ensure homogeneous and uniform activation. The activation sequence of Provon Chemicals was used.

CHAPTER 4

EXPERIMENTAL RESULTS AND DISCUSSION

4.1 INFLUENCE OF THE CHEMICAL COMPOSITION OF THE MELT

4.1.1 Introduction

In this chapter, specific intrinsic reaction rates of SO_3 formation are evaluated as a function of the chemical composition of the melt. The variables are:

- Alkali metal cation
- Ratio of alkali metal cation to vanadium pentoxide
- Ratio of sodium to potassium
- Ratio of hydroxide to sulphate as initial anions in the catalyst formulation.

Following the procedures outlined in Chapter 3, experimental runs were conducted to evaluate the intrinsic reaction rates at five different temperature levels (400°C to 600°C). Throughout this section the reaction rates will be intrinsic rates expressed in moles of SO_3 formed per catalyst mass per unit time.

4.1.2 Promotion action of the alkali metal cations

Here the alkali metal promotors on the activity, the alkali metal oxide/vanadium pentoxide ratio was kept constant at a M_2O/V_2O_5 mole ratio of 2.5 with M being *Li, Na, K, Cs*. The catalyst formulations are given in Appendix A1 while the results and calculations are summarized in Appendix B1.

As seen in figure (29) the catalytic activity increases as the molecular weight and ionic radius of the alkali metal cations increases, and the ionization potential decreases.

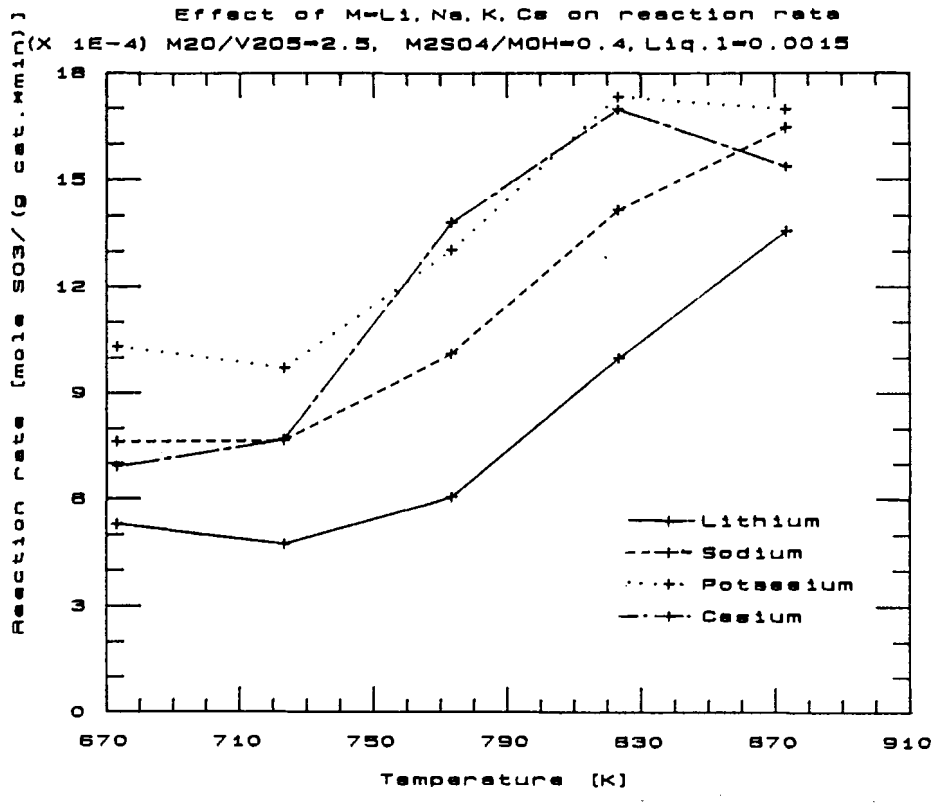

Figure 29. : Promotion action of different group 1 elements.

The promoting action therefore increases in order $Li < Na < K \simeq Cs$. Although the peak activity of *K* and *Cs* promoted catalysts are off the same order, *K* promoted catalysts have a higher activity at lower temperatures than the *Cs* promoted counterparts. From figure (29) it is concluded that with increasing atomic number of alkali metal promoters, the peak activity moves towards lower temperatures.

To obtain the activation energies, Equations (31a) and (33) were used. The linear portion of the Arrhenius relationship between $°C \wedge 55°C$ was used.

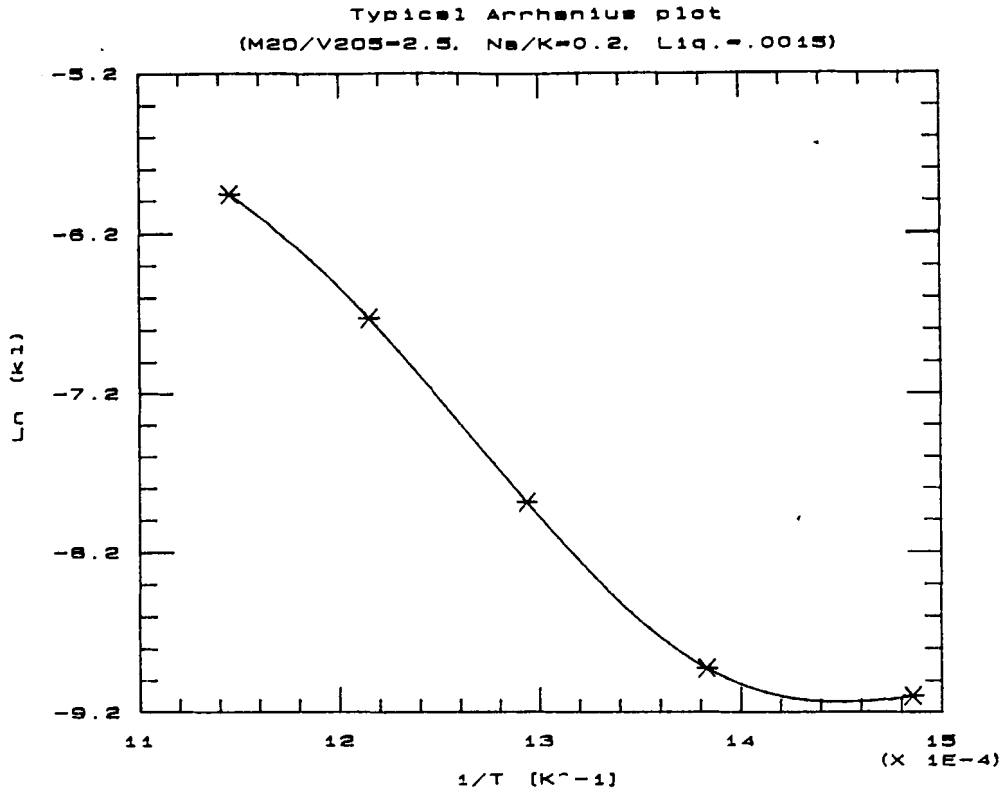

Figure 30. : A typical Arrhenius plot obtained from intrinsic rate data.

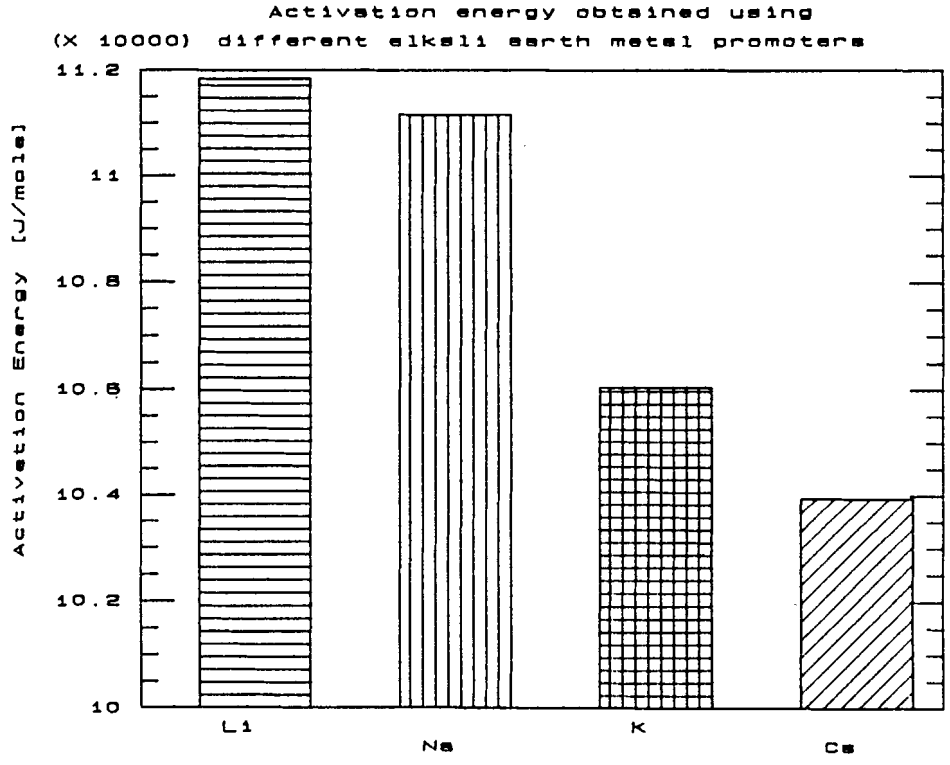

Figure 31. : Activation energy as a function of the type of alkali earth metal promoter.

In figure (31) the activation energies for various promoters are given and it is seen that there is a decrease in activation energy as the size of the cation increases.

Discussion

As discussed in the literature survey the melting point and viscosity of the catalyst mixture, decreases with increasing atomic weight and radius of the alkali metal used. Low molecular weight alkali metals tend to form sulphates, M_2SO_4, while higher molecular weight metals tend to produce pyrosulphates, $M_2S_2O_7$. There is evidence of partial formation of even higher sulphates, $M_2S_3O_{10}$, in the case of *Cs*. The pyrosulphates have lower melting points than the corresponding sulphates and may form eutectic mixtures with sulphates which can result in even lower melting points. It must be mentioned at this point that the reactant compositions ($SO_2/O_2/N_2$ mixture) also have an effect on the final chemical composition of catalyst melt (i.e. the sulphate pyrosulphate ratio) and therefore could also have an effect on the catalyst melting point. For this reason the reactant composition was kept constant during all the experiments.

Reactant diffusivities, in particular that of oxygen, increases with a decrease in viscosity of the melt. Furthermore the melt viscosity decreases with increasing temperature. Since diffusion and viscosity are activated processes, their temperature dependence will be affected by the temperature at which the melt first is formed, and this is dependent on the molecular weight of the group 1 promotors and their tendencies to form higher sulphates. So, from a viscosity and melting temperature point of view, a lower activation energy and higher activity can be expected for increasing molecular weight promoters. This at least partially explains the trend in figures (29) and (30).

In conclusion the activation energy to overcome the physical barriers of viscosity and melting point on diffusion as influenced by the type of alkali metal in the melt, contribute significantly to the measured activation energy.

There are other factors, such as the increase in the V_2O_5 solubility with increasing molecular weight of the alkali metals that may increase the vanadium availability for reaction. The interactions of the different alkali metals in the ionic melt (different ionic radius and electronegativity) may also contribute to the differences in activation energy.

The nonlinearity of Arrhenius plots (figure 30) at $\pm 450°C$ is probably related to a change in the state of the active component of the catalyst. It is possible that under these high temperature conditions a decomposition of the pyrosulphate and a volatilization of the SO_3 occurs. This can be expressed by the following reaction

$$S_2O_7^{2-} \rightleftarrows SO_4^{2-} + SO_3.$$

A change in activation energy indicates a shift in controlling mechanism of the reaction.

4.1.3 Effect of the Alkali metal: Vanadium ratio on activity

The alkali metal promoter used for these experiments was potassium. The potassium oxide to vanadium pentoxide molar ratio was varied while the total moles of active constituents (i.e. the liquid loading) were kept constant (0.0015 mole catalyst per gram support material). The catalyst formulations are given in Appendix A1 while the calculations and results are given in Appendix B1.

Because of the multivariable nature of the data, multivariable regression analysis on the data was necessary to quantify the relationships between variables. The multiple regression model uses least squares, up to third order cross linked relationships, to estimate the regression model. The dependant variable is reaction rate and the two independent variables are temperature and the M_2O/V_2O_5 molar ratio. A regression fit with a R-squared of 0.96 has been obtained (Appendix C1.1). The residual plot and the predicted versus observed value plot revealed no irregularities (Appendix C1.2 and 1.3).

From figures (32) and (33) it can be seen that an optimum M_2O/V_2O_5 mole ratio exists at each temperature. This optimum ratio is more pronounced at lower temperatures than at higher temperatures. The locus of the maxima moves towards lower M_2O/V_2O_5 ratios at higher temperatures (dotted line on figure 33). At the optimum temperature, 845K, the optimum M_2O/V_2O_5 mole ratio was 2.8.

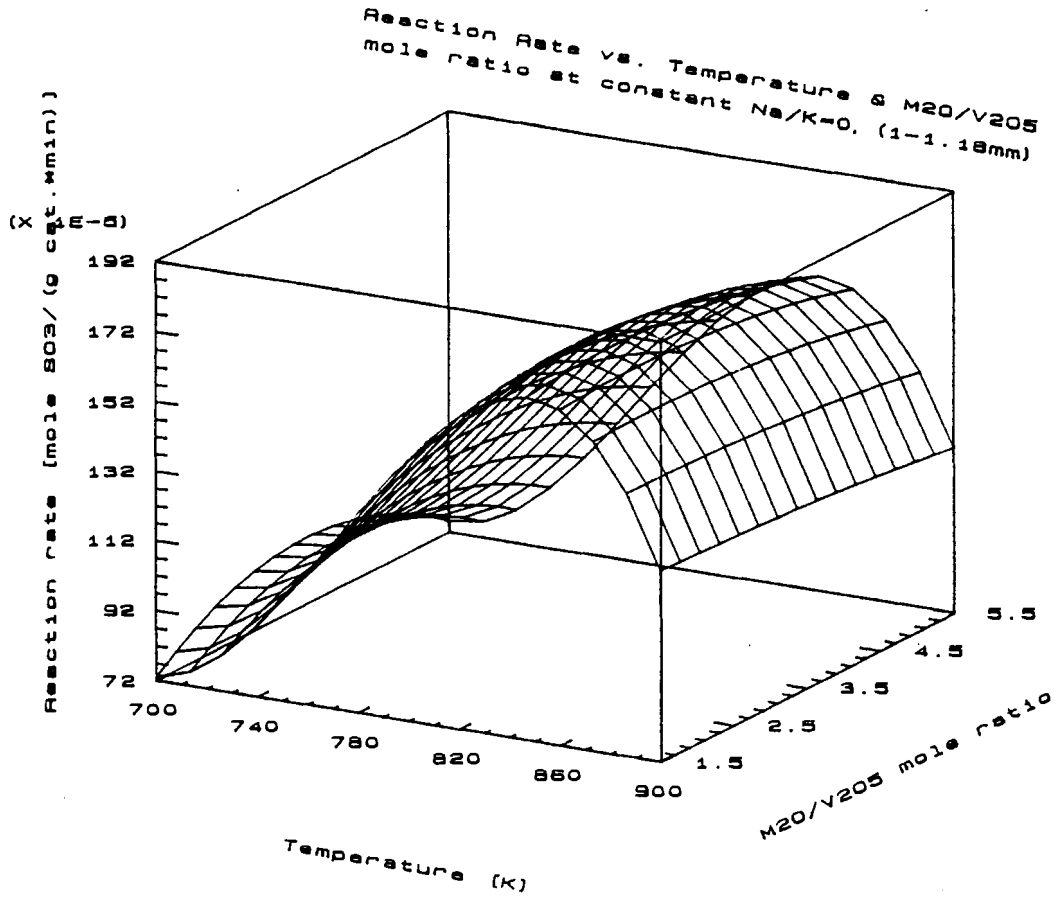

Figure 32. : Surface plot of reaction rate as a function of the M_2O/V_2O_5 mole ratio ($M = K$) and temperature. The liquid loading = 0,0015 mole catalyst/g celite.

Discussion

An optimum M_2O/V_2O_5 mole ratio and the temperature dependence of this optimum ratio can be attributed to the following factors:

- The solubility of V_2O_5 in the $K_2S_2O_7 - K_2SO_4$ mixture increases with increasing temperature; thus an increase in V_2O_5 active sites available for reaction.
- An increase in viscosity of the melt with increasing V_2O_5 concentration. Thus a high V_2O_5 concentration in the melt could lead to lower reaction rates due to increasing diffusion resistance (Tandy, 1956: 69).
- On the other hand, low concentrations of V_2O_5 in the melt would result in a decrease in active catalytic sites and would therefore also result in lower reaction rates.

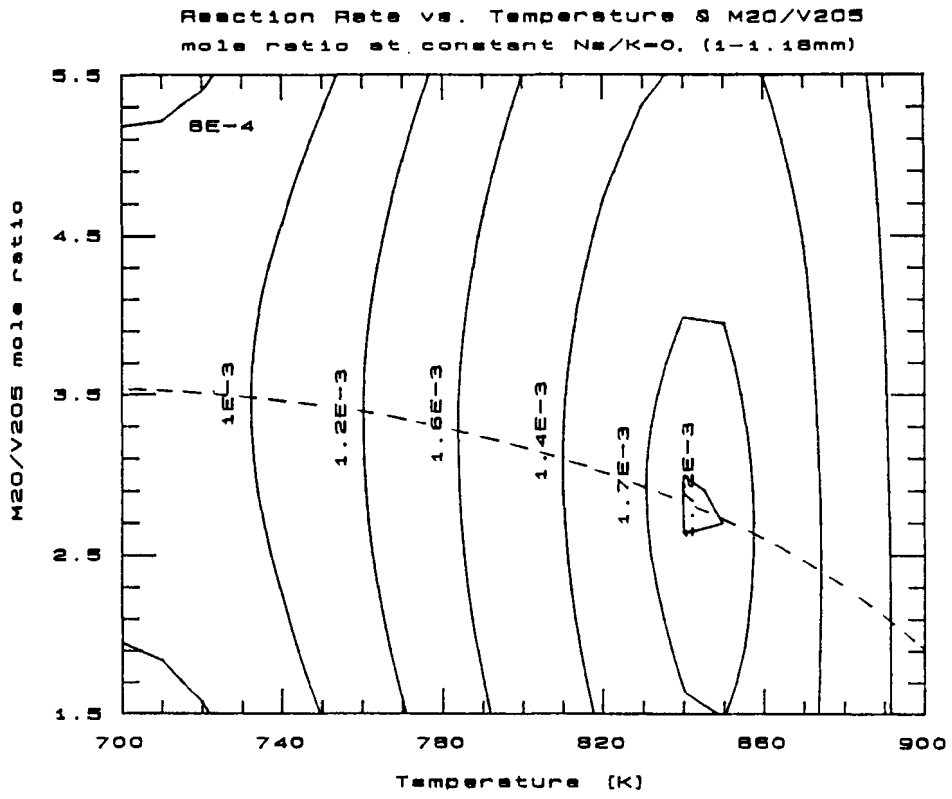

Figure 33. : Contour plot of reaction rate as a function of reaction M_2O/V_2O_5 mole ratio ($M = K$) and temperature. The liquid loading was 0.0015 mole catalyst/g celite.

The less pronounced optimum M_2O/V_2O_5 ratio on reaction rate at higher temperatures can be due to the reduced influence of the V_2O_5 concentration on the melt viscosity. Therefore the effect of V_2O_5 concentration on viscosity and consequently diffusion resistance is not as severe at higher temperatures.

The decrease of the optimum M_2O/V_2O_5 (increase in V_2O_5 concentration) mole ratio locus with increasing temperature (dotted line in figure 33) is most probably the result of increasing V_2O_5 solubility in the melt with temperature.

4.1.4 Mixtures of different alkali metals and different V_2O_5 concentrations

In the previous section the only alkaline earth metal used was potassium. In this section mixtures of sodium and potassium were used and their M_2O/V_2O_5 (M = Na and K mixtures) ratios were also varied. Therefore the three independent variables were Na/K, M_2O/V_2O_5 mole

ratios and temperature while the dependent variable was reaction rate. The liquid loading was kept constant at 0,0015 mole catalyst per gram support material. The formulations, results and calculations are given in Appendix A2 and B2 respectively.

Effect of *Na/K* mole ratio

With a constant M_2O/V_2O_5 mole ratio of 2.5 and varying *Na/K* mole ratios am excellent multiple regression fit with a R-squared of 0.97 was obtained (Appendix C2). The residula plot and predicted value plot revealed no inconsistencies (Appendix C2.1 and C2.2).

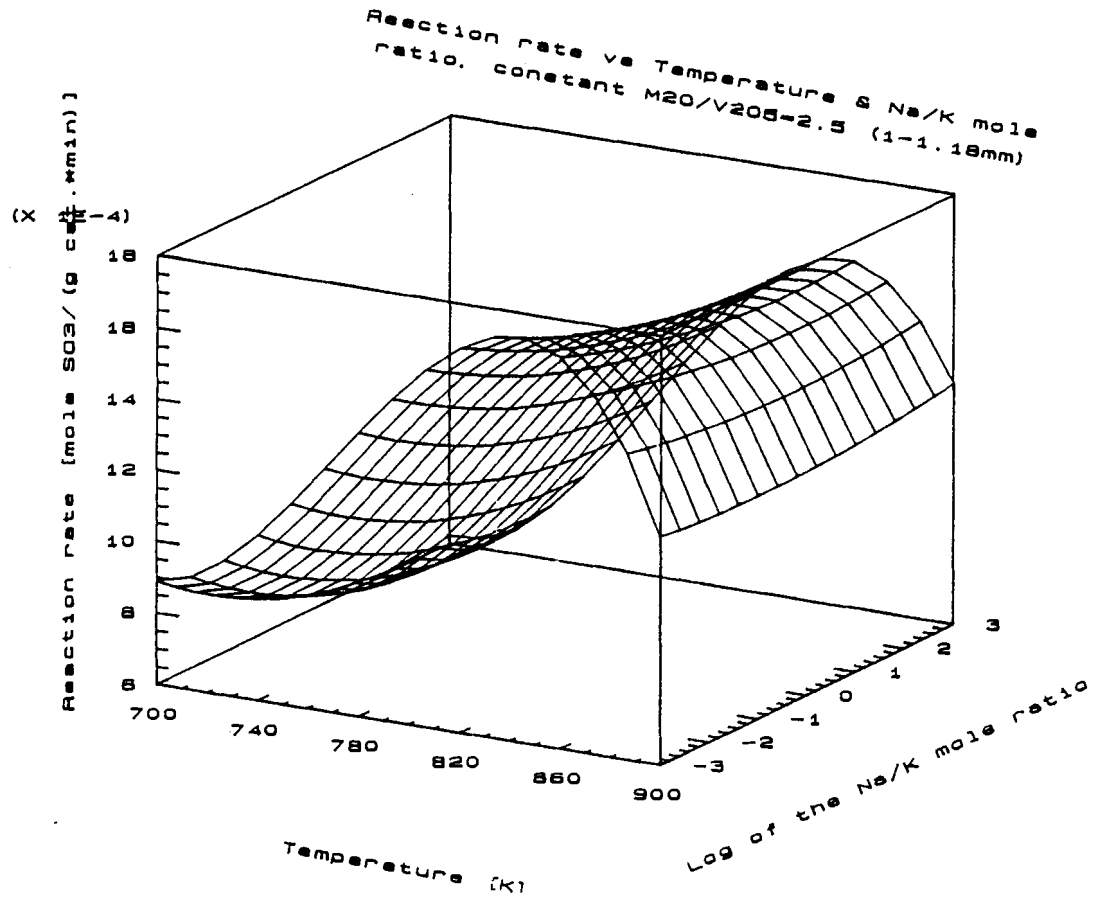

Figure 34. : Reaction rate versus temperature at different *Na/K* mole ratios. Constant M_2O/V_2O_5 mole ratio of 2.5.

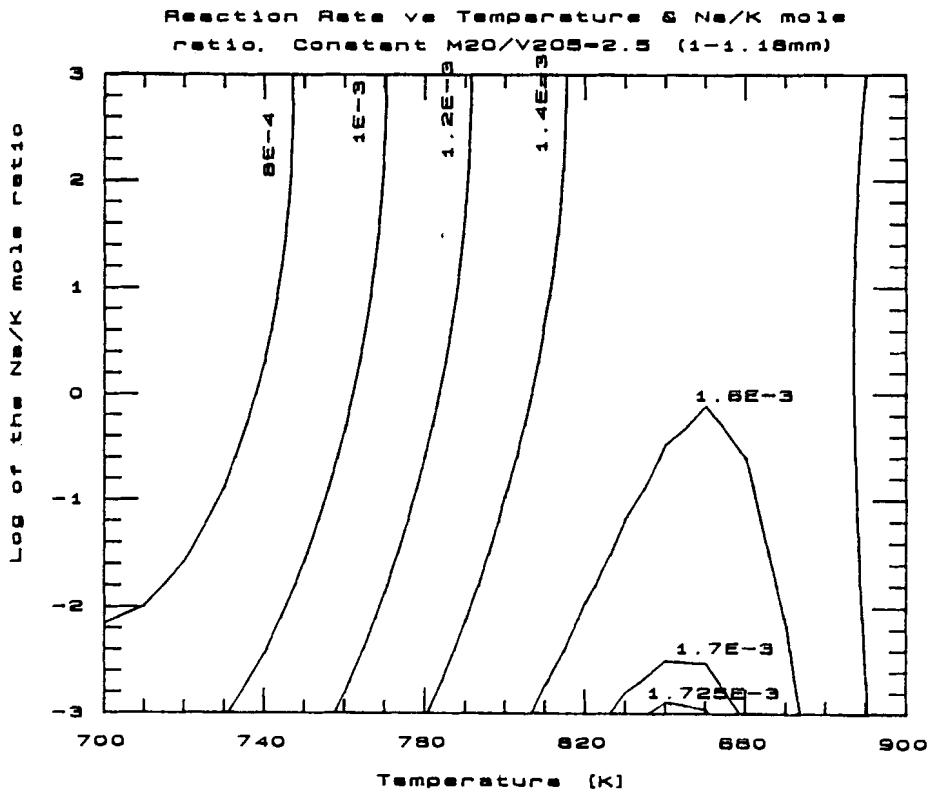

Figure 35. : Contour plot of reaction rate versus temperature and *Na/K* mole ratio. Constant M_2O/V_2O_5 mole ratio of 2.5.

From figures (34) and (35) it is concluded that **partial replacement of the potassium by sodium decreases activity at all temperature levels**. This is in agreement with the results obtained by Tandy (1956: 72). This has implications on strike temperature.

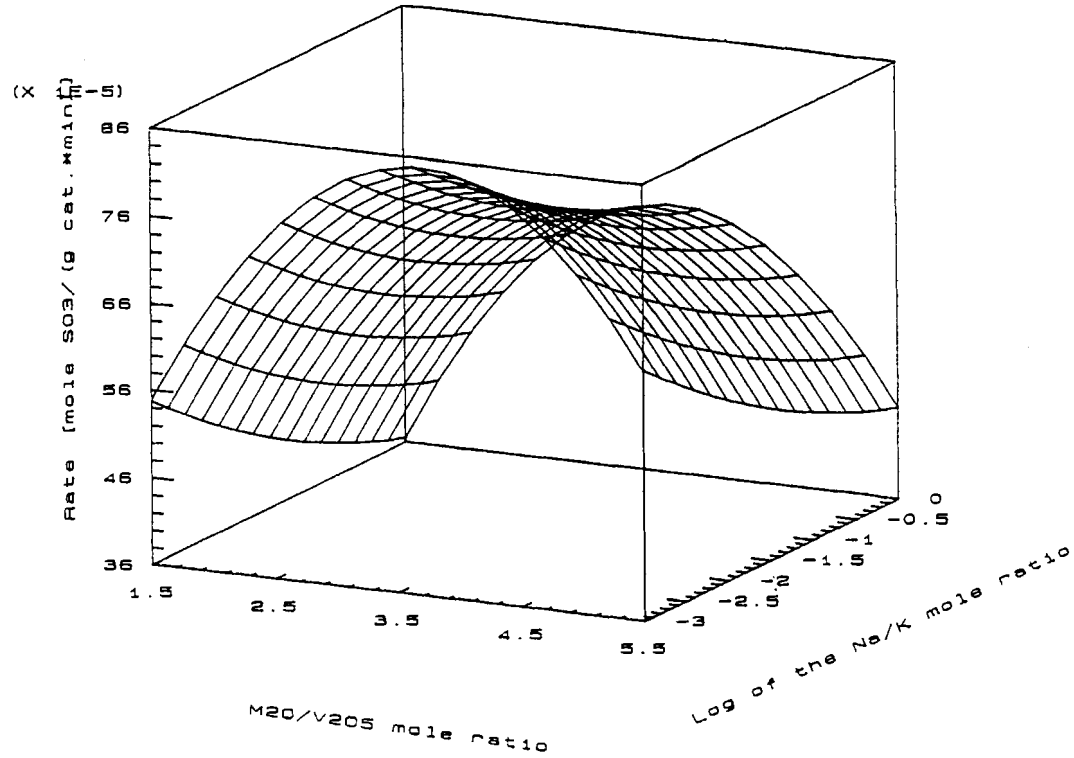

Figure 36. : Surface plot of reaction rate versus Na/K and M_2O/V_2O_5 mole ratio at 450°C.

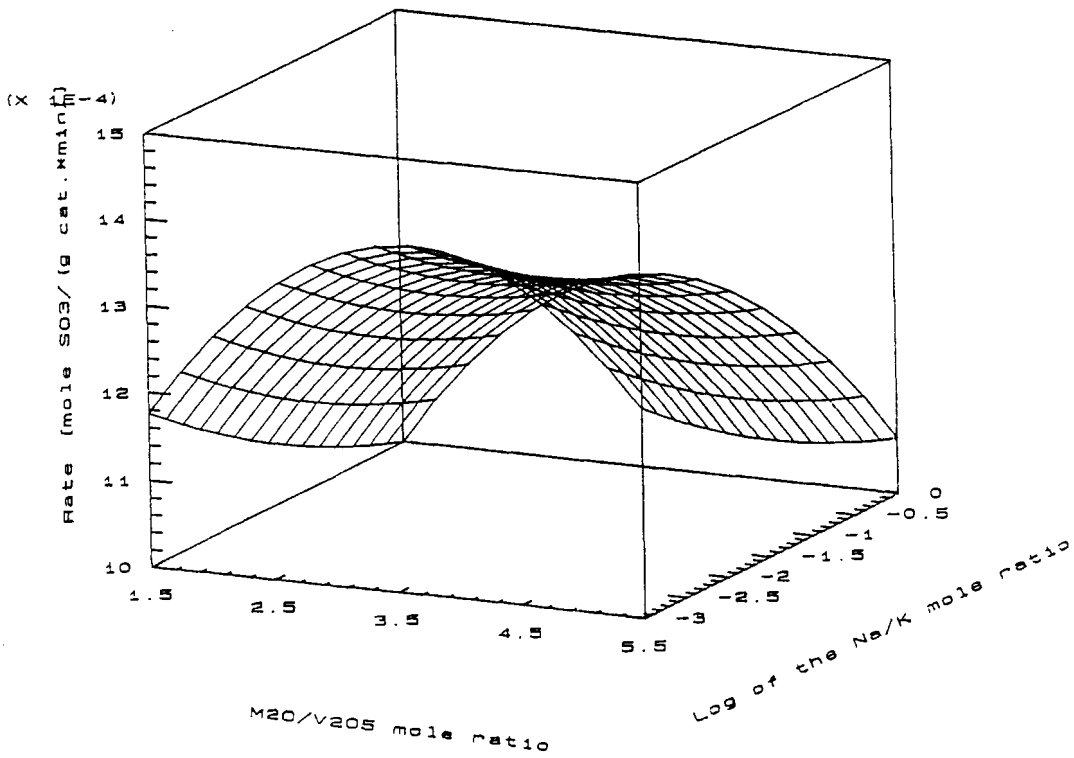

Figure 37. : Surface plot of reaction rate versus Na/K and M_2O/V_2O_5 mole ratio at 500°C.

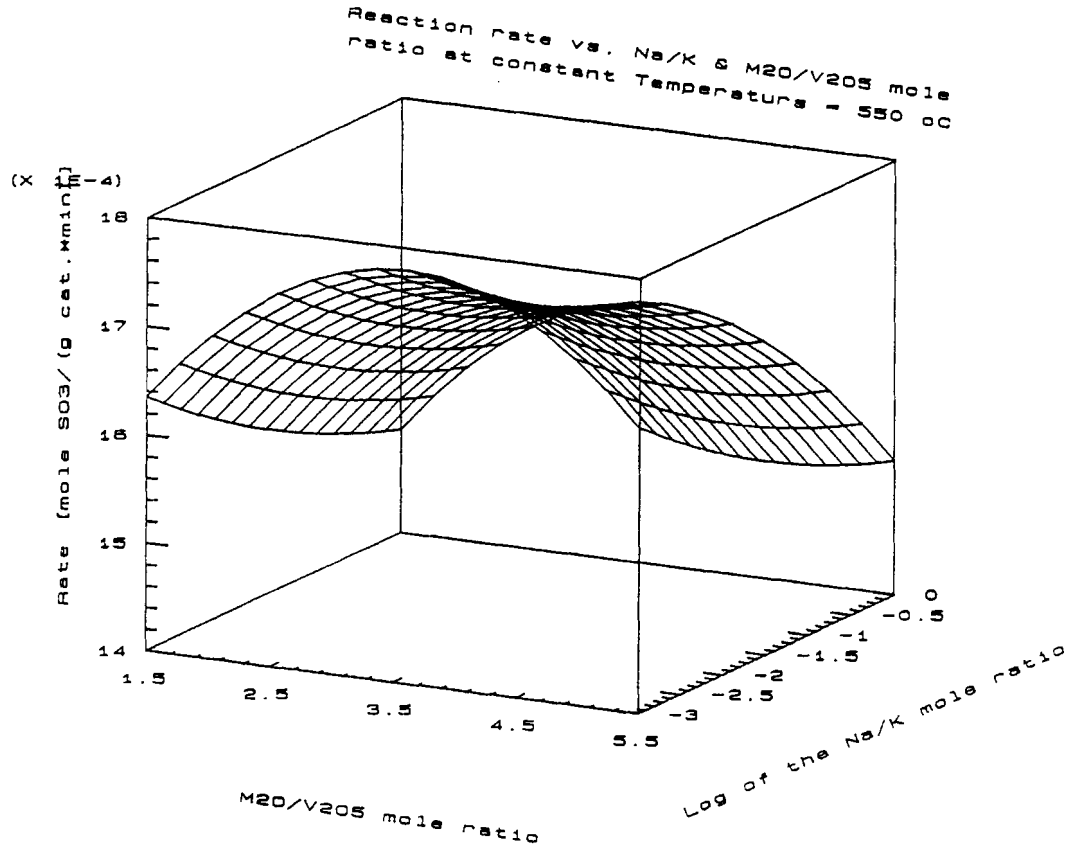

Figure 38. : Surface plot of reaction rate versus *Na/K* and M_2O/V_2O_5 mole ratio at 550°C.

Effect of *Na/K* and M_2O/V_2O_5 ratio

Three temperature levels were chosen. The data is in Appendix A2 and B2 and is graphically represented in figures (36), (37) and (39), each graph representing a different temperature. A fourth order regression fit gave a R-squared of 0,95 (Appendix C3). The residual and predicted value plots indicate no discrepancy (Appendix C3.1 and C3.2).

From figure (36), (37), (38) it is concluded that there is a common general trend of decreasing activity with increasing partial replacement of potassium with sodium and it holds at all M_2O/V_2O_5 mole ratios and all temperature levels. The optimum M_2O/V_2O_5 ratio is independent of the *Na/K* mole ratio. The optimum M_2O/V_2O_5 ratio is more pronounced at lower

temperatures (figure 36) than at higher temperatures (figure 38); the same tendency as in the previous section.

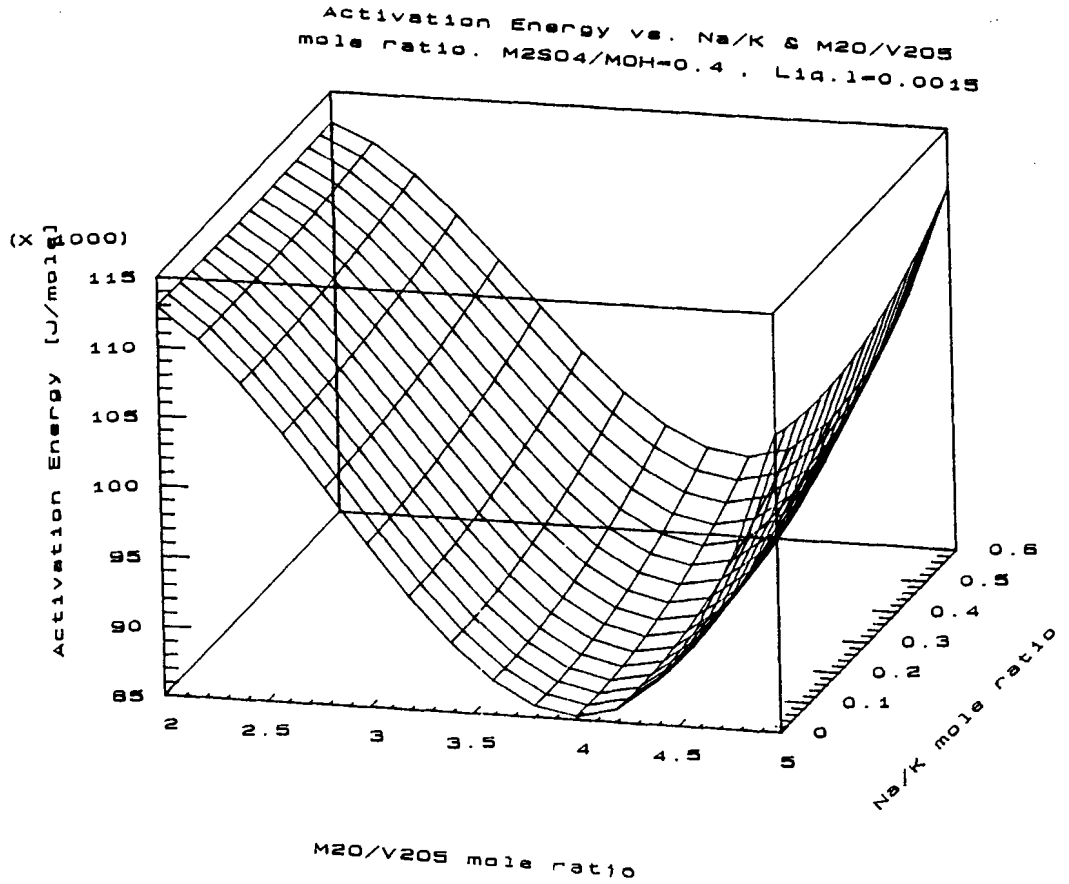

Figure 39. : Surface plot of activation energy as a function of M_2O/V_2O_5 and *Na/K* mole ratios.

Effect of *Na/K* and M_2O/V_2O_5 mole ratios on activation energy

Activation energies obtained from slopes of Arrhenius plots were modelled by a multivariable regression fit with a R-squared of 0.91 (Appendix B2, C4, C4.1, C4.2).

From figure (39 and (40) it is concluded that the minimum activation energy occurs with a melt composition when no sodium is present (potassium only). At high vanadium concentrations ($M_2O/V_2O_5 \simeq 2$) the activation energy is independent of the *Na/K* mole ratio. At low vanadium concentrations, notably near the minimum value, the activation energy drops with decreasing *Na/K* mole ratio.

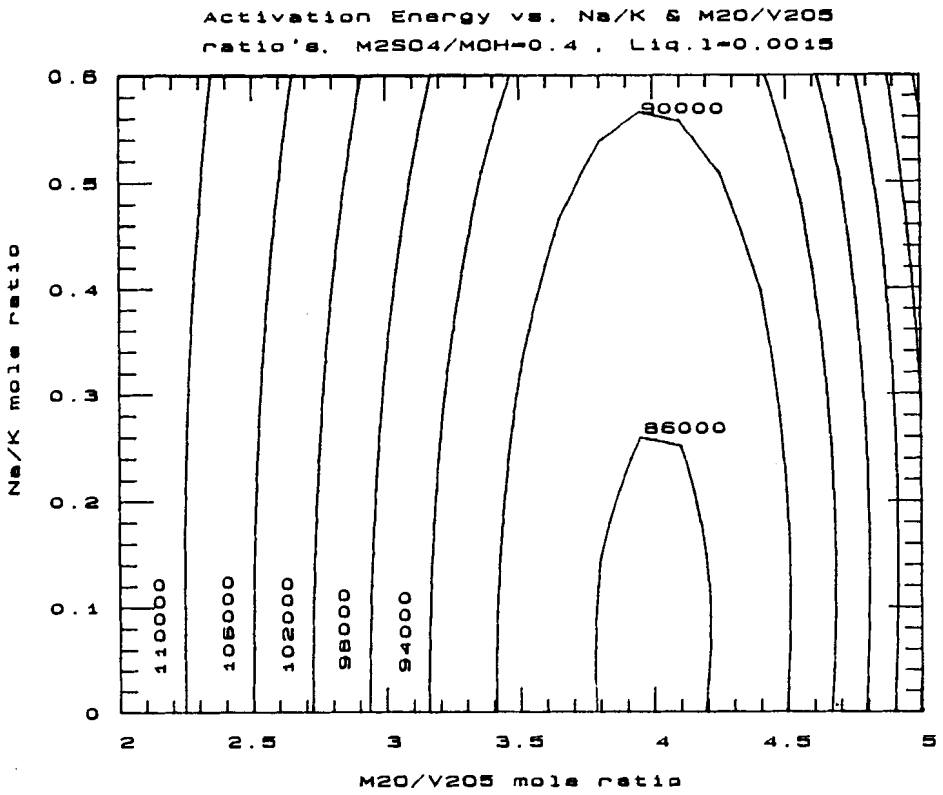

Figure 40. : Contour plot of activation energy as a function of M_2O/V_2O_5 and *Na/K* mole ratios.

Discussion

The decrease in activity when sodium displaces potassium is probably due to viscosity changes (Tandy, 1956:72). Addition of sodium results in lower $M_2S_2O_7/M_2SO_4$ ratios because less pyrosulphate forms with sodium than with potassium. The increase in melting point of the mixture is due to sulphates that have higher melting points than the corresponding pyrosulphates and possibly because the system is moving away from the eutectic sulphate/pyrosulphate mixture.

The reason why the optimum M_2O/V_2O_5 mole ratio is relatively independent of the *Na/K* mole ratio is not clear. The optimum M_2O/V_2O_2 mole ratio is determined by the opposing factors: the influence of V_2O_5 on the viscosity and the effect of V_2O_5 concentration on availability of active sites in the melt. The dependence of these factors on the *Na/K* mole ratio is the only possible explanation. In general the activation energy is more sensitive to the M_2O/V_2O_5 ratio than the *Na/K* mole ratio. The same arguments of the previous paragraph can be used to explain this tendency. The catalyst composition at the minimum activation energy represents the composition where highest activity or temperature sensitivity is obtained.

4.1.5 Effect of the hydroxide/sulphate ratio as initial chemicals

The raw materials used to manufacture the catalyst can effect the mechanical properties and activity of the final product. Usually alkali metal sulphates and -hydroxides are used as initial chemicals. These sulphates or hydroxides are converted to sulphates and pyrosulphates during activation and reaction. Based on the idea that the hydroxides could react with the silica catalyst support to form thin layers of alkali metal silicates and these in turn can affect sintering and mechanical stability, resulted in conducting the following experiments:

With a constant $Na/K = 0.2$ mole ratio the M_2SO_4/MOH ratios were varied. The multivariable regression model fitted through the data gave a R-squared of 0.98; also the residual and predicted value plots showed no inconsistencies (Appendix C5.1, C5.2 and C5.3). The catalyst formulations and calculations are in Appendix A3 and B3 respectively.

From figure (41) and (42) it is concluded that the starting components used have a pronounced effect on the activity of the final catalyst. The optimum ratio of M_2SO_4 to MOH is one. Therefore equivalent amounts of sulphate and hydroxides should be used as initial chemicals during catalyst preparation.

Discussion

An optimum hydroxide/sulphate ratio for reagents is concluded to be due to the following factors:

- At high hydroxide levels excessive sodium and to a lesser extent potassium silicates form. These lower melting point alkali metal silicates formed on the diatom particles enhance sintering between particles. At high hydroxide levels collapsing of the pore structures occur and result in decreased activity.
- During the manufacturing it was observed that high sulphate and low hydroxide levels produced a shiny surface; probably a skin effect. This skin effectively forms a high diffusion resistance barrier that will lead to a decrease in activity.

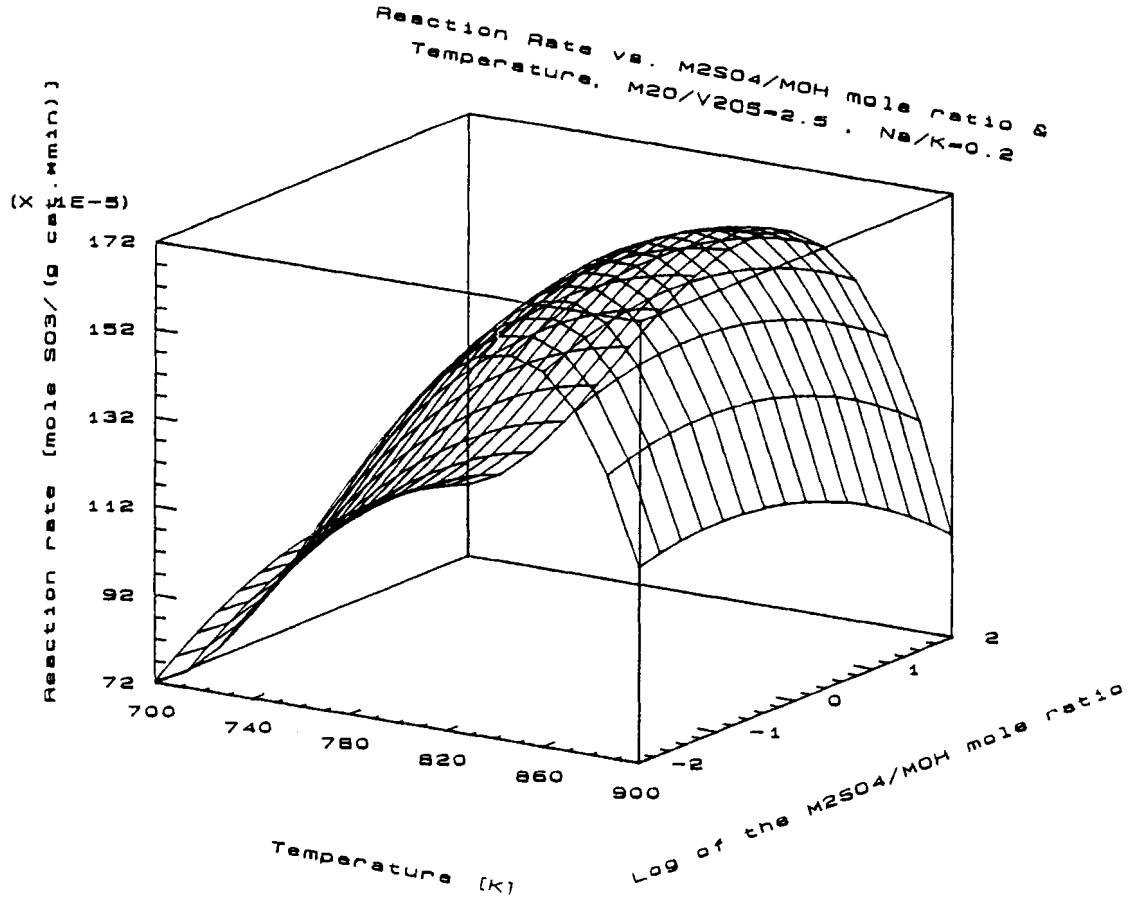

Figure 41. : Reaction rate versus M_2SO_4/MOH mole ratio of the initial chemicals.

Apart from the effect of the hydroxide ratio on the activity of the catalyst, the initial M_2SO_4/MOH ratio used can also have a significant effect on the mechanical strength of the catalyst. The lower melting point sodium and potassium silicate layers on the diatom particles probably act as binders. This ratio therefore is also an important variable in the manufacturing process of the catalyst.

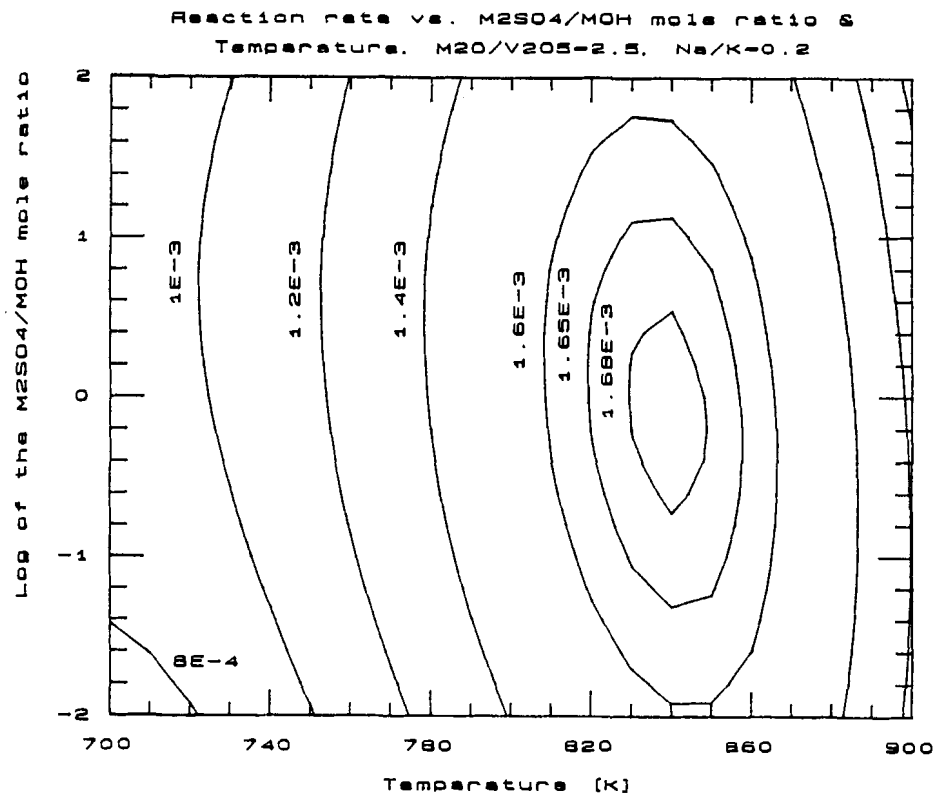

Figure 42. : Contour plot of the reaction rate versus the M_2SO_4/MOH mole ratio of the initial chemicals.

4.2 EFFECT OF LIQUID LOADING

4.2.1 Introduction

In the previous section low liquid loadings on the support were used to preclude diffusion limitations and to ensure a homogeneous catalytic reaction in the liquid phase. In this section the effect of liquid loading on reaction kinetics was investigated. Small particles were used to eliminate any gas phase diffusion effects. Large particles were used to investigate the combined effect of gas and liquid phase diffusion on the overall effectiveness factors.

4.2.2 Liquid phase transport resistance and liquid distribution

The effect of liquid loading on the liquid diffusion resistance was determined with catalyst particle sizes of 1-1,18mm. A constant composition was used and tests were done at five different temperature levels between 400°C and 600°C. In each case only the amount of liquid

on the carrier matrix was varied. The formulations are given in Appendix A4 with the results and calculations in Appendix B4 and B6.

The reactions are expressed in terms of the rate of SO_3 formation per unit volume of active melt. A multiple regression fit through the data was obtained with a R-squared of 0,98. The residual plot and predicted versus observed value plots reveiled no discrepansies (Appendix C 6.1 - 6.3). The liquid loading factor was calculated using equations (1) and (2) and was based on the assumption that melt density is practically independent of temperature in this range. The melt density was indirectly determined by regression analysis between the experimental data and the liquid effectiveness factor model described by equations (38) to (44). The indirectly calculated melt density of $2,2 g/cm^3$ is in agreement with the density of 2,0 g/cm^3 quoted by Neth et al. (1980:45). At very low liquid loadings the reaction rate per unit volume of melt is considerable higher than at higher liquid loadings where it levels off (figure 43 and 44). The maxima shifted towards higher temperatures at lower liquid loadings (figure 44).

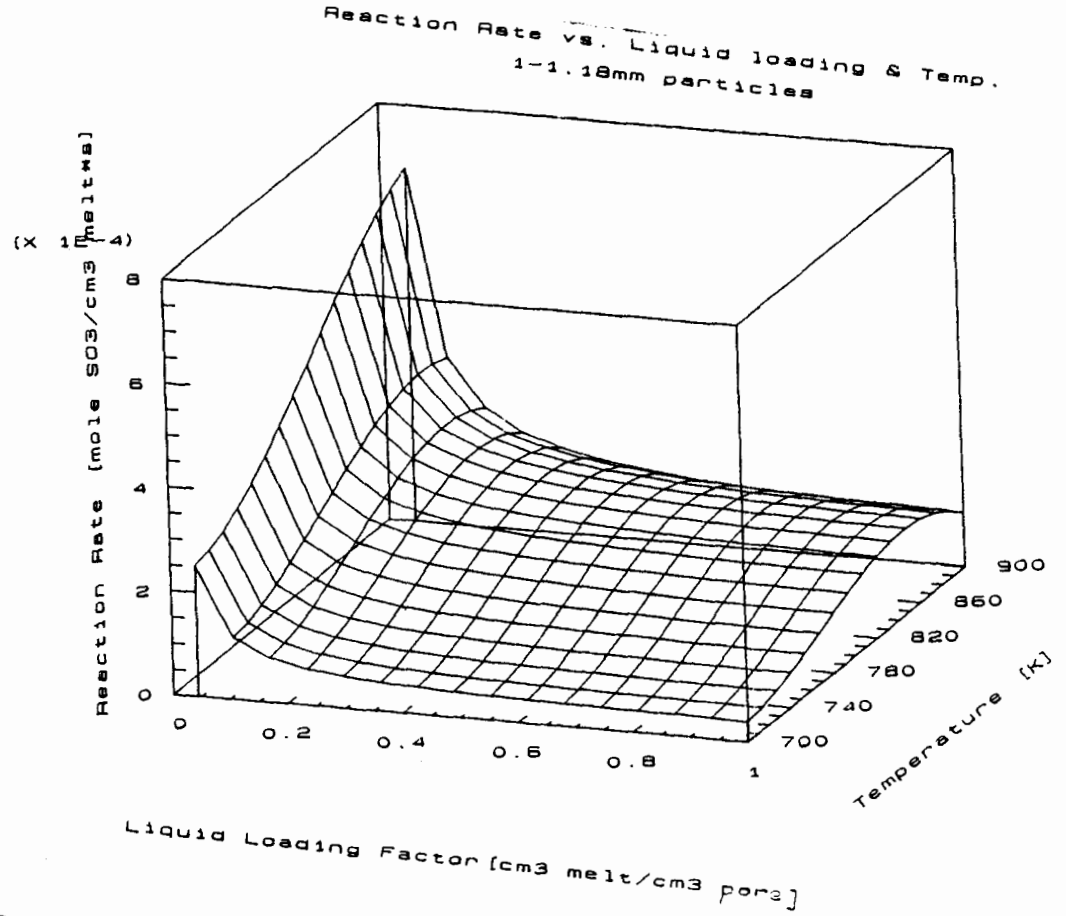

Figuur 43. : Reaction rate per unit volume melt versus temperature and liquid loading at constant melt composition. Catalyst size 1-1,18mm.

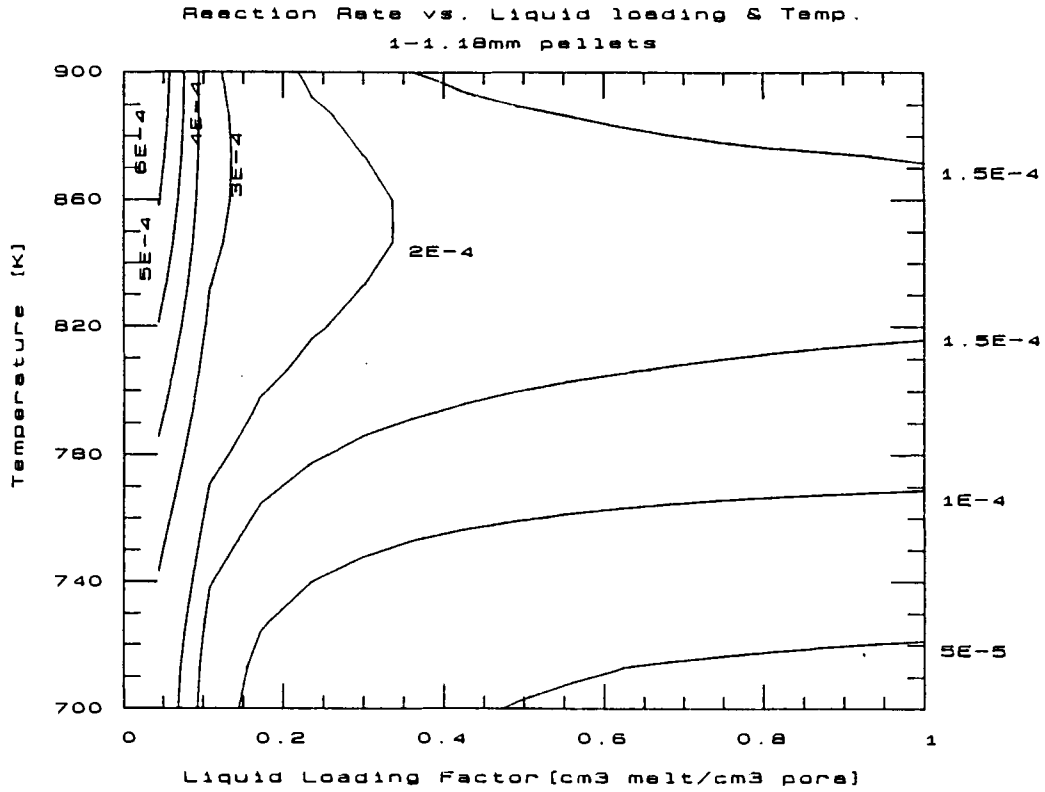

Figure 44. : Contour plot of reaction per unit volume melt versus temperature and liquid loading.

Liquid effectiveness factor, η_L

The liquid effectiveness factor calculations were based on the assumption that the catalyst formulation with very low liquid loading of 0,00015 mole catalyst/g celite revealed intrinsic rates, Equation (34). The liquid effectiveness factor at each temperature level and liquid loading is the actual observed reaction rate divided by the intrinsic reaction rate (0,00015 mole catalyst/g celiter base case). An acceptable plane fit with a R-squared of 0,89 was fitted through the data. (See appendix C7.1-C7.3). From figure (45) it is clear that the liquid effectiveness factor is highly dependant on liquid loading and only slightly dependent on temperature. This observation is in agreement with the findings of Neth **et al.** (1980: 95). The slight decrease of η_L with temperature can be attributed to viscosity changes with temperature. To simplify the calculations from here on, η_L will be assumed to be only a function of the liquid loading factor and the average value at each liquid loading will be used (figure 46).

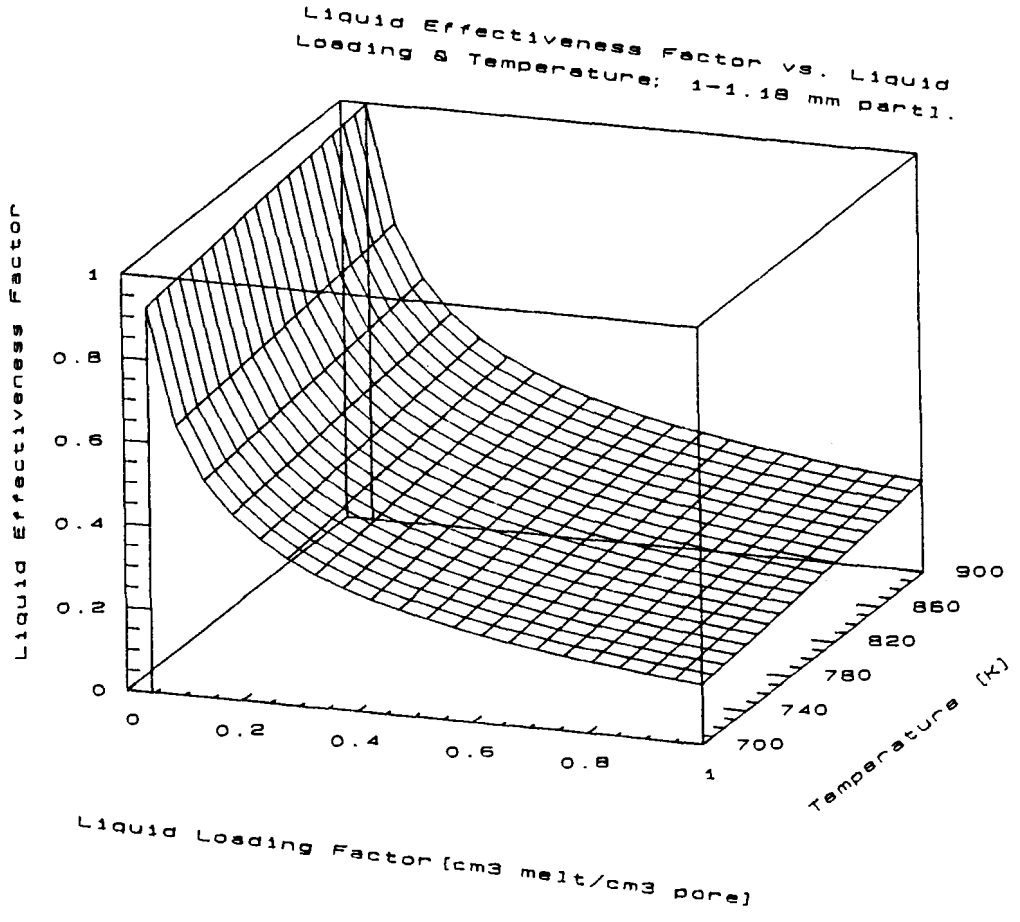

Figure 45. : Liquid effectiveness factor vs. liquid loading and temperature for 1-1,18 mm particels using the 0,00015 mole catalyst/g celite sample as reference basis.

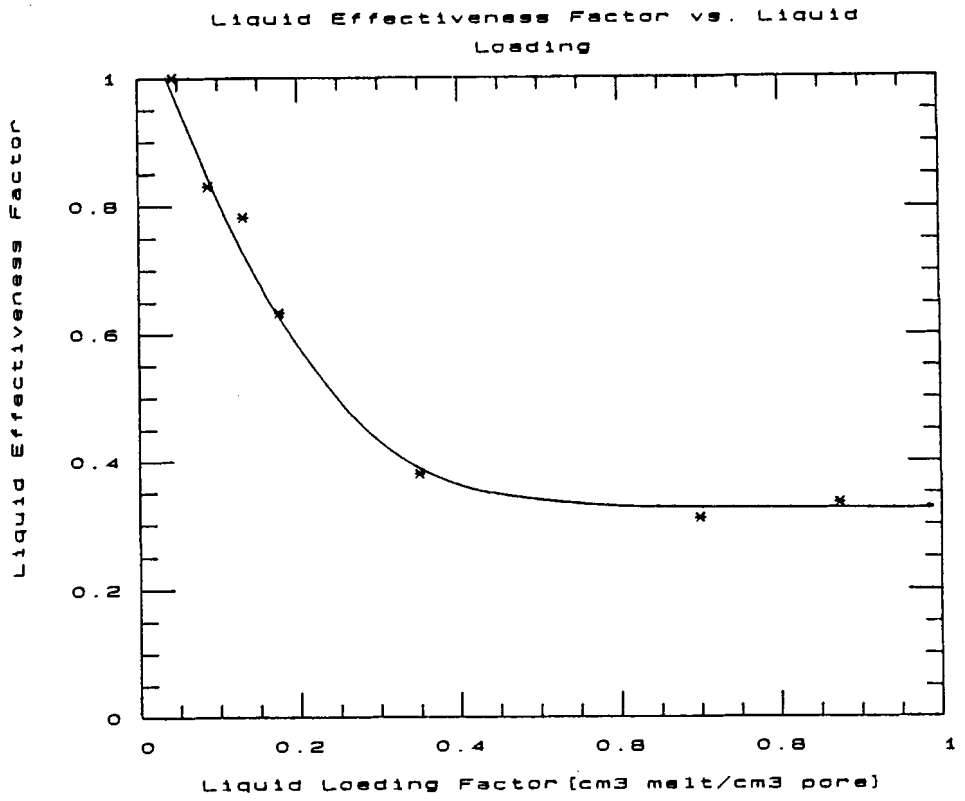

Figure 46. : Average liquid effectiveness factor vs. liquid loading factor for 1-1,18mm particles using the 0,00015 mole catalyst/g celite sample as reference basis.

Liquid effectiveness factor η_L, Thiele Modulus, ϕ_L, relationship

The Thiele modulus was determined by a regression fit at fixed values for the coefficients, H_{O_2} and $D_{O_2,eff}$ in equation (38) at each temperature level (Appendix B4). These calculations were based on the assumption that η_L is independent of temperature. In figure (52) the experimentally determined average η_L is plotted against the Thiele modulus ϕ_L.

Liquid distribution, δ

The mean thickness of the melt was calculated from the experimental data by rearranging equation (38) and by substituting equations (40) - (43). If the liquid effectiveness factor is plotted against the experimentally calculated mean melt thickness (figure 47) the same trend is observed as in figure (46) which gives rise to the idea that there must be a linear relationship between the mean melt thickness and liquid loading factor.

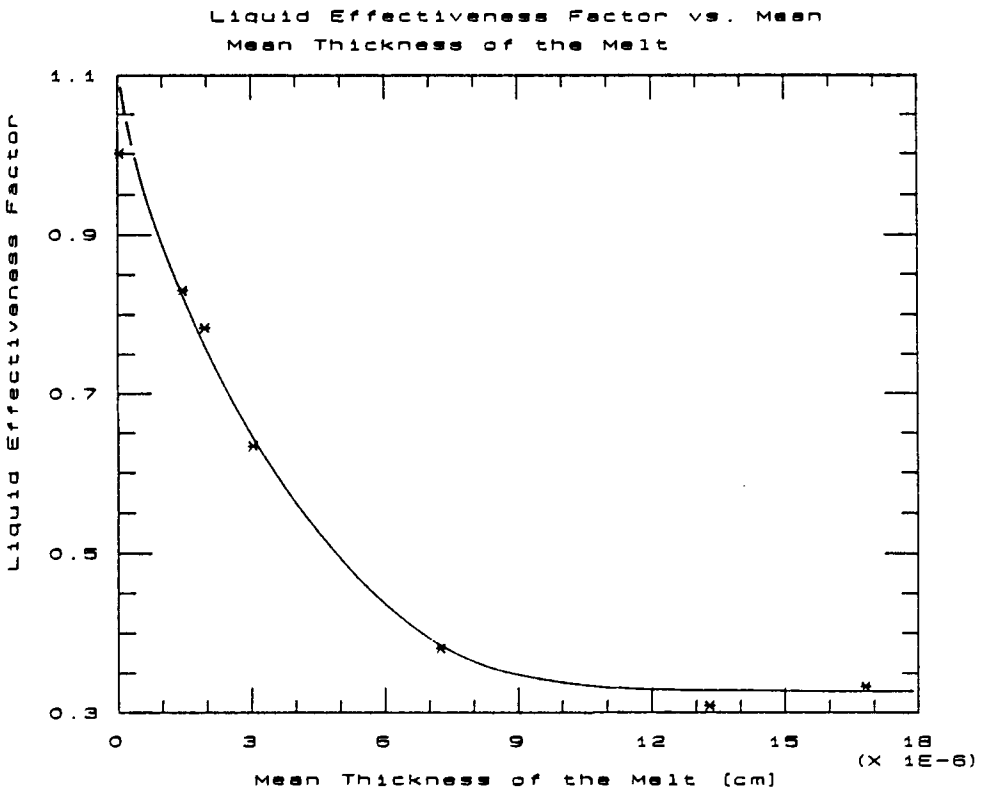

Figure 47. : Liquid effectiveness factor vs. the mean melt thickness for 1-1,18mm particles.

This was the case and from figure (48) it is clear that the mean melt thickness is proportional to the liquid loading within experimental error which is in agreement with the simplified liquid distribution model (Equation 5); the slope $s = 2{,}1 \times 10^{5}$. In figure (49) and (50) the experimentally determined δ is plotted together with the uniform liquid film - and dispersed liquid plug model. The experimental δ is in close agreement with the uniform liquid distribution model at liquid loadings up to $\pm 0{,}6 cm^3$ melt $/cm^3$ pores.

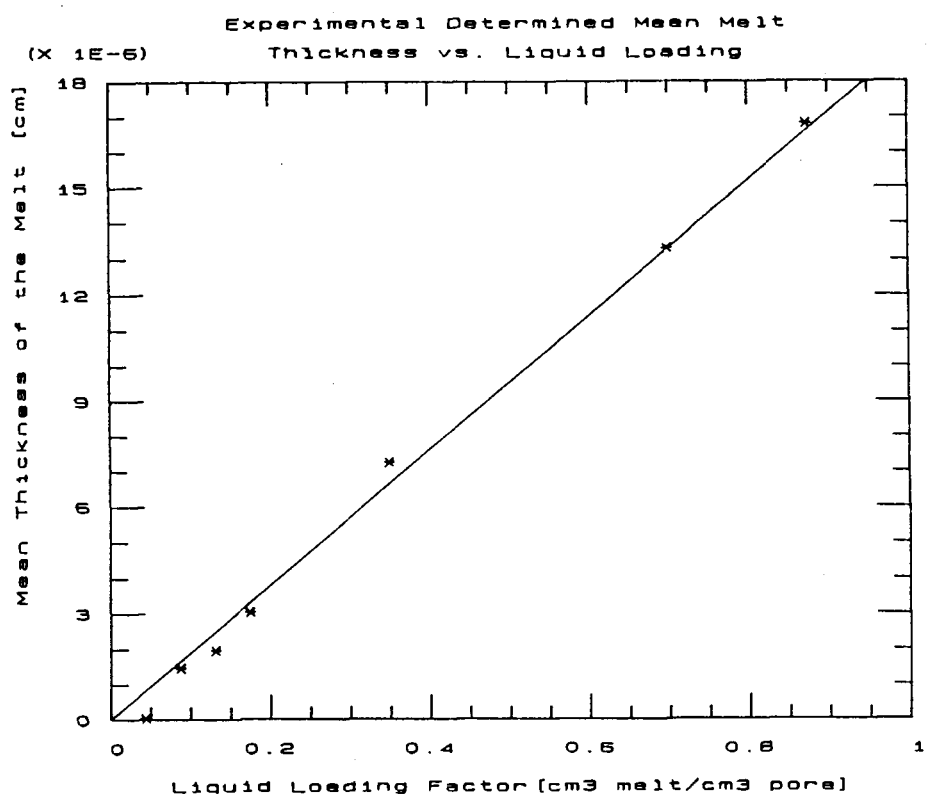

Figure 48. : Experimentally calculated mean melt thickness vs. liquid loading factor.

At very **high liquid loadings** the experimental δ deviates from the uniform model, most likely because of the **formation of liquid clusters.**

Influence of liquid loading, η_L, on activation energy

The observed activation energy was calculated from the slope of the Arrhenius plot of the experimentally determined rate constants (Appendix B4). It can be seen from figure (51) that there is a substantial drop in activation energy as the liquid loading increases.

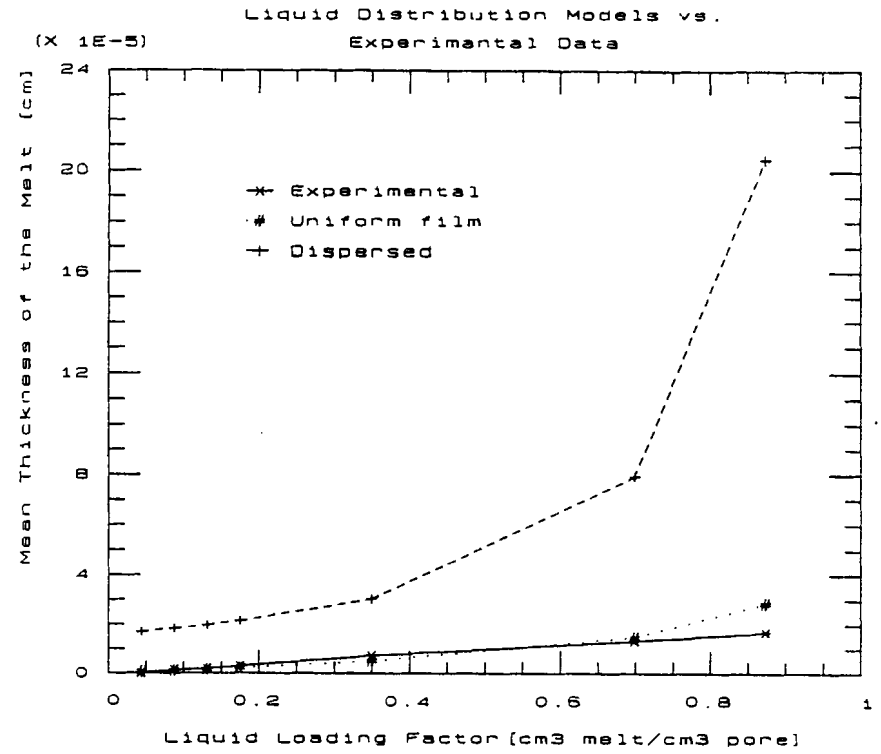

Figure 49. : Comparison between the experimentally determined liquid melt thickness, the uniform film - and dispersed plug model.

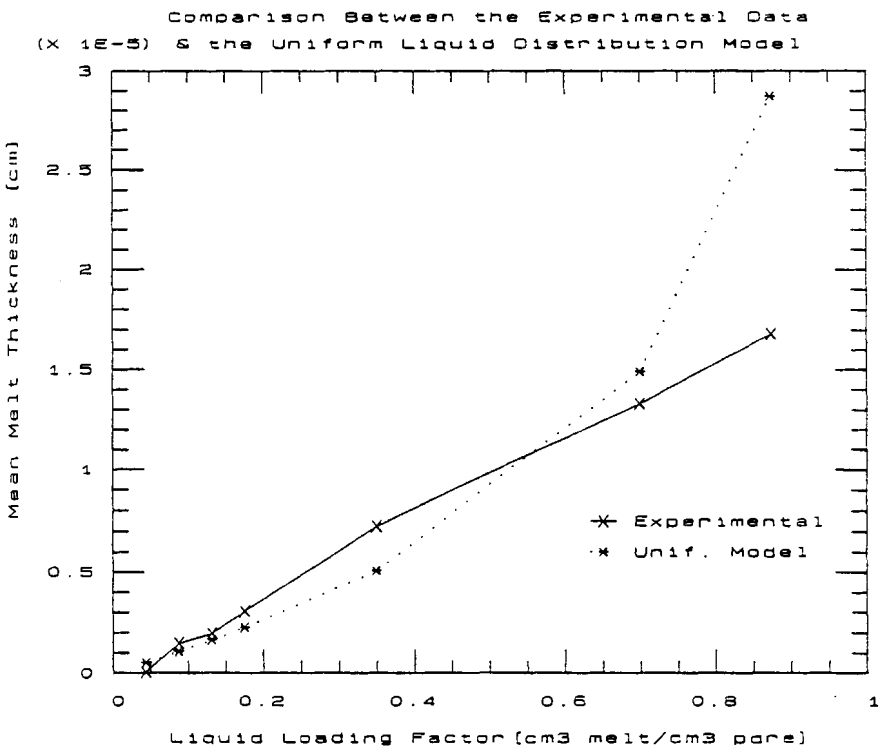

Figure 50. : Comparison between experimental data and the uniform model.

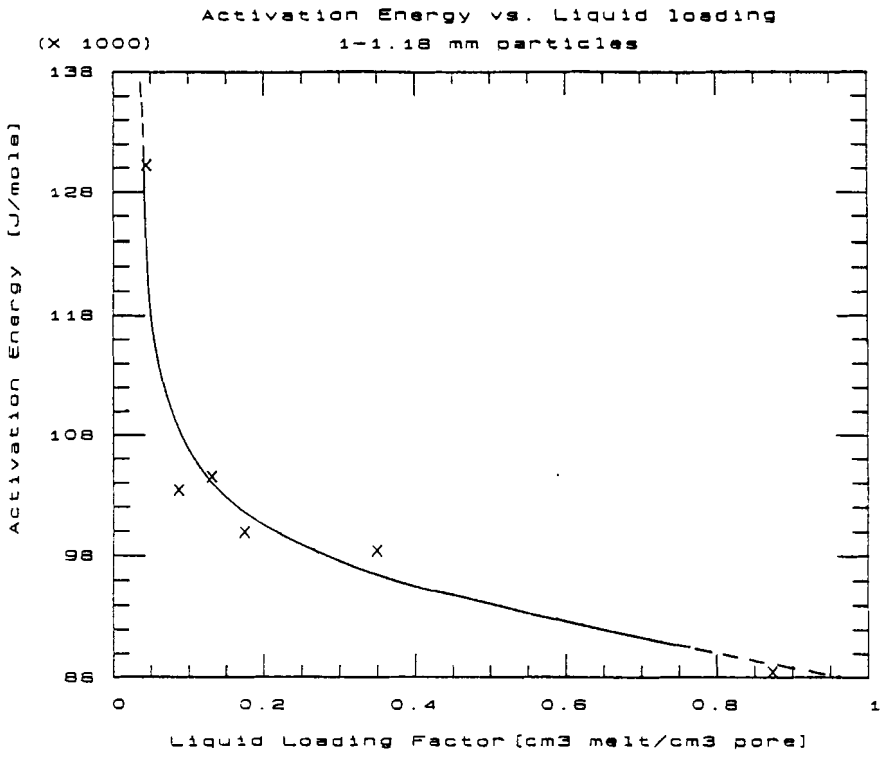

Figure 51. : Activation energy vs. liquid loading factor.

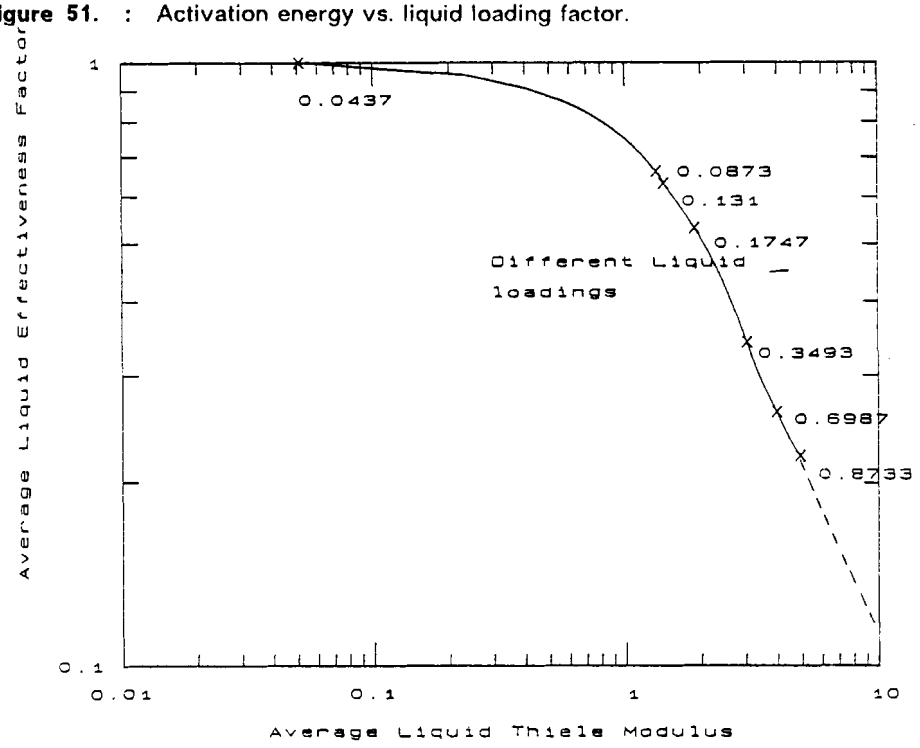

Figure 52. : Liquid effectiveness factor vs. Thiele modulus for different liquid loading factors.

Physical properties as influenced by liquid loading

Since reaction rates in SLP systems depend on liquid dispersion in the pores and internal surface areas of the exposed liquid/gas interface, measurements such as internal surface

area, pore volume were conducted. These experiments were intended to give better insight in the nature of how the liquid is distributed.

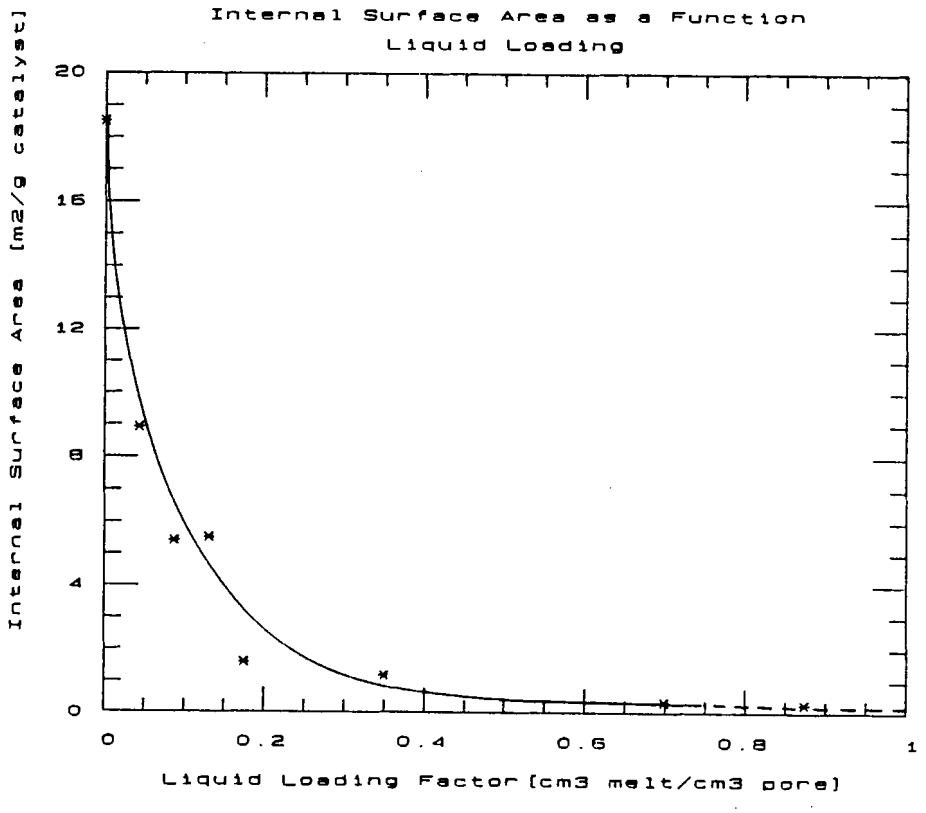

Figure 53. : Internal surface area as a function of the liquid loading factor.

The internal surface area shows a considerable drop when the liquid loading is increased from 0 to 0,2 cm^3 melt /cm^3 pore volume. Beyond 0,4 cm^3 melt /cm^3 pore the internal surface area is very low and gradually drops towards zero.

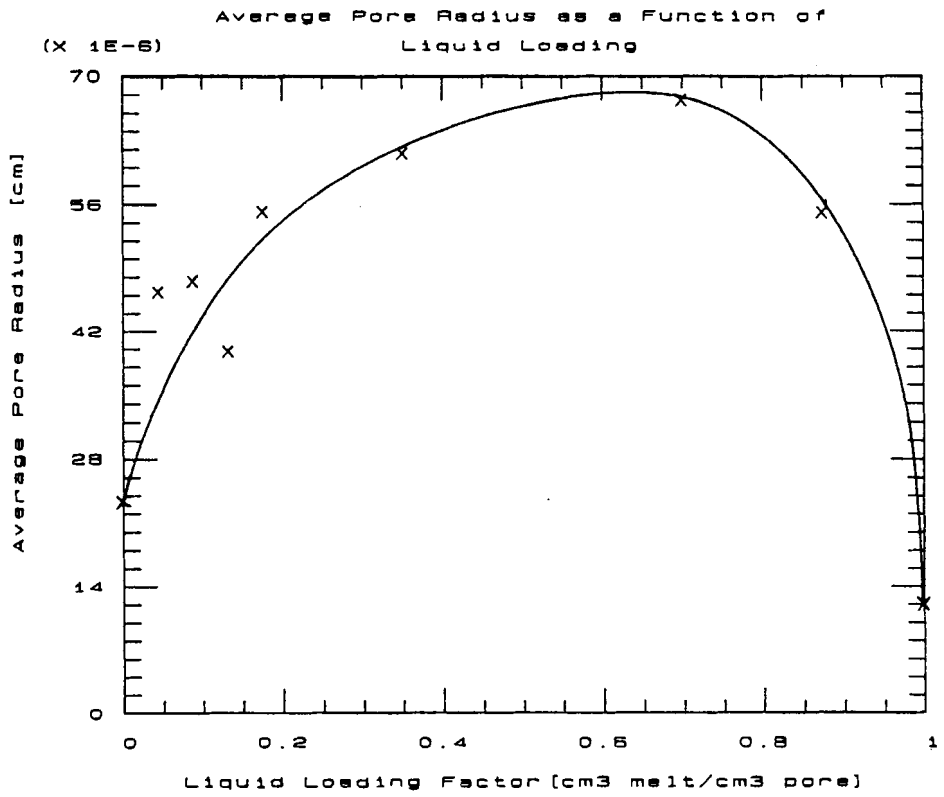

Figure 54. : Average pore radius as a function of liquid loading.

The pore volumes and pore size distributions were measured by a high pressure mercury porometer. The weighted average pore radius is calculated in Appendix B6. At low liquid loadings the average pore radius is small, but the average pore radius increases with increasing liquid loadings up to about 0,6 cm^3 melt $/cm^3$ pore whereafter it declined drastically.

Figure (55) shows that the pore volume drops rapidly and then levels off when the liquid loading is increased. At very high liquid loadings the pore volume suddenly drops to zero.

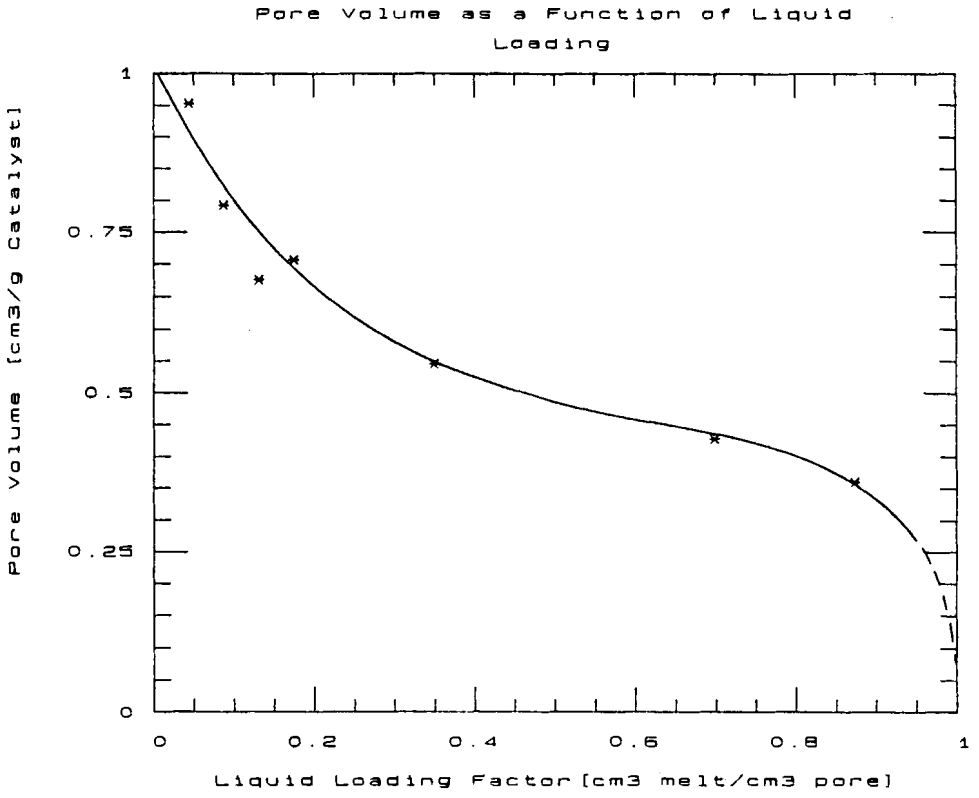

Figure 55. : Pore volume vs. liquid loading factor.

Discussion

High reaction rates per unit volume melt are observed at very low, liquid loadings as seen in figure (43) and (44). This is because the reaction is unhindered by diffusion and takes place as a homogeneous catalytic reaction throughout the liquid phase. When the liquid loading is increased, the rate per unit volume active melt drops dramatically due to liquid phase diffusion resistance. At higher liquid loadings, α, only a small portion of the liquid film is effectively used since the reaction zone is very thin; $\pm 9 \times 10^{-7}$ cm according to Holroyd & Kenney (1971: 1963). Figure (45) illustrates this phenomenon that only a thin surface layer is effective during reaction since the liquid effectiveness factor is highly dependent on liquid loading. The liquid effectiveness factor, η_L, is only slightly dependent on temperature in the range 400°C to 600°C. This is most likely attributable to viscosity changes of the melt with temperature.

At very low liquid loadings ($0 - 0{,}2 cm^2$ melt $/cm^3$ pore) the oxidation rate is indirectly proportional to the liquid volume. This is the linear part of figures (46) and (47). In this range of α the reaction rate is primarily a homogeneous reaction in the liquid phase. With increasing

liquid loading the effectiveness factor decreases until it finally becomes proportional to the surface area of the melt.

The mean thickness of the melt calculated from the experimental data is proportional to the liquid loading factor α. For values less than $0{,}6 cm^3$ melt $/cm^3$ pore the measured liquid melt thickness behaves like the uniform film distribution model. In this range the average measured mean melt thickness is less than half the mean pore radius of the support material ($r_p = 2{,}34 \times 10^{-5}$ cm). For liquid loadings above $0{,}6 cm^3$ melt $/cm^3$ pore the mean melt thickness is larger than half the mean pore radius. In this liquid loading region the liquid can reduce the gas/liquid surface area further by coalescence to clusters which form continuous liquid regions that are larger than the pore dimensions. It can be concluded that the **liquid distribution can change with liquid loading and pore size distribution.**

The drop in the apparent activation energy is due to liquid phase diffusion effects. It can be explained as follows: Taking logs and differentiating with respect to temperature and noting that both the reaction rate and to a lesser extent the diffusional process are temperature dependent gives

$$\frac{d(\ln k_{i,obs})}{dT} = \frac{1}{2}\left[\frac{d(\ln k_i)}{dT} + \frac{d(\ln D_i)}{dT}\right]$$

where $k_{i,obs}$ = observed rate constant
k_i = intrinsic rate constant
D_i = Diffusion coefficient

with Arrhenius temperature dependencies for both reaction and diffusion we have

$$k_i = k_{i,o} e^{-E_{true}/RT}$$

and

$$D_i = D_{i,o} e^{-E_{diff}/RT}$$

With

E_{true} = Activation energy of the reaction alone
E_{obs} = Observed activation energy
E_{diff} = Activation energy due to diffusion alone

Substituting these equations give

$$E_{obs} = \frac{E_{true} + E_{diff}}{2}$$

Since E_{diff} for liquid diffusion in the ionic molten salt melt is usually about 3 times smaller than E_{true} (Gay **et al.**, 1983: vol. 2) the observed activation energy if influenced by strong pore diffusion is roughly:

$$E_{obs} \simeq \frac{E_{true} + E_{true}/3}{2}$$
$$\simeq \frac{2}{3} E_{true}$$

This can explain the drop in activation energy from 130 J/mole to ± 88 J/mole with increasing liquid loading.

From the liquid effectiveness factor η_L versus Thiele modulus plot (figure 52) it is concluded that from a liquid loading of 0,087 cm^3 melt $/cm^3$ pore upwards the reaction rate is strongly influenced by liquid phase diffusion. From the profile of the effectiveness factor, Thiele modulus plot it can be deduced that the liquid film is isothermal because η_L is always less than unity. This is probably because of the high thermal conductivity of the liquid film and carrier matrix.

The substantial drop in internal surface area (figure 53) with increasing liquid loading is attributable to the tendency of the liquid to minimize the high energy gas/liquid surface area and maximize the low energy liquid/solid surface area. The liquid is drawn into the smaller pores first because most of the infernal surface area is associated with the smaller pores. This can be seen in figure (54) where the average pore radius is small at low liquid loadings and gradually increase as the liquid loading mounts towards $0,6cm^3$ melt $/cm^3$ pore. From this liquid loading upwards liquid cluster formation causes a drop in average pore radius down to zero when the whole pore matrix is filled with liquid. Figure (55) also confirms this where the initial drop in pore volume arises from the filling of the small pores and the formation of liquid films on the walls of the larger pores. This is the case up to a liquid loading of $\pm 0,6cm^3$ pore $/cm^3$ melt from whereon the formation of liquid clusters results in the sudden drop in pore volume.

4.2.3 Influence on the gas phase and overall transport resistance

The combined effect of liquid loading on the liquid phase and gas phase transport resistance was determined simultaneously using 6 mm diameter catalyst pellets with the same constant composition and levels of liquid loadings as in the previous chapter. These pellets were tested at 550°C. The results and calculations are given in Appendix B5.

Reaction rate as influenced by liquid loading

Here the focus is on reaction rate and the way it is influenced by both liquid- and gas phase diffusion. The reaction rate can either be expressed in terms of *mole* SO_3 formed per unit volume liquid or per unit mass. The reaction rate per unit volume melt drops rapidly as the liquid loading is increased up to 0,2cm^3/ melt /cm^3 (figure 56).

For higher liquid loadings the reaction rate asymptotically levels off.

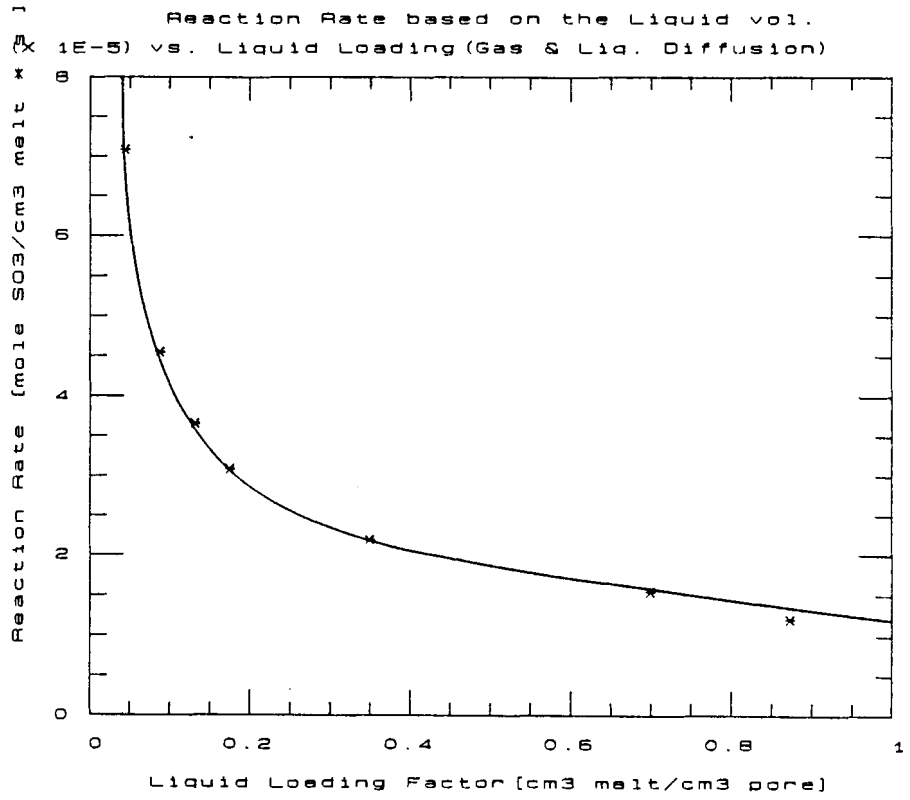

Figure 56. : Reaction rate per unit volume melt vs. liquid loading at 550°C 6mm pellets.

The reaction rate per unit pellet mass has an optimum at about 0,25cm^3/ melt cm^3 pore liquid loading (figure 57). This is in agreement with the results of Livbjerg **et al.** (1976: 223) at similar average pore sizes.

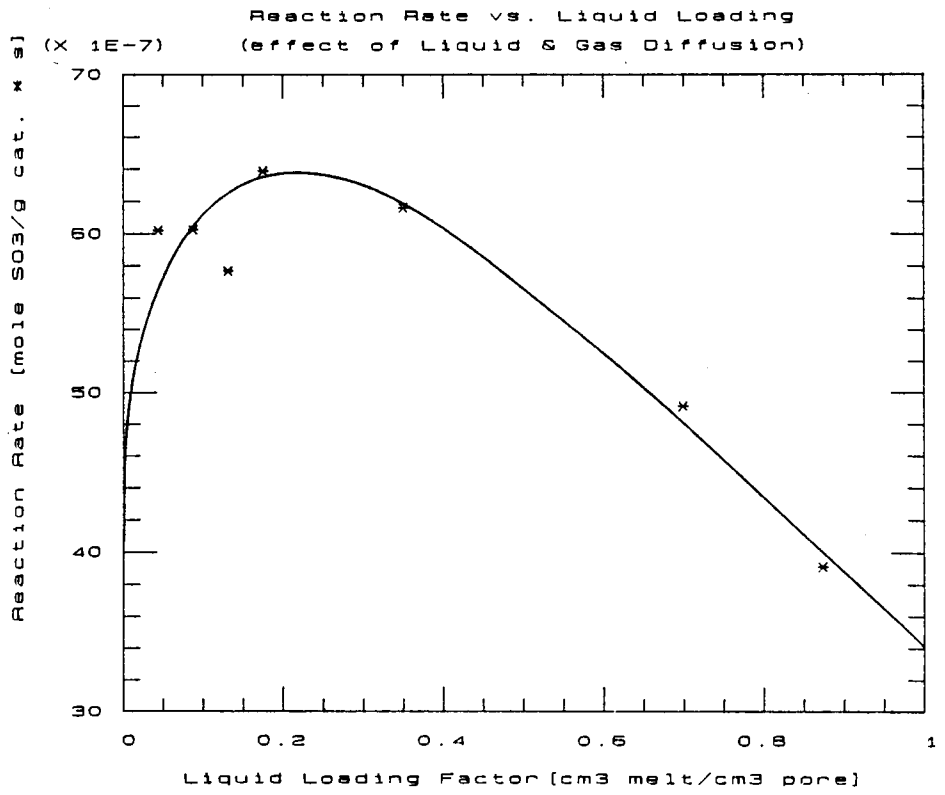

Figure 57. : Reaction rate per unit mass vs. liquid loading at 550°C with 6mm pellets.

The observed rate constant as a function of liquid loading shows an optimum of about 0,3cm^3 melt /cm^3 pore (figure 58). At very low liquid loadings the rate constant is proportional to the mean melt thickness as seen in figure (59).

Effectiveness factors as influenced by liquid loading

The gas phase effectiveness factor can be separated from the overall effectiveness factor. This is done by division with the liquid phase effectiveness factor. Equation (56) divided by Equation (45). See Appendix B5.

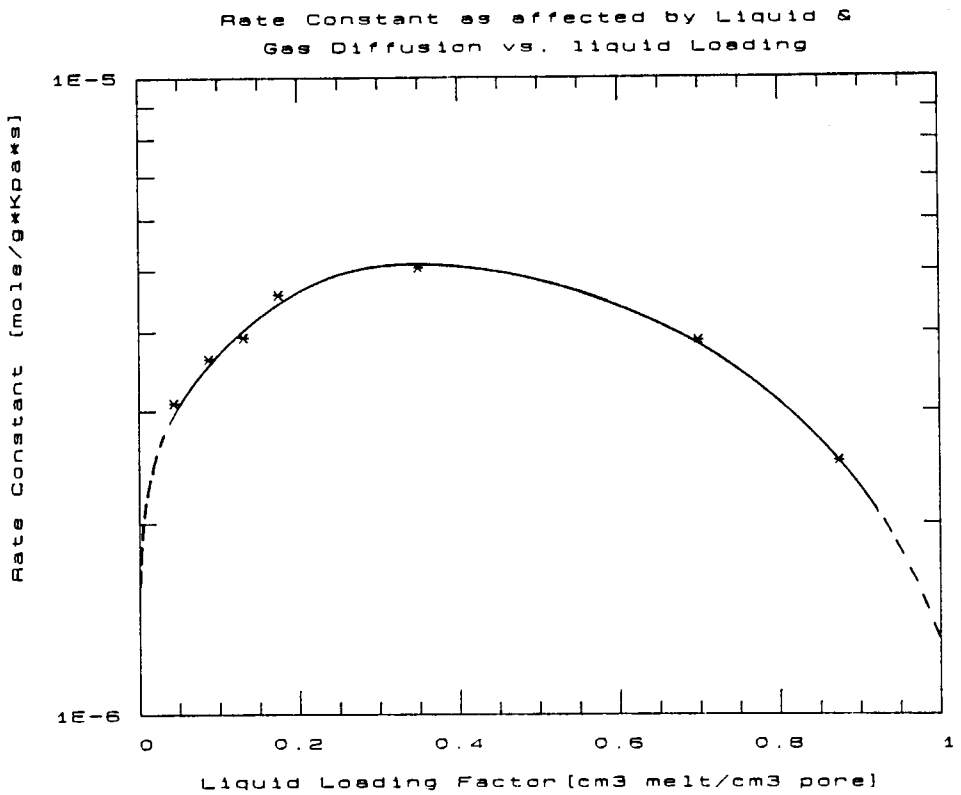

Figure 58. : Observed rate constant vs. liquid loading. Calculated from rate data at 550°C using 6mm pellets.

The overall effectiveness factor was obtained for each level of liquid loading using the same reference formulation i.e. 0,0005*mole* catalyst/g celite crushed to 1-1,18mm size. The gas and liquid effectiveness factor of the reference sample was assumed to be unity.

Figure (60) suggests an independence of the gas phase effectiveness factor to liquid loading over a wide range of liquid loadings. It declines rapidly only at very high liquid loadings.

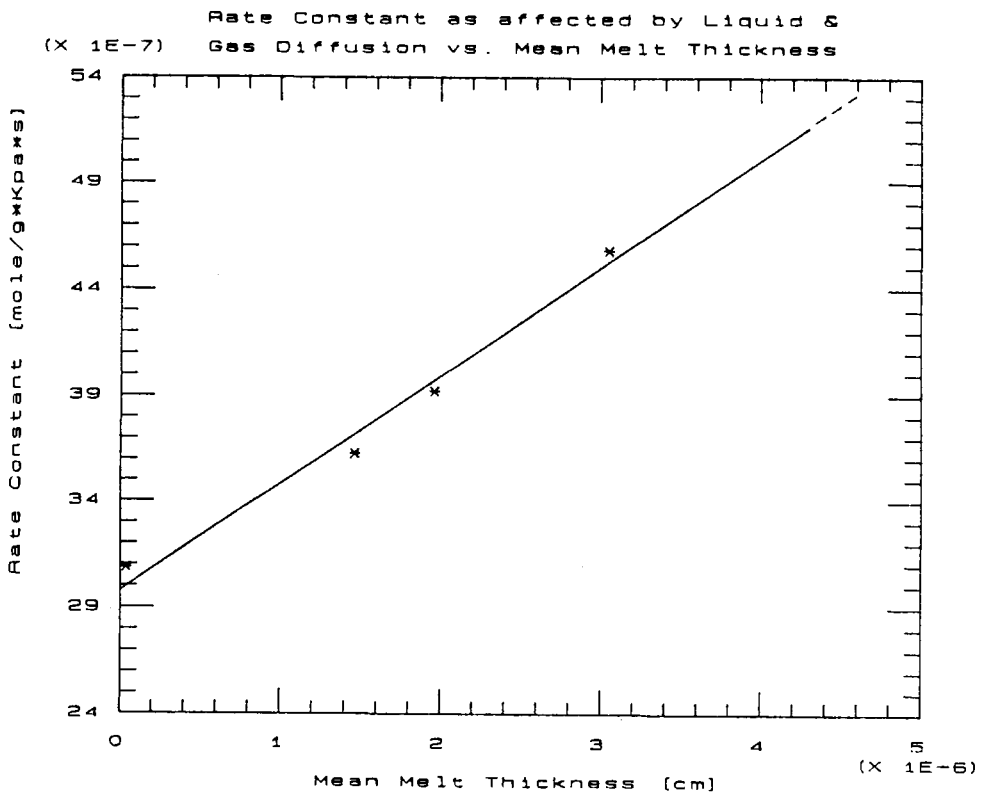

Figuur 59. : Observed rate constant at low liquid loadings as a function of the mean thickness of the melt.

In figure (61) the individual contribution of liquid and gas phase diffusion can be seen. The overall effectiveness factor is primarily influenced by liquid phase diffusion at low liquid loadings, wheres at high liquid loadings it is principally dependent on the gas pore diffusion.

Figure (62) shows the relationship between that part of the rate equation (equation 56) which depends on the liquid loading i.e. α, η_L and η_G versus the liquid loading factor. At temperatures close to 550°C there is not much improvement when α is increased from 0,3 to 0,8cm^3 melt /cm^3 pore . In industrial catalysts the optimum liquid loading, α is usually close to 0,3cm^3 melt /cm^3 pore (Neth **et al.**, 1980: 53).

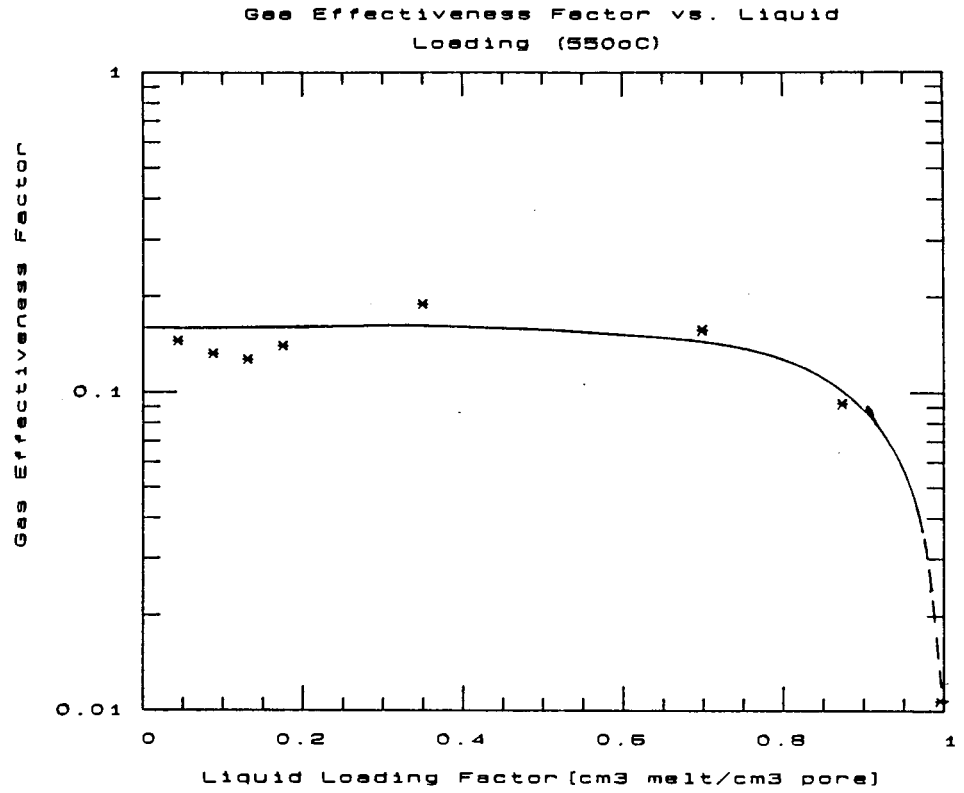

Figure 60. : Gas phase effectiveness factor as a function of liquid loading at 550°C using 6mm pellets.

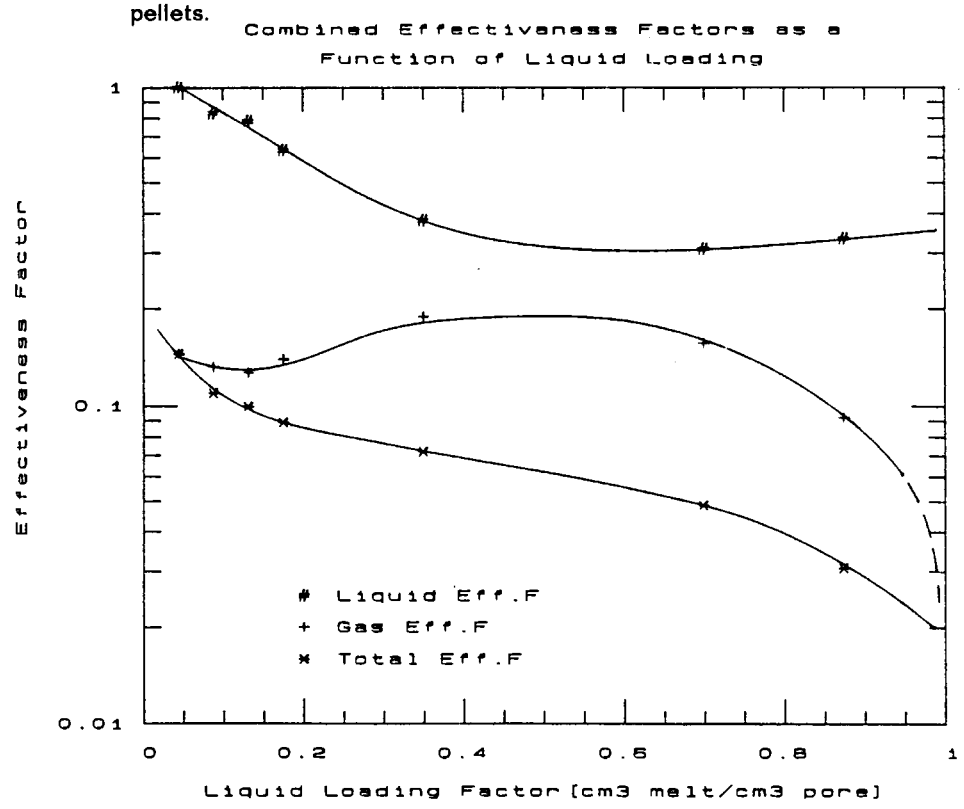

Figure 61. : Liquid-, gas- and overall effectiveness factor vs. liquid loading.

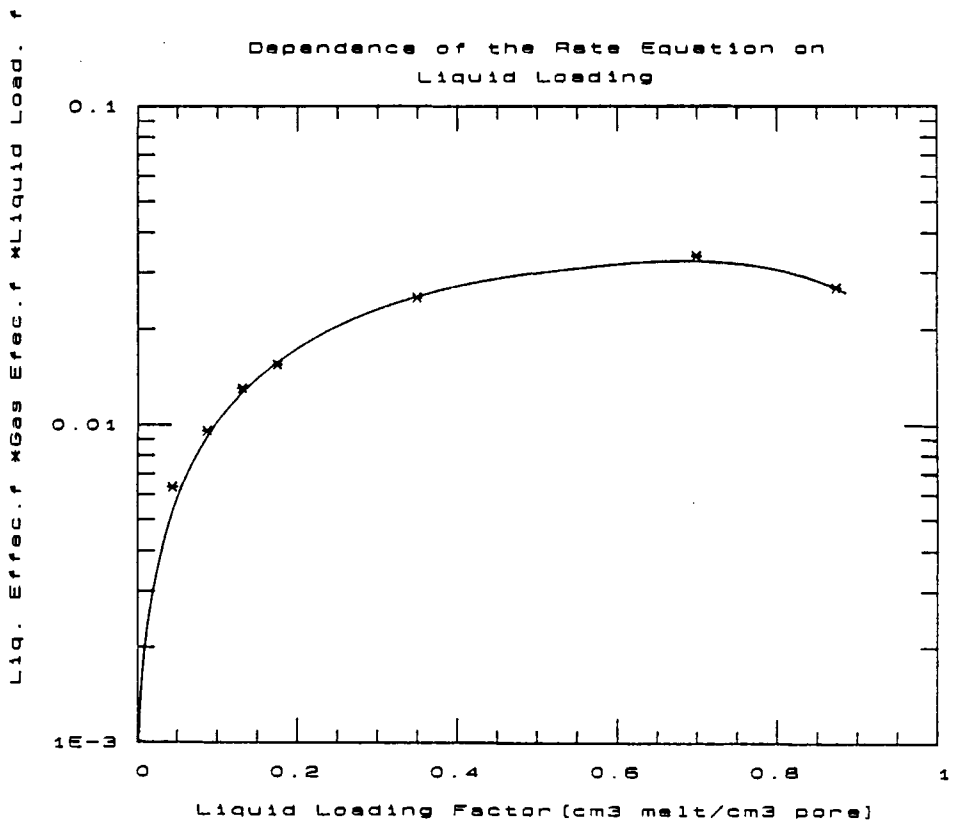

Figuur 62. : Relationship between the product $\alpha.\eta_L.\eta_G$ and liquid loading factor at a temperature of 550°C.

Discussion

An optimal liquid loading for a given pore structure is due to

- High liquid loadings lead to a gradual disappearance of the residual pore system and increasing pore gas phase diffusion. This can be seen in figure (60) where the gas phase effectiveness factor drops rapidly for liquid loadings above $\alpha = 0{,}8 cm^3$ melt/cm^3 pore.
- At liquid loadings of up to $0{,}4 cm^3$/ melt /cm^3 pore the reaction rate is sensitive to liquid loading while the pore diffusion remains relatively constant (figure 47 & 60).
- At very low liquid loadings the reaction rate, expressed per unit mass of catalyst and carrier matrix, is proportional to the volume or thickness of active melt. In other words the number of active sites present, because the melt is still extensively utilized in this region (see figure 59). The liquid phase effectiveness is still reasonably high in this region (figure 61).

- The change in liquid distribution from a uniform distribution to cluster formation also contributes to the drop in reaction rate at high liquid loadings.

The deduction from figure (61) is that the principle diffusion restriction, for the pore structure used in this study, is residual pore gas phase diffusion, and it remains almost constant for liquid loadings up to $0{,}8cm^3$ melt $/cm^3$ pore . The liquid effectiveness in this region drops rapidly and levels off at a liquid loading of about 0,6 upwards.

The controlling diffusion resistance is highly dependent on the pore structure and pore size distribution and it can easily become liquid phase diffusion controlled if a carrier matrix with slightly larger pores is used and vice versa.

The pore structure and pore size distribution was kept constant in this study. It can be concluded that the optimal liquid loading for a given pore size distribution occurs where the diffusion resistance is evenly divided between liquid phase diffusion and pore diffusion. In this case it is relatively insensitive to the pore structure because of a bimodal pore distribution. With all factors taken into account, the optimal liquid loading is at about $0{,}3cm^3$ melt $/cm^3$ pores for the carrier matrix, and is in agreement with other studies (Livbjerg **et al.**, 1976: 198 and Neth **et al.**, 1980: 53) using similar pore structures.

4.2.4 Direct observation of catalyst sample by scanning electron microscopy (SEM)

In this section the rapidly cooled catalysts were studied at room temperature by means of a scanning electron microscope (SEM) which gives an independent and more direct characterization of the active component.

In the first part the individual diatom species that were common in the Celite 209 batch used were studied. In the second part the effect of liquid loading on the catalyst distribution was investigated. The catalyst samples at different liquid loadings were exposed to the reaction mixture at 550°C for five hours to ensure that no further liquid migration occurred. After five hours the reactor was shut down and the hot samples quenched in liquid nitrogen. This rapid quenching prevented alternations in the active component dispersion on solidification of the melt, which could be the case if the catalyst was allowed to cool down slowly. The samples were cut in half and the surfaces cleaned with purified compressed nitrogen to remove all the loose debris. The samples were vacuum treated to remove all volatile matter and was coated with carbon vapour.

The next few pages contain SEM photographs of the more common diatomite species in the Celite 209 batch used at different magnifications. The well defined pores of the diatomite species are clearly visible. More SEM microphotographs of diatoms in the Celite 209 batch are shown in Appendix A5.

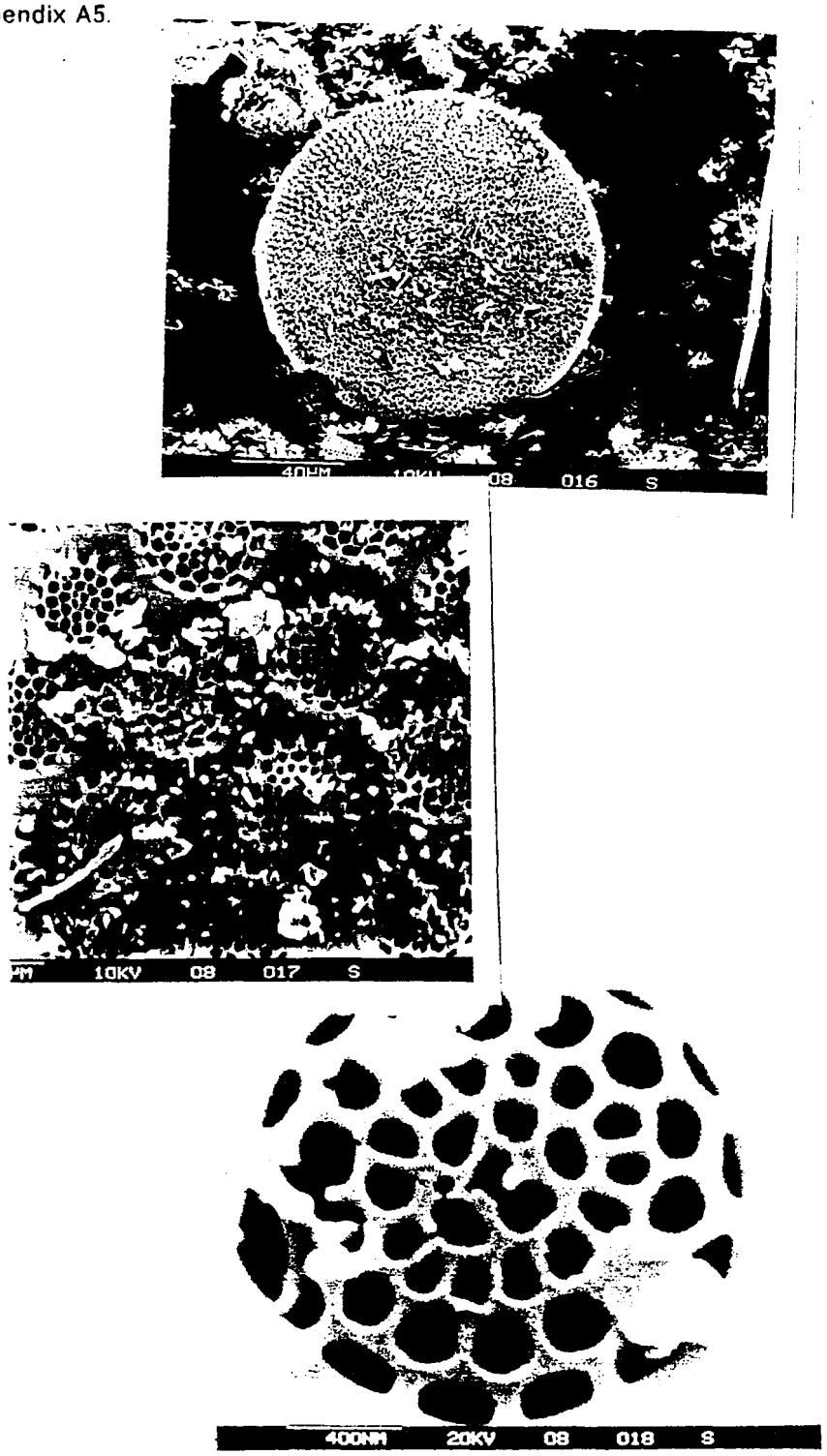

Figure 63. : SEM microphotograph of a typical Pill Box diatom from above, with the pores at different magnifications.

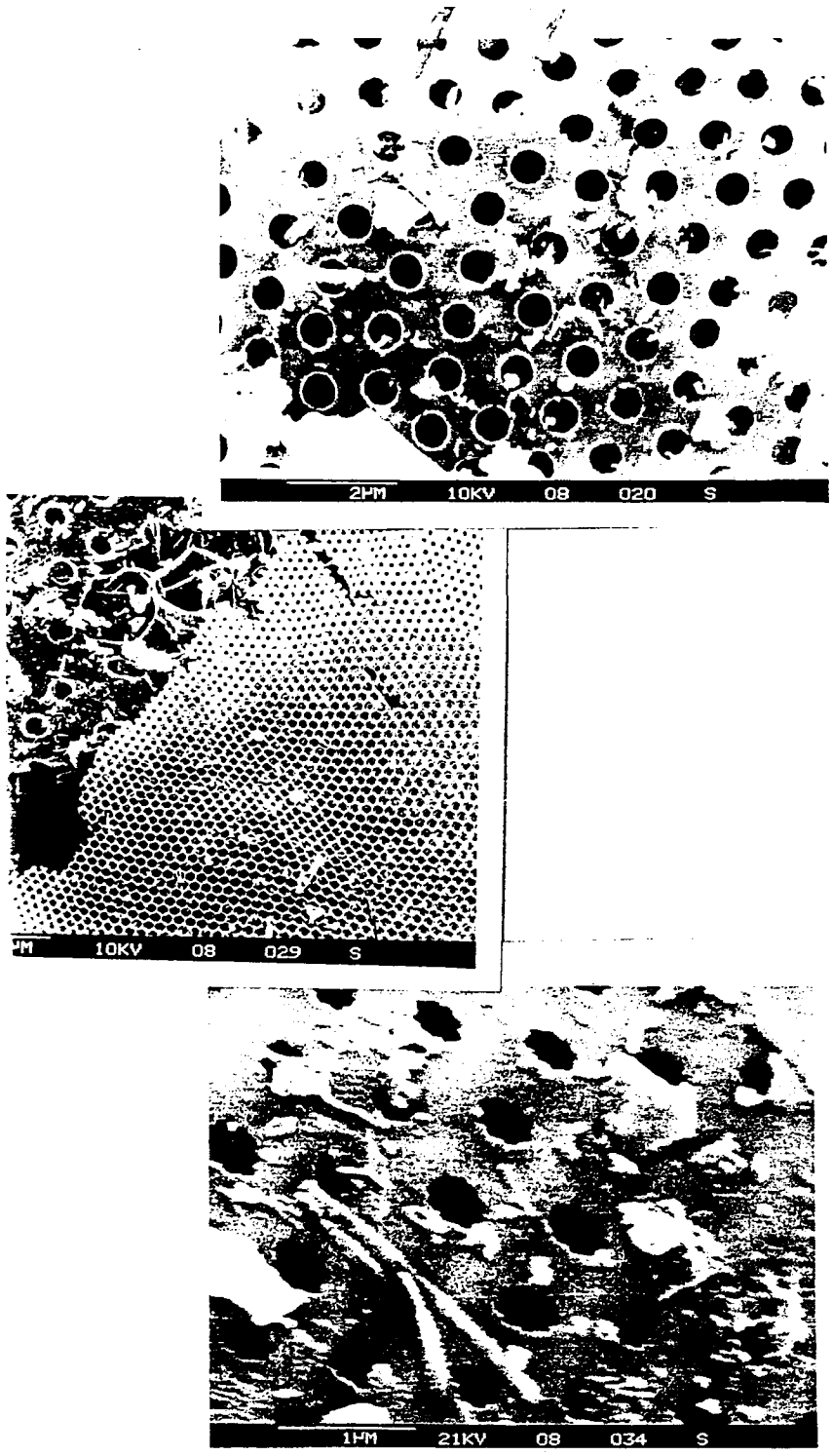

Figure 64. : SEM microphotograph showing typical pore sizes and shapes of Celite 209.

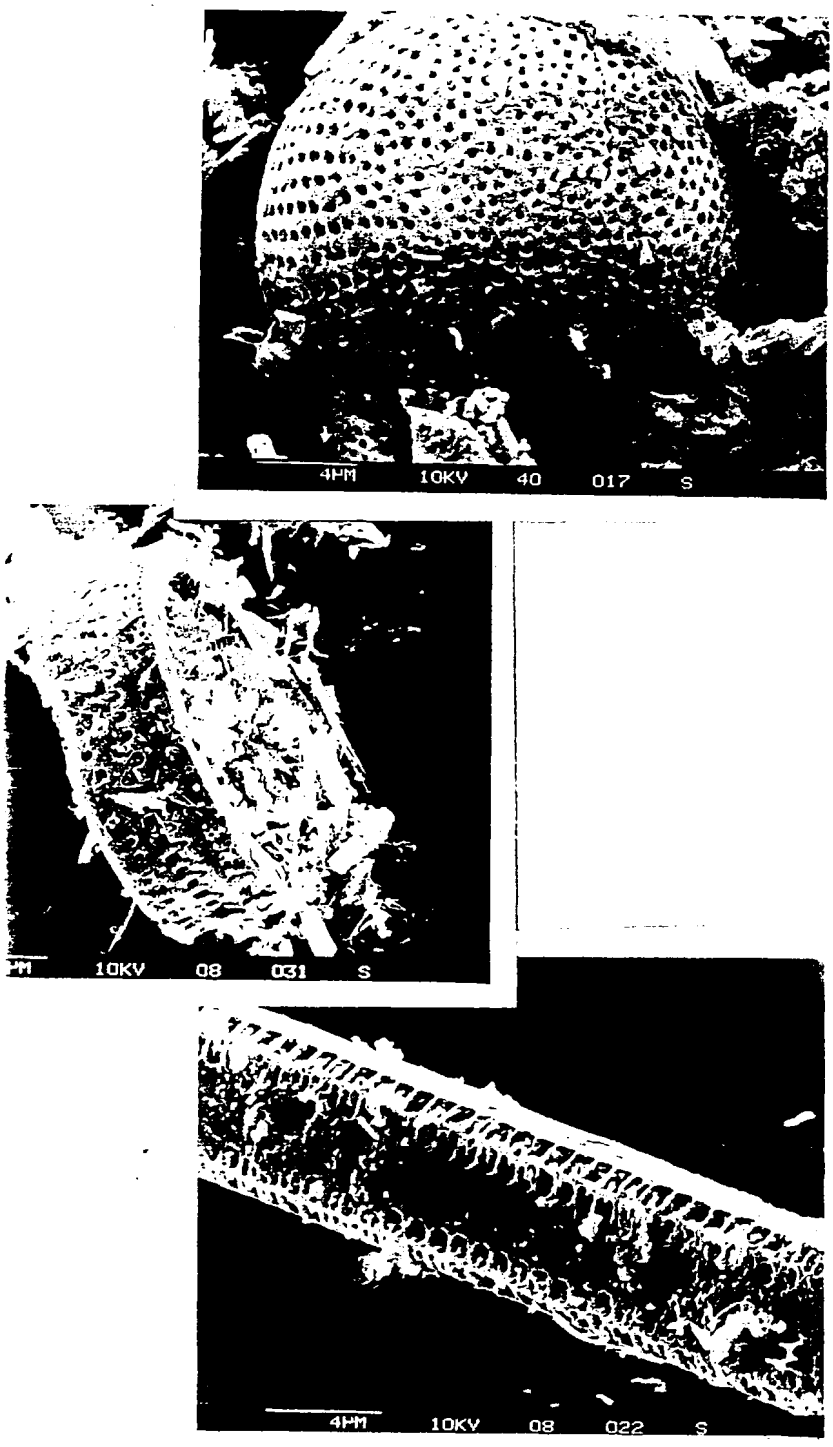

Figure 65. : SEM microphotograph of common diatom shapes in the Celite 209 batch.

In figure (66) the effect of liquid loading at low loadings can be seen. At very low liquid loadings, 0,0005*mole* catalyst/g Celite, the mircopores within the diatom particles are exclusively filled while the outside surface of the diatom particles are free of catalyst melt.

At slightly higher liquid loadings (0,001 and 0,002 mole catalyst/g Celite) the outer surface of the diatoms in the carrier matrix are coated with a thin catalyst film, but the residual gas pore system are still largely unfilled.

Figure (67) and (68) confirm cluster formation at high liquid loadings, $0{,}6cm^3$ melt $/cm^3$ pore . EDAX analyses of Vanadium confirms that the darker regions on the photographs are indeed catalyst clusters. This can clearly be seen in figure (68) where the Vanadium density EDAX analyses are superimposed upon the SEM microphotograph of a cluster.

Discussion

The SEM microphotographs of the diatom particles which are the building blocks of the catalyst matrix give better insight into the geometry of the pore system. The smaller pores of the bidispersed pore structure are primarily the tiny interconnected pores and voids within the diatoms. The larger pores in the pore structure consist mainly of voids between the diatom particles. For this reason the particle size distribution of the diatomite is very important, since a lot of broken diatoms and fines can greatly reduce the residual pore system (RPS).

The SEM microphotographs of rapidly quenched samples confirms the conclusion in the previous section based on rate data that the melt tends to form clusters in the bidispersed pore structure for liquid loadings higher than $0{,}6cm^3$ melt $/cm^3$ pore . EDAX scanner analyses of the observed darker regions in the microphotographs (figures 67 & 68) confirm that the darker areas are indeed catalyst clusters. The cluster size, $\pm 100 - 200\mu m$, greatly exceed the pore dimensions (mean pore radius of the support, $\pm 0{,}25\mu m$.) The size of the clusters depends on the liquid loading and the support pore size distribution (Livbjerg **et al.**, 1976: 229).

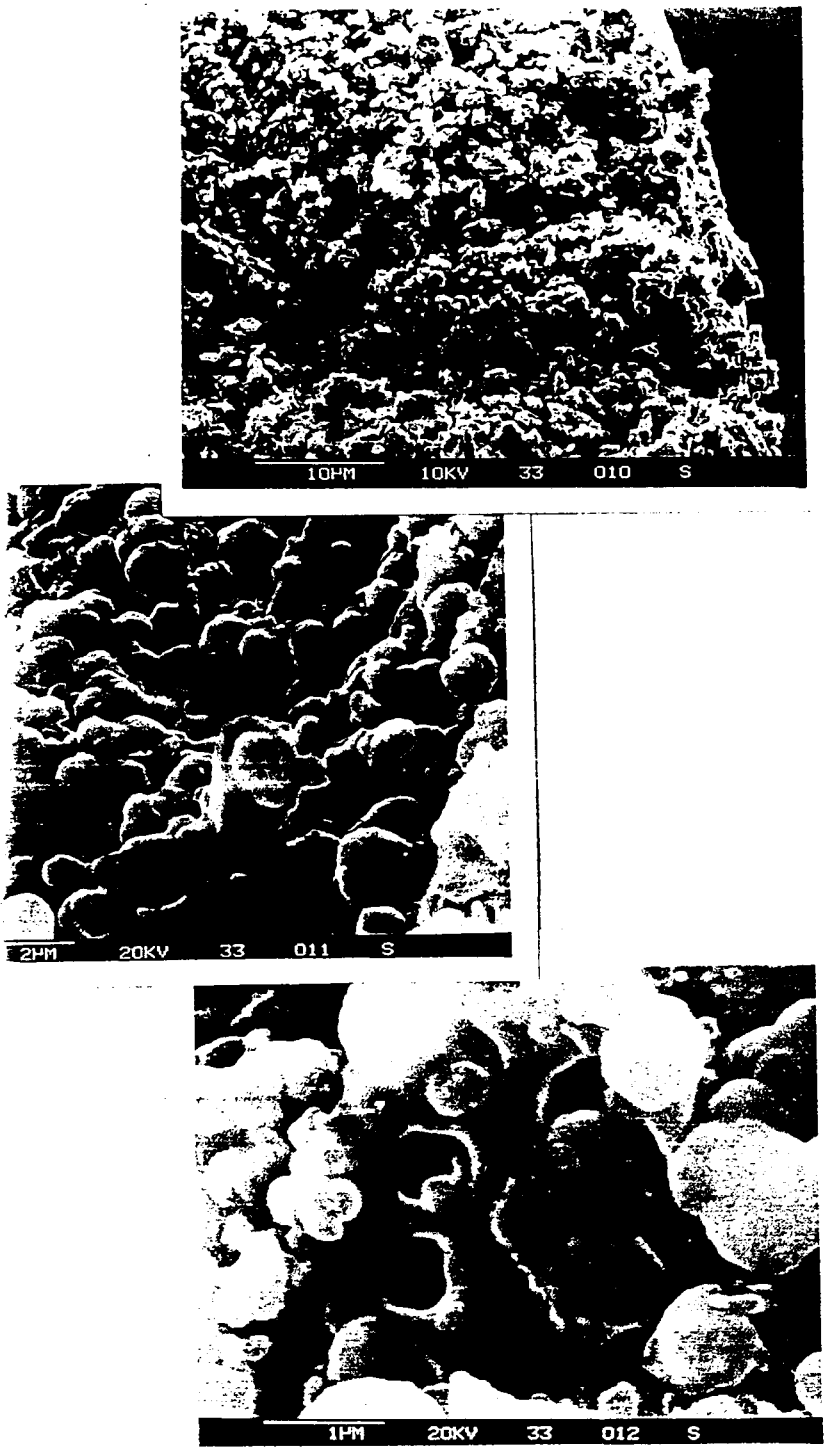

Figure 66. : SEM microphotographs of catalyst samples at different liquid loadings of 0,0005; 0,001; 0,002*mole* catalyst/g Celite from top to bottom.

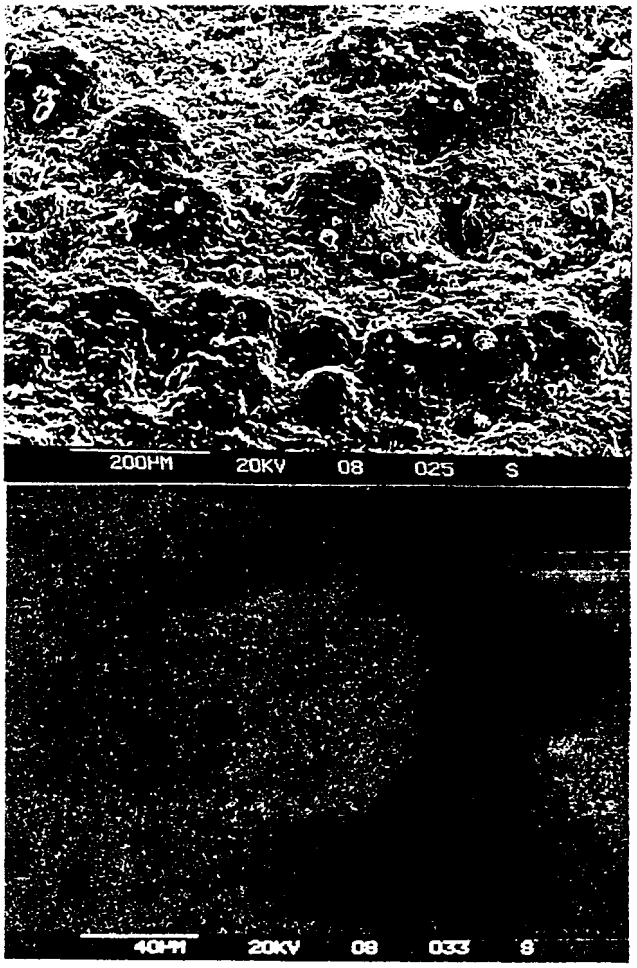

Figure 67. : SEM microphotograph and EDAX analyses Vanadium density photograph of a high liquid loading (0,008 mole catalyst/g Celite) catalyst sample. The large liquid clusters are clearly visible.

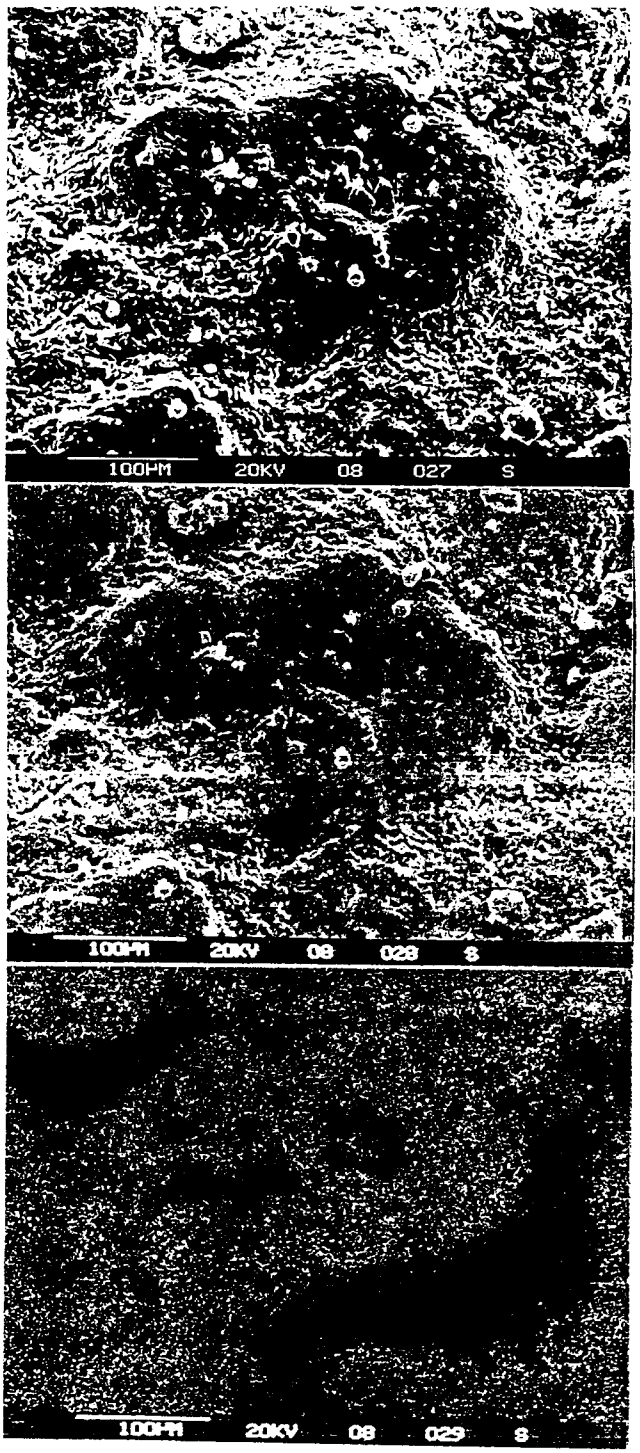

Figure 68. : EDAX analyzer Vanadium density superimposed upon the SEM microphotograph of a single liquid cluster. The catalyst liquid loading was 0.008 mole catalyst/g Celite.

4.3 EFFECT OF PELLET GEOMETRY AND SIZE

4.3.1 Introduction

This section describes the effect of pellet geometry and size on:

- Activity
- Bed used pressure drop
- Crush strength
- Attrition resistance

The above variables are interactive, and from an economic point of view, certain tradeoffs are required to optimise the final shape.

Sizes and shapes of catalyst particles influence the effectiveness of catalyst utilization by way of reactant and product diffusion into and out of the particle. Diffusion path length affects the overall reaction rate, and is related to the global effectiveness factor n.

In shaping a particle, material can be removed from the interior, such as in rings. In doing this the effective diffusional path is reduced and increases the reaction rate per unit mass. However continued removal eventually reduces the reaction rate per unit reactor bed volume, because less catalyst is available. Therefore the tradeoff between pellet effectiveness and bulk density has to be optimized. Furthermore, removal of material from the interior, also reduces the crush strength.

Selectively shaping the exterior of the particle, such as producing serrated protruding edges also increases global effectiveness diffusion, however, the sharp edges are more prone to attrition.

Smaller particles imply denser bed packing with associated increases in gas pressure drops across the catalyst bed.

The shapes selected for this study are shown in figure (69).

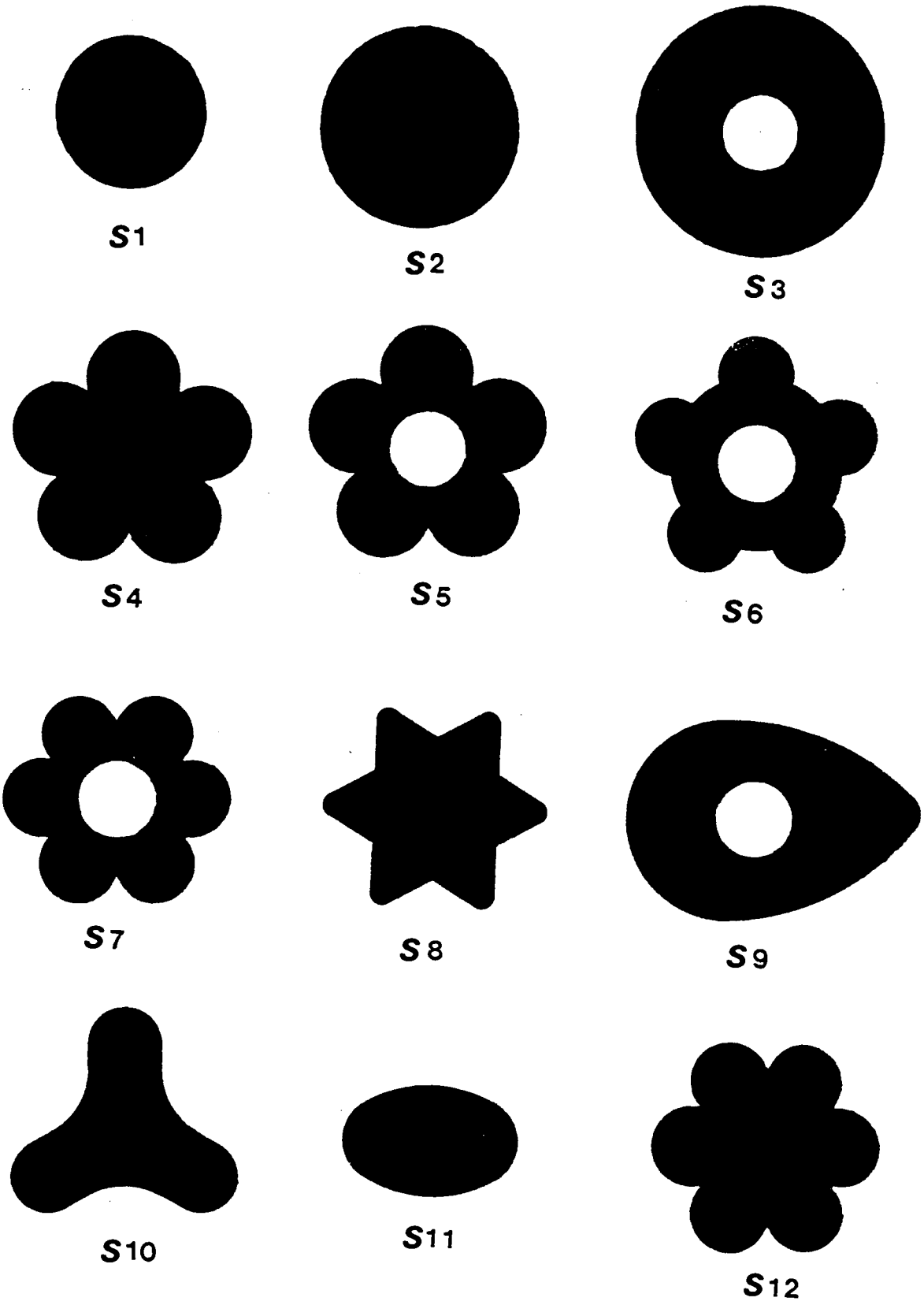

Figure 69. : Catalyst pellet shapes used in this study (Scale 4.2:1).

The shapes were manufactured using an industrial bonnet extruder fitted with a die that contains the different shapes. Due to the differences in cross sectional area of the various shapes, it was difficult to control the die pressure. **This could result in experimental error**

because die pressure affects the pore size distribution as shown in figure (17). The liquid composition and loading (Provon, LB-formulation) were kept constant.

4.3.2 Effect of particle geometry and size on reaction rate

The reaction rate was measured at five different temperatures between 400°C and 600°C. Since the level of liquid loading was kept constant only the gas effectiveness factor was affected by the pellet geometry.

In table (10) there are listed the raction rate per unit mass, the gass effectiveness factor, the volume to surface area ratio of the pellet, activation energies, bed bulk densities and the reation rate per bed volume for the different shapes. The results listed in table (10) have been extracted from Appendices A6 and B7 respectively. The reaction rates per mass listed were extracted from the data in Appendix B7 at 500°C. The gas effectiveness factor, η_G, was calculated using Equation (34) and taking the ratio between the reaction rate obtained for the various shapes relative to a crushed 1-1,18mm reference sample of the same formulation. The volume to external surface area ratio of the various shapes were calculated from geometric measurements. Activation energies were obtained from Arrhenius plots. Bed bulk densities were experimentally determined as outlined in Chapter 3. The reaction rates per bed volume were calculated by multiplying the measured reaction rate per mass by bed bulk densities.

Discussion

The only reasonable relationships between the various measurements and calculations listed in table (10), were the relationships between the reaction rate and V_k/F_k. This is shown in figure (70). Data scatter was probably due to varying die pressures during extrusion. Alterations in die pressures result in changes in pore structure (figure 17) and this in turn affects the reaction rate. Due to this variation it became necessary to compare similar shapes rather than the whole spectrum.

Table 10: Reaction rate related factors for the various shapes

Shape No.	Reaction rate per mass $\left(\frac{\text{mole}SO_3}{kg\ \text{min}}\right)$	η_G	$\frac{V_k}{F_k}$	Activation energies (J/mole)	Bed Bulk density (Kg/m^3)	Reaction rate per bed volume $\left(\frac{\text{mole}\ SO_3}{kgm^3}\right)$ at 500°C
S 1	1,696	0,169	1,200	60750	625	17,667
S 2	1,335	0,133	1,500	50230	610	13,569
S 3	1,447	0,144	1,355	49300	575	13,868
S 4	1,303	0,130	1,341	42060	621	13,483
S 5	1,497	0,149	1,007	50580	576	14,380
S 6	1,661	0,165	1,024	51860	541	14,994
S 7	1,705	0,170	0,975	55620	562	15,967
S 8	1,705	0,170	1,136	52650	585	16,635
S 9	1,620	0,162	1,160	57700	607	16,379
S10	1,714	0,170	1,150	59130	557	15,906
S11	1,687	0,168	1,094	63400	638	17,933
S12	1,620	0,162	1,325	57680	604	16,298

Shapes S1, S2 and S11 will be considered first; the general trend and absolute value are consistent for S1 and S11. The effect of particle radius (V_k/F_K) when S1 and S2 are compared, is consistent with theory, in that the larger particles have a lower gas effectiveness factor, bulk density, activation energies and reaction rates.

When comparing shapes S5, S6 and S7 all containing lobes and a hole, one would expect similar trends. This is indeed the case.

The effect of a hole can be seen when comparing S4 with S5 and S12 to S7. By including a hole in the structure the reaction rate, effectiveness and bulk density move into a more favourable direction.

It is difficult to draw any logical conclusions from the remaining structures.

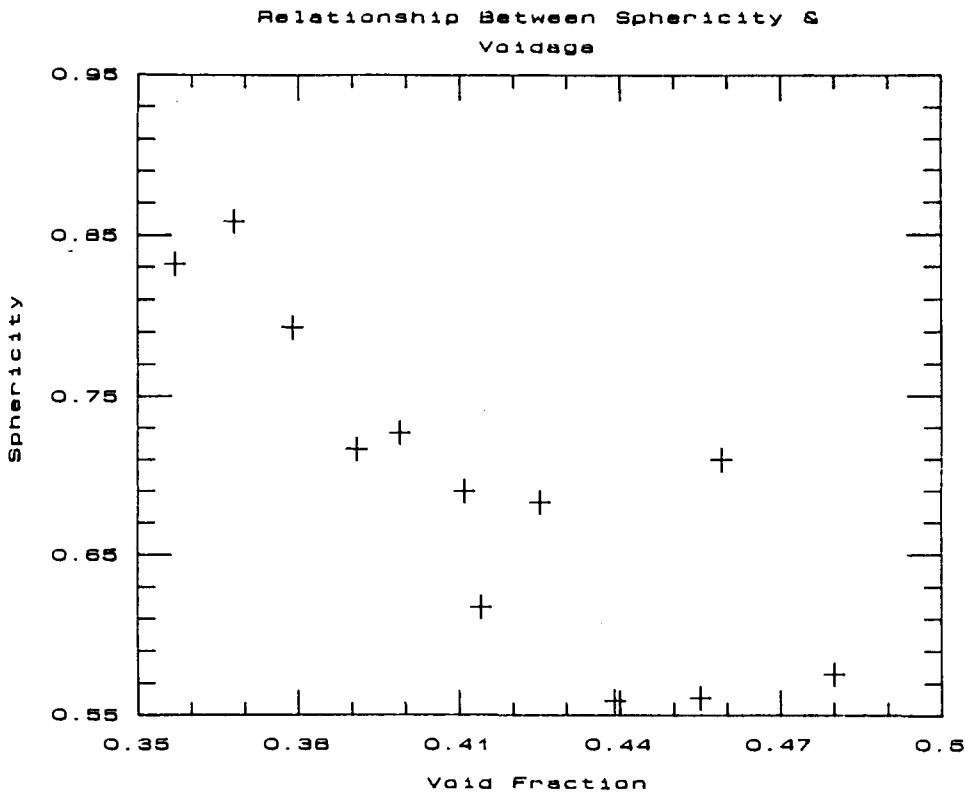

Figuur 70. : Relationship between reaction rate and the volume/external surface area of the pellet (500°C).

4.3.3 Pressure drop

Pressure drop generally requires a large sample for accurary. Following the procedures outlined in section (3.3.1) pressure drops have been measured in a 300mm deep bed using air at room temperature and atmospheric pressure. These measurements provided relative comparisons between the shape of individual catalysts. However extrapolation to actual operating conditions is dangerous.

The shape related variables that affect the pressure drop across the catalyst bed are:

- Bed void fraction, ε
- Effective diameter, dp as defined in equation (57)
- Sphericity of the pellet ϕ_s, as defined in equation (58).

The relationship between these variables can be seen in the Ergun equation, equation (59). The sphericity and effective diameter were calculated from the pellet geometrical dimensions (Appendix B9) and are shown in table (11) together with the experimentally determined void fraction, ε. The voidage can only experimentally be accurately determined.

An average pellet length for all the shapes of 10mm ± 1mm were ensured by hand picking of the samples.

Table 11: Shape related variables in bed pressure drop

Shape No.	d_p	ϕ_s	ε	ΔP $u_o = 0{,}5 m/s$ mmH_2O/m bed
S 1	8,653	0,832	0.357	77,5
S 2	10,483	0,859	0.368	54,8
S 3	11,788	0,690	0.411	32,3
S 4	11,227	0,717	0.391	39,9
S 5	10,781	0,561	0.455	34,0
S 6	10,670	0,576	0.480	35,5
S 7	10,471	0,599	0.439	40,1
S 8	9,975	0,683	0.425	39,9
S 9	11,269	0,618	0.414	40,0
S10	9,725	0,710	0.459	37,3
S11	8,277	0,793	0.379	60,6
S12	10,942	0,727	0.399	48,3

According to Kunii (1977: 64) the void fraction, ε, is related to the sphericity of the particle (figure 15). To check if this relationship holds the sphericity was plotted against the void fraction for the different shapes (figure 71). The pressure drop for various superficial air velocities is shown in figure (72) and table (11).

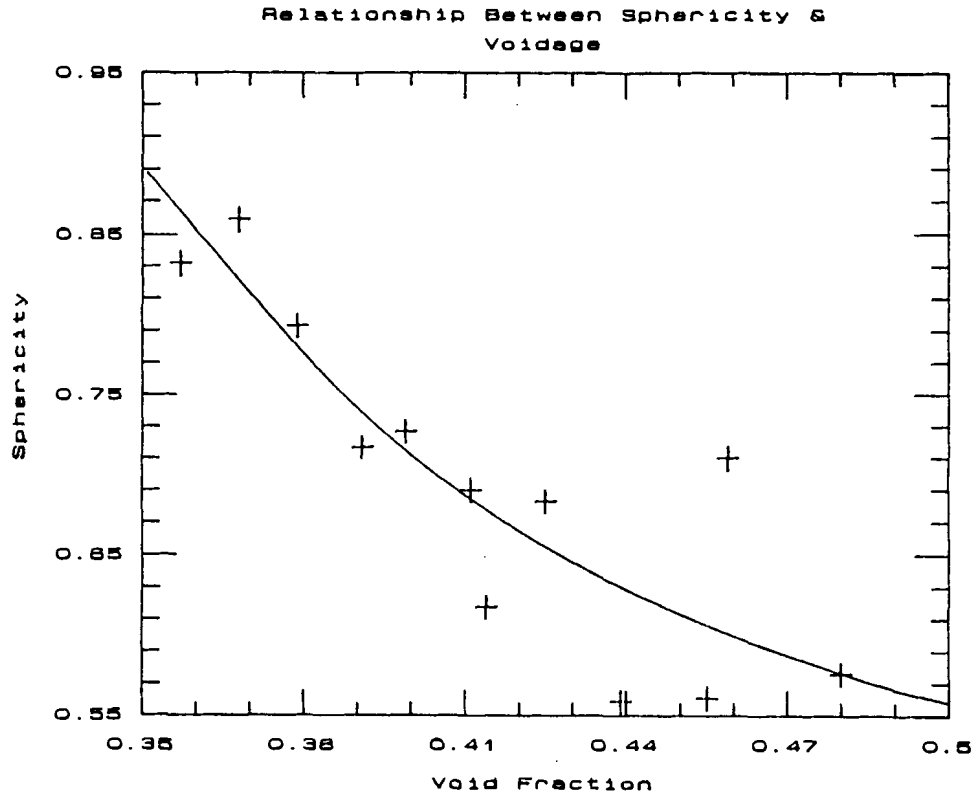

Figure 71. : Relationship between sphericity and voidage.

Pressure drops at intermediate velocities are shown in Appendix A7. Pressure drops calculated using the Ergun equation, equation (59), were more conservative (± 30% higher) than the experimentally determined pressure drops. Both experimental and calculated pressure drops revealed the same relative comparison of one shape with the other.

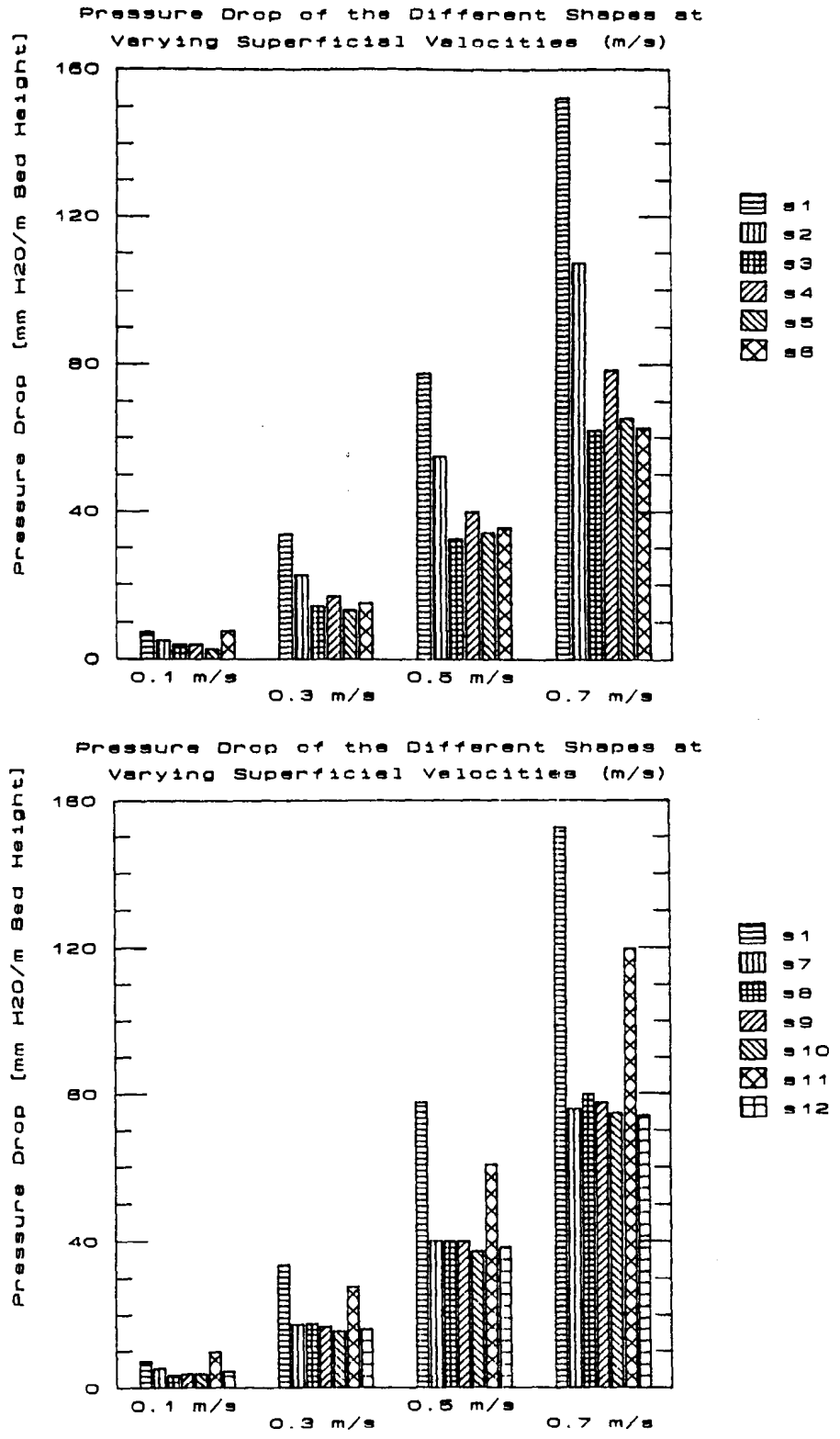

Figure 72. : Pressure drop at various superficial velocities.

Discussion

Pressure drops across the catalyst bed can be reduced by increasing the diameter of the catalyst particles, which in turn increases the size of voids between them. This will cause a drop in activity which is related to the amount of exposed pellet surface per unit volume. An alternative way to achieve high void fractions is to change the geometric shape of the catalyst pellets in such that the surface area per unit volume is kept the same (or increased) while the bulk density decreases. Ultimately the reaction rate per unit volume of reactor will drop because less catalyst is available. Another important factor is the "dirt holding capacity" which will improve as the average size of voids between the pellets increases. It is important to keep a good balance between dirt holding and filtering ability; in other words dirt must move further into the bed without passing through to the second bed to any great extent. The dust holding capacity of the beds have important operational consequences and can increase the plant availability by reducing the annual screening frequency.

The shapes can be ranked from low to high bed pressure drops: $S3 < S6 \simeq S5 < S12 \simeq S10 < S7 < S9 < S8 \simeq S4 < S1 < S11 < S1$. This ranking agrees with the predicted order obtained from the Ergun equation.

4.3.4 Mechanical strength and attrition resistance

A primary engineering goal in the design of a catalyst is to develop a pellet that has the mechanical strength to minimise dust formation, cracking or failure while in service. Such failures, which can cause the pressure drop across the reactor to become prohibitively large, and can cause frequent plant shutdowns.

Crush Strength

The bulk crush strength was measured employing a variably loaded piston at the top of a sample mass. Force versus displacement is then a representation of the differential crush strength of the catalyst. The area under the displacement versus force curve is inversely proportional to the integral crush strength of the catalyst. A smaller displacement at a given pressure indicates a greater strength. The catalyst shapes were tested at room temperature; the 6mm pellet was tested at temperatures up to 600°C to evaluate the effect of temperature on crush strength. The test results are in Appendix B10. The crush strengths of the various shapes are shown in table (12).

Table 12: Mechanical strengths

Shape No.	Crush Strength	Attrition Resistance
S 1	0,093	7,0
S 2	0,87	11,0
S 3	0,099	3,0
S 4	0,110	1,5
S 5	0,104	2,5
S 6	0,061	3.0
S 7	0,101	2,5
S 8	0,112	4,0
S 9	0,085	1,5
S10	0,100	2,0
S11	0,126	3,0
S12	0,100	4,5

The variation of crush strength with temperature can be seen in figure (73) and Appendix B11. There is a sharp drop in crush strength when the temperature was increased from 25°C to 300°C. The crush strength remains fairly constant in the temperature range 300°C to 600°C.

Attrition Resistance

Attrition loss was measured as the percentage weight loss of the sample after 1500 revolutions in the 300mm diameter attrition mill. Tests were conducted at room temperature and are shown in table (12).

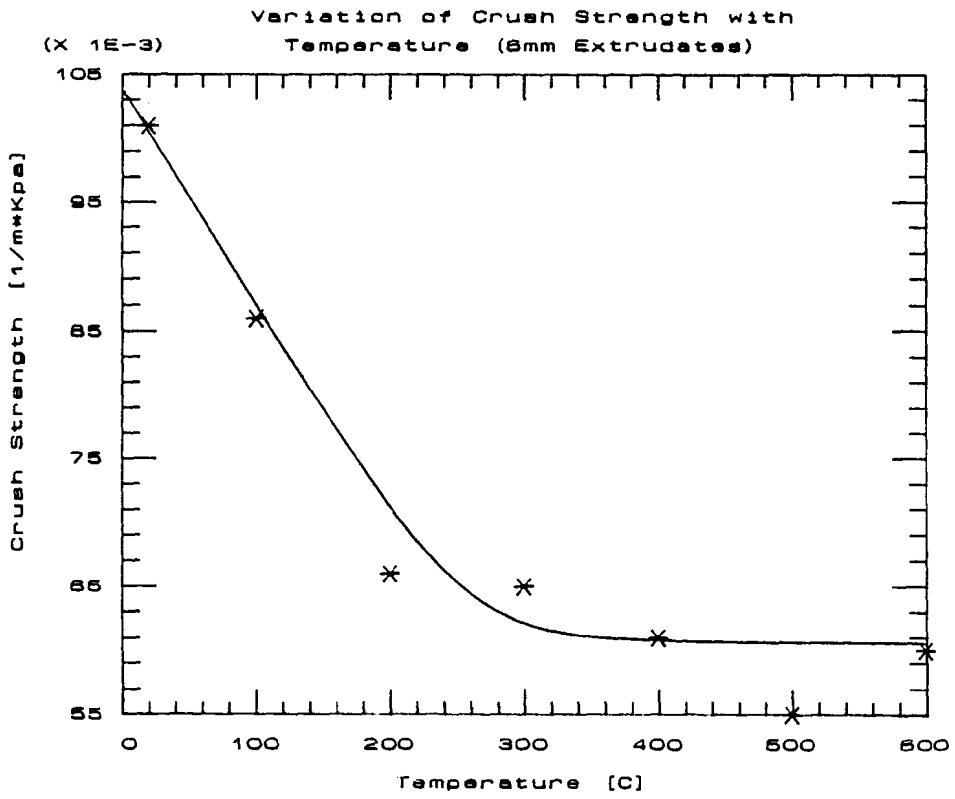

Figure 73. : Effect of temperature on the crush strength (6mm extrudates, LB formulation).

Discussion

The crush strength of a catalyst pellet has two components i.e. the geometrical strength of the shape and the inherent strength of the catalyst material. The inherent catalyst material strength is a function of the degree of sintering between the diatom particles which is affected by mainly the *NaOH* content in the initial catalyst formulation. At room temperature the active melt which is an amorphous solid contributes to the catalyst strength as can be seen in figure (73). When the temperature is increased above the melting point of the active constituents which is known to be around 300°*C* the crush strength levels off. At this point the crush strength is only affected by the strength of the carrier matrix due to sintering. In conclusion, the inherent strength of the catalyst material at room temperature are both affected by the degree of liquid loading and the amount of sintering between the diatoms.

The shapes can be ranked from strong to weak: $S1 > S2 \simeq S3 > S4 \simeq S5 \simeq S6 \simeq S7 \simeq S8 > S9 \simeq S10 \simeq S11 > S12$. The ranking order was not the same as expected, most likely due to different inherent material strengths due to variations in the die pressure during extrusion.

The attrition resistances of different shapes except shape S1 and S2 were all in the same order of magnitude. The only explanation is that the attrition resistance is much more sensitive to the inherent material strength than by the pellet geometry. The shapes can roughly be ranked from the most resistant as follows: $S4 \simeq S9 > S10 \simeq S5 \simeq S6 \simeq S7 \simeq S11 \simeq S3 > S8 \simeq S12 > S1 > S2$. Again the ranking order was not as expected, probably due to variations in the die pressure during manufacturing.

CHAPTER 5

CONCLUSIONS AND RECOMMENDTATIONS

5.1 CONCLUSIONS

Literature survey

- The literature on the catalytic oxidation of sulphur dioxide over vanadium based catalysts is voluminous. However most of the results in earlier publications were based on measurements with mass transfer restrictions and the kinetics and mechanisms presented by them are uncertain. The fact that the active ingredients is in a molten state at operating conditions were also often disregarded by earlier publications.

- The models of Neth **et al.** (1980: 43-46) and Livbjerg **et al.** (1976: 216) were the most complete taking into account reaction kinetics, simultaneous diffusion effects in both the liquid and gas phases and liquid distribution.

Chemical composition of the active constituent

- The catalytic activity increases as the molecular weight and ionic radius of the alkali metal cation promoters increases.

- The peak activity moves toward lower temperatures with increasing molecular weight of the alkali metal cation promoter.

- The chemical compositions of the active constituents are dependent on temperature and the reactant composition ($SO_2/SO_3/O_2/N_2$ ratios). This change in chemical composition which affects the activity is not permanent and can best be explained by the decomposition of alkali metal pyrosulphates to sulphates and vice versa.

- There is an optimum M_2O/V_2O_5 mole ratio which is more pronounced at lower temperatures. At higher temperatures the optimum activity occurs at lower M_2O/V_2O_5 mole ratios. At the peak temperature the optimum M_2O/V_2O_5 mole ratio was 2.8.

- There is a common general trend of decreasing activity and increasing activation energy with increasing partial replacement of potassium by sodium. This trend holds at all

M_2O/V_2O_5 mole ratios and temperature levels. The optimum M_2O/V_2O_5 ratio is independent of the Na/K mole ratio.

- The raw chemicals used to make the catalyst, i.e. the M_2SO_4/MOH ratio, have an effect on the activity and strength of the final catalyst. A one to one M_2SO_4/MOH mole ratio yielded the highest activity.

Active constituent loading

- there is a sharp drop in reaction rate per volume active melt, liquid effectiveness factor and activation energy when the liquid loading is increased due to increased liquid phase diffusion resistance. Only a small portion of the liquid film is effective during reaction since the liquid effectiveness factor, η_L, is highly dependent on liquid loading. The liquid effectiveness factor, n_L, is only slightly dependent on temperature in the range 400°C to 600°C.

- Liquid distribution or dissipation within the pore structure of the support is an important parameter to take into account in the design of the SLP V_2O_5 catalyst system. The liquid dispersion, described by the mean melt thickness, δ is proportional to the liquid loading factor. Direct observations by SEM as well as indirect calculations from rate data indicate a uniform liquid distribution for liquid loadings up to $0,6cm^3$ melt $/cm^3$ pores. At higher liquid loadings cluster formation occurs. The cluster size greatly exceed the pore dimentions. It must be mentioned that the abovementioned liquid dispersion is specific to the pore size distribution of the support used in this study. Other supports with different pore size distribution can result in a different liquid dispersion and distribution.

- The liquid is preferably drawn into the smaller pores first before larger and larger pores are filled with increased liquid loading for liquid loadings up to $0,6cm^3$ melt $/cms^3$ pore. Physical property measurments such as the change in internal surface area, average pore radius and pore volume support this.

- There is an optimal liquid loading for the pore structure used in this study. It is $0,3cm^3$ melt $/cm^3$ pores. This optimum is the result of a trade off between the effective utilization of the active liquid and the gradual disappearance of the residual pore system with increased liquid loading. The controlling diffusion resistance is residual pore gas diffusion for this pore structure, but it can easily become liquid phase diffusion controlled if a carrier matrix with slightly larger pores is used and vice versa.

Influence of pellet geometry and size on activity

- Various shapes produced different rate data, however there was no overall consistency when comparing the shapes and this was concluded due to variations in die pressures during extrusion of the different shapes.

- Increased effective pellet radius (V_k/F_k ratio) results in a decrease in the gas effectiveness factor, bed bulk density, activation energies and reaction rates.

- Inclusion of a hole into the shape results in more favourable gas effectiveness factors lower bed bulk densities and higher reaction rates per bed volume.

Pressure drop

- Experimentally determined pressure drops and predicted pressure drops using the Ergun equation correlated well.

- The introduction of exotic shapes resulted in activity comparable to small particles, however there was a considerable decrease in bed pressure drop.

Mechanical strength

- The inherent material strength of the catalyst at room temperature is affected by both the degree of liquid loading and the amount of sintering between the diatom particles. At operating conditions, the active constituents are in the molten state, then the crush strength is only affected by the amount of sintering which occurred. This in turn depends on the M_2SO_4/MOH ratio in the raw mix, during manufacturing.

- Attrition resistance appears to be more dependent on the inherent material strength rather than the geometric shape of the catalyst pellet.

- The mechanical strength of the different shapes were not in the same order as expected, probably due to variations in die pressure during extrusion.

5.2 RECOMMENDATIONS

- In the formulation of catalysts for a complete multibed industrial reactor it must be realized that each bed operates under different reactant conditions. In this study the conditions simulate those of a typical first bed. It could be useful to optimize the catalyst formulation for lower bed conditions.

- It is possible to introduce temporary lower strike temperature characteristic to the catalyst provided that subsequent to activation the catalyst is cooled down under a high SO_3 partial pressure. This will enhance pyrosulphate formation with lower melting points.

- From the experience gained in work an ideal catalyst would require a global effectiveness factor close to unity. This implies that both the liquid and gas phase effectiveness factors must approach unity. This would imply a pronounced bimodal pore size distribution, with small pores that lead to a highly dispersed liquid phase and large pores that will enhance rapid mass transfer of reactants and products to and from the active regions.

- Analytical techniques developed here gave excellent results and can be considered for on-stream analysis.

- Local raw materials are always an advantage to the manufacturer. The preliminary results and discussions on the high surface area amorphous silica looks very promising. The extrapolated advantages from the knowledge gained in this work regarding this raw material are:

    - The high surface area and small pores size distribution would lead to much lower liquid loadings for equivalent activity.

    - Because of the small particles shear resistance in the extruder die is very low and consequently preformation of exotic shapes would be easier. The small particles imply many more contact points between particle surfaces in the pellet which leads to a higher mechanical strength.

    - The lower active constituent loadings necessary for comparable activity would lead to less stickyness and therefore less dust holding problems under operating conditions.

    - The high surface area and low liquid loading approaches the more conventional heterogenous catalyst.

REFERENCES

ARIS, R. 1975. The mathematical theory of diffusion and reaction in permeable catalyst. Oxford: Clarendon Press. Vol 182.

BAZAROVA, Z.G., BORESKOV, G.K., KEFELI, L.M., KARAKCHIEV, L.G., OSTANNKOVICH, A.A. 1968. *Dolcl, Akod. NAUK USSR (Transl.)*, 5:1132

BORESKOV, G.K., BUYANOV, R.A., IVANOV, A.A. 1967. *Kinet. Katal.*, 8(1): 153-159 (English version p.126-132).

BORESKOV, G.K., DZIS'KO, V.A., TARASOVA, D.V., BALAGANSKAYA, G.P. 1970. *Kinet. Katal. (USSR)*, 11(1):181-186.

BORESKOV, G.M., POLYAKOVA, G.P., INVANOV, A.A., MASTIKHIN, V.M. 1973. *Kinet. Katal. (USSR)*, 210(3):626-629.

DIFFORD, A.M.R. & SPENCER, M.S. 1973 Catalyst test reactor types and examples of their Applications. *AICHE Symposium series*, 143 (70):42-47.

DONOVAN, R.J., PALERMO, J.S. 1978. Minimizing catalyst pressure drop: an interim report. *Sulphur* 138: 39-40, September/October.

DONOVAN, R.J., SMITH, R.M., PATERMO, J.S. 1977. The role of catalyst engineering in sulphuric acid plant operations. *Sulphur*, 131:46-50, July/August.

DONOVAN, J.R. STOLK, R.D., UNLAND, M.L. ca. 1983. Oxidation catalyst for Sulfuric Acid Production. (*In* Applied Industrial Catalyst, Vol.2, chapter 7, p.245-286).

EKLUND, R.B. 1956. The Rate of oxidation of Sulphur Dioxide with a commercial Vanadium catalyst. Stokholm: Almquist-Wiksell.

FLOOD, H. & FORLAND, T. 1947. *Acta Chem. Scand*, 1: 592-604.

FRAZER, J.H., & KIRKPATRICK, W.J. 1940. *J. Am. Chem. Soc.*, 62: 1659.

FULTON, W.J. 1986. Building the mathematical model of the catalyst and reactor. *Chemical Engineering*, 118-124, February 17.

FULTON, W.J. 1986. Making the catalyst. *Chemical Engineering*, 59-63, July 7.

FULTON, W.J. 1986. Selecting the catalyst configuration. *Chemical Engineering*, 97-101, May 12.

GAY, R.J. & LOVERING, G.D. 1983. Molten Salt Techniques, Vol. 1 & 2. New York: Plenum Press. 272p.

GLUECK, A.R. & KENNEY, C.N. 1968. The Kinetics of the Oxidation of Sulphur dioxide over molten Salts. *Chemical Engineering Science*, 23: 1257-1265, 23 January.

GOLDMAN, M., CANJAR, N.L., BECKMAN, R.B. 1957. *J. Appl. Chem.*, 7: 274-291.

GRYDGAARD, P., JENSEN'HOLM, H., LIVBJERG, H., VILLADSEN, J. 1978. *ACS Symp. Ser.*, 65:582-595.

HANSEN, N.H. 1979. Technical University of Denmark, Chemistry Department. Lyngby. Denmark (Thesis (Ph.D.)).

HASSAN, S.A. & ISKANDAR, F.T. 1975. Catalytic and Surface characteristics of Newly Imported, Exhausted and Regenerated V_2O_5 Catalysts used in H_2SO_4 manufacturing. *Journal of Catalysis,* 43:243-271, May 1.

HOLROYD, F.P.B. & KENNEY, C.N. 1971. Sulphur dioxide oxidation kinetics over molten salts: The adsorption of sulphur dioxide in vanadium pentoxide/potassium pyrosulphate melts.*Chemical Engineering Science*, 26: 1963-1970.

JENSEN-HOLM, H. 1978. Supported liquid phase catalysis for sulfur dioxide oxidation. Instituttet for Kemiteknik, Denmarks Tekniske Hojskole, Lyngby (Thesis (Ph.D.)).

JIRU, P. & JARA, V. 1960. *Proceedings of the 2nd International Congress on Catalysis, Editions Tecknip. Paris*, 2: 2113-2120.

KAKINOKI, D.V., SAHARA, N., KAMATA, I., AIGAMI, Y. 1962. *Shokubar*, 4: 113.

KOVENKLIOGLU, S. & DELANCEY, G.B. 1978. Catalyst effectiveness in sulfur dioxide oxidation. *Chemical Engineering Science*, 34: 841-846, November 8.

KUNII, D. & LEVENSPIEL, O. 1977. Fluidization Engineering. New York: Robert E. Krieger Publishing Company. 64p.

LEVENSPIEL, O. 1972. Chemical Reaction Engineering, Second Edition. New York, London, Sydney, Toronto: John Wiley & Sons, Inc. 460p.

LIVBJERG, H., JENSEN, K.F., VILLADSEN, J. 1976. Sulfur Dioxide Oxidqation on Supported Molten $V_2O_5 - K_2S_2O_7$ Catalyst, The influence of Liquid Diffusion Resistance. **Journal of Catalysis,** 45: 216-230, July 26.

LIVBJERG, H., SORENSEN, B., VILLADSEN, J. 1974. Dispersion, Mass Transport, and chemical Reaction in Supported Liquid Phase Catalyst for SO_2 Oxidation. (*In* Chemical Reaction Engineering - II, 19: 242-258, January 2).

LIVBJERG, H., VILLADSEN, J. 1971. Kinetics and Effectiveness Factor for SO_2 Oxidation on an Industrial Vanadium catalyst. *Chemical Engineering Science*, 27(1): 21-38, April 4.

LUX, H. 1939. *Z. Electrochem* 45: 303-310.

MARS, P. & MAESSEN, J.G.M. 1964. The Mechanism and the kinetics of Sulfur Dioxide Oxidation on Catalysis Containing Vanadium and Alkali Oxides. *Proc. 3rd Int. Congr. Cat.*, 1: 266-

MOKHLEWOV, I.P., IKRAMOV, S.A., DEVYUZHKINA, V.I. 1976. *Khim. Promst.* (Moscow) (Eng. preface only), 3: 226.

NETH, N., KAUTZ, G., HUSTER, H.J., WAGNER, U. 1980. On the Kinetics of SO_2 Oxidation. *German Chemical Engineering*, 3: 43-44.

REGNER, A. & SIMECEK, A. 1968. *Collect. Czech. Chem. Commun.*, 33: 2540.

RONY, P.R. 1969. Diffusion Kinetics within Supported liquid Phase Catalysis. *Journal of Catalysis,* 14: 142-147, January 13.

SANDER, U.H.F., ROTHE, U., KOLA, R. ca. 1981. Sulphur, Sulphur Dioxide and Sulphuric Acid. *Industrial Chemistry and Technology*, p.261-377.

SCHOUBYE, P. & ALBJERG, A. 1978. Pressure drop and dust accumulation in sulphuric acid converters. *Sulphur*, 138: 34-36, September/October.

SIMICEK, A. 1970. SO_2 oxidation catalysts. *Journal of catalysis*, 18: 83-89.

SIMONOVA, L.G., LAPINA, O.B., MASTIKHIN, V.M., DZISKO, V.A. 1982. Effect of the type and content of alkaline promoters on the properties of vanadium catalysts for SO_2 oxidation. *React. Kinet. Catal. Lett.* 22(1-2): 59-62, May.

TAMURA, A., HUDGINS, R.R., SILVESTON, P.L. 1975. Loss of Activity of commercial Vanadia SO_2 Oxidation Catalysts during Run-in Period. *Journal of Catalysis*, 42: 122-130, August 5.

TANDY, G.H. 1956. SO_2 oxidation catalysts, *J. Applied Chem.*, 6: 68-74.

TARASOVA, D.V., BORESKOV, G.K., DZIS'KO, V.V. 1968. *Kinet. Catal (USSR)*, 9: 1111-

TOPSOE, H. & NIELSEN, A. 1948. *Trans. Danish Acad. Tech. Sci.*, 1: 1-3.

URBANEK, A. & TRELA, M. 1980. Catalytic Oxidation of Sulfur Dioxide. *Catal. Rev. - Sci. Eng.*, 21(1): 73-133.

WEEKMAN, V.W. 1974. Laboratory Reactors and Their Limitations. *AICHE Journal*, 20(5): 833-840, September.

WEISS, J.M., DOWNS, C.R., BURNS, R.M. 1923. SO_2 oxidation. *Ind. Eng. Chem.*, 15: 965-

WEYCHERT, S. & URBANEK, A. 1969. *Int. Chem. Eng.*, 9(3): 396-403.

APPENDIX A

APPENDIX A1:
Formulations: Different M and M_2O/V_2O_5 mole ratios

FORMULATIONS: DIFFERENT M & M2O/V2O5 MOLE RATIO'S

DRY MASS REQUIRED (G) :	400
G H2O / G CELITE :	1.1
LIQUID LOADING, MOLE CATALYST/G CELITE :	0.0015
G.GRM/G CELITE :	0.025
K2SO4/KOH MOLE RATIO :	0.4

RAW MATERIAL PROPERTIES:

CELITE 209:	M/M % PURITY
VOLATILES	6.60%
SIO2	86.70%
AL2O3	3.30%
FE2O3	1.20%
P2O5	0.20%
TIO2	0.50%
CAO	0.50%
MGO	0.80%
NA2O & K2O	100.00%
TOTAL MASS REQ. (G)	2863.539

NH4VO3 :	M/M % PURITY
MM (G/MOLE)	116.978
NH4VO3	93.00%
OTHER	7.00%
TOTAL MASS REQ. (G)	284.703

NAOH :	M/M % PURITY
MM (G/MOLE)	39.99707
NAOH	98.00%
OTHER	2.00%
TOTAL MASS REQ. (G)	6.194

NA2SO4 :	M/M % PURITY
MM (G/MOLE)	142.03114
NA2SO4	99.00%
OTHER	1.00%
TOTAL MASS REQ. (G)	8.709

LIOH :	M/M % PURITY
MM (G/MOLE)	23.9483
LIOH	98.00%
OTHER	2.00%
TOTAL MASS REQ. (G)	3.750

L12SO4 :	M/M % PURITY
MM (G/MOLE)	109.9396
L12SO4	98.00%
OTHER	2.00%
TOTAL MASS REQ. (G)	6.886

KOH :	M/M % PURITY
MM (G/MOLE)	56.1056
KOH	85.00%
OTHER	15.00%
TOTAL MASS REQ. (G)	49.840

K2SO4 :	M/M % PURITY
MM (G/MOLE)	174.2542
K2SO4	99.00%
OTHER	1.00%
TOTAL MASS REQ. (G)	53.161

CSOH.H2O :	M/M % PURITY
MM (G/MOLE)	167.9279
CS.SALT	92.00%
OTHER	8.00%
TOTAL MASS REQ. (G)	24.706

CS2SO4 :	M/M % PURITY
MM (G/MOLE)	361.8684
CS.SALT	98.00%
OTHER	2.00%
TOTAL MASS REQ. (G)	20.643

FORMULATIONS :

LITHIUM :

H2O/V2O5 MOLE RATIO.	2.5
CHEMICAL	MASS (G)
CELITE 209	368.003
GUM	8.593
AHV	37.057
LIOH	3.750
L12SO4	6.886
NAOH	0.000
NA2SO4	0.000
KOH	0.000
K2SO4	0.000
CSOH.H2O	0.000
CS2SO4	0.000
WATER	378.086

SODIUM :

H2O/V2O5 MOLE RATIO.	2.5
CHEMICAL	MASS (G)
CELITE 209	361.969
GUM	8.499
AHV	36.651
LIOH	0.000
L12SO4	0.000
NAOH	6.194
NA2SO4	8.709
KOH	0.000
K2SO4	0.000
CSOH.H2O	0.000
CS2SO4	0.000
WATER	373.942

POTASSIUM :

H2O/V2O5 MOLE RATIO.	2.5
CHEMICAL	MASS (G)
CELITE 209	358.168
GUM	8.127
AHV	36.000
LIOH	0.000
L12SO4	0.000
NAOH	0.000
NA2SO4	0.000
KOH	9.824
K2SO4	10.532
CSOH.H2O	0.000
CS2SO4	0.000
WATER	368.398

CESIUM :

H2O/V2O5 MOLE RATIO.	2.5
CHEMICAL	MASS (G)
CELITE 209	335.194
GUM	7.827
AHV	33.753
LIOH	0.000
L12SO4	0.000
NAOH	0.000
NA2SO4	0.000
KOH	0.000
K2SO4	0.000
CSOH.H2O	24.706
CS2SO4	20.643
WATER	344.378

POTASSIUM :

H2O/V2O5 MOLE RATIO.	1.5
CHEMICAL	MASS (G)
CELITE 209	349.008
GUM	8.149
AHV	49.202
LIOH	0.000
L12SO4	0.000
NAOH	0.000
NA2SO4	0.000
KOH	8.509
K2SO4	0.000
CSOH.H2O	0.000
CS2SO4	358.571
WATER	379.657

POTASSIUM :

H2O/V2O5 MOLE RATIO.	3.5
CHEMICAL	MASS (G)
CELITE 209	364.430
GUM	8.499
AHV	28.542
LIOH	0.000
L12SO4	0.000
NAOH	0.000
NA2SO4	0.000
KOH	10.922
K2SO4	11.649
CSOH.H2O	0.000
CS2SO4	0.000
WATER	374.415

POTASSIUM :

H2O/V2O5 MOLE RATIO.	5
CHEMICAL	MASS (G)
CELITE 209	369.232
GUM	8.629
AHV	21.707
LIOH	0.000
L12SO4	0.000
NAOH	0.000
NA2SO4	0.000
KOH	11.862
K2SO4	12.636
CSOH.H2O	0.000
CS2SO4	0.000
WATER	379.657

APPENDIX A2:
Formulations: Different Na/K and M_2O/V_2O_5 mole ratios

FORMULATIONS: DIFFERENT NA/K & M2O/V2O5 RATIO'S

DRY MASS REQUIRED (G) :	500
G H2O / G CELITE :	1.1
LIQUID LOADING, MOLE CATALYST/G CELITE :	0.0015
G GUM/G CELITE :	0.025
M2SO4/MOH MOLE RATIO :	0.4

RAW MATERIAL PROPERTIES:

CELITE 209:

	M/M % PURITY
VOLITILES	6.60%
SIO2	86.70%
AL2O3	3.30%
FE2O3	1.20%
P2O5	0.20%
TIO2	0.20%
CAO	0.50%
MGO	0.50%
Na2O & K2O	0.80%
	100.00%
TOTAL MASS REQ. (G)	4072.163

NH4VO3 :

	M/M % PURITY
MM (G/MOLE)	116.978
NH4VO3	93.00%
OTHER	7.00%
	100.00%
TOTAL MASS REQ. (G)	374.111

NAOH :

	M/M % PURITY
MM (G/MOLE)	39.99707
NAOH	98.00%
OTHER	2.00%
	100.00%
TOTAL MASS REQ. (G)	1.456

NA2SO4 :

	M/M % PURITY
MM (G/MOLE)	142.03714
NA2SO4	99.00%
OTHER	1.00%
	100.00%
TOTAL MASS REQ. (G)	21.298

KOH :

	M/M % PURITY
MM (G/MOLE)	56.1056
KOH	85.00%
OTHER	15.00%
	100.00%
TOTAL MASS REQ. (G)	91.558

K2SO4 :

	M/M % PURITY
MM (G/MOLE)	174.2542
K2SO4	99.00%
OTHER	1.00%
	100.00%
TOTAL MASS REQ. (G)	97.660

FORMULATIONS :

SODIUM / POTASSIUM:

M2O/V2O5 MOLE RATIO.	2
NA/K MOLE RATIO.	0.1

CHEMICAL	MASS (G)
CELITE 209	443.826
GUM	10.363
AMV	52.141
NAOH	0.064
NA2SO4	0.901
KOH	10.364
K2SO4	11.055
WATER	455.987

SODIUM / POTASSIUM:

M2O/V2O5 MOLE RATIO.	2
NA/K MOLE RATIO.	0.2

CHEMICAL	MASS (G)
CELITE 209	444.271
GUM	10.374
AMV	52.193
NAOH	0.118
NA2SO4	1.654
KOH	9.510
K2SO4	10.144
WATER	456.444

SODIUM / POTASSIUM:

M2O/V2O5 MOLE RATIO.	2
NA/K MOLE RATIO.	0.6

CHEMICAL	MASS (G)
CELITE 209	445.497
GUM	10.402
AMV	52.337
NAOH	0.265
NA2SO4	3.731
KOH	7.152
K2SO4	7.629
WATER	457.704

SODIUM / POTASSIUM:

M2O/V2O5 MOLE RATIO.	2.5
NA/K MOLE RATIO.	0.1

CHEMICAL	MASS (G)
CELITE 209	449.043
GUM	10.485
AMV	45.218
NAOH	0.069
NA2SO4	0.977
KOH	11.235
K2SO4	11.984
WATER	461.347

SODIUM / POTASSIUM:

M2O/V2O5 MOLE RATIO.	2.5
NA/K MOLE RATIO.	0.2

CHEMICAL	MASS (G)
CELITE 209	449.530
GUM	10.497
AMV	45.267
NAOH	0.127
NA2SO4	1.793
KOH	10.310
K2SO4	10.997
WATER	461.848

SODIUM / POTASSIUM:

M2O/V2O5 MOLE RATIO.	2.5
NA/K MOLE RATIO.	0.6

CHEMICAL	MASS (G)
CELITE 209	450.876
GUM	10.528
AMV	45.402
NAOH	0.288
NA2SO4	4.046
KOH	7.756
K2SO4	8.273
WATER	463.230

SODIUM / POTASSIUM:

M2O/V2O5 MOLE RATIO.	5
NA/K MOLE RATIO.	0.1

CHEMICAL	MASS (G)
CELITE 209	462.638
GUM	10.803
AMV	27.176
NAOH	0.084
NA2SO4	1.174
KOH	13.505
K2SO4	14.405
WATER	475.314

SODIUM / POTASSIUM:

M2O/V2O5 MOLE RATIO.	5
NA/K MOLE RATIO.	0.2

CHEMICAL	MASS (G)
CELITE 209	463.241
GUM	10.817
AMV	27.211
NAOH	0.153
NA2SO4	2.155
KOH	12.395
K2SO4	13.221
WATER	475.934

SODIUM / POTASSIUM:

M2O/V2O5 MOLE RATIO.	5
NA/K MOLE RATIO.	0.6

CHEMICAL	MASS (G)
CELITE 209	464.909
GUM	10.856
AMV	27.309
NAOH	0.346
NA2SO4	4.867
KOH	9.330
K2SO4	9.952
WATER	477.648

APPENDIX A3:
Formulations: Different M_2SO_4/MOH mole ratios

FORMULATIONS: DIFFERENT M2SO4/MOH MOLE RATIO'S:

DRY MASS REQUIRED (G) :	500
G H2O / G CELITE :	1.1
G GUM/G CELITE :	0.025

RAW MATERIAL PROPERTIES:

CELITE 209:

	M/M % PURITY
VOLITILES	6.60%
SIO2	86.70%
AL2O3	3.30%
FE2O3	1.20%
P2O5	0.20%
TIO2	0.20%
CAO	0.50%
MGO	0.50%
NA2O & K2O	0.80%
	100.00%
TOTAL MASS REQ. (G)	1668.378

NH4VO3 :

	M/M % PURITY
MM (G/MOLE)	116.978
NH4VO3	93.00%
OTHER	7.00%
	100.00%
TOTAL MASS REQ. (G)	224.003

NaOH :

	M/M % PURITY
MM (G/MOLE)	39.99707
NAOH	98.00%
OTHER	2.00%
	100.00%
TOTAL MASS REQ. (G)	0.489

NA2SO4 :

	M/M % PURITY
MM (G/MOLE)	142.03714
NA2SO4	99.00%
OTHER	1.00%
	100.00%
TOTAL MASS REQ. (G)	18.827

KOH :

	M/M % PURITY
MM (G/MOLE)	56.1056
KOH	85.00%
OTHER	15.00%
	100.00%
TOTAL MASS REQ. (G)	39.570

K2SO4 :

	M/M % PURITY
MM (G/MOLE)	174.2542
K2SO4	99.00%
OTHER	1.00%
	100.00%
TOTAL MASS REQ. (G)	115.485

FORMULATIONS :

SODIUM / POTASSIUM:	
M2O/V2O5 MOLE RATIO.	2.5
NA/K MOLE RATIO.	0.2
MOLE CAT./G CELITE	0.0020
M2SO4/MOH MOLE RATIO	0
CHEMICAL	MASS (G)
CELITE 209	441.365
GUM	10.306
AMV	59.260
NAOH	0.200
NA2SO4	0.000
KOH	16.197
K2SO4	0.000
WATER	453.459

SODIUM / POTASSIUM:	
M2O/V2O5 MOLE RATIO.	2.5
NA/K MOLE RATIO.	0.2
MOLE CAT./G CELITE	0.0020
M2SO4/MOH MOLE RATIO	0.4
CHEMICAL	MASS (G)
CELITE 209	429.586
GUM	10.031
AMV	57.678
NAOH	0.162
NA2SO4	2.284
KOH	13.137
K2SO4	14.012
WATER	441.356

SODIUM / POTASSIUM:	
M2O/V2O5 MOLE RATIO.	2.5
NA/K MOLE RATIO.	0.2
MOLE CAT./G CELITE	0.0020
M2SO4/MOH MOLE RATIO	1
CHEMICAL	MASS (G)
CELITE 209	418.418
GUM	9.770
AMV	56.179
NAOH	0.127
NA2SO4	4.450
KOH	10.236
K2SO4	27.296
WATER	429.883

SODIUM / POTASSIUM:	
M2O/V2O5 MOLE RATIO.	2.5
NA/K MOLE RATIO.	0.2
MOLE CAT./G CELITE	0.0020
M2SO4/MOH MOLE RATIO	1000000
CHEMICAL	MASS (G)
CELITE 209	379.009
GUM	8.850
AMV	50.887
NAOH	0.000
NA2SO4	12.092
KOH	0.000
K2SO4	74.176
WATER	389.394

FORMULATIONS: DIFFERENT LIQUID LOADINGS:

DRY MASS REQUIRED (G) :	500
G H2O / G CELITE :	1.1
G GUM/G CELITE :	0.025
M2SO4/MOH MOLE RATIO :	0.4

RAW MATERIAL PROPERTIES:

CELITE 209:

	M/M % PURITY
VOLITILES	6.60%
SIO2	86.70%
AL2O3	3.30%
FE2O3	1.20%
P2O5	0.20%
TIO2	0.20%
CAO	0.50%
MGO	0.50%
NA2O & K2O	0.80%
	100.00%
TOTAL MASS REQ. (G)	2292.953

NH4VO3 :

	M/M % PURITY
MM (G/MOLE)	116.978
NH4VO3	93.00%
OTHER	7.00%
	100.00%
TOTAL MASS REQ. (G)	523.142

NAOH :

	M/M % PURITY
MM (G/MOLE)	39.99707
NAOH	98.00%
OTHER	2.00%
	100.00%
TOTAL MASS REQ. (G)	1.473

NA2SO4 :

	M/M % PURITY
MM (G/MOLE)	142.03714
NA2SO4	99.00%
OTHER	1.00%
	100.00%
TOTAL MASS REQ. (G)	20.719

KOH :

	M/M % PURITY
MM (G/MOLE)	56.1056
KOH	85.00%
OTHER	15.00%
	100.00%
TOTAL MASS REQ. (G)	119.152

K2SO4 :

	M/M % PURITY
MM (G/MOLE)	174.2542
K2SO4	99.00%
OTHER	1.00%
	100.00%
TOTAL MASS REQ. (G)	127.094

FORMULATIONS :

SODIUM / POTASSIUM:

M2O/V2O5 MOLE RATIO.	2.5
NA/K MOLE RATIO.	0.2
MOLE CAT./G CELITE	0.0005

CHEMICAL	MASS (G)
CELITE 209	495.545
GUM	11.571
AMV	16.633
NAOH	0.047
NA2SO4	0.659
KOH	3.788
K2SO4	4.041
WATER	509.123

SODIUM / POTASSIUM:

M2O/V2O5 MOLE RATIO.	2.5
NA/K MOLE RATIO.	0.2
MOLE CAT./G CELITE	0.0010

CHEMICAL	MASS (G)
CELITE 209	471.417
GUM	11.008
AMV	31.647
NAOH	0.089
NA2SO4	1.253
KOH	7.208
K2SO4	7.688
WATER	484.334

SODIUM / POTASSIUM:

M2O/V2O5 MOLE RATIO.	2.5
NA/K MOLE RATIO.	0.2
MOLE CAT./G CELITE	0.0020

CHEMICAL	MASS (G)
CELITE 209	429.586
GUM	10.031
AMV	57.678
NAOH	0.162
NA2SO4	2.284
KOH	13.137
K2SO4	14.012
WATER	441.356

SODIUM / POTASSIUM:

M2O/V2O5 MOLE RATIO.	2.5
NA/K MOLE RATIO.	0.2
MOLE CAT./G CELITE	0.0040

CHEMICAL	MASS (G)
CELITE 209	364.837
GUM	8.519
AMV	97.969
NAOH	0.276
NA2SO4	3.880
KOH	22.314
K2SO4	23.801
WATER	374.834

SODIUM / POTASSIUM:

M2O/V2O5 MOLE RATIO.	2.5
NA/K MOLE RATIO.	0.2
MOLE CAT./G CELITE	0.0080

CHEMICAL	MASS (G)
CELITE 209	280.332
GUM	6.546
AMV	150.554
NAOH	0.424
NA2SO4	5.963
KOH	34.291
K2SO4	36.576
WATER	288.013

SODIUM / POTASSIUM:

M2O/V2O5 MOLE RATIO.	2.5
NA/K MOLE RATIO.	0.2
MOLE CAT./G CELITE	0.0100

CHEMICAL	MASS (G)
CELITE 209	251.236
GUM	5.866
AMV	168.660
NAOH	0.475
NA2SO4	6.680
KOH	38.415
K2SO4	40.975
WATER	258.120

APPENDIX A5:
Sem Microphotographs

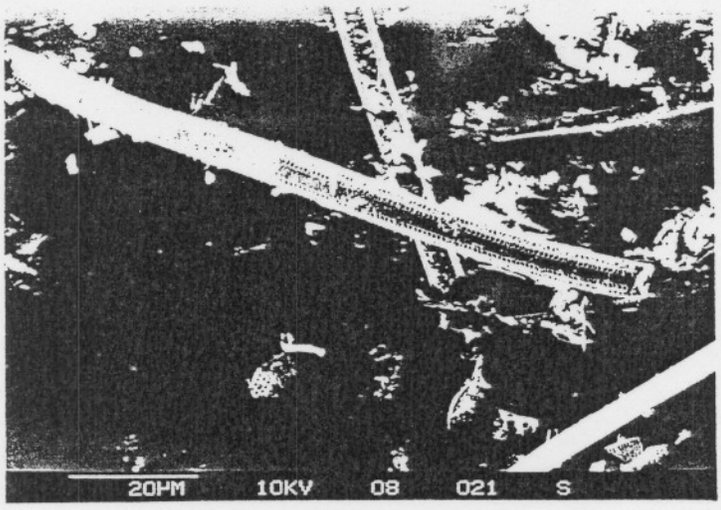

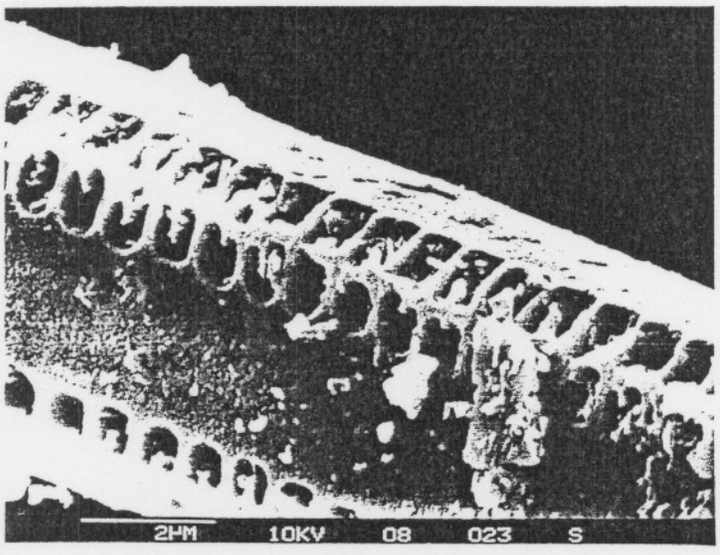

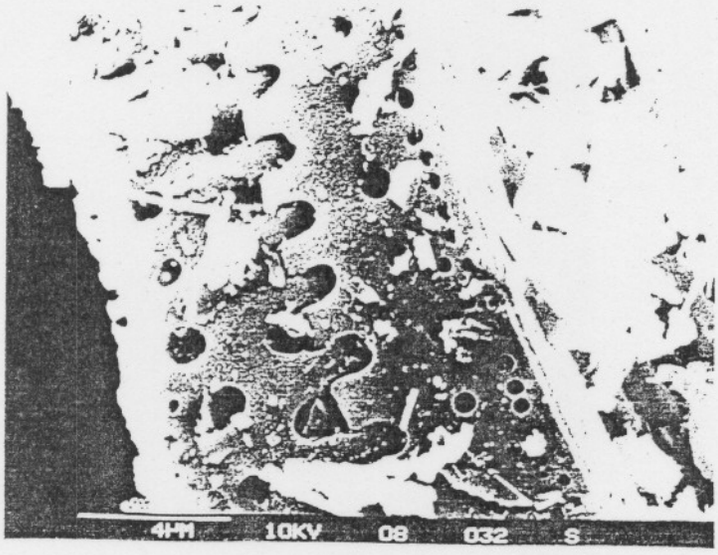

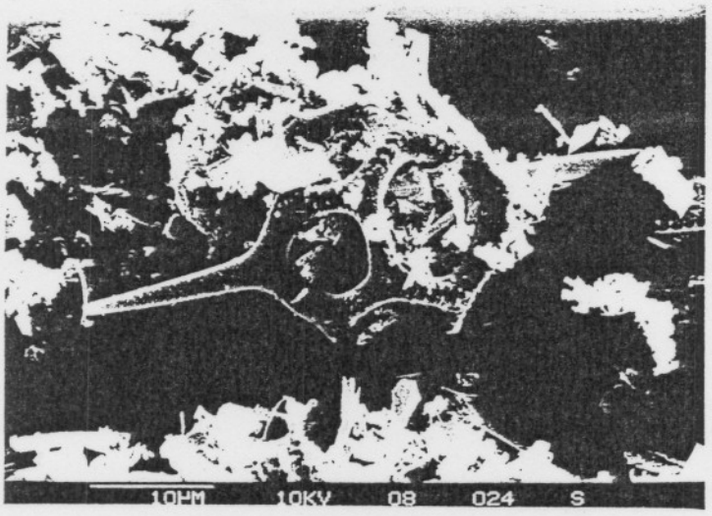
10UM 10KV 08 024 S

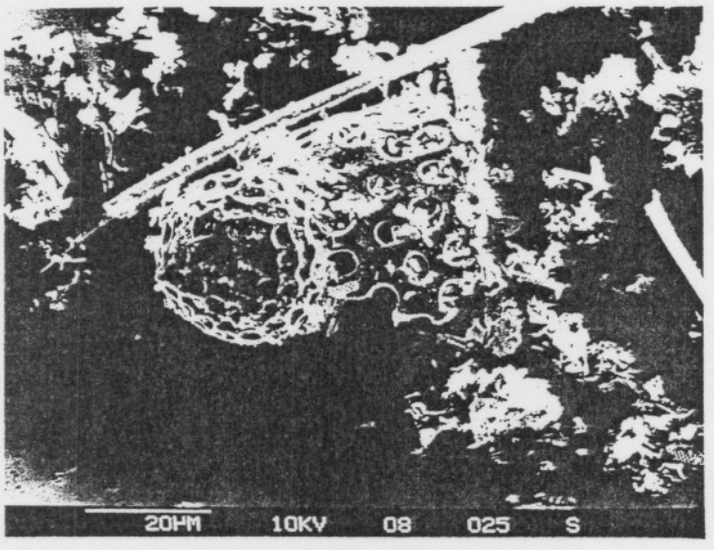
20UM 10KV 08 025 S

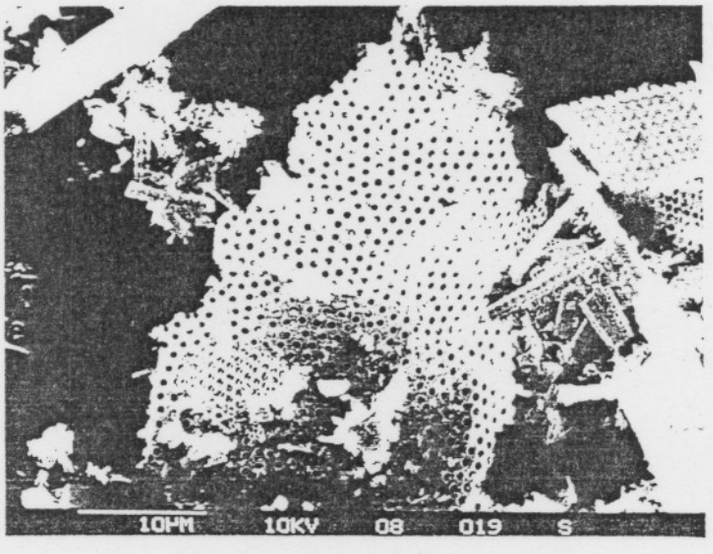
10UM 10KV 08 019 S

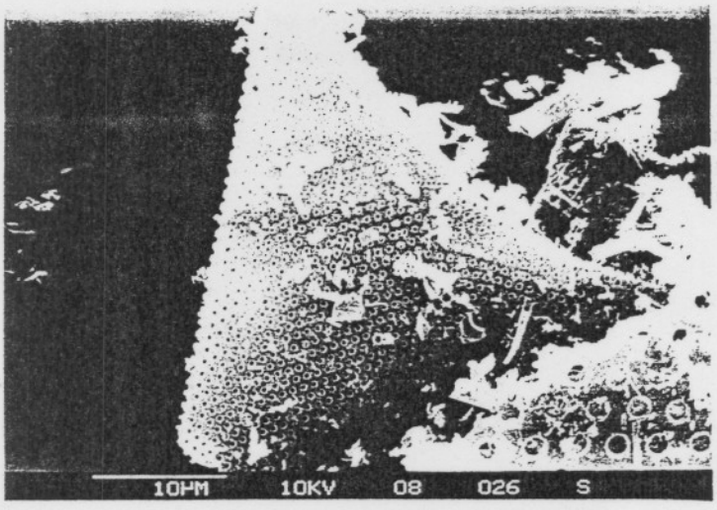
10UM 10KV 08 026 S

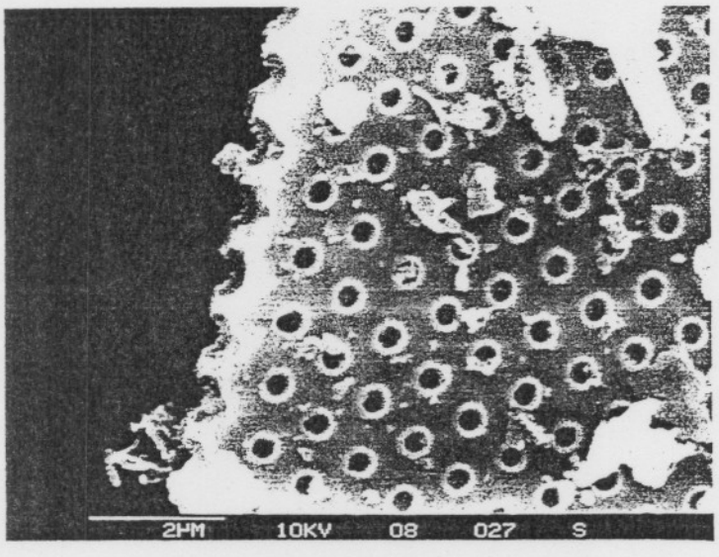
2UM 10KV 08 027 S

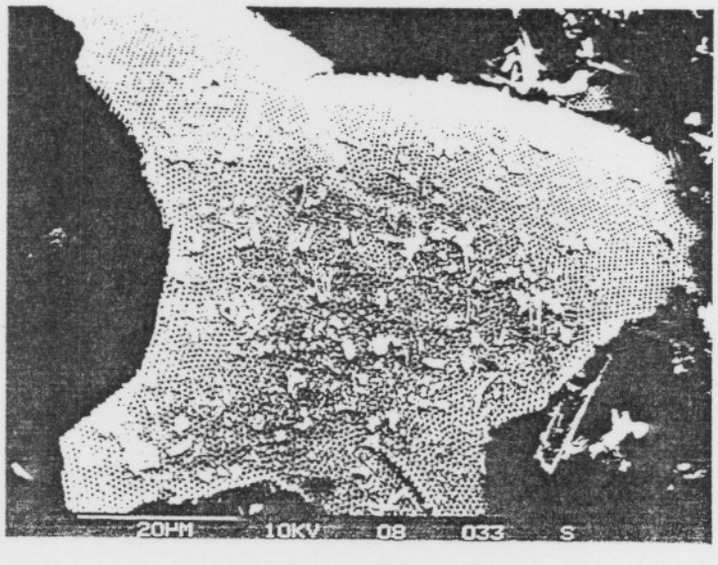
20UM 10KV 08 033 S

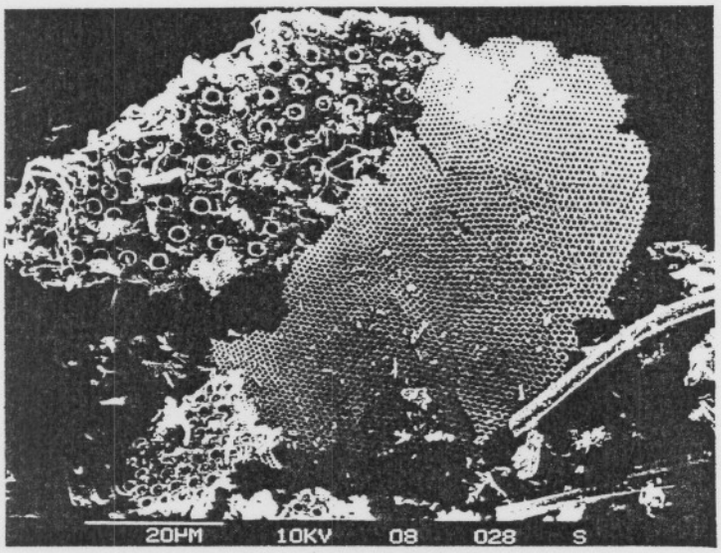
20HM 10KV 08 028 S

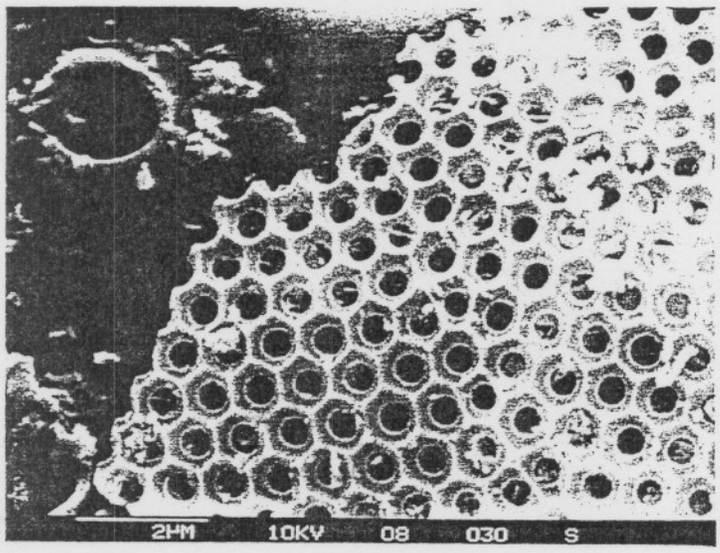
2HM 10KV 08 030 S

APPENDIX A6:
Reaction rate vs. temperature for the different shapes

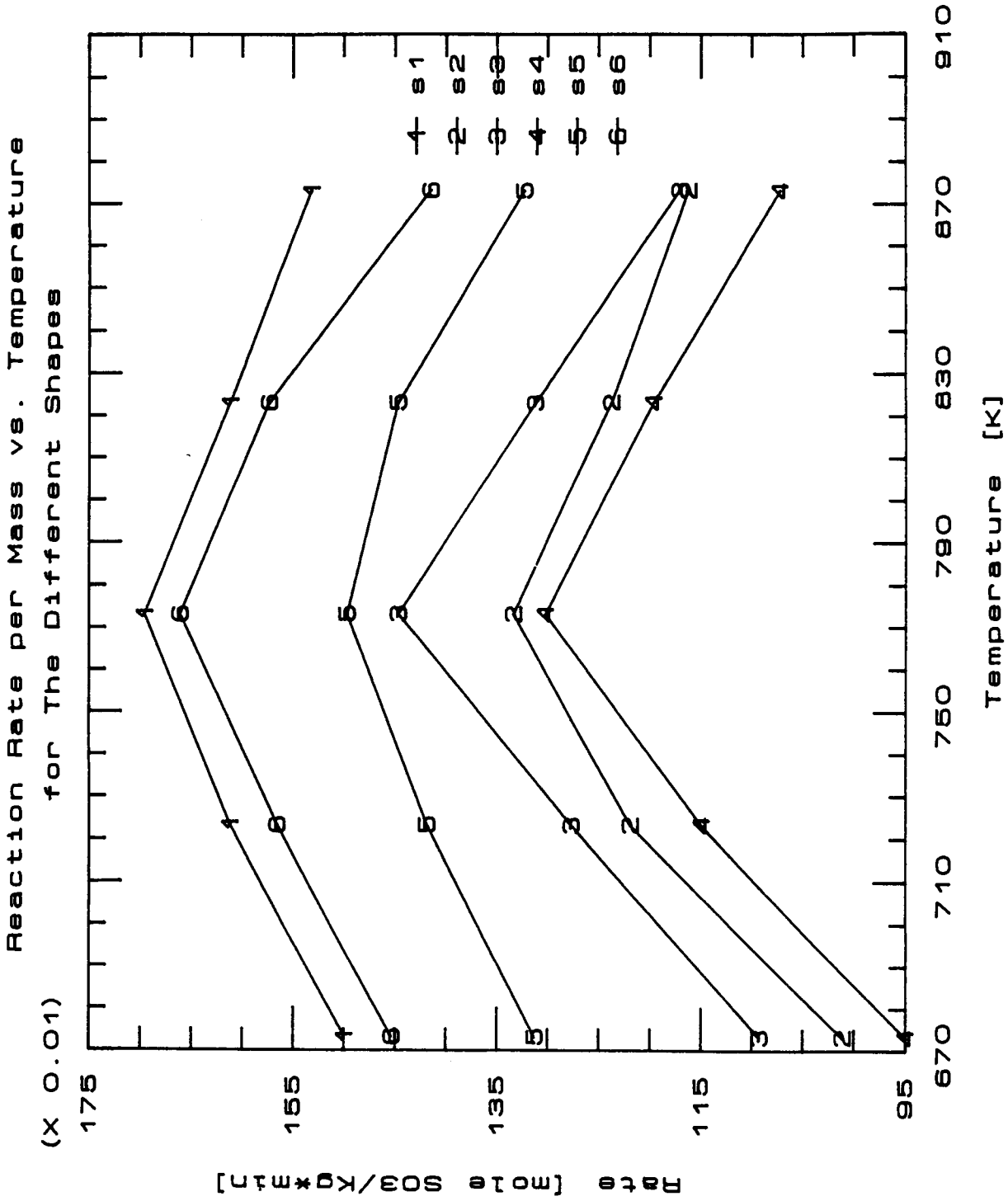

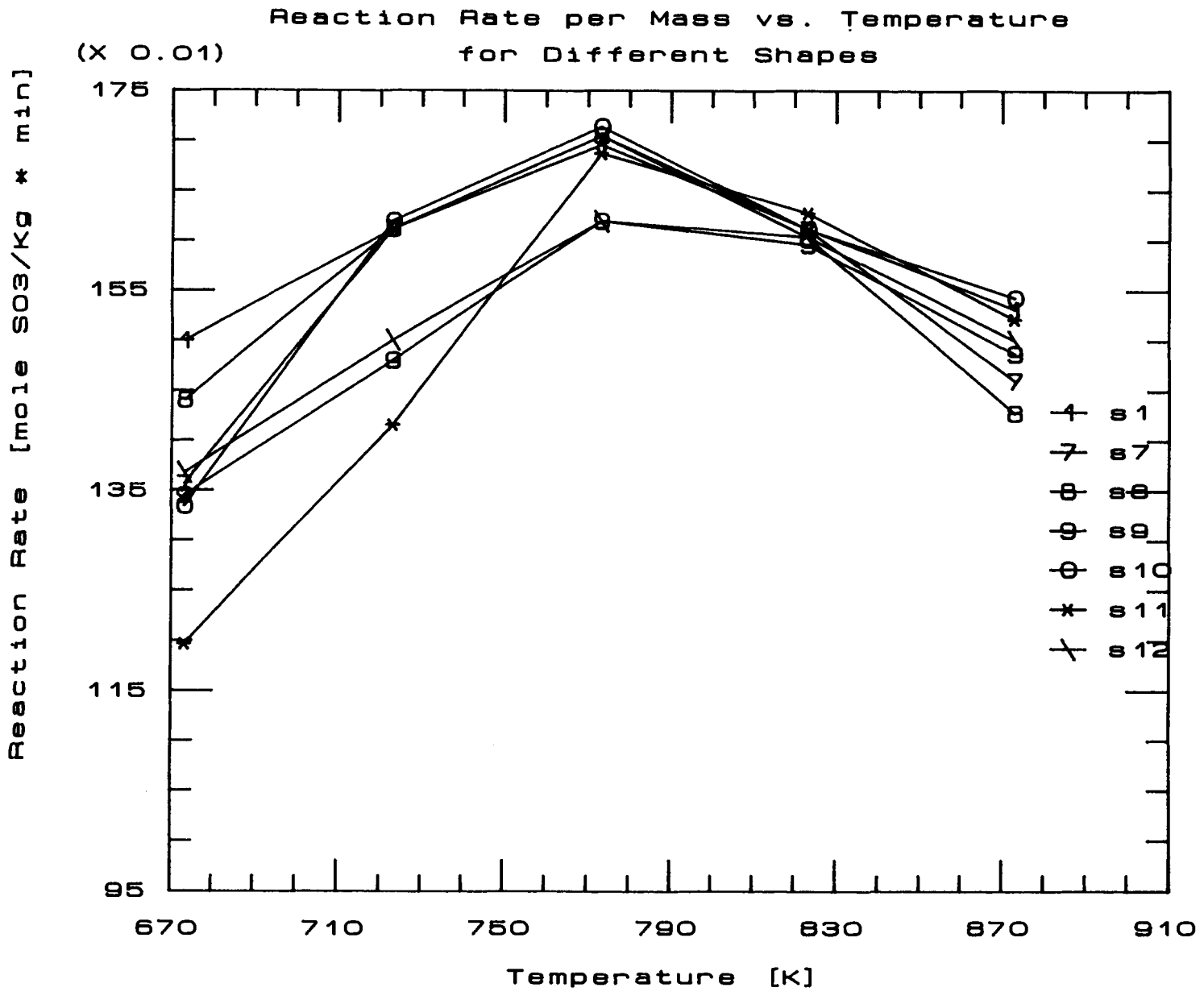
Reaction Rate per Mass vs. Temperature
for Different Shapes
(X 0.01)
Reaction Rate [mole SO3/Kg * min]
175
155
135
115
95
670
710
750
790
830
870
910
Temperature [K]
s1
s7
s8
s9
s10
s11
s12

APPENDIX A7:
Bed pressure drops versus superficial velocity

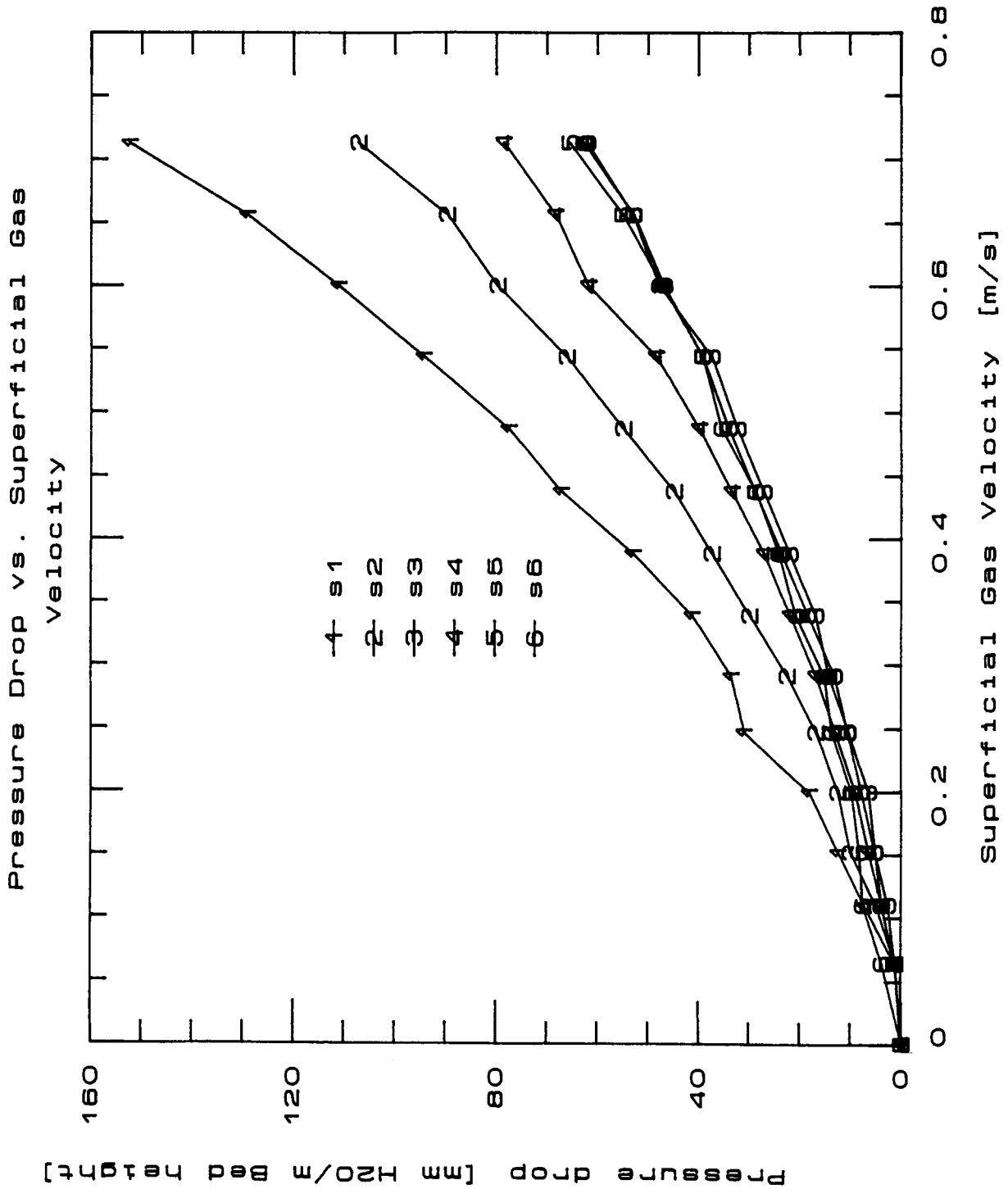

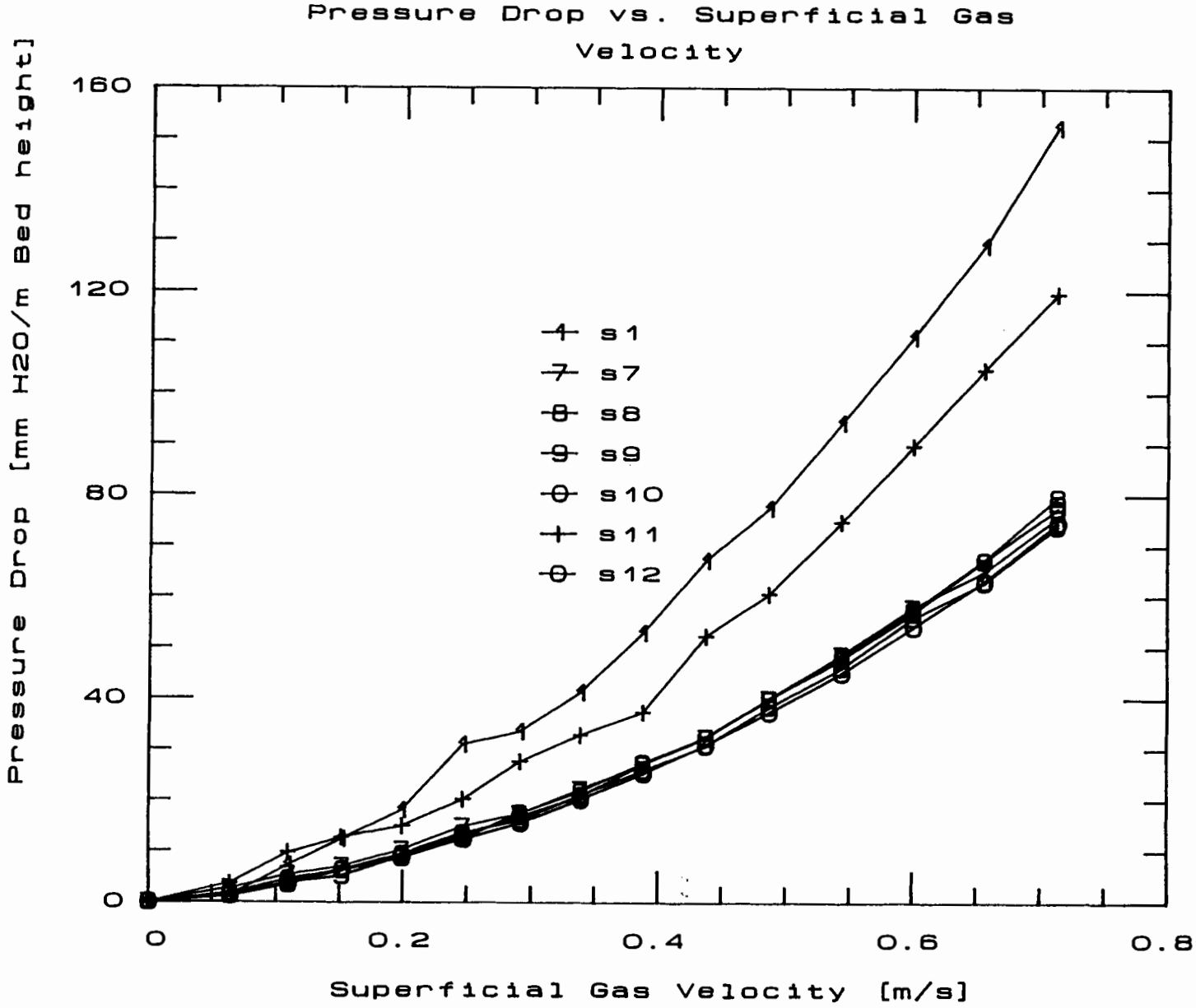
Pressure Drop vs. Superficial Gas Velocity
Pressure Drop [mm H20/m Bed height]
160
120
80
40
0
0
0.2
0.4
0.6
0.8
Superficial Gas Velocity [m/s]
s1
s7
s8
s9
s10
s11
s12

APPENDIX B

APPENDIX B1:
Results: Different M and M_2O/V_2O_5 MOLE RATIOS

DIFFERENT M & M2O/V2O5 MOLE RATIO'S

CATALYST PELLET SIZE: 1-1.18MM
CATALYST DILUTION : 3 G CAT + 3 G CERAMIC
TIME BETWEEN TEMP. RUNS : 60 MIN
TITRATION SOLUT. STRENGTH (N): 1.00
TITRATER CORRECTION FACTOR : 2.04722
LIQUID LOADING MOLE CATALYST/G CELITE : 0.0015
PARAMETER S 0.5

GAS COMPOSITION(MOLE %):

SO2	8.00%
O2	10.00%
N2	82.00%

REACTOR CONDITIONS :

LINEAR VELOCITY (M/S)	0.2
REACTOR DIAMETER (M)	0.032
MASS OF CATALYST (KG)	0.003
ATM. PRESSURE (KPA)	87.326

FORMULATION:

LITHIUM
M2O/V2O5 MOLE RATIO : 2.5

TEMP. (OC)	PRESSURE (KPAG)	N (MOLES/MIN)	SO3 (MOLES/MIN)	%CONVERSION (MOLE SO3/ MOLE SO2 FE (CORRECTED)	R (MOL SO3/ G*MIN)	PO2 (KPA)	PSO2 (KPA)	PSO3 (KPA)	Q	KP	KC	WI	DIST. FROM EQUILIBRIUM	KL (MOLE SO3/ G*MIN*KPA)	LN(KL) (MOLE SO3/ G*MIN*KPA)
400	10	0.16784	0.00324675	11.8116%	0.0005206	9.3160	6.8990	0.9240	7.4662	48.3505	15.8680	0.8388	1.0000	6.765E-05	-9.6012
450	10	0.15623	0.00290697	11.3611%	0.0004733	9.3327	6.9330	0.8886	7.8020	14.9744	3.8850	0.7162	1.0000	7.081E-05	-9.5555
500	10	0.14613	0.00371747	15.5332%	0.0006052	9.1850	6.6178	1.2170	5.4378	5.3968	1.1410	0.5091	0.9998	1.295E-04	-8.9522
550	10	0.13725	0.00613496	27.2924%	0.0009989	8.7658	5.7236	2.1485	2.6640	2.2018	0.3889	0.2542	0.9949	4.501E-04	-7.7060
600	10	0.12939	0.00833333	39.3240%	0.0013560	8.3328	4.7998	3.1107	1.5430	0.9954	0.1499	0.1055	0.9117	1.693E-03	-6.3811

FORMULATION:

SODIUM
M2O/V2O5 MOLE RATIO : 2.5

TEMP (OC)	PRESSURE (KPAG)	N (MOLES/MIN)	SO3 (MOLES/MIN)	%CONVERSION (MOLE SO3/ MOLE SO2 FE (CORRECTED)	R (MOL SO3/ G*MIN)	PO2 (KPA)	PSO2 (KPA)	PSO3 (KPA)	Q	KP	KC	WI	DIST. FROM EQUILIBRIUM	KL (MOLE SO3/ G*MIN*KPA)	LN(KL) (MOLE SO3/ G*MIN*KPA)
400	10	0.16784	0.00467289	16.9999%	0.0007608	9.1329	6.5067	1.3327	4.8824	48.3505	15.8680	0.8064	1.0000	1.033E-04	-9.1777
450	10	0.15623	0.00469483	18.3484%	0.0007644	9.0850	6.4045	1.4392	4.4501	14.9744	3.8850	0.6498	1.0000	1.295E-04	-8.9519
500	10	0.14613	0.00621118	25.9530%	0.0010113	8.8137	5.8258	2.0419	2.8531	5.3968	1.1410	0.4140	0.9993	2.774E-04	-8.1901
550	10	0.13725	0.00869565	38.6040%	0.0014158	8.3559	4.8491	3.0593	1.5850	2.2018	0.3889	0.1934	0.9831	8.910E-04	-7.0231
600	10	0.12939	0.01010101	47.6655%	0.0016446	8.0301	4.1540	3.7834	1.0980	0.9954	0.1499	0.0833	0.7985	3.079E-03	-5.7832

FORMULATION:

POTASSIUM
M2O/V2O5 MOLE RATIO : 2.5

TEMP. (OC)	PRESSURE (KPAG)	N (MOLES/MIN)	SO3 (MOLES/MIN)	%CONVERSION (MOLE SO3/ MOLE SO2 FE (CORRECTED)	R (MOL SO3/ G*MIN)	PO2 (KPA)	PSO2 (KPA)	PSO3 (KPA)	Q	KP	KC	WI	DIST. FROM EQUILIBRIUM	KL (MOLE SO3/ G*MIN*KPA)	LN(KL) (MOLE SO3/ G*MIN*KPA)
400	10	0.16784	0.00632911	23.0252%	0.0010305	8.9184	6.0490	1.8094	3.3431	48.3505	15.8680	0.7731	1.0000	1.495E-04	-8.8085
450	10	0.15623	0.00595238	23.2632%	0.0009691	8.9099	6.0309	1.8283	3.2986	14.9744	3.8850	0.6110	0.9999	1.780E-04	-8.6335
500	10	0.14613	0.008	33.4275%	0.0013025	8.5455	5.2536	2.6380	1.9916	5.3968	1.1410	0.3614	0.9984	4.224E-04	-7.7695
550	10	0.13725	0.01063829	47.3261%	0.0017321	8.0424	4.1804	3.7560	1.1130	2.2018	0.3889	0.1575	0.9602	1.424E-03	-6.5540
600	10	0.12939	0.01041666	49.1551%	0.0016960	7.9758	4.0382	3.9040	1.0344	0.9954	0.1499	0.0798	0.7664	3.475E-03	-5.6621

FORMULATION:

CESIUM
M2O/V2O5 MOLE RATIO : 2.5

TEMP. (OC)	PRESSURE (KPAG)	N (MOLES/MIN)	SO3 (MOLES/MIN)	%CONVERSION (MOLE SO3/ MOLE SO2 FE (CORRECTED)	R (MOL SO3/ G*MIN)	PO2 (KPA)	PSO2 (KPA)	PSO3 (KPA)	Q	KP	KC	WI	DIST. FROM EQUILIBRIUM	KL (MOLE SO3/ G*MIN*KPA)	LN(KL) (MOLE SO3/ G*MIN*KPA)
400	10	0.16784	0.00423728	15.4152%	0.0006899	9.1891	6.6267	1.2077	5.4871	48.3505	15.8680	0.8158	1.0000	9.204E-05	-9.2933
450	10	0.15623	0.00471698	18.4350%	0.0007680	9.0819	6.3979	1.4460	4.4245	14.9744	3.8850	0.6491	1.0000	1.303E-04	-8.9450
500	10	0.14613	0.00847457	35.4104%	0.0013798	8.4741	5.1012	2.7967	1.8240	5.3968	1.1410	0.3488	0.9980	4.678E-04	-7.6676
550	10	0.13725	0.01041666	46.3402%	0.0016960	8.0783	4.2569	3.6762	1.1500	2.2018	0.3889	0.1613	0.9639	1.351E-03	-6.6071
600	10	0.12939	0.00943396	44.5178%	0.0015360	8.1445	4.3982	3.5290	1.2463	0.9954	0.1499	0.0911	0.8523	2.429E-03	-6.0202

FORMULATION:

POTASSIUM
M2O/V2O5 MOLE RATIO : 1.5

TEMP (oC)	PRESSURE (KPAG)	N (MOLES/MIN)	SO3 (MOLES/MIN)	%CONVERSION (MOLE SO3/ MOLE SO2 FE (CORRECTED)	R (MOL SO3/ G*MIN)	PO2 (KPA)	PSO2 (KPA)	PSO3 (KPA)	Q	KP	KC	WI	DIST. FROM EQUILIBRIUM	KL (MOLE SO3/ G*MIN*KPA)	LN(KL) (MOLE SO3/ G*MIN*KPA)
400	10	0.16784	0.00431162	15.6856%	0.0007020	9.1795	6.6062	1.2290	5.3753	48.3505	15.8680	0.8141	1.0000	9.394E-05	-9.2729
450	10	0.15623	0.00429255	16.7762%	0.0006989	9.1408	6.5236	1.3150	4.9608	14.9744	3.8850	0.6634	1.0000	1.153E-04	-9.0683
500	10	0.14613	0.00680272	28.4247%	0.0011076	8.7252	5.6170	2.2386	2.5181	5.3968	1.1410	0.3956	0.9990	3.212E-04	-8.0434
550	10	0.13725	0.01052631	46.8280%	0.0017139	8.0606	4.2160	3.7157	1.1355	2.2018	0.3889	0.1504	0.9621	1.387E-03	-6.5809
600	10	0.12939	0.00966183	45.5931%	0.0015731	8.1055	4.3149	3.6159	1.1933	0.9954	0.1499	0.0884	0.8357	2.628E-03	-5.9415

FORMULATION:

POTASSIUM
M2O/V2O5 MOLE RATIO : 2

TEMP (oC)	PRESSURE (KPAG)	N (MOLES/MIN)	SO3 (MOLES/MIN)	%CONVERSION (MOLE SO3/ MOLE SO2 FE (CORRECTED)	R (MOL SO3/ G*MIN)	PO2 (KPA)	PSO2 (KPA)	PSO3 (KPA)	Q	KP	KC	WI	DIST. FROM EQUILIBRIUM	KL (MOLE SO3/ G*MIN*KPA)	LN(KL) (MOLE SO3/ G*MIN*KPA)
400	10	0.16784	0.00471698	17.1603%	0.0007680	9.1272	6.4945	1.3453	4.8274	48.3505	15.8680	0.8054	1.0000	1.045E-04	-9.1666
450	10	0.15623	0.00442477	17.2909%	0.0007204	9.1625	6.4845	1.3558	4.7827	14.9744	3.8850	0.6588	1.0000	1.199E-04	-9.0291
500	10	0.14613	0.00694444	29.0169%	0.0011307	8.7040	5.5917	2.2858	2.4463	5.3968	1.1410	0.3913	0.9990	3.323E-04	-8.0095
550	10	0.13725	0.01030927	45.8624%	0.0016785	8.0957	4.2940	3.6376	1.1804	2.2018	0.3889	0.1631	0.9655	1.316E-03	-6.6329
600	10	0.12939	0.00990099	48.7216%	0.0016121	8.0644	4.2273	3.7071	1.1403	0.9954	0.1499	0.0856	0.8164	2.861E-03	-5.8565

FORMULATION:

POTASSIUM
M2O/V2O5 MOLE RATIO : 3.5

TEMP (oC)	PRESSURE (KPAG)	N (MOLES/MIN)	SO3 (MOLES/MIN)	%CONVERSION (MOLE SO3/ MOLE SO2 FE (CORRECTED)	R (MOL SO3/ G*MIN)	PO2 (KPA)	PSO2 (KPA)	PSO3 (KPA)	Q	KP	KC	WI	DIST. FROM EQUILIBRIUM	KL (MOLE SO3/ G*MIN*KPA)	LN(KL) (MOLE SO3/ G*MIN*KPA)
400	10	0.16784	0.00515463	18.7525%	0.0008392	9.0706	6.3738	1.4711	4.3326	48.3505	15.8680	0.7963	1.0000	1.163E-04	-9.0603
450	10	0.15623	0.00515463	20.1457%	0.0008392	9.0210	6.2681	1.5813	3.9659	14.9744	3.8850	0.6351	1.0000	1.465E-04	-8.8285
500	10	0.14613	0.00793365	33.1637%	0.0012925	8.5551	5.2740	2.6167	2.0155	5.3968	1.1410	0.3632	0.9984	4.166E-04	-7.7834
550	10	0.13725	0.01058201	47.0768%	0.0017250	8.0515	4.1998	3.7357	1.1242	2.2018	0.3889	0.1584	0.9611	1.405E-03	-6.5675
600	10	0.12939	0.00909090	42.8990%	0.0014802	8.2033	4.5236	3.3985	1.3311	0.9954	0.1499	0.0954	0.8741	2.165E-03	-6.1354

FORMULATION:

POTASSIUM
M2O/V2O5 MOLE RATIO : 5

TEMP (oC)	PRESSURE (KPAG)	N (MOLES/MIN)	SO3 (MOLES/MIN)	%CONVERSION (MOLE SO3/ MOLE SO2 FE (CORRECTED)	R (MOL SO3/ G*MIN)	PO2 (KPA)	PSO2 (KPA)	PSO3 (KPA)	Q	KP	KC	WI	DIST. FROM EQUILIBRIUM	KL (MOLE SO3/ G*MIN*KPA)	LN(KL) (MOLE SO3/ G*MIN*KPA)
400	10	0.16784	0.00561797	20.4381%	0.0009147	9.0106	6.2458	1.6044	3.8928	48.3505	15.8680	0.7870	1.0000	1.290E-04	-8.9557
450	10	0.15623	0.00510204	19.9390%	0.0008307	9.0283	6.2837	1.5650	4.0151	14.9744	3.8850	0.6367	1.0000	1.445E-04	-8.8471
500	10	0.14613	0.00641025	26.7848%	0.0010437	8.7840	5.7623	2.1081	2.7335	5.3968	1.1410	0.4077	0.9992	2.917E-04	-8.1340
550	10	0.13725	0.01030927	45.8624%	0.0016782	8.0957	4.2940	3.6376	1.1804	2.2018	0.3889	0.1631	0.9655	1.316E-03	-6.6329
600	10	0.12939	0.00961538	45.3730%	0.0015655	8.1134	4.3319	3.5982	1.2039	0.9954	0.1499	0.0889	0.8393	2.586E-03	-5.9577

SUMMARY OF ACTIVATION ENERGY

COMPOSITION M2O/V2O5 2.5: M	ACTIVATION ENERGY (J/MOLE)
LI	111838.57
NA	111150.48
K	106049.24
CS	103941.49

ASSUME MELT DENCITY(G/CM^3) : 2
MM K2S2O7 : 254.33
MM V2O5 : 181.88

COMPOSITION POTASSIUM M2O/V2O5	G CAT/ G CELITE	CV (G V2O5/ CM^3 MELT)	CV^2	ACTIVATION ENERGY (J/MOLE)	LN(Z2*AL)	Z2*AL (MOLE SO3 G*MIN*KPA
1.5	0.1690125	0.6456800	0.4169002	114047.75	9.863177	1.92E+04
	0.1726315	0.5267761	0.277493	114407.12	9.944114	2.08E+04
2.5	0.1752225	0.4440548	0.197185	106049.24	8.905916	7.37E+03
3.5	0.1786725	0.3393172	0.115146	98145.270	7.534380	1.87E+03
5	0.1816125	0.2502597	0.062629	106417.36	8.723003	6.14E+03

APPENDIX B2: Results: Different Na/K and M_2O/V_2O_5 mole ratios

DIFFERENT NA/K & M2O/V2O5 RATIO'S:

CATALYST PELLET SIZE: 1-1.18MM
CATALYST DILUTION = 3 G CAT ' 3 G CERAMIC
TIME BETWEEN TEMP. RUNS = 60 MIN
TITRATION SOLUT. STRENGTH (N): 1.00
TITRATER CORRECTION FACTOR : 2.04722
LIQUID LOADIND MOLE CATALYST/G CELITE = 0.0015
M2SO4/MOH MOLE RATIO = 0.4
PARAMETER S = 0.5
CONSTANT FOR KP EQUATION, A = 4956
CONSTANT FOR KP EQUATION, B = 4.678

GAS COMPOSITION(MOLE %):

SO2	8.00%
O2	10.00%
N2	82.00%

REACTOR CONDITIONS :

LINEAR VELOCITY (M/S)	0.2
REACTOR DIAMETER (M)	0.032
MASS OF CATALYST (KG)	0.003
ATM. PRESSURE (KPA)	87.326

FORMULATION:

M2O/V2O5 = 2
NA/K = 0.1

TEMP. (OC)	PRESSURE (KPAG)	N (MOLES/MIN)	SO3 (MOLES/MIN)	%CONVERSION (MOLE SO3/ MOLE SO2 FE (CORRECTED)	R (MOL SO3/ G*MIN)	PO2 (KPA)	PSO2 (KPA)	PSO3 (KPA)	Q	KP	KC	WI	DIST. FROM EQUILIBRIUM	KL (MOLE SO3/ G*MIN*KPA)
400	10	0.16784	0.00316455	11.5126%	0.000515	9.3274	6.9216	0.9005	7.6861	48.3505	15.8680	0.8408	1.0000	6.570E-05
450	10	0.15623	0.00320512	12.5263%	0.000521	9.2915	6.8451	0.9802	6.9832	14.9744	3.8850	0.7038	1.0000	7.980E-05
500	10	0.14613	0.00574712	24.0140%	0.000935	8.8831	5.9737	1.8879	3.1642	5.3968	1.1410	0.4293	0.9994	2.455E-04
550	10	0.13725	0.00854008	37.9919%	0.001390	8.3809	4.9025	3.0037	1.6321	2.2018	0.3889	0.1966	0.9842	8.573E-04
600	10	0.12939	0.00840336	39.6545%	0.001368	8.3208	4.7743	3.1373	1.5218	0.9954	0.1499	0.1045	0.9087	1.732E-03

FORMULATION:

M2O/V2O5 = 2
NA/K = 0.2

TEMP. (OC)	PRESSURE (KPAG)	N (MOLES/MIN)	SO3 (MOLES/MIN)	%CONVERSION (MOLE SO3/ MOLE SO2 FE (CORRECTED)	R (MOL SO3/ G*MIN)	PO2 (KPA)	PSO2 (KPA)	PSO3 (KPA)	Q	KP	KC	WI	DIST. FROM EQUILIBRIUM	KL (MOLE SO3/ G*MIN*KPA)
400	10	0.16784	0.0030644	11.1482%	0.000498	9.3402	6.9491	0.8719	7.9700	48.3505	15.8680	0.8433	1.0000	6.334E-05
450	10	0.15623	0.00331125	12.9411%	0.000539	9.2768	6.8137	1.0128	6.7273	14.9744	3.8850	0.6996	1.0000	8.308E-05
500	10	0.14613	0.00576923	24.1064%	0.000939	8.8798	5.9667	1.8952	3.1483	5.3968	1.1410	0.4285	0.9994	2.470E-04
550	10	0.13725	0.0091743	40.8133%	0.001493	8.2789	4.6848	3.2305	1.4502	2.2018	0.3889	0.1840	0.9791	1.002E-03
600	10	0.12939	0.0086956	41.0335%	0.001415	8.2709	4.6678	3.2482	1.4370	0.9954	0.1499	0.1005	0.8953	1.902E-03

FORMULATION:

M2O/V2O5 = 2
NA/K = 0.6

TEMP. (OC)	PRESSURE (KPAG)	N (MOLES/MIN)	SO3 (MOLES/MIN)	%CONVERSION (MOLE SO3/ MOLE SO2 FE (CORRECTED)	R (MOL SO3/ G*MIN)	PO2 (KPA)	PSO2 (KPA)	PSO3 (KPA)	Q	KP	KC	WI	DIST. FROM EQUILIBRIUM	KL (MOLE SO3/ G*MIN*KPA)
400	10	0.16784	0.003676	13.3732%	0.000598	9.2615	6.7811	1.0469	6.4776	48.3505	15.8680	0.8285	1.0000	7.800E-05
450	10	0.15623	0.00387596	15.1481%	0.000631	9.1986	6.6469	1.1866	5.6015	14.9744	3.8850	0.6781	1.0000	1.012E-04
500	10	0.14613	0.00607903	25.4008%	0.000989	8.8335	5.8680	1.9980	2.9369	5.3968	1.1410	0.4182	0.9993	2.681E-04
550	10	0.13725	0.00961538	42.7756%	0.001565	8.2078	4.5331	3.3885	1.3378	2.2018	0.3889	0.1756	0.9746	1.115E-03
600	10	0.12939	0.00922618	43.5373%	0.001502	8.1801	4.4741	3.4499	1.2969	0.9954	0.1499	0.0937	0.8659	2.265E-03

FORMULATION:

M2O/V2O5 = 2.5
NA/K = 0.1

TEMP. (OC)	PRESSURE (KPAG)	N (MOLES/MIN)	SO3 (MOLES/MIN)	%CONVERSION (MOLE SO3/ MOLE SO2 FE (CORRECTED)	R (MOL SO3/ G*MIN)	PO2 (KPA)	PSO2 (KPA)	PSO3 (KPA)	Q	KP	KC	WI	DIST. FROM EQUILIBRIUM	KL (MOLE SO3/ G*MIN*KPA)
400	10	0.16784	0.00490196	17.8333%	0.000798	9.1033	6.4435	1.3985	4.6075	48.3505	15.8680	0.8016	1.0000	1.094E-04
450	10	0.15623	0.00442477	17.2930%	0.000720	9.1225	6.4845	1.3558	4.7827	14.9744	3.8850	0.6588	1.0000	1.199E-04
500	10	0.14613	0.00806451	33.6971%	0.001313	8.5358	5.2329	2.6595	1.9676	5.3968	1.1410	0.3597	0.9983	4.284E-04
550	10	0.13725	0.0106383	47.3262%	0.001732	8.0424	4.1804	3.7560	1.1130	2.2018	0.3889	0.1575	0.9602	1.424E-03
600	10	0.12939	0.00909166	42.9025%	0.001480	8.2032	4.5233	3.3987	1.3309	0.9954	0.1499	0.0953	0.8740	2.165E-03

FORMULATION:

M2O/V2O5 : 2.5
NA/K : 1000000

TEMP. (OC)	PRESSURE (KPAG)	N (MOLES/MIN)	SO3 (MOLES/MIN)	%CONVERSION (MOLE SO3/ MOLE SO2 FE (CORRECTED)	R (MOL SO3/ G*MIN)	PO2 (KPA)	PSO2 (KPA)	PSO3 (KPA)	Q	KP	KC	WI	DIST. FROM EQUILIBRIUM	KL (MOLE SO3/ G*MIN*KPA)
400	10	0.16784	0.00467289	16.9999%	0.000760	9.1329	6.5067	1.3327	4.8824	48.3505	15.8680	0.8064	1.0000	1.033E-04
450	10	0.15623	0.00469483	18.3404%	0.000764	9.0850	6.4045	1.4392	4.4501	14.9744	3.8850	0.6498	1.0000	1.295E-04
500	10	0.14613	0.00621118	25.9530%	0.001011	8.8137	5.8258	2.0419	2.8531	5.3968	1.1410	0.4140	0.9993	2.774E-04
550	10	0.13725	0.00869565	38.6840%	0.001415	8.3559	4.8491	3.0593	1.5850	2.2018	0.3889	0.1934	0.9831	8.910E-04
600	10	0.12939	0.01010101	47.6655%	0.001644	8.0301	4.1540	3.7834	1.0980	0.9954	0.1499	0.0833	0.7985	3.079E-03

FORMULATION:

M2O/V2O5 : 2.5
NA/K : 0

TEMP. (OC)	PRESSURE (KPAG)	N (MOLES/MIN)	SO3 (MOLES/MIN)	%CONVERSION (MOLE SO3/ MOLE SO2 FE (CORRECTED)	R (MOL SO3/ G*MIN)	PO2 (KPA)	PSO2 (KPA)	PSO3 (KPA)	Q	KP	KC	WI	DIST. FROM EQUILIBRIUM	KL (MOLE SO3/ G*MIN*KPA)
400	10	0.16784	0.00632911	23.0252%	0.001030	8.9184	6.0490	1.8094	3.3431	48.3505	15.8680	0.7731	1.0000	1.495E-04
450	10	0.15623	0.00595238	23.2632%	0.000969	8.9099	6.0309	1.8283	3.2986	14.9744	3.8850	0.6110	0.9999	1.780E-04
500	10	0.14613	0.008	33.4275%	0.001302	8.5455	5.2536	2.6380	1.9916	5.3968	1.1410	0.3614	0.9984	4.254E-04
550	10	0.13725	0.01063829	47.3261%	0.001732	8.0424	4.1804	3.7560	1.1130	2.2018	0.3889	0.1575	0.9602	1.424E-03
600	10	0.12939	0.01041666	49.1551%	0.001696	7.9758	4.0382	3.9040	1.0344	0.9954	0.1499	0.0798	0.7664	3.475E-03

FORMULATION:

M2O/V2O5 : 1.5
NA/K : 0

TEMP. (OC)	PRESSURE (KPAG)	N (MOLES/MIN)	SO3 (MOLES/MIN)	%CONVERSION (MOLE SO3/ MOLE SO2 FE (CORRECTED)	R (MOL SO3/ G*MIN)	PO2 (KPA)	PSO2 (KPA)	PSO3 (KPA)	Q	KP	KC	WI	DIST. FROM EQUILIBRIUM	KL (MOLE SO3/ G*MIN*KPA)
400	10	0.16784	0.00431162	15.6856%	0.000702	9.1795	6.6062	1.2290	5.3753	48.3505	15.8680	0.8141	1.0000	9.394E-05
450	10	0.15623	0.00429255	16.7762%	0.000698	9.1408	6.5236	1.3150	4.9608	14.9744	3.8850	0.6634	1.0000	1.153E-04
500	10	0.14613	0.00680272	28.4247%	0.001107	8.7252	5.6370	2.2386	2.5181	5.3968	1.1410	0.3956	0.9990	3.212E-04
550	10	0.13725	0.01052631	46.8280%	0.001713	8.0606	4.2190	3.7157	1.1355	2.2018	0.3889	0.1594	0.9621	1.387E-03
600	10	0.12939	0.00966183	45.5931%	0.001573	8.1055	4.3149	3.6159	1.1933	0.9954	0.1499	0.0884	0.8357	2.628E-03

FORMULATION:

M2O/V2O5 : 2
NA/K : 0

TEMP. (OC)	PRESSURE (KPAG)	N (MOLES/MIN)	SO3 (MOLES/MIN)	%CONVERSION (MOLE SO3/ MOLE SO2 FE (CORRECTED)	R (MOL SO3/ G*MIN)	PO2 (KPA)	PSO2 (KPA)	PSO3 (KPA)	Q	KP	KC	WI	DIST. FROM EQUILIBRIUM	KL (MOLE SO3/ G*MIN*KPA)
400	10	0.16784	0.00471698	17.1603%	0.000768	9.1272	6.4945	1.3453	4.8274	48.3505	15.8680	0.8054	1.0000	1.045E-04
450	10	0.15623	0.00442477	17.2929%	0.000720	9.1225	6.4845	1.3558	4.7827	14.9744	3.8850	0.6588	1.0000	1.199E-04
500	10	0.14613	0.00694444	29.0169%	0.001130	8.7040	5.5917	2.2858	2.4463	5.3968	1.1410	0.3913	0.9990	3.323E-04
550	10	0.13725	0.01030927	45.8624%	0.001678	8.0957	4.2940	3.6376	1.1804	2.2018	0.3889	0.1631	0.9655	1.316E-03
600	10	0.12939	0.00990099	46.7216%	0.001612	8.0644	4.2273	3.7071	1.1403	0.9954	0.1499	0.0856	0.8164	2.861E-03

FORMULATION:

M2O/V2O5 : 3.5
NA/K : 0

TEMP. (OC)	PRESSURE (KPAG)	N (MOLES/MIN)	SO3 (MOLES/MIN)	%CONVERSION (MOLE SO3/ MOLE SO2 FE (CORRECTED)	R (MOL SO3/ G*MIN)	PO2 (KPA)	PSO2 (KPA)	PSO3 (KPA)	Q	KP	KC	WI	DIST. FROM EQUILIBRIUM	KL (MOLE SO3/ G*MIN*KPA)
400	10	0.16784	0.00515463	18.7525%	0.000839	9.0706	6.3738	1.4711	4.3326	48.3505	15.8680	0.7963	1.0000	1.162E-04
450	10	0.15623	0.00515463	20.1454%	0.000839	9.0210	6.2681	1.5813	3.9639	14.9744	3.8850	0.6351	1.0000	1.465E-04
500	10	0.14613	0.0079365	33.1622%	0.001292	8.5551	5.2740	2.6167	2.0155	5.3968	1.1410	0.3632	0.9984	4.166E-04
550	10	0.13725	0.01058201	47.0758%	0.001722	8.0515	4.1998	3.7357	1.1242	2.2018	0.3889	0.1584	0.9611	1.405E-03
600	10	0.12939	0.00909090	42.8990%	0.001480	8.2033	4.5236	3.3985	1.3311	0.9954	0.1499	0.0954	0.8741	2.165E-03

FORMULATION:

M2O/V2O5 : 5
NA/K : 0.1

TEMP. (OC)	PRESSURE (KPAG)	N (MOLES/MIN)	SO3 (MOLES/MIN)	%CONVERSION (MOLE SO3/ MOLE SO2 FE (CORRECTED)	R (MOL SO3/ G*MIN)	PO2 (KPA)	PSO2 (KPA)	PSO3 (KPA)	Q	KP	KC	WI	DIST. FROM EQUILIBRIUM	KL (MOLE SO3/ G*MIN*KPA)
400	10	0.16784	0.004245	15.4432%	0.000691	9.1881	6.6246	1.2099	5.4753	48.3505	15.8680	0.8156	1.0000	9.223E-05
450	10	0.15623	0.00406455	15.8851%	0.000661	9.1725	6.5911	1.2447	5.2952	14.9744	3.8850	0.6713	1.0000	1.075E-04
500	10	0.14613	0.00662028	27.6624%	0.001077	8.7525	5.6953	2.1779	2.6150	5.3968	1.1410	0.4011	0.9991	3.073E-04
550	10	0.13725	0.00909090	40.4424%	0.001480	8.2923	4.7135	3.2007	1.4727	2.2018	0.3889	0.1856	0.9798	9.817E-04
600	10	0.12939	0.0089686	42.3218%	0.001460	8.2242	4.5682	3.3520	1.3628	0.9954	0.1499	0.0969	0.8811	2.079E-03

FORMULATION:

M2O/V2O5 : 2.5
NA/K : 0.2

TEMP. (OC)	PRESSURE (KPAG)	N (MOLES/MIN)	SO3 (MOLES/MIN)	%CONVERSION (MOLE SO3/ MOLE SO2 FE (CORRECTED)	R (MOL SO3/ G*MIN)	PO2 (KPA)	PSO2 (KPA)	PSO3 (KPA)	Q	KP	KC	WI	DIST. FROM EQUILIBRIUM	KL (MOLE SO3/ G*MIN*KPA)
400	10	0.16784	0.0053192	19.3512%	0.000866	9.0493	6.3284	1.5185	4.1676	48.3505	15.8680	0.7930	1.0000	1.207E-04
450	10	0.15623	0.00526315	20.5695%	0.000856	9.0059	6.2358	1.6148	3.8616	14.9744	3.8850	0.6317	1.0000	1.506E-04
500	10	0.14613	0.0067114	28.0432%	0.001092	8.7389	5.6662	2.2082	2.5659	5.3968	1.1410	0.3983	0.9991	3.142E-04
550	10	0.13725	0.01010101	44.9360%	0.001644	8.1293	4.3658	3.5628	1.2254	2.2018	0.3889	0.1668	0.9685	1.252E-03
600	10	0.12939	0.01	47.1889%	0.001628	8.0474	4.1910	3.7448	1.1191	0.9954	0.1499	0.0845	0.8077	2.966E-03

FORMULATION:

M2O/V2O5 : 5
NA/K : 0.2

TEMP. (OC)	PRESSURE (KPAG)	N (MOLES/MIN)	SO3 (MOLES/MIN)	%CONVERSION (MOLE SO3/ MOLE SO2 FE (CORRECTED)	R (MOL SO3/ G*MIN)	PO2 (KPA)	PSO2 (KPA)	PSO3 (KPA)	Q	KP	KC	WI	DIST. FROM EQUILIBRIUM	KL (MOLE SO3/ G*MIN*KPA)
400	10	0.16784	0.005	18.1899%	0.000814	9.0906	6.4165	1.4267	4.4975	48.3505	15.8680	0.7995	1.0000	1.120E-04
450	10	0.15623	0.00480769	18.7895%	0.000782	9.0693	6.3710	1.4740	4.3221	14.9744	3.8850	0.6462	1.0000	1.336E-04
500	10	0.14613	0.00746268	31.1824%	0.001215	8.6263	5.4259	2.4585	2.2069	5.3968	1.1410	0.3763	0.9987	3.748E-04
550	10	0.13725	0.00990099	44.0461%	0.001612	8.1617	4.4347	3.4910	1.2703	2.2018	0.3889	0.1704	0.9712	1.194E-03
600	10	0.12939	0.00961538	45.3739%	0.001565	8.1134	4.3319	3.5982	1.2039	0.9954	0.1499	0.0889	0.8393	2.586E-03

FORMULATION:

M2O/V2O5 : 2.5
NA/K : 0.6

TEMP. (OC)	PRESSURE (KPAG)	N (MOLES/MIN)	SO3 (MOLES/MIN)	%CONVERSION (MOLE SO3/ MOLE SO2 FE (CORRECTED)	R (MOL SO3/ G*MIN)	PO2 (KPA)	PSO2 (KPA)	PSO3 (KPA)	Q	KP	KC	WI	DIST. FROM EQUILIBRIUM	KL (MOLE SO3/ G*MIN*KPA)
400	10	0.16784	0.00431034	15.6810%	0.000701	9.1797	6.6066	1.2286	5.3772	48.3505	15.8680	0.8142	1.0000	9.390E-05
450	10	0.15623	0.00436681	17.0664%	0.000711	9.1305	6.5017	1.3379	4.8595	14.9744	3.8850	0.6608	1.0000	1.178E-04
500	10	0.14613	0.00677966	28.3284%	0.001103	8.7287	5.6444	2.2309	2.5300	5.3968	1.1410	0.3963	0.9990	3.194E-04
550	10	0.13725	0.00970873	43.1909%	0.001580	8.1927	4.5010	3.4220	1.3153	2.2018	0.3889	0.1739	0.9735	1.140E-03
600	10	0.12939	0.00934579	44.1017%	0.001521	8.1596	4.4304	3.4955	1.2675	0.9954	0.1499	0.0922	0.8582	2.358E-03

FORMULATION:

M2O/V2O5 : 5
NA/K : 0.6

TEMP. (OC)	PRESSURE (KPAG)	N (MOLES/MIN)	SO3 (MOLES/MIN)	%CONVERSION (MOLE SO3/ MOLE SO2 FE (CORRECTED)	R (MOL SO3/ G*MIN)	PO2 (KPA)	PSO2 (KPA)	PSO3 (KPA)	Q	KP	KC	WI	DIST. FROM EQUILIBRIUM	KL (MOLE SO3/ G*MIN*KPA)
400	10	0.16784	0.00416666	15.1583%	0.000678	9.1983	6.6461	1.1874	5.5971	48.3505	15.8680	0.8173	1.0000	9.024E-05
450	10	0.15623	0.00423728	16.5602%	0.000689	9.1485	6.5400	1.2980	5.0386	14.9744	3.8850	0.6653	1.0000	1.134E-04
500	10	0.14613	0.00621118	25.9530%	0.001011	8.8137	5.8258	2.0419	2.8531	5.3968	1.1410	0.4140	0.9993	2.774E-04
550	10	0.13725	0.00961538	42.7756%	0.001565	8.2078	4.5331	3.3885	1.3378	2.2018	0.3889	0.1756	0.9746	1.115E-03
600	10	0.12939	0.00943396	44.5178%	0.001536	8.1445	4.3982	3.5290	1.2463	0.9954	0.1499	0.0911	0.8523	2.429E-03

FORMULATION:

M2O/V2O5 = 5
NA/K = 0

TEMP. (oC)	PRESSURE (KPAG)	N (MOLES/MIN)	SO3 (MOLES/MIN)	%CONVERSION (MOLE SO3/ MOLE SO2 FE (CORRECTED)	R (MOL SO3/ G*MIN)	PO2 (KPA)	PSO2 (KPA)	PSO3 (KPA)	Q	KP	KC	WI	DIST. FROM EQUILIBRIUM	KL (MOLE SO3/ G*MIN*KPA)
400	10	0.16784	0.00561797	20.4381%	0.000914	9.0106	6.2458	1.6044	3.8928	48.3505	15.8680	0.7870	1.0000	1.290E-04
450	10	0.15623	0.00510204	19.9398%	0.000830	9.0283	6.2837	1.5650	4.0151	14.9744	3.8850	0.6367	1.0000	1.445E-04
500	10	0.14613	0.00641025	26.7848%	0.001043	8.7840	5.7623	2.1081	2.7335	5.3968	1.1410	0.4077	0.9992	2.917E-04
550	10	0.13725	0.01030927	45.8624%	0.001678	8.0957	4.2940	3.6376	1.1804	2.2018	0.3889	0.1631	0.9655	1.316E-03
600	10	0.12939	0.00961538	45.3739%	0.001565	8.1134	4.3319	3.5982	1.2039	0.9954	0.1499	0.0889	0.8393	2.586E-03

SUMMARY OF ACTIVATION ENERGY:

M2O/V2O5	NA/K MOLE RATIO 0	0.1	0.2	0.6	1000000
1.5	114048				
2	114407	110330	113617	112918	
2.5	106049	104628	107932	107805	111159
3.5	98143				
5	106417	105640	105570	110998	

APPENDIX B3:
Results for different M_2SO_4/MOH mole ratios

DIFFERENT M2SO4/MOH MOLE RATIO'S

CATALYST PELLET SIZE: 1-1.18MM
CATALYST DILUTION : 3 G CAT + 3 G CERAMIC
TIME BETWEEN TEMP. RUNS : 60 MIN
TITRATION SOLUT. STRENGTH (N): 1.00
TITRATER CORRECTION FACTOR : 2.04722
LIQUID LOADING MOLE CATALYST/G CELITE : 0.002
M2O/V2O5 MOLE RATIO : 2.5
NA/K MOLE RATIO : 0.2
PARAMETER S : 0.5

GAS COMPOSITION(MOLE %):

SO2	8.00%
O2	10.00%
N2	82.00%

REACTOR CONDITIONS :

LINEAR VELOCITY (M/S)	0.2
REACTOR DIAMETER (M)	0.032
MASS OF CATALYST (KG)	0.003
ATM. PRESSURE (KPA)	87.326

FORMULATION:

M2SO4/MOH MOLE RATIO : 0

TEMP. (OC)	PRESSURE (KPAG)	N (MOLES/MIN)	SO3 (MOLES/MIN)	%CONVERSION (MOLE SO3/ MOLE SO2 FE (CORRECTED)	R (MOL SO3/ G*MIN)	Po2 (KPA)	Pso2 (KPA)	Pso3 (KPA)	Q	KP	Kc	Wi	DIST. FROM EQUILIBRIUM	KL (MOLE SO3/ G*MIN*KPA)
400	10	0.16784	0.00442477	16.0972%	0.000720	9.1649	6.5751	1.2615	5.2122	48.3505	15.8680	0.8117	1.0000	9.685E-05
450	10	0.15623	0.00526315	20.5695%	0.000856	9.0059	6.2356	1.6148	3.8616	14.9744	3.8850	0.6317	1.0000	1.506E-04
500	10	0.14613	0.00738007	30.8371%	0.001201	8.6387	5.4523	2.4310	2.2428	5.3968	1.1410	0.3787	0.9987	3.678E-04
550	10	0.13725	0.00900900	40.0780%	0.001466	8.3055	4.7416	3.1713	1.4951	2.2018	0.3889	0.1872	0.9805	9.623E-04
600	10	0.12939	0.00921658	43.4920%	0.001500	8.1818	4.4777	3.4463	1.2993	0.9954	0.1499	0.0938	0.8665	2.257E-03

FORMULATION:

M2SO4/MOH MOLE RATIO : 0.4

TEMP. (OC)	PRESSURE (KPAG)	N (MOLES/MIN)	SO3 (MOLES/MIN)	%CONVERSION (MOLE SO3/ MOLE SO2 FE (CORRECTED)	R (MOL SO3/ G*MIN)	Po2 (KPA)	Pso2 (KPA)	Pso3 (KPA)	Q	KP	Kc	Wi	DIST. FROM EQUILIBRIUM	KL (MOLE SO3/ G*MIN*KPA
400	10	0.16784	0.00595238	21.6547%	0.000969	8.9672	6.1533	1.7008	3.6179	48.3505	15.8680	0.7804	1.0000	1.385E-04
450	10	0.15623	0.0054945	21.4737%	0.000894	8.9737	6.1671	1.6864	3.6569	14.9744	3.8850	0.6246	0.9999	1.596E-04
500	10	0.14613	0.00819672	34.2495%	0.001334	8.5159	5.1905	2.7037	1.9198	5.3968	1.1410	0.3561	0.9982	4.408E-04
550	10	0.13725	0.01010101	44.9360%	0.001644	8.1293	4.3658	3.5628	1.2254	2.2018	0.3889	0.1668	0.9685	1.252E-03
600	10	0.12939	0.00909090	42.8990%	0.001480	8.2033	4.5236	3.3985	1.3311	0.9954	0.1499	0.0954	0.8741	2.165E-03

FORMULATION:

M2SO4/MOH MOLE RATIO : 1

TEMP. (OC)	PRESSURE (KPAG)	N (MOLES/MIN)	SO3 (MOLES/MIN)	%CONVERSION (MOLE SO3/ MOLE SO2 FE (CORRECTED)	R (MOL SO3/ G*MIN)	Po2 (KPA)	Pso2 (KPA)	Pso3 (KPA)	Q	KP	Kc	Wi	DIST. FROM EQUILIBRIUM	KL (MOLE SO3/ G*MIN*KPA
400	10	0.16784	0.00602409	21.9156%	0.000980	8.9579	6.1335	1.7215	3.5630	48.3505	15.8680	0.7790	1.0000	1.406E-04
450	10	0.15623	0.00561797	21.9562%	0.000914	8.9565	6.1304	1.7247	3.5545	14.9744	3.8850	0.6209	0.9999	1.645E-04
500	10	0.14613	0.00826446	34.5325%	0.001345	8.5057	5.1687	2.7264	1.8958	5.3968	1.1410	0.3543	0.9982	4.473E-04
550	10	0.13725	0.01036269	46.1001%	0.001687	8.0870	4.2755	3.6568	1.1692	2.2018	0.3889	0.1622	0.9647	1.333E-03
600	10	0.12939	0.00961538	45.3739%	0.001565	8.1134	4.3319	3.5982	1.2039	0.9954	0.1499	0.0889	0.8393	2.586E-03

FORMULATION:

M2SO4/MOH MOLE RATIO : 1000000

TEMP. (OC)	PRESSURE (KPAG)	N (MOLES/MIN)	SO3 (MOLES/MIN)	%CONVERSION (MOLE SO3/ MOLE SO2 FE (CORRECTED)	R (MOL SO3/ G*MIN)	Po2 (KPA)	Pso2 (KPA)	Pso3 (KPA)	Q	KP	Kc	Wi	DIST. FROM EQUILIBRIUM	KL (MOLE SO3/ G*MIN*KPA
400	10	0.16784	0.0054945	19.9889%	0.000894	9.0266	6.2799	1.5689	4.0028	48.3505	15.8680	0.7895	1.0000	1.255E-04
450	10	0.15623	0.00581395	22.7221%	0.000946	8.9292	6.0721	1.7854	3.4010	14.9744	3.8850	0.6150	0.9999	1.724E-04
500	10	0.14613	0.00833333	34.8203%	0.001356	8.4954	5.1466	2.7494	1.8719	5.3968	1.1410	0.3525	0.9981	4.539E-04
550	10	0.13725	0.00913242	40.6270%	0.001486	8.2856	4.6992	3.2155	1.4614	2.2018	0.3889	0.1848	0.9794	9.917E-04
600	10	0.12939	0.00840336	39.6545%	0.001368	8.3208	4.7743	3.1373	1.5218	0.9954	0.1499	0.1045	0.9087	1.732E-03

SUMMARY OF ACTIVATION ENERGY

M2SO4/MOH MOLE RATIO	LOG(M2SO4/MOH)	ACTIVATION ENERGY (J/MOLE)
0.001	-3	95186.1913
0.4	-0.397940	93470.2777
1	0	98439.0790
1000	3	81220.2671

APPENDIX B4: Results for different liquid loadings

DIFFERENT LIQUID LOADINGS

CATALYST PELLET SIZE: 1-1.18MM
CATALYST DILUTION : 3 G CAT + 3 G CERAMIC
TIME BETWEEN TEMP. RUNS = 60 MIN
TITRATION SOLUT. STRENGTH (N): 1.00
TITRATER CORRECTION FACTOR : 2.04722
NA/K MOLE RATIO : 0.2
M2O/V2O5 MOLE RATIO: 2.5
PARAMETER S: 0.5
MELT DENCITY (ASSUMP.)(G/CM^3): 2.2
ASSUMED M2SO4/M2S2O7 MOLE RATIO: 1
PORE VOL. OF SUPPORT,VP,(CM^3 PORES/G CEL.): 1.0472
APPARENT DENCITY OF THE SUPPORT(G/CM^3): 0.712

GAS COMPOSITION(MOLE %):

SO2	8.00%
O2	10.00%
N2	82.00%

REACTOR CONDITIONS.:

LINEAR VELOCITY (M/S)	0.2
REACTOR DIAMETER (M)	0.035
MASS OF CATALYST (KG)	0.003
ATM. PRESSURE (KPA)	87.326

MOLECULAR WEIGHTS:

	MM
K2S2O7	254.33
NA2S2O7	222.16
V2O5	181.88
K2SO4	174.27
NA2SO4	142.04

FORMULATION:

Gv,G V2O5/G CEL.: 0.0259828 G K2SO4/ G CEL.: 0.0259330 CM^3 ACTIVE MELT : 0.12464490
G NA2SO4/ G CEL.: 0.0042273 G K2S2O7/G CEL.: 0.0378467 CV (G V2O5/CM^3 MELT): 0.56820281
G NA2S2O7/G CAL.: 0.0066119 G CATALYST/G CEL.: 0.1006019 LIQUID LOADING FACTOR: 0.04366705

MOLE CAT./G CELITE : 0.0005

TEMP. (OC)	PRESSURE (KPAG)	N (MOLES/MIN)	SO3 (MOLES/MIN)	%CONVERSION (MOLE SO3/ MOLE SO2 FEED)	PSO2 (KPA)	PO2 (KPA)	PSO3 (KPA)	KC	KP^-0.5 (KPA)	Q	DISTANCE FROM EQUILIBRIUM	WI	RL (MOLE SO3/ CM3 MELT*S)	RV (MOLE SO3/ CM3 PELLET*S
400	10	0.16784	0.00409836	14.9098%	6.6649	9.2071	1.1679	15.8680	48.3505	5.7070	1.0000	0.8109	2.677E-04	8.715E-06
450	10	0.15623	0.00416666	16.2843%	6.5609	9.1583	1.2762	3.8850	14.9744	5.1409	1.0000	0.6677	2.721E-04	8.861E-06
500	10	0.14613	0.00454545	18.9939%	6.3556	9.0620	1.4901	1.1410	5.3968	4.2651	0.9998	0.4735	2.969E-04	9.666E-06
550	10	0.13725	0.00729927	32.4720%	5.3270	8.5799	2.5616	0.3889	2.2018	2.0796	0.9944	0.2242	4.767E-04	1.552E-05
600	10	0.12939	0.00858369	40.5055%	4.7086	8.2900	3.2057	0.1499	0.9954	1.4688	0.9436	0.1020	5.606E-04	1.825E-05

FORMULATION:

Gv,G V2O5/G CEL.: 0.0519657 G K2SO4/ G CEL.: 0.0518660 CM^3 ACTIVE MELT : 0.22841155
G NA2SO4/ G CEL.: 0.0084547 G K2S2O7/G CEL.: 0.0756934 CV (G V2O5/CM^3 MELT): 0.56820281
G NA2S2O7/G CAL.: 0.0132238 G CATALYST/G CEL.: 0.2012038 LIQUID LOADING FACTOR: 0.08733410

MOLE CAT./G CELITE : 0.001

TEMP. (OC)	PRESSURE (KPAG)	N (MOLES/MIN)	SO3 (MOLES/MIN)	%CONVERSION (MOLE SO3/ MOLE SO2 FEED)	PSO2 (KPA)	PO2 (KPA)	PSO3 (KPA)	KC	KP^-0.5 (KPA)	Q	DISTANCE FROM EQUILIBRIUM	WI	RL (MOLE SO3/ CM3 MELT*S)	RV (MOLE SO3/ CM3 PELLET*S
400	10	0.16784	0.00454545	16.5363%	6.5418	9.1494	1.2961	15.8680	48.3505	5.0473	1.0000	0.8091	1.620E-04	1.055E-05
450	10	0.15623	0.00425531	16.2307%	6.5347	9.1460	1.2735	3.8850	14.9744	5.0130	1.0000	0.6647	1.617E-04	9.876E-06
500	10	0.14613	0.00539083	20.5051%	6.0871	8.9162	1.7698	1.1410	5.3968	3.4395	0.9997	0.4416	1.921E-04	1.251E-05
550	10	0.13725	0.00896860	39.8983%	4.7555	8.3120	3.1569	0.3889	2.2018	1.5061	0.9891	0.1880	3.197E-04	2.082E-05
600	10	0.12939	0.00884955	41.7600%	4.6116	8.2446	3.3067	0.1499	0.9954	1.3946	0.9371	0.0985	3.154E-04	2.054E-05

FORMULATION:

Gv,G V2O5/G CEL.: 0.0779485 G K2SO4/ G CEL.: 0.0777991 CM^3 ACTIVE MELT : 0.31614029
G NA2SO4/ G CEL.: 0.0126821 G K2S2O7/G CEL.: 0.1135401 CV (G V2O5/CM^3 MELT): 0.56820281
G NA2S2O7/G CAL.: 0.0198357 G CATALYST/G CEL.: 0.3018057 LIQUID LOADING FACTOR: 0.13100116

MOLE CAT./G CELITE : 0.0015

TEMP. (OC)	PRESSURE (KPAG)	N (MOLES/MIN)	SO3 (MOLES/MIN)	%CONVERSION (MOLE SO3/ MOLE SO2 FEED)	PSO2 (KPA)	PO2 (KPA)	PSO3 (KPA)	KC	KP^-0.5 (KPA)	Q	DISTANCE FROM EQUILIBRIUM	WI	RL (MOLE SO3/ CM3 MELT*S)	RV (MOLE SO3/ CM3 PELLET*S
400	10	0.16784	0.0053192	19.3512%	6.3284	9.0493	1.5185	15.8680	48.3505	4.1676	1.0000	0.7930	1.370E-04	1.338E-05
450	10	0.15623	0.00526315	20.5695%	6.2358	9.0059	1.6148	3.8850	14.9744	3.8616	1.0000	0.6317	1.355E-04	1.324E-05
500	10	0.14613	0.0067114	28.0432%	5.6662	8.7389	2.2082	1.1410	5.3968	2.5659	0.9994	0.3903	1.758E-04	1.717E-05
550	10	0.13725	0.01010101	44.9360%	4.3658	8.1293	3.5628	0.3889	2.2018	1.2254	0.9831	0.1668	3.601E-04	3.517E-05
600	10	0.12939	0.01	47.1889%	4.1910	8.0474	3.7448	0.1499	0.9954	1.1191	0.8999	0.0845	2.575E-04	2.515E-05

FORMULATION:

MOLE CAT./G CELITE : 0.002

Gv,G V2O5/G CEL.: 0.1039314 G K2SO4/ G CEL.: 0.1037321 CM'3 ACTIVE MELT : 0.39128257
G NA2SO4/ G CEL.: 0.0169095 G K2S2O7/G CEL.: 0.1513869 CV (G V2O5/CM'3 MELT): 0.56820281
G NA2S2O7/G CAL.: 0.0264476 G CATALYST/G CEL.: 0.4024076 LIQUID LOADING FACTOR: 0.1746682

TEMP. (oC)	PRESSURE (KPAG)	N (MOLES/MIN)	SO3 (MOLES/MIN)	%CONVERSION (MOLE SO3/ MOLE SO2 FEED)	PSO2 (KPA)	PO2 (KPA)	PSO3 (KPA)	KC	KP -0.5 (KPA)	Q	DISTANCE FROM EQUILIBRIUM	WI	RL (MOLE SO3/ CM3 MELT*S)	RV (MOLE SO3/ CM3 PELLET*S
400	10	0.16784	0.00515463	18.7525%	6.3738	9.0706	1.4711	15.8680	48.3505	4.3326	1.0000	0.7963	1.072E-04	1.397E-05
450	10	0.15623	0.00505050	19.7384%	6.2990	9.0355	1.5491	3.8850	14.9744	4.0663	1.0000	0.6304	1.051E-04	1.369E-05
500	10	0.14613	0.00793650	33.1622%	5.2740	8.5551	2.6167	1.1410	5.3968	2.0155	0.9990	0.3632	1.651E-04	2.151E-05
550	10	0.13725	0.01010101	44.9360%	4.3958	8.1293	3.5628	0.3889	2.2018	1.2254	0.9831	0.1668	2.102E-04	2.737E-05
600	10	0.12939	0.00956937	45.1568%	4.3487	8.1213	3.5806	0.1499	0.9954	1.2145	0.9157	0.0895	1.991E-04	2.593E-05

FORMULATION:

MOLE CAT./G CELITE : 0.004

Gv,G V2O5/G CEL.: 0.2078628 G K2SO4/ G CEL.: 0.2074642 CM'3 ACTIVE MELT : 0.60808181
G NA2SO4/ G CEL.: 0.0338190 G K2S2O7/G CEL.: 0.3027738 CV (G V2O5/CM'3 MELT): 0.56820281
G NA2S2O7/G CAL.: 0.0528952 G CATALYST/G CEL.: 0.8048152 LIQUID LOADING FACTOR: 0.34933642

TEMP. (oC)	PRESSURE (KPAG)	N (MOLES/MIN)	SO3 (MOLES/MIN)	%CONVERSION (MOLE SO3/ MOLE SO2 FEED)	PSO2 (KPA)	PO2 (KPA)	PSO3 (KPA)	KC	KP -0.5 (KPA)	Q	DISTANCE FROM EQUILIBRIUM	WI	RL (MOLE SO3/ CM3 MELT*S)	RV (MOLE SO3/ CM3 PELLET*S
400	10	0.16784	0.00595238	21.6547%	6.1533	8.9672	1.7008	15.8680	48.3505	3.6179	1.0000	0.7804	7.969E-05	2.076E-05
450	10	0.15623	0.00537634	21.0119%	6.2022	8.9902	1.6499	3.8850	14.9744	3.7595	1.0000	0.6282	7.198E-05	1.875E-05
500	10	0.14613	0.00714285	29.8460%	5.5202	8.6745	2.3519	1.1410	5.3968	2.1505	0.9993	0.3855	9.563E-05	2.491E-05
550	10	0.13725	0.00980392	43.6143%	4.4602	8.1773	3.4561	0.3889	2.2018	1.3028	0.9840	0.1721	1.311E-04	3.419E-05
600	10	0.12939	0.00961538	45.3730%	4.3319	8.1134	3.5982	0.1499	0.9954	1.2039	0.9142	0.0809	1.287E-04	3.353E-05

FORMULATION:

MOLE CAT./G CELITE : 0.008

Gv,G V2O5/G CEL.: 0.4157257 G K2SO4/ G CEL.: 0.4149285 CM'3 ACTIVE MELT : 0.84109634
G NA2SO4/ G CEL.: 0.0676380 G K2S2O7/G CEL.: 0.6055476 CV (G V2O5/CM'3 MELT): 0.56820281
G NA2S2O7/G CAL.: 0.1057904 G CATALYST/G CEL.: 1.6096304 LIQUID LOADING FACTOR: 0.69867285

TEMP. (oC)	PRESSURE (KPAG)	N (MOLES/MIN)	SO3 (MOLES/MIN)	%CONVERSION (MOLE SO3/ MOLE SO2 FEED)	PSO2 (KPA)	PO2 (KPA)	PSO3 (KPA)	KC	KP -0.5 (KPA)	Q	DISTANCE FROM EQUILIBRIUM	WI	RL (MOLE SO3/ CM3 MELT*S)	RV (MOLE SO3/ CM3 PELLET*S
400	10	0.16784	0.00588235	21.3999%	6.1727	8.9763	1.6806	15.8680	48.3505	3.6729	1.0000	0.7818	5.694E-05	2.966E-05
450	10	0.15623	0.00526315	20.5695%	6.2358	9.0059	1.6148	3.8850	14.9744	3.8616	1.0000	0.6317	5.094E-05	2.654E-05
500	10	0.14613	0.00784313	32.7720%	5.3040	8.5691	2.5856	1.1410	5.3968	2.0514	0.9990	0.3657	7.502E-05	3.955E-05
550	10	0.13725	0.01030927	45.8655%	4.2940	8.0957	3.5376	0.3889	2.2018	1.1804	0.9817	0.1631	9.875E-05	5.188E-05
600	10	0.12939	0.0100001	47.1893%	4.1910	8.0474	3.7449	0.1499	0.9954	1.1191	0.8999	0.0845	9.679E-05	5.042E-05

FORMULATION:

MOLE CAT./G CELITE : 0.01

Gv,G V2O5/G CEL.: 0.5196571 G K2SO4/ G CEL.: 0.5186607 CM'3 ACTIVE MELT : 0.91090757
G NA2SO4/ G CEL.: 0.0845476 G K2S2O7/G CEL.: 0.7569345 CV (G V2O5/CM'3 MELT): 0.56820281
G NA2S2O7/G CAL.: 0.1322380 G CATALYST/G CEL.: 2.0120380 LIQUID LOADING FACTOR: 0.87334107

TEMP. (oC)	PRESSURE (KPAG)	N (MOLES/MIN)	SO3 (MOLES/MIN)	%CONVERSION (MOLE SO3/ MOLE SO2 FEED)	PSO2 (KPA)	PO2 (KPA)	PSO3 (KPA)	KC	KP -0.5 (KPA)	Q	DISTANCE FROM EQUILIBRIUM	WI	RL (MOLE SO3/ CM3 MELT*S)	RV (MOLE SO3/ CM3 PELLET*S
400	10	0.16784	0.00454545	16.5363%	6.5418	9.1494	1.2961	15.8680	48.3505	5.0473	1.0000	0.8091	4.062E-05	2.645E-05
450	10	0.15623	0.00454545	17.7646%	6.4407	9.1057	1.3931	3.8850	14.9744	4.6292	1.0000	0.6548	4.062E-05	2.645E-05
500	10	0.14613	0.00657894	27.4897%	5.7085	8.7587	2.1642	1.1410	5.3968	2.5377	0.9994	0.4024	5.880E-05	3.829E-05
550	10	0.13725	0.01098901	46.8864%	4.0591	7.9856	3.8825	0.3889	2.2018	1.0456	0.9764	0.1516	9.821E-05	6.395E-05
600	10	0.12939	0.01020408	48.1519%	4.1162	8.0124	3.8228	0.1499	0.9954	1.0768	0.8914	0.0822	9.120E-05	5.939E-05

RATE CONSTANT:

RATE CONSTANT * LIQUID EFFECTIVENESS FACTOR, KL*NL

TEMP (oC)	1/T	LIQUID LOADING FACTOR (CM3 MELT/CM3 PORES) 0.0437	0.0873	0.1310	0.1747	0.3493	0.6987	0.8733
400	0.001485	3.550E-05	2.189E-05	1.909E-05	1.485E-05	1.139E-05	8.114E-06	5.488E-06
450	0.001382	4.450E-05	2.495E-05	2.382E-05	1.822E-05	1.275E-05	8.955E-06	6.814E-06
500	0.001293	6.921E-05	4.870E-05	4.968E-05	5.320E-05	2.862E-05	2.425E-05	1.669E-05
550	0.001214	2.492E-04	2.069E-04	1.951E-04	1.577E-04	9.468E-05	7.696E-05	8.308E-05
600	0.001145	7.025E-04	4.146E-04	4.211E-04	2.992E-04	1.952E-04	1.583E-04	1.554E-04

LIQUID EFFECTIVENESS FACTOR:

EFFECTIVENESS FACTORS, ASSUME NL=1 FOR THE 0.0005 MOLE CAT./ G CEL. SAMPLE

TEMP (oC)	1/T	LIQUID LOADING FACTOR (CM3 MELT/CM3 PORES) 0.0437	0.0873	0.1310	0.1747	0.3493	0.6987	0.8733
400	0.001485	1	0.616	0.538	0.418	0.321	0.229	0.155
450	0.001382	1	0.561	0.535	0.409	0.286	0.201	0.153
500	0.001293	1	0.704	0.718	0.769	0.414	0.350	0.241
550	0.001214	1	0.830	0.783	0.633	0.380	0.309	0.333
600	0.001145	1	0.590	0.599	0.426	0.278	0.225	0.221
AVARAGE NL:		1.00	0.66	0.63	0.53	0.34	0.26	0.22

ACTIVATION ENERGY:

LN (RATE CONSTANT (MOL/CM3 MELT. * KPA * SEC.))

TEMP (oC)	1/T	LIQUID LOADING FACTOR (CM3 MELT/CM3 PORES) 0.0437	0.0873	0.1310	0.1747	0.3493	0.6987	0.8733
400	0.001485	-1.02E+01	-1.07E+01	-1.09E+01	-1.11E+01	-1.14E+01	-1.17E+01	-1.21E+01
450	0.001382	-1.00E+01	-1.06E+01	-1.06E+01	-1.09E+01	-1.13E+01	-1.16E+01	-1.19E+01
500	0.001293	-9.58E+00	-9.93E+00	-9.91E+00	-9.84E+00	-1.05E+01	-1.06E+01	-1.10E+01
550	0.001214	-8.30E+00	-8.48E+00	-8.54E+00	-8.76E+00	-9.27E+00	-9.47E+00	-9.40E+00
600	0.001145	-7.26E+00	-7.79E+00	-7.77E+00	-8.11E+00	-8.54E+00	-8.75E+00	-8.77E+00
ACTIVATION ENERGY =		130189	103390	104506	99881	98372	102697	88445

MEAN THICKNESS OF THE MELT:

PORE RADIUS OF SUPPORT(CM): 2.3400E-05 CONSTANT S = 2.100E-05
GAS PHASE TORYUOSITY FACTOR = 2
AEL: 0.237 ,BEL: 6250
POROSITY OF THE CARRIER: 0.63806

LIQ. LOAD. FACTOR		0.0437	0.0873	0.1310	0.1747	0.3493	0.6987	0.8733
	TEMP(oC)							
	400	0.0508	1.456	1.750	2.349	3.103	4.365	6.452
CALCULATED	450	0.0508	1.658	1.762	2.406	3.490	4.975	6.354
THIELE	500	0.0508	1.172	1.129	0.978	2.374	2.838	4.147
MODULUS	550	0.0508	0.800	0.938	1.398	2.603	3.226	2.988
	600	0.0508	1.548	1.516	2.301	3.592	4.443	4.524
AVG. THIELE MODULUS:		0.0508	1.3267	1.4189	1.8863	3.0322	3.9694	4.8929
	TEMP(oC)							
	400	1.29E-08	5.27E-07	7.84E-07	1.21E-06	2.29E-06	4.55E-06	7.39E-06
	450	2.43E-08	1.12E-06	1.50E-06	2.36E-06	4.87E-06	9.79E-06	1.37E-05
DELTA(CM)	500	4.05E-08	1.37E-06	1.70E-06	1.78E-06	5.93E-06	1.03E-05	1.60E-05
	550	5.06E-08	1.23E-06	1.88E-06	3.23E-06	8.38E-06	1.51E-05	1.62E-05
	600	6.91E-08	3.03E-06	3.93E-06	6.68E-06	1.48E-05	2.66E-05	3.07E-05
EXP.DELTA. AVG.(CM):		3.95E-08	1.46E-06	1.96E-06	3.05E-06	7.25E-06	1.33E-05	1.68E-05
UNIF.FILM.DELTA(CM):		5.224E-07	1.070E-06	1.644E-06	2.249E-06	5.067E-06	1.489E-05	2.871E-05
DIS.PLUGS.DELTA(CM):		1.694E-05	1.831E-05	1.982E-05	2.149E-05	3.040E-05	7.920E-05	2.046E-04

APPENDIX B5:
Results: Different liquid loadings for 6mm pellets

DIFFERENT LIQUID LOADINGS

CATALYST PELLET SIZE: 6 MM	
TIME BETWEEN TEMP. RUNS : 60 MIN	
TITRATION SOLUT. STRENGTH (N):	1.00
TITRATER CORRECTION FACTOR :	2.04722
NA/K MOLE RATIO :	0.2
H2O/V2O5 MOLE RATIO:	2.5
PARAMETER S:	0.5
MELT DENCITY (ASSUMP.)(G/CM^3):	2.2
ASSUMED H2SO4/H2S2O7 MOLE RATIO:	1
PORE VOL. OF SUPPORT,VP,(CM^3 PORES/G CEL.):	1.0472
APPARENT DENCITY OF THE SUPPORT(G/CM^3):	0.712

GAS COMPOSITION(MOLE %):

SO2	8.00%
O2	10.00%
N2	82.00%

REACTOR CONDITIONS :

LINEAR VELOCITY (M/S)	0.2
REACTOR DIAMETER (M)	0.032
MASS OF CATALYST (KG)	0.003
ATM. PRESSURE (KPA)	87.326

MOLECULAR WEIGHTS:

	MM
K2S2O7	254.33
NA2S2O7	222.16
V2O5	181.88
K2SO4	174.27
NA2SO4	142.04

LIQUID LOADING FACTOR:

SAMPLE MASS (G) :	19.78300	GV,G V2O5/G CEL.:	0.00000	G K2SO4/ G CEL.:	0.00000	CM^3 ACTIVE MELT :	0.00000
MOLE CAT./G CELITE :	0.00000	G NA2SO4/ G CEL.:	0.00000	G K2S2O7/G CEL.:	0.00000	CV (G V2O5/CM^3 MELT):	0.00000
		G NA2S2O7/G CAL.:	0.00000	G CATALYST/G CEL.:	0.00000	LIQUID LOADING FACTOR:	0.00000
SAMPLE MASS (G) :	19.78300	GV,G V2O5/G CEL.:	0.02598	G K2SO4/ G CEL.:	0.02593	CM^3 ACTIVE MELT :	0.82195
MOLE CAT./G CELITE :	0.00050	G NA2SO4/ G CEL.:	0.00423	G K2S2O7/G CEL.:	0.03785	CV (G V2O5/CM^3 MELT):	0.56820
		G NA2S2O7/G CAL.:	0.00661	G CATALYST/G CEL.:	0.10060	LIQUID LOADING FACTOR:	0.04367
SAMPLE MASS (G) :	23.25600	GV,G V2O5/G CEL.:	0.05197	G K2SO4/ G CEL.:	0.05187	CM^3 ACTIVE MELT :	1.50622
MOLE CAT./G CELITE :	0.00100	G NA2SO4/ G CEL.:	0.00845	G K2S2O7/G CEL.:	0.07569	CV (G V2O5/CM^3 MELT):	0.56820
		G NA2S2O7/G CAL.:	0.01322	G CATALYST/G CEL.:	0.20120	LIQUID LOADING FACTOR:	0.08733
SAMPLE MASS (G) :	27.01900	GV,G V2O5/G CEL.:	0.07795	G K2SO4/ G CEL.:	0.07780	CM^3 ACTIVE MELT :	2.08473
MOLE CAT./G CELITE :	0.00150	G NA2SO4/ G CEL.:	0.01268	G K2S2O7/G CEL.:	0.11354	CV (G V2O5/CM^3 MELT):	0.56820
		G NA2S2O7/G CAL.:	0.01984	G CATALYST/G CEL.:	0.30181	LIQUID LOADING FACTOR:	0.13100
SAMPLE MASS (G) :	25.46600	GV,G V2O5/G CEL.:	0.10393	G K2SO4/ G CEL.:	0.10373	CM^3 ACTIVE MELT :	2.58025
MOLE CAT./G CELITE :	0.00200	G NA2SO4/ G CEL.:	0.01691	G K2S2O7/G CEL.:	0.15139	CV (G V2O5/CM^3 MELT):	0.56820
		G NA2S2O7/G CAL.:	0.02645	G CATALYST/G CEL.:	0.40241	LIQUID LOADING FACTOR:	0.17467
SAMPLE MASS (G) :	29.10300	GV,G V2O5/G CEL.:	0.20786	G K2SO4/ G CEL.:	0.20746	CM^3 ACTIVE MELT :	4.00989
MOLE CAT./G CELITE :	0.00400	G NA2SO4/ G CEL.:	0.03382	G K2S2O7/G CEL.:	0.30277	CV (G V2O5/CM^3 MELT):	0.56820
		G NA2S2O7/G CAL.:	0.05290	G CATALYST/G CEL.:	0.80482	LIQUID LOADING FACTOR:	0.34934
SAMPLE MASS (G) :	35.52700	GV,G V2O5/G CEL.:	0.41573	G K2SO4/ G CEL.:	0.41493	CM^3 ACTIVE MELT :	5.54647
MOLE CAT./G CELITE :	0.00800	G NA2SO4/ G CEL.:	0.06764	G K2S2O7/G CEL.:	0.60555	CV (G V2O5/CM^3 MELT):	0.56820
		G NA2S2O7/G CAL.:	0.10579	G CATALYST/G CEL.:	1.60963	LIQUID LOADING FACTOR:	0.69867
SAMPLE MASS (G) :	37.72100	GV,G V2O5/G CEL.:	0.51966	G K2SO4/ G CEL.:	0.51866	CM^3 ACTIVE MELT :	6.00683
MOLE CAT./G CELITE :	0.01000	G NA2SO4/ G CEL.:	0.08455	G K2S2O7/G CEL.:	0.75693	CV (G V2O5/CM^3 MELT):	0.56820
		G NA2S2O7/G CAL.:	0.13224	G CATALYST/G CEL.:	2.01204	LIQUID LOADING FACTOR:	0.87334

REACTION RATES:

LIQ. LOAD. FACTOR	TEMP. (oC)	PRESSURE (KPAG)	N (MOLES/MIN)	SO3 (MOLES/MIN)	%CONVERSION (MOLE SO3/ MOLE SO2 FE	PSO2 (KPA)	PO2 (KPA)	PSO3 (KPA)	KC	KP (KPA0.5) :	Q :	DISTANCE FROM EQUILIBRIU
0.0000	550	10	0.13725	0	0.0000%	7.7861	9.7326	0.0000	0.3889	2.2018		
0.0437	550	10	0.13725	0.00714285	31.7761%	5.3804	8.6049	2.5060	0.3889	2.2018	2.1470	0.9948
0.0873	550	10	0.13725	0.00840336	37.3037%	4.9494	8.4029	2.9549	0.3889	2.2018	1.6750	0.9912
0.1310	550	10	0.13725	0.00934579	41.5762%	4.6259	8.2512	3.2919	0.3889	2.2018	1.4052	0.9873
0.1747	550	10	0.13725	0.00975609	43.4015%	4.4847	8.1851	3.4390	0.3889	2.2018	1.3041	0.9852
0.3493	550	10	0.13725	0.01075268	47.8350%	4.1408	8.0239	3.7971	0.3889	2.2018	1.0905	0.9784
0.6987	550	10	0.13725	0.0104712	46.5028%	4.2381	8.0695	3.6958	0.3889	2.2018	1.1467	0.9806
0.8733	550	10	0.13725	0.00884955	39.3686%	4.7963	8.3312	3.1143	0.3889	2.2018	1.5401	0.9896

WI	RL (MOLE SO3/ CM^3 MELT*S)	RV (MOLE SO3/ CM^3 PELLET*S	RG (MOLE SO3/ G CAT PELLET*S)	KL*NL*NG (MOLE / CM^3* KPA	KL*NL*NG (MOLE / G * KPA *S)
	0.000E+00	0.000E+00	0.000E+00	0.000E+00	
0.2280	7.075E-05	2.303E-06	6.018E-06	3.625E-05	3.083E-06
0.1995	4.542E-05	2.958E-06	6.022E-06	2.734E-05	3.625E-06
0.1807	3.650E-05	3.565E-06	5.765E-06	2.480E-05	3.917E-06
0.1730	3.078E-05	4.009E-06	6.385E-06	2.206E-05	4.577E-06
0.1555	2.183E-05	5.686E-06	6.158E-06	1.708E-05	5.043E-06
0.1603	1.537E-05	8.007E-06	4.912E-06	1.212E-05	3.872E-06
0.1903	1.199E-05	7.810E-06	3.910E-06	7.643E-06	2.492E-06

GAS EFFECTIVENESS FACTOR:

LIQ. LOAD. FACTOR	KL*NL*NG (MOLE / CM3*KPA*S)	KL*NL (MOLE / CM3*KPA*S)	NG	NL	NG*NL	NG*NL*LF
0.0000						
0.0437	3.625E-05	2.492E-04	0.145	1.000	0.145	0.006
0.0873	2.734E-05	2.069E-04	0.132	0.830	0.110	0.010
0.1310	2.480E-05	1.951E-04	0.127	0.783	0.100	0.013
0.1747	2.206E-05	1.577E-04	0.140	0.633	0.089	0.015
0.3493	1.708E-05	9.468E-05	0.189	0.380	0.072	0.025
0.6987	1.212E-05	7.696E-05	0.157	0.309	0.049	0.034
0.8733	7.643E-06	8.308E-05	0.092	0.333	0.031	0.027

SURFACE AREA'S & PORE SIZE DISTRIBUTIONS:

NA/K MOLE RATIO : 0.2
M2O/V2O5 MOLE RATIO : 2.5

LIQ. LOAD (MOLE CAT/ CELITE)	SURFACE AREA (M'2/G CAT.)	PORE-DIAMATER(130o ANGLE) (ANGSTRONG)	PORE SIZE DISTRIBUTION 8840	4420	2357	1179	707	505	393	321	253	196	161	136	118	104	93	80
0.0000	18.50		0.043	0.190	0.094	0.403	0.016	0.038	0.012	0.004	0.008	0.005	0.003	0.002	0.002	0.001	0.001	0.001
0.0005	8.90		0.229	0.283	0.240	0.055	0.021	0.006	0.003	0.002	0.002	0.002						0.001
0.0010	5.40		0.219	0.227	0.145	0.093	0.017	0.004	0.003	0.001	0.001				0.001		0.002	
0.0015	5.50	DELTA PV	0.058	0.387	0.158	0.047	0.003	0.006	0.002	0.002	0.001	0.001			0.001			
0.0020	1.60	(CC/G)	0.287	0.178	0.143	0.036	0.009	0.005			0.001		0.006		0.001		0.002	
0.0040	1.18		0.270	0.184	0.034	0.039	0.006	0.002				0.001			0.001		0.001	
0.0080	0.34		0.207	0.120	0.006	0.017	0.002	0.001			0.001							
0.0100	0.27		0.137	0.093	0.048	0.015	0.005	0.001	0.001		0.002		0.001		0.001		0.002	

68	59	52	47	42	38	36	TOTAL PORE VOLUME (CC/G)	AV. PORE RADIUS (CM)
0.001	0.002	0.002	0.001		0.001	0.005	0.851	2.34E-05
	0.001		0.001		0.002	0.001	0.952	4.63E-05
	0.001				0.002	0.001	0.792	4.75E-05
					0.001	0.002	0.675	3.97E-05
		0.001			0.001	0.003	0.706	5.52E-05
	0.002					0.002	0.545	6.15E-05
0.001	0.001						0.427	6.73E-05
0.003			0.006		0.004	0.001	0.359	5.50E-05

APPENDIX B6:
Physical properties for different liquid loadings

APPENDIX B7:
Results for the different shapes

DIFFERENT SHAPES ; LB FORMULATION

TIME BETWEEN TEMP. RUNS : 60 MIN
TITRATION SOLUT. STRENGTH (N): 1.00
TITRATER CORRECTION FACTOR : 2.04722
PARAMETER S : 0.5
CONSTANT FOR KP EQUATION, A : 4956
CONSTANT FOR KP EQUATION, B : 4.678

GAS COMPOSITION(MOLE %):

SO2	8.00%
O2	10.00%
N2	82.00%

REACTOR CONDITIONS :

LINEAR VELOCITY (M/S)	0.2
REACTOR DIAMETER (M)	0.032
MASS OF CATALYST (KG)	0.003
ATM. PRESSURE (KPA)	87.326

SHAPE S1 (6MM PELLETS)

CATALYST MASS (KG) : 0.0190001 FK.PELLET EXT. SURFACE AREA(MM2): 282.7433
VK.PELLET VOL.(MM3): 339.292 VK/FK. VOLUME/SURFACE RATIO (MM): 1.200
CATALYST BULK DENCITY (KG/M3) : 625

TEMP. (OC)	PRESSURE (KPAG)	N (MOLES/MIN)	SO3 (MOLES/MIN)	%CONVERSION (MOLE SO3/ MOLE SO2 FE (CORRECTED)	R (MOL SO3/ KG*MIN)	RV (MOL SO3/ M3*S)	PO2 (KPA)	PSO2 (KPA)	PSO3 (KPA)	Q	KP	KC	WI	DIST. FROM EQUILIBRIUM	KL (MOLE SO3/ G*MIN*KPA)
400	10	0.16784	0.00990099	36.0197%	1.612103	16.79274	8.4521	5.0544	2.8455	1.7763	48.3505	15.8680	0.7081	1.0000	2.694E-01
450	10	0.15623	0.00990099	38.6952%	1.612103	16.79274	8.3555	4.8483	3.0602	1.5843	14.9744	3.8850	0.5080	0.9996	3.800E-01
500	10	0.14613	0.01041666	43.5254%	1.696066	17.66736	8.1806	4.4751	3.4490	1.2975	5.3968	1.1410	0.3013	0.9954	6.913E-01
550	10	0.13725	0.00869565	38.6840%	1.415846	14.74840	8.3559	4.8491	3.0593	1.5850	2.2018	0.3889	0.1934	0.9831	8.910E-01
600	10	0.12939	0.0077821	36.7228%	1.267100	13.19896	8.4267	5.0003	2.9019	1.7231	0.9954	0.1499	0.1136	0.9320	1.421E+00

SHAPE S2 (8MM PELLETS)

CATALYST MASS (KG) : 0.01962415 FK.PELLET EXT. SURFACE AREA(MM2): 402.124
VK.PELLET VOL.(MM3): 603.186 VK/FK. VOLUME/SURFACE RATIO (MM): 1.500
CATALYST BULK DENCITY (KG/M3) : 610

TEMP. (OC)	PRESSURE (KPAG)	N (MOLES/MIN)	SO3 (MOLES/MIN)	%CONVERSION (MOLE SO3/ MOLE SO2 FE (CORRECTED)	R (MOL SO3/ KG*MIN)	RV (MOL SO3/ M3*S)	PO2 (KPA)	PSO2 (KPA)	PSO3 (KPA)	Q	KP	KC	WI	DIST. FROM EQUILIBRIUM	KL (MOLE SO3/ G*MIN*KPA)
400	10	0.16784	0.00621118	22.5962%	1.011319	10.28174	8.9337	6.0817	1.7754	3.4255	48.3505	15.8680	0.7754	1.0000	1.460E-01
450	10	0.15623	0.00749063	29.2750%	1.219642	12.39969	8.6947	5.5720	2.3064	2.4159	14.9744	3.8850	0.5684	0.9999	2.468E-01
500	10	0.14613	0.00819672	34.2495%	1.334609	13.56853	8.5159	5.1905	2.7037	1.9198	5.3968	1.1410	0.3561	0.9982	4.408E-01
550	10	0.13725	0.00760456	33.8301%	1.238192	12.58829	8.5310	5.2227	2.6702	1.9559	2.2018	0.3889	0.2170	0.9897	6.757E-01
600	10	0.12939	0.00714285	33.7063%	1.163016	11.82399	8.5355	5.2322	2.6603	1.9668	0.9954	0.1499	0.1239	0.9501	1.158E+00

SHAPE S3 (10MM RING)

CATALYST MASS (KG) : 0.0172058 FK.PELLET EXT. SURFACE AREA(MM2): 633.031
VK.PELLET VOL.(MM3): 857.655 VK/FK. VOLUME/SURFACE RATIO (MM): 1.355
CATALYST BULK DENCITY (KG/M3) : 575

TEMP. (OC)	PRESSURE (KPAG)	N (MOLES/MIN)	SO3 (MOLES/MIN)	%CONVERSION (MOLE SO3/ MOLE SO2 FE (CORRECTED)	R (MOL SO3/ KG*MIN)	RV (MOL SO3/ M3*S)	PO2 (KPA)	PSO2 (KPA)	PSO3 (KPA)	Q	KP	KC	WI	DIST. FROM EQUILIBRIUM	KL (MOLE SO3/ G*MIN*KPA)
400	10	0.16784	0.0067114	24.4160%	1.092766	10.47109	8.8687	5.9431	1.9198	3.0957	48.3505	15.8680	0.7659	1.0000	1.609E-01
450	10	0.15623	0.00784313	30.6526%	1.277037	12.23681	8.6453	5.4665	2.4163	2.2624	14.9744	3.8850	0.5592	0.9998	2.642E-01
500	10	0.14613	0.00888888	37.1416%	1.447310	13.86840	8.4116	4.9680	2.9355	1.6924	5.3968	1.1410	0.3382	0.9976	5.100E-01
550	10	0.13725	0.00806451	35.8763%	1.313083	12.58221	8.4573	5.0654	2.8340	1.7874	2.2018	0.3889	0.2067	0.9873	7.608E-01
600	10	0.12939	0.00719424	33.9488%	1.171383	11.22442	8.5267	5.2136	2.6797	1.9456	0.9954	0.1499	0.1230	0.9489	1.177E+00

SHAPE S4 (5 LOBE SOLID DAISY)

CATALYST MASS (KG) : 0.01647495 FK.PELLET EXT. SURFACE AREA(MM2): 552.498
VK.PELLET VOL.(MM3): 740.988 VK/FK. VOLUME/SURFACE RATIO (MM): 1.341
CATALYST BULK DENCITY (KG/M3) : 621

TEMP. (OC)	PRESSURE (KPAG)	N (MOLES/MIN)	SO3 (MOLES/MIN)	%CONVERSION (MOLE SO3/ MOLE SO2 FE (CORRECTED)	R (MOL SO3/ KG*MIN)	RV (MOL SO3/ M3*S)	PO2 (KPA)	PSO2 (KPA)	PSO3 (KPA)	Q	KP	KC	WI	DIST. FROM EQUILIBRIUM	KL (MOLE SO3/ G*MIN*KPA)
400	10	0.16784	0.00704225	25.6196%	1.146636	11.86921	8.8257	5.8513	2.0154	2.9033	48.3505	15.8680	0.7597	1.0000	1.710E-01
450	10	0.15623	0.00809716	31.6454%	1.318399	13.64719	8.6096	5.3904	2.4955	2.1600	14.9744	3.8850	0.5526	0.9998	2.772E-01
500	10	0.14613	0.008	33.4275%	1.302579	13.48343	8.5455	5.2536	2.6380	1.9916	5.3968	1.1410	0.3614	0.9984	4.224E-01
550	10	0.13725	0.00735294	32.7107%	1.197223	12.39286	8.5713	5.3087	2.5806	2.0571	2.2018	0.3889	0.2229	0.9908	6.324E-01
600	10	0.12939	0.00662251	31.2509%	1.078293	11.16177	8.6238	5.4206	2.4640	2.1999	0.9954	0.1499	0.1331	0.9615	9.771E-01

SHAPE S5 (5 LOBE DAISY WITH HOLE)

CATALYST MASS (KG) : 0.0176183 FK,PELLET EXT. SURFACE AREA(MM2): 651.402
VK,PELLET VOL.(MM3): 656.172 VK/FK, VOLUME/SURFACE RATIO (MM): 1.007
CATALYST BULK DENCITY (KG/M3) : 576

TEMP. (OC)	PRESSURE (KPAG)	N (MOLES/MIN)	SO3 (MOLES/MIN)	%CONVERSION (MOLE SO3/ MOLE SO2 FE (CORRECTED)	R (MOL SO3/ KG*MIN)	RV (MOL SO3/ M3*S)	Po2 (KPA)	Pso2 (KPA)	Pso3 (KPA)	Q	KP	KC	Wi	DIST. FROM EQUILIBRIUM	KL (MOLE SO3/ G*MIN*KPA)
400	10	0.16784	0.00806451	29.3386%	1.313083	12.61216	0.6924	5.5671	2.3115	2.4085	48.3505	15.8680	0.7409	1.0000	2.039E-01
450	10	0.15623	0.00871459	34.0585%	1.418930	13.62882	0.5228	5.2052	2.6884	1.9361	14.9744	3.8850	0.5370	0.9998	3.101E-01
500	10	0.14613	0.0091954	38.4224%	1.497217	14.38077	0.3651	4.8693	3.0383	1.6026	5.3968	1.1410	0.3305	0.9973	5.430E-01
550	10	0.13725	0.00888888	39.5436%	1.447310	13.90141	0.3248	4.7826	3.1284	1.5289	2.2018	0.3889	0.1896	0.9815	6.344E-01
600	10	0.12939	0.00813008	38.3649%	1.323759	12.71470	0.3674	4.8737	3.0337	1.6065	0.9954	0.1499	0.1084	0.9198	1.587E+00

SHAPE S6 (5 LOBE CASTLE WITH HOLE)

CATALYST MASS (KG) : 0.015644 FK,PELLET EXT. SURFACE AREA(MM2): 621.062
VK,PELLET VOL.(MM3): 636.132 VK/FK, VOLUME/SURFACE RATIO (MM): 1.024
CATALYST BULK DENCITY (KG/M3) : 541

TEMP. (OC)	PRESSURE (KPAG)	N (MOLES/MIN)	SO3 (MOLES/MIN)	%CONVERSION (MOLE SO3/ MOLE SO2 FE (CORRECTED)	R (MOL SO3/ KG*MIN)	RV (MOL SO3/ M3*S)	Po2 (KPA)	Pso2 (KPA)	Pso3 (KPA)	Q	KP	KC	Wi	DIST. FROM EQUILIBRIUM	KL (MOLE SO3/ G*MIN*KPA)
400	10	0.16784	0.00892857	32.4820%	1.453771	13.11947	0.5795	5.3262	2.5624	2.0786	48.3505	15.8680	0.7254	1.0000	2.336E-01
450	10	0.15623	0.00961538	37.5789%	1.565599	14.12866	0.3958	4.9343	2.9706	1.6611	14.9744	3.8850	0.5119	0.9997	3.623E-01
500	10	0.14613	0.01020408	42.6371%	1.661453	14.99369	0.2128	4.5430	3.3774	1.3454	5.3968	1.1410	0.3062	0.9958	6.634E-01
550	10	0.13725	0.00966747	43.0073%	1.574080	14.20520	0.1994	4.5152	3.4072	1.3252	2.2018	0.3889	0.1746	0.9740	1.129E+00
600	10	0.12939	0.00869565	41.0338%	1.415846	12.77723	0.2709	4.6678	3.2482	1.4370	0.9954	0.1499	0.1005	0.8953	1.902E+00

SHAPE S7 (6 LOBE DAISY WITH HOLE)

CATALYST MASS (KG) : 0.0155954 FK,PELLET EXT. SURFACE AREA(MM2): 616.484
VK,PELLET VOL.(MM3): 601.104 VK/FK, VOLUME/SURFACE RATIO (MM): 0.975
CATALYST BULK DENCITY (KG/M3) : 562

TEMP. (OC)	PRESSURE (KPAG)	N (MOLES/MIN)	SO3 (MOLES/MIN)	%CONVERSION (MOLE SO3/ MOLE SO2 FE (CORRECTED)	R (MOL SO3/ KG*MIN)	RV (MOL SO3/ M3*S)	Po2 (KPA)	Pso2 (KPA)	Pso3 (KPA)	Q	KP	KC	Wi	DIST. FROM EQUILIBRIUM	KL (MOLE SO3/ G*MIN*KPA)
400	10	0.16784	0.00833333	30.3165%	1.356853	12.70668	0.6573	5.4922	2.3894	2.2985	48.3505	15.8680	0.7361	1.0000	2.129E-01
450	10	0.15623	0.00990099	38.6952%	1.612103	15.09704	0.3555	4.8483	3.0602	1.5843	14.9744	3.8850	0.5080	0.9996	3.800E-01
500	10	0.14613	0.0104712	43.7532%	1.704946	15.96650	0.1723	4.4574	3.4673	1.2855	5.3968	1.1410	0.3000	0.9953	6.986E-01
550	10	0.13725	0.00990099	44.0461%	1.612103	15.09704	0.1617	4.4347	3.4910	1.2703	2.2018	0.3889	0.1704	0.9712	1.194E+00
600	10	0.12939	0.0089686	42.3218%	1.460289	13.67533	0.2242	4.5682	3.3520	1.3628	0.9954	0.1499	0.0969	0.8011	2.079E+00

SHAPE S8 (DAVID STAR)

CATALYST MASS (KG) : 0.01954165 FK,PELLET EXT. SURFACE AREA(MM2): 457.424
VK,PELLET VOL.(MM3): 519.744 VK/FK, VOLUME/SURFACE RATIO (MM): 1.136
CATALYST BULK DENCITY (KG/M3) : 585

TEMP. (OC)	PRESSURE (KPAG)	N (MOLES/MIN)	SO3 (MOLES/MIN)	%CONVERSION (MOLE SO3/ MOLE SO2 FE (CORRECTED)	R (MOL SO3/ KG*MIN)	RV (MOL SO3/ M3*S)	Po2 (KPA)	Pso2 (KPA)	Pso3 (KPA)	Q	KP	KC	Wi	DIST. FROM EQUILIBRIUM	KL (MOLE SO3/ G*MIN*KPA)
400	10	0.16784	0.00884955	32.1945%	1.440905	14.05891	0.5899	5.3483	2.5394	2.1061	48.3505	15.8680	0.7268	1.0000	2.308E-01
450	10	0.15623	0.00990099	38.6952%	1.612103	15.72029	0.3555	4.8483	3.0602	1.5843	14.9744	3.8850	0.5080	0.9996	3.800E-01
500	10	0.14613	0.0104712	43.7532%	1.704946	16.63516	0.1723	4.4574	3.4673	1.2855	5.3968	1.1410	0.3000	0.9953	6.986E-01
550	10	0.13725	0.00985221	43.8201%	1.604160	15.65179	0.1695	4.4516	3.4735	1.2816	2.2018	0.3889	0.1713	0.9718	1.180E+00
600	10	0.12939	0.00877192	41.3937%	1.428265	13.93558	0.2579	4.6400	3.2772	1.4158	0.9954	0.1499	0.0995	0.8915	1.950E+00

SHAPE S9 (TEARDROP WITH HOLE)

CATALYST MASS (KG) : 0.02056415 FK,PELLET EXT. SURFACE AREA(MM2): 645.932
VK,PELLET VOL.(MM3): 749.352 VK/FK, VOLUME/SURFACE RATIO (MM): 1.160
CATALYST BULK DENCITY (KG/M3) : 607

TEMP. (OC)	PRESSURE (KPAG)	N (MOLES/MIN)	SO3 (MOLES/MIN)	%CONVERSION (MOLE SO3/ MOLE SO2 FE (CORRECTED)	R (MOL SO3/ KG*MIN)	RV (MOL SO3/ M3*S)	PO2 (KPA)	PSO2 (KPA)	PSO3 (KPA)	Q	KP	KC	WI	KL (MOLE SO3/ G*MIN*KPA)
400	10	0.16784	0.00826446	30.0660%	1.345639	13.60396	0.6663	5.5114	2.3695	2.3260	48.3505	15.8680	0.7373	2.106E-01
450	10	0.15623	0.00909090	35.5292%	1.480203	14.96436	0.4698	5.0921	2.8062	1.8146	14.9744	3.8850	0.5277	3.313E-01
500	10	0.14613	0.00995024	41.5764%	1.620122	16.37089	0.2512	4.6258	3.2919	1.4052	5.3968	1.1410	0.3122	6.313E-01
550	10	0.13725	0.00980392	43.6143%	1.596208	16.13004	0.1773	4.4682	3.4561	1.2928	2.2018	0.3889	0.1721	1.166E+00
600	10	0.12939	0.00913242	43.0948%	1.486962	15.03269	0.1962	4.5084	3.4143	1.3205	0.9954	0.1499	0.0948	2.195E+00

SHAPE S10 (3 POINTED STAR)

CATALYST MASS (KG) : 0.01910995 FK,PELLET EXT. SURFACE AREA(MM2): 418.672
VK,PELLET VOL.(MM3): 481.632 VK/FK, VOLUME/SURFACE RATIO (MM): 1.150
CATALYST BULK DENCITY (KG/M3) : 557

TEMP. (OC)	PRESSURE (KPAG)	N (MOLES/MIN)	SO3 (MOLES/MIN)	%CONVERSION (MOLE SO3/ MOLE SO2 FE (CORRECTED)	R (MOL SO3/ KG*MIN)	RV (MOL SO3/ M3*S)	PO2 (KPA)	PSO2 (KPA)	PSO3 (KPA)	Q	KP	KC	WI	KL (MOLE SO3/ G*MIN*KPA)
400	10	0.16784	0.00819672	29.8195%	1.334609	12.38606	0.6752	5.5303	2.3498	2.3535	48.3505	15.8680	0.7385	2.083E-01
450	10	0.15623	0.00995024	38.8076%	1.620122	15.03581	0.3486	4.8334	3.0757	1.5715	14.9744	3.8850	0.5068	3.831E-01
500	10	0.14613	0.01052631	43.9835%	1.713919	15.90631	0.1639	4.4306	3.4859	1.2736	5.3968	1.1410	0.2988	7.061E-01
550	10	0.13725	0.00990099	44.0461%	1.612103	14.96139	0.1617	4.4347	3.4910	1.2703	2.2018	0.3889	0.1704	1.194E+00
600	10	0.12939	0.00947867	44.7288%	1.543340	14.32322	0.1369	4.3819	3.5461	1.2357	0.9954	0.1499	0.0906	2.467E+00

SHAPE S11 (EGG)

CATALYST MASS (KG) : 0.02347565 FK,PELLET EXT. SURFACE AREA(MM2): 271.312
VK,PELLET VOL.(MM3): 296.88 VK/FK, VOLUME/SURFACE RATIO (MM): 1.094
CATALYST BULK DENCITY (KG/M3) : 638

TEMP. (OC)	PRESSURE (KPAG)	N (MOLES/MIN)	SO3 (MOLES/MIN)	%CONVERSION (MOLE SO3/ MOLE SO2 FE (CORRECTED)	R (MOL SO3/ KG*MIN)	RV (MOL SO3/ M3*S)	PO2 (KPA)	PSO2 (KPA)	PSO3 (KPA)	Q	KP	KC	WI	KL (MOLE SO3/ G*MIN*KPA)
400	10	0.16784	0.00735294	26.7499%	1.197223	12.72486	0.7852	5.7650	2.1053	2.7383	48.3505	15.8680	0.7539	1.808E-01
450	10	0.15623	0.00869565	33.9844%	1.415846	15.04853	0.5255	5.2109	2.6825	1.9425	14.9744	3.8850	0.5375	3.091E-01
500	10	0.14613	0.01036269	43.2998%	1.687278	17.93348	0.1887	4.4925	3.4308	1.3095	5.3968	1.1410	0.3025	6.841E-01
550	10	0.13725	0.01	44.4866%	1.628224	17.30581	0.1457	4.4006	3.5265	1.2479	2.2018	0.3889	0.1686	1.222E+00
600	10	0.12939	0.00934579	44.1017%	1.521704	16.17365	0.1596	4.4304	3.4955	1.2675	0.9954	0.1499	0.0922	2.358E+00

SHAPE S12 (SIX LOBE SOLID DAISY)

CATALYST MASS (KG) : 0.01907295 FK,PELLET EXT. SURFACE AREA(MM2): 517.52
VK,PELLET VOL.(MM3): 685.92 VK/FK, VOLUME/SURFACE RATIO (MM): 1.325
CATALYST BULK DENCITY (KG/M3) : 604

TEMP. (OC)	PRESSURE (KPAG)	N (MOLES/MIN)	SO3 (MOLES/MIN)	%CONVERSION (MOLE SO3/ MOLE SO2 FE (CORRECTED)	R (MOL SO3/ KG*MIN)	RV (MOL SO3/ M3*S)	PO2 (KPA)	PSO2 (KPA)	PSO3 (KPA)	Q	KP	KC	WI	KL (MOLE SO3/ G*MIN*KPA)
400	10	0.16784	0.00840336	30.5713%	1.368255	13.76465	0.6482	5.4727	2.4098	2.2710	48.3505	15.8680	0.7340	2.153E-01
450	10	0.15623	0.00921658	36.0203%	1.500665	15.09669	0.4521	5.0543	2.8456	1.7762	14.9744	3.8850	0.5246	3.386E-01
500	10	0.14613	0.00995024	41.5764%	1.620122	16.29842	0.2512	4.6258	3.2919	1.4052	5.3968	1.1410	0.3122	6.313E-01
550	10	0.13725	0.00985221	43.0291%	1.604160	16.13785	0.1695	4.4516	3.4736	1.2816	2.2018	0.3889	0.1713	1.100E+00
600	10	0.12939	0.00921658	43.4920%	1.500665	15.09669	0.1818	4.4777	3.4463	1.2993	0.9954	0.1499	0.0930	2.257E+00

ACTIVATION ENERGY VS SHAPE:

SHAPE	ACTIVATION ENERGY (J/MOLE)
REF	87032.480
S1	40752.345
S2	50229.755
S3	49301.166
S4	42060.993
S5	50500.792
S6	51855.485
S7	55618.910
S8	52649.926
S9	57703.841
S10	59134.863
S11	63396.418
S12	57678.843

APPENDIX B8:
Results for reference LB catalyst

REFERENCE RUN, LB & STANDARD FORMULATIONS :

CATALYST PELLET SIZE: 1-1.18MM
CATALYST DILUTION : 3 G CAT + 3 G CERAMIC
TIME BETWEEN TEMP. RUNS : 60 MIN
TITRATION SOLUT. STRENGTH (N): 1.00
TITRATER CORRECTION FACTOR : 2.04722
PARAMETER S : 0.5
CONSTANT FOR KP EQUATION, A : 4956
CONSTANT FOR KP EQUATION, B : 4.678

GAS COMPOSITION(MOLE %):

SO2	8.00%
O2	10.00%
N2	82.00%

REACTOR CONDITIONS :

LINEAR VELOCITY (M/S)	0.2
REACTOR DIAMETER (M)	0.032
MASS OF CATALYST (KG)	0.003
ATM. PRESSURE (KPA)	87.326

FORMULATION:

LB FORMULATION, RUN 1

TEMP. (OC)	PRESSURE (KPAG)	N (MOLES/MIN)	SO3 (MOLES/MIN)	%CONVERSION (MOLE SO3/ MOLE SO2 FE (CORRECTED)	R (MOL SO3/ G*MIN)	PO2 (KPA)	PSO2 (KPA)	PSO3 (KPA)	Q	KP	KC	WI	DIST. FROM EQUILIBRIUM	KL (MOLE SO3/ G*MIN*KPA)
400	10	0.16784	0.00352113	12.8098%	0.000573	9.2815	6.8237	1.0025	6.8065	48.3505	15.8680	0.8322	1.0000	7.423E-05
450	10	0.15623	0.00524691	20.5060%	0.000854	9.0042	6.2407	1.6098	3.8766	14.9744	3.8850	0.6322	1.0000	1.500E-04
500	10	0.14613	0.00546875	22.8508%	0.000890	8.9246	6.0623	1.7956	3.3762	5.3968	1.1410	0.4389	0.9995	2.275E-04
550	10	0.13725	0.0065359	29.0760%	0.001064	8.7019	5.5872	2.2905	2.4393	2.2018	0.3889	0.2435	0.9938	5.055E-04
600	10	0.12939	0.00869995	41.0541%	0.001416	8.2702	4.6662	3.2499	1.4358	0.9954	0.1499	0.1005	0.8951	1.905E-03
550	10	0.13725	0.00661157	29.4126%	0.001076	8.6898	5.5614	2.3174	2.3999	2.2018	0.3889	0.2415	0.9936	5.164E-04
500	10	0.14613	0.00666666	27.8562%	0.001085	8.7456	5.6805	2.1933	2.5899	5.3968	1.1410	0.3997	0.9991	3.108E-04
450	10	0.15623	0.00555555	21.7123%	0.000904	8.9652	6.1489	1.7053	3.6057	14.9744	3.8850	0.6228	0.9999	1.620E-04
400	10	0.16784	0.0043478	15.8172%	0.000707	9.1749	6.5963	1.2394	5.3222	48.3505	15.8680	0.8134	1.0000	9.486E-05

ACTIVATION ENERGY (J/MOLE) = 87032.4873

FORMULATION:

LB FORMULATION, RUN 2

TEMP. (OC)	PRESSURE (KPAG)	N (MOLES/MIN)	SO3 (MOLES/MIN)	%CONVERSION (MOLE SO3/ MOLE SO2 FE (CORRECTED)	R (MOL SO3/ G*MIN)	PO2 (KPA)	PSO2 (KPA)	PSO3 (KPA)	Q	KP	KC	WI	DIST. FROM EQUILIBRIUM	KL (MOLE SO3/ G*MIN*KPA)
400	10	0.16784	0.00617283	22.4567%	0.001005	8.9386	6.0923	1.7643	3.4530	48.3505	15.8680	0.7761	1.0000	1.449E-04
450	10	0.15623	0.00636942	24.8930%	0.001037	8.8516	5.9067	1.9577	3.0172	14.9744	3.8850	0.5990	0.9999	1.956E-04
500	10	0.14613	0.00687285	28.7178%	0.001119	8.7147	5.6146	2.2620	2.4825	5.3968	1.1410	0.3935	0.9990	3.267E-04
550	10	0.13725	0.00692041	30.7866%	0.001126	8.6405	5.4565	2.4270	2.2485	2.2018	0.3889	0.2335	0.9925	5.627E-04
600	10	0.12939	0.00757575	35.7491%	0.001233	8.4619	5.0752	2.8238	1.7973	0.9954	0.1499	0.1168	0.9384	1.330E-03

ACTIVATION ENERGY (J/MOLE) = 65481.0019

FORMULATION:

STANDARD FORMULATION

TEMP. (OC)	PRESSURE (KPAG)	N (MOLES/MIN)	SO3 (MOLES/MIN)	%CONVERSION (MOLE SO3/ MOLE SO2 FE (CORRECTED)	R (MOL SO3/ G*MIN)	PO2 (KPA)	PSO2 (KPA)	PSO3 (KPA)	Q	KP	KC	WI	DIST. FROM EQUILIBRIUM	KL (MOLE SO3/ G*MIN*KPA)
400	10	0.16784	0.00625	22.7374%	0.001017	8.9286	6.0709	1.7866	3.3980	48.3505	15.8680	0.7746	1.0000	1.471E-04
450	10	0.15623	0.00666666	26.0547%	0.001085	8.8101	5.8181	2.0500	2.8381	14.9744	3.8850	0.5907	0.9999	2.086E-04
500	10	0.14613	0.008	33.4275%	0.001302	8.5455	5.2536	2.6380	1.9916	5.3968	1.1410	0.3614	0.9984	4.224E-04
550	10	0.13725	0.00892857	39.7202%	0.001453	8.3184	4.7692	3.1426	1.5176	2.2018	0.3889	0.1888	0.9812	9.435E-04
600	10	0.12939	0.00892857	42.1329%	0.001453	8.2311	4.5828	3.3367	1.3734	0.9954	0.1499	0.0974	0.8833	2.052E-03

ACTIVATION ENERGY (J/MOLE) = 65414.3595

PRESSURE DROP:

TEMPERATURE (oC) : 25
AIR PRESSURE (KPA) : 87.33
BEDDIAMETER (M) : 0.19
DENCITY ETHYL ALCOHOL (G/CM3)(25oC) : 0.78522

EKSPERIMENTAL RESULTS:

ROTAMETER (L/MIN) (AIR @ 15oC & 760 MM HG)	AIR LINEAR VELOCITY (M/S)	PRESSURE DROP (MM ETANOL)											
	SHAPE :	S1	S2	S3	S4	S5	S6	S7	S8	S9	S10	S11	S12
	BEDHEIGHT (M):	0.304	0.315	0.304	0.305	0.300	0.104	0.145	0.315	0.304	0.305	0.105	0.225
90.0	0.064	0.5	0.5	0.5	0.5	0.5	0.5	0.5	0.5	0.5	0.5	0.5	0.5
155.0	0.109	2.8	2.0	1.5	1.5	1.0	1.0	1.0	1.4	1.5	1.5	1.3	1.3
215.0	0.152	4.8	4.0	2.5	2.5	2.0	1.1	1.3	2.5	2.5	2.5	1.7	1.8
282.5	0.199	7.0	5.0	2.5	3.5	3.0	1.3	1.9	3.5	3.5	3.5	2.0	2.7
350.0	0.247	12.0	6.7	4.0	5.0	4.0	1.8	2.8	5.0	5.0	4.8	2.7	3.9
412.5	0.291	13.0	9.0	5.5	6.5	5.0	2.0	3.2	7.0	6.5	6.0	3.7	4.6
480.0	0.339	16.0	12.0	6.5	8.5	7.0	2.8	4.1	8.7	8.0	7.8	4.4	6.0
550.0	0.388	20.5	15.0	8.5	10.5	9.0	3.2	5.0	11.0	10.5	9.8	5.0	7.4
620.0	0.438	26.0	18.0	10.5	13.0	11.0	3.8	6.0	13.0	12.5	12.0	7.0	8.8
690.0	0.487	30.0	22.0	12.5	15.5	13.0	4.7	7.4	16.0	15.5	14.5	8.1	11.0
770.0	0.543	36.5	26.5	14.5	18.8	15.0	5.2	9.0	19.4	18.5	17.5	10.0	13.2
850.0	0.600	43.0	32.0	18.5	24.0	18.0	6.2	10.7	23.0	22.0	21.0	12.0	16.0
930.0	0.656	50.0	36.0	20.5	26.5	21.0	7.0	12.0	27.0	26.0	24.5	14.0	18.0
1010.0	0.713	59.0	43.0	24.0	30.5	25.0	8.3	14.0	32.0	30.0	29.0	16.0	21.2

LINEAR VELOCITY (M/S)	PRESSURE DROP (MM H2O/M BED HEIGHT)											
SHAPE :	S1	S2	S3	S4	S5	S6	S7	S8	S9	S10	S11	S12
0.064	1.3	1.2	1.3	1.3	1.3	3.8	2.7	1.2	1.3	1.3	3.7	1.7
0.109	7.2	5.0	3.9	3.9	2.6	7.6	5.4	3.5	3.9	3.9	9.7	4.5
0.152	12.4	10.0	5.5	6.4	5.2	8.3	7.0	6.2	5.2	6.4	13.7	6.3
0.199	18.1	12.5	6.5	9.0	7.9	9.8	10.3	8.7	9.0	9.0	15.0	9.4
0.247	31.0	16.7	10.3	12.9	10.5	13.6	14.9	12.5	12.9	12.4	20.2	13.6
0.291	33.6	22.4	14.2	16.7	13.1	15.1	17.3	17.4	16.8	15.4	27.7	16.1
0.339	41.3	29.9	16.8	21.9	18.3	20.8	22.2	21.7	20.7	20.1	32.9	20.9
0.388	53.0	37.4	22.0	27.0	23.6	24.2	27.1	27.4	27.1	25.2	37.4	25.8
0.438	67.2	44.9	27.1	33.5	28.8	28.7	32.5	32.4	32.3	30.9	52.3	30.7
0.487	77.5	54.8	32.3	39.9	34.0	35.5	40.1	39.9	40.0	37.3	60.6	38.4
0.543	94.3	66.1	37.5	48.4	39.3	39.3	48.7	48.4	47.8	45.1	74.8	46.1
0.600	111.1	79.8	47.8	61.8	47.1	46.8	57.9	57.3	56.8	54.1	89.7	55.8
0.656	129.1	89.7	53.0	68.5	55.0	52.9	65.0	67.3	67.5	63.1	104.7	62.8
0.713	152.4	107.2	62.0	78.5	65.4	62.7	75.8	79.8	77.5	74.7	119.7	74.0

ERGUN EQUATION PREDICTIONS:

DENCITY OF THE AIR (KG/M3): 1.02163
VISCOSITY OF AIR (PA*S) : 1.8E-05

AIR LINEAR VELOCITY (M/S)	SHAPE :	S1	S2	S3	S4	S5	S6	S7	S8	S9	S10	S11	S12
	SURFACE OF PELLET (MM2) :	282.74	402.12	633.03	552.50	651.40	621.06	616.48	457.42	645.93	418.67	271.31	517.52
	VOLUME OF PELLET (MM3) :	339.29	603.19	857.66	740.99	656.17	636.13	601.10	519.74	749.35	481.63	296.88	685.92
	EFFFECTIVE DIAM.,DP,(MM):	8.653	10.483	11.788	11.227	10.781	10.670	10.471	9.975	11.269	9.725	8.277	10.942
	SPHERICITY :	0.832	0.859	0.690	0.717	0.561	0.576	0.559	0.683	0.618	0.710	0.793	0.727
	VOID FRACTION:	0.357	0.368	0.411	0.391	0.455	0.480	0.439	0.425	0.414	0.459	0.379	0.399
	MAX.PART. REYNOLD NUMBER:	342	415	467	444	427	422	414	395	446	385	328	433
0.064		4.6	2.8	2.1	2.7	2.2	1.7	2.8	2.5	2.7	1.7	4.2	2.5
0.109		9.7	6.1	4.6	5.7	4.7	3.7	5.8	5.3	5.6	3.7	8.9	5.3
0.152		15.7	10.2	7.6	9.4	7.7	6.0	9.4	8.6	9.2	6.1	14.4	8.6
0.199		24.0	15.8	11.8	14.6	11.8	9.2	14.3	13.2	14.2	9.4	21.9	13.6
0.247		34.0	22.6	16.9	20.8	16.7	13.0	20.1	18.7	20.1	13.4	30.9	19.4
0.291		44.6	29.9	22.4	27.5	21.9	17.1	26.3	24.6	26.4	17.7	40.5	25.5
0.339		57.7	39.0	29.1	35.7	28.3	22.2	34.0	31.8	34.3	22.9	52.2	33.3
0.388		73.0	49.6	37.0	45.4	35.7	28.1	42.9	40.3	43.4	29.1	66.0	42.3
0.438		90.0	61.5	45.9	56.2	44.0	34.7	53.8	49.8	53.6	36.0	81.2	52.4
0.487		108.7	74.6	55.6	68.1	53.2	42.0	63.7	60.2	64.8	43.6	98.1	63.5
0.543		132.3	91.1	67.9	83.1	64.7	51.1	77.4	73.3	78.9	53.5	119.5	77.3
0.600		158.1	109.3	81.5	99.5	77.4	61.1	92.5	87.7	94.5	63.7	142.3	92.9
0.656		186.3	129.1	96.2	117.5	91.1	72.0	108.8	103.4	111.3	75.1	167.5	109.6
0.713		216.7	150.6	112.1	136.9	106.0	83.9	126.5	120.4	129.6	87.5	194.7	127.7

APPENDIX B10:
Mechanical crush strength

EFFECT OF CATALYST SHAPE ON MECHANICAL STRENGTH:

LB FORMULATION
ROOM TEMPERATURE

PRESSURE GUAGE (KPA) (MOLE/G CEL.)	DISPLACEMENT (INCHES) (*10E-3) S1	S2	S3	S4	S5	S6	S7	S8	S9	S10	S11	S12
500	19.5	19.0	20.0	24.0	20.5	49.0	14.0	11.5	10.5	15.5	16.0	21.0
1000	59.5	71.0	66.0	66.5	61.5	134.0	51.5	51.0	50.5	47.5	47.0	57.5
1500	99.0	112.0	95.0	96.0	95.0	179.0	84.0	84.0	98.5	77.0	69.0	91.5
2000	134.5	153.5	136.5	114.0	116.0	219.0	114.0	114.0	123.0	103.5	94.0	123.5
2500	169.0	188.5	159.0	141.5	146.5	259.0	148.5	134.5	173.5	131.0	118.0	156.5
3000	188.0	210.5	184.5	163.5	172.5	281.0	178.5	158.0	210.0	154.5	144.0	177.0
3500	218.0	232.5	201.5	184.0	191.0	308.0	200.0	179.0	241.0	192.0	159.0	197.0
4000	246.0	264.0	226.5	198.0	210.0	366.0	224.0	202.5	267.5	228.5	184.0	224.0
4500	268.5	278.5	247.5	215.0	238.5	397.0	250.0	220.5	293.0	258.0	198.0	245.5
5000	290.5	301.5	268.0	236.0	271.5	429.0	274.0	244.0	338.5	299.5	217.0	273.0
5500	312.0	324.5	285.0	258.0	255.5	455.0	298.5	265.0	368.5	335.5	235.0	293.0
6000	326.5	362.5	301.5	283.5	329.5	511.0	317.5	284.0	392.0	357.5	255.0	314.0

INTERGRAL CRUSH STRENGTH (1/(M*KPA))

% INTERGRAL CRUSH STRENGTH RELATIVE TO THE 6MM LB CATALYST

PRESSURE ON THE CATALYST (KPA)	AREA UNDER THE CURVE (KPA * M) (MOLE/ G CEL.) S1	S2	S3	S4	S5	S6	S7	S8	S9	S10	S11	S12
78	0.000	0.000	0.000	0.000	0.000	0.000	0.000	0.000	0.000	0.000	0.000	0.000
274	0.196	0.223	0.213	0.225	0.203	0.454	0.163	0.155	0.151	0.156	0.156	0.195
469	0.393	0.454	0.400	0.403	0.388	0.777	0.336	0.335	0.370	0.309	0.288	0.370
664	0.579	0.659	0.574	0.521	0.524	0.988	0.491	0.491	0.550	0.448	0.404	0.534
860	0.753	0.849	0.733	0.634	0.651	1.186	0.651	0.617	0.736	0.582	0.526	0.695
1055	0.886	0.990	0.852	0.757	0.792	1.340	0.811	0.726	0.952	0.708	0.650	0.828
1251	1.008	1.099	0.958	0.862	0.902	1.462	0.939	0.836	1.119	0.860	0.752	0.928
1446	1.151	1.232	1.062	0.948	0.995	1.673	1.052	0.947	1.262	1.043	0.851	1.045
1641	1.277	1.346	1.176	1.025	1.113	1.893	1.176	1.050	1.391	1.207	0.948	1.165
1837	1.387	1.439	1.279	1.119	1.266	2.050	1.300	1.153	1.567	1.383	1.030	1.287
2032	1.495	1.553	1.372	1.226	1.308	2.194	1.421	1.263	1.754	1.576	1.122	1.405
2228	1.584	1.705	1.455	1.344	1.452	2.397	1.529	1.362	1.887	1.720	1.216	1.506
	0.093	0.087	0.099	0.110	0.104	0.061	0.101	0.112	0.085	0.100	0.126	0.100
	100.00%	92.73%	106.29%	118.17%	111.64%	65.26%	108.51%	119.87%	91.24%	107.18%	134.83%	107.58%

TEMPERATURE vs STRENGTH :6MM LB SAMPLE

PRESSURE GUAGE (KPA)	DISPLACEMENT (INCHES)													
	20 oC		100 oC		200 oC		300 oC		400 oC		500 oC		600 oC	
300	0.0000	0.0000	0.0000	0.0000	0.0000	0.0000	0.0000	0.0000	0.0000	0.0000	0.0000	0.0000	0.0000	0.0000
400	0.0180	0.0145	0.0295	0.0160	0.0250	0.0290	0.0275	0.0140	0.0220	0.0290	0.0280	0.0300	0.0170	0.0400
600	0.0420	0.0390	0.0650	0.0355	0.0600	0.0530	0.0645	0.0465	0.0590	0.0610	0.0610	0.0660	0.0520	0.0650
800	0.0650	0.0615	0.0840	0.0530	0.0810	0.0740	0.0920	0.0665	0.0900	0.0865	0.0960	0.0920	0.0785	0.0920
1000	0.0825	0.0750	0.1010	0.0685	0.1000	0.0875	0.1110	0.0820	0.1035	0.1090	0.1225	0.1155	0.1020	0.1150
1200	0.1030	0.0935	0.1130	0.0835	0.1160	0.1045	0.1335	0.1050	0.1240	0.1270	0.1435	0.1370	0.1250	0.1415
1400	0.1160	0.1020	0.1280	0.1000	0.1310	0.1205	0.1510	0.1255	0.1450	0.1515	0.1730	0.1610	0.1420	0.1700
1600	0.1250	0.1120	0.1440	0.1100	0.1510	0.1335	0.1660	0.1390	0.1630	0.1740	0.1890	0.1830	0.1530	0.1900
1800	0.1335	0.1220	0.1580	0.1180	0.1650	0.1465	0.1885	0.1575	0.1780	0.1930	0.2070	0.2090	0.1760	0.2130
2000	0.1450	0.1300	0.1740	0.1265	0.1850	0.1630	0.2090	0.1750	0.1920	0.2090	0.2240	0.2270	0.1970	0.2400
2200	0.1525	0.1385	0.1865	0.1350	0.2000	0.1830	0.2295	0.1900	0.2090	0.2230	0.2430	0.2480	0.2060	0.2560
2400	0.1540	0.1500	0.1990	0.1475	0.2190	0.1940	0.2470	0.2010	0.2150	0.2460	0.2570	0.2650	0.2180	0.2750
2600	0.1655	0.1565	0.2120	0.1610	0.2400	0.2170	0.2595	0.2200	0.2315	0.2580	0.2760	0.2870	0.2350	0.2790
2800	0.1725	0.1640	0.2245	0.1670	0.2530	0.2300	0.2715	0.2380	0.2475	0.2835	0.3000	0.3010	0.2520	0.2845
3000	0.1800	0.1710	0.2315	0.1730	0.2650	0.2480	0.2870	0.2500	0.2675	0.3000	0.3190	0.3160	0.2710	0.3190
3200	0.1890	0.1815	0.2410	0.1840	0.2790	0.2685	0.3000	0.2730	0.2885	0.3220	0.3330	0.3385	0.2850	0.3490
3400	0.1905	0.1920	0.2580	0.1925	0.2960	0.2820	0.3120	0.2810	0.3000	0.3315	0.3530	0.3530	0.2910	0.3590
3600	0.2020	0.2020	0.2690	0.2000	0.3160	0.2980	0.3290	0.3000	0.3160	0.3445	0.3675	0.3670	0.3080	0.3750
3800	0.2110	0.2035	0.2815	0.2080	0.3400	0.3135	0.3450	0.3125	0.3270	0.3535	0.3860	0.3910	0.3350	0.3910
4000	0.2195	0.2145	0.2920	0.2225	0.3550	0.3345	0.3630	0.3310	0.3380	0.3925	0.4040	0.4160	0.3465	0.4000
4200	0.2260	0.2225	0.3000	0.2300	0.3700	0.3500	0.3790	0.3400	0.3525	0.4145	0.4320	0.4365	0.3580	0.4280
4400	0.2310	0.2270	0.3060	0.2360	0.3830	0.3625	0.3920	0.3550	0.3710	0.4330	0.4380	0.4530	0.3695	0.4470
4600	0.2370	0.2345	0.3150	0.2435	0.4020	0.3810	0.4150	0.3645	0.3820	0.4460	0.4470	0.4690	0.3770	0.4600
4800	0.2435	0.2415	0.3240	0.2560	0.4150	0.3950	0.4285	0.3860	0.3900	0.4565	0.4550	0.4730	0.3950	0.4740
5000	0.2490	0.2480	0.3425	0.2625	0.4410	0.4130	0.4370	0.4010	0.4040	0.4670	0.4730	0.4860	0.4050	0.4880
5200	0.2650	0.2535	0.3560	0.2730	0.4480	0.4245	0.4585	0.4130	0.4200	0.4810	0.4850	0.5030	0.4090	0.4985
5400	0.2720	0.2630	0.3670	0.2785	0.4630	0.4340	0.4700	0.4180	0.4380	0.5000	0.5010	0.5130	0.4270	0.5185
5600	0.2810	0.2700	0.3815	0.2880	0.4775	0.4490	0.4800	0.4270	0.4430	0.5085	0.5125	0.5250	0.4360	0.5340
5800	0.2900	0.2750	0.3900	0.2970	0.4950	0.4655	0.4900	0.4390	0.4600	0.5190	0.5240	0.5370	0.4545	0.5470
6000	0.2960	0.2820	0.4000	0.3030	0.5000	0.4790	0.5000	0.4650	0.4700	0.5320	0.5335	0.5545	0.4630	0.5635

PROCESSED RESULTS:

PRESSURE ON THE CATALYST (KPA)	DISPLACEMENT (MM)							AREA UNDER THE CURVE (KPA * M) TEMPERATURE(OC):						
	20 oC	100 oC	200 oC	300 oC	400 oC	500 oC	600 oC	20 oC	100 oC	200 oC	300 oC	400 oC	500 oC	600 oC
0	0.000	0.000	0.000	0.000	0.000	0.000	0.000	0.000	0.000	0.000	0.000	0.000	0.000	0.000
39	0.413	0.578	0.686	0.527	0.648	0.737	0.724	0.008	0.011	0.013	0.010	0.012	0.014	0.014
117	1.029	1.276	1.435	1.410	1.524	1.613	1.486	0.056	0.072	0.083	0.076	0.085	0.092	0.086
195	1.607	1.740	1.969	2.013	2.242	2.388	2.165	0.103	0.118	0.133	0.134	0.147	0.156	0.143
274	2.000	2.153	2.381	2.451	2.699	3.023	2.756	0.141	0.152	0.170	0.174	0.193	0.211	0.192
352	2.496	2.496	2.800	3.029	3.188	3.562	3.219	0.176	0.182	0.202	0.214	0.230	0.257	0.234
430	2.769	2.896	3.194	3.512	3.766	4.245	3.835	0.206	0.211	0.234	0.256	0.272	0.305	0.276
508	3.010	3.228	3.613	3.974	4.280	4.724	4.356	0.226	0.239	0.266	0.289	0.314	0.350	0.320
586	3.245	3.509	3.956	4.394	4.716	5.283	4.940	0.244	0.263	0.296	0.333	0.351	0.391	0.363
664	3.493	3.816	4.420	4.877	5.093	5.726	5.550	0.263	0.286	0.327	0.365	0.383	0.430	0.410
743	3.696	4.083	4.864	5.328	5.486	6.236	5.867	0.281	0.309	0.363	0.399	0.413	0.466	0.446
821	3.861	4.401	5.245	5.690	5.855	6.629	6.261	0.295	0.332	0.395	0.431	0.443	0.503	0.474
899	4.089	4.737	5.804	6.090	6.217	7.150	6.528	0.311	0.357	0.432	0.460	0.472	0.538	0.500
977	4.274	4.972	6.134	6.471	6.744	7.633	6.814	0.327	0.379	0.467	0.491	0.506	0.578	0.521
1055	4.458	5.137	6.515	6.820	7.207	8.064	7.493	0.341	0.395	0.494	0.519	0.545	0.613	0.559
1133	4.705	5.398	6.953	7.277	7.753	8.528	8.052	0.358	0.412	0.526	0.551	0.565	0.648	0.607
1211	4.858	5.721	7.341	7.531	8.020	8.966	8.255	0.374	0.435	0.559	0.579	0.576	0.684	0.637
1290	5.131	5.956	7.798	7.988	8.388	9.328	8.674	0.390	0.456	0.592	0.606	0.641	0.715	0.662
1368	5.264	6.217	8.299	8.350	8.642	9.868	9.220	0.406	0.476	0.629	0.639	0.666	0.750	0.699
1446	5.512	6.534	8.757	8.814	9.277	10.414	9.481	0.421	0.498	0.667	0.671	0.700	0.793	0.731
1524	5.696	6.731	9.144	9.131	9.741	11.030	9.982	0.438	0.518	0.700	0.701	0.743	0.838	0.761
1602	5.817	6.883	9.468	9.487	10.211	11.316	10.370	0.450	0.532	0.727	0.728	0.780	0.873	0.795
1680	5.988	7.093	9.944	9.900	10.516	11.506	10.630	0.461	0.546	0.759	0.758	0.810	0.892	0.821
1759	6.160	7.366	10.287	10.370	10.751	11.786	11.036	0.475	0.565	0.791	0.792	0.831	0.910	0.847
1837	6.312	7.684	10.846	10.643	11.062	12.179	11.341	0.487	0.588	0.826	0.821	0.852	0.937	0.874
1915	6.585	7.988	11.081	11.068	11.443	12.548	11.525	0.504	0.612	0.857	0.848	0.879	0.966	0.894
1993	6.795	8.198	11.392	11.278	11.913	12.878	12.008	0.523	0.633	0.878	0.873	0.913	0.994	0.930
2071	6.998	8.503	11.767	11.519	12.084	13.176	12.319	0.539	0.653	0.905	0.891	0.938	1.018	0.951
2149	7.176	8.725	12.198	11.798	12.433	13.475	12.719	0.554	0.673	0.937	0.911	0.958	1.042	0.978
2228	7.341	8.928	12.433	12.256	12.725	13.818	13.037	0.567	0.690	0.963	0.940	0.983	1.067	1.007
TOTAL AREA UNDER THE CURVE (KPA*M) :								10	12	15	15	16	18	17
INTERGREL CRUSH STRENGTH OF THE CATALYST								0.101	0.086	0.066	0.065	0.061	0.055	0.060

* THE AREA UNDER THE CURVE (DISPLACEMENT VS. PRESSURE) IS INVERSELY PROPORTIONAL TO THE INTERGRAL CRUCH STRENGTH OF THE CATALYST

APPENDIX C

APPENDIX C1.1:
Statistics for different M_2O/V_2O_5 mole ratios

Model fitting results for: r31

Independent variable	coefficient	std. error	t-value	sig.level
CONSTANT	0.312593	0.040276	7.7612	0.0000
t31	-0.00124	0.000156	-7.9276	0.0000
mv31	0.002618	0.002375	1.1025	0.2866
t31*t31	1.62661E-6	2.023833E-7	8.0373	0.0000
mv31*mv31	-0.000223	0.000164	-1.3591	0.1930
t31*mv31	-4.262143E-6	5.68088E-6	-0.7503	0.4640
t31*t31*t31	-7.03137E-10	8.71205E-11	-8.0709	0.0000
t31*t31*mv31	1.510632E-9	3.559976E-9	0.4243	0.6770
t31*mv31*mv31	2.435335E-7	2.111503E-7	1.1534	0.2657

R-SQ. (ADJ.) = 0.9425	SE=	0.000092	MAE=	0.000058	DurbWat= 1.699
Previously: 0.9465		0.000089		0.000057	1.717

25 observations fitted, forecast(s) computed for 0 missing val. of dep. var.

Analysis of Variance for the Full Regression

Source	Sum of Squares	DF	Mean Square	F-Ratio	P-value
Model	0.00000343027	8	0.000000428784	50.2164	.0000
Error	0.000000136620	16	8.53872E-9		
Total (Corr.)	0.00000356689	24			

R-squared = 0.961698 Stnd. error of est. = 9.24052E-5
R-squared (Adj. for d.f.) = 0.942547 Durbin-Watson statistic = 1.69924

Residual Summary

Number of observations = 25 (0 missing values excluded)
Residual average = -5.82817E-17
Residual variance = 8.53872E-9
Residual standard error = 9.24052E-5

Coeff. of skewness = -0.199258 standardized value = -0.406734
Coeff. of kurtosis = -0.160802 standardized value = -0.164118

Durbin-Watson statistic = 1.69924

APPENDIX C1.2

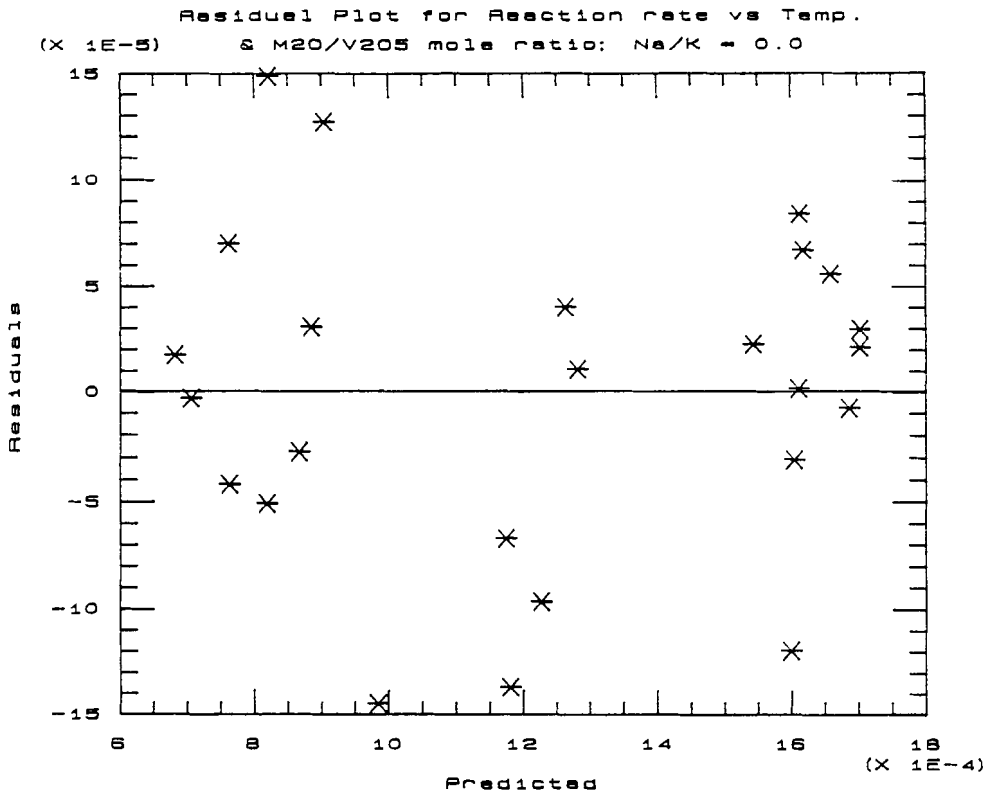

APPENDIX C1.3

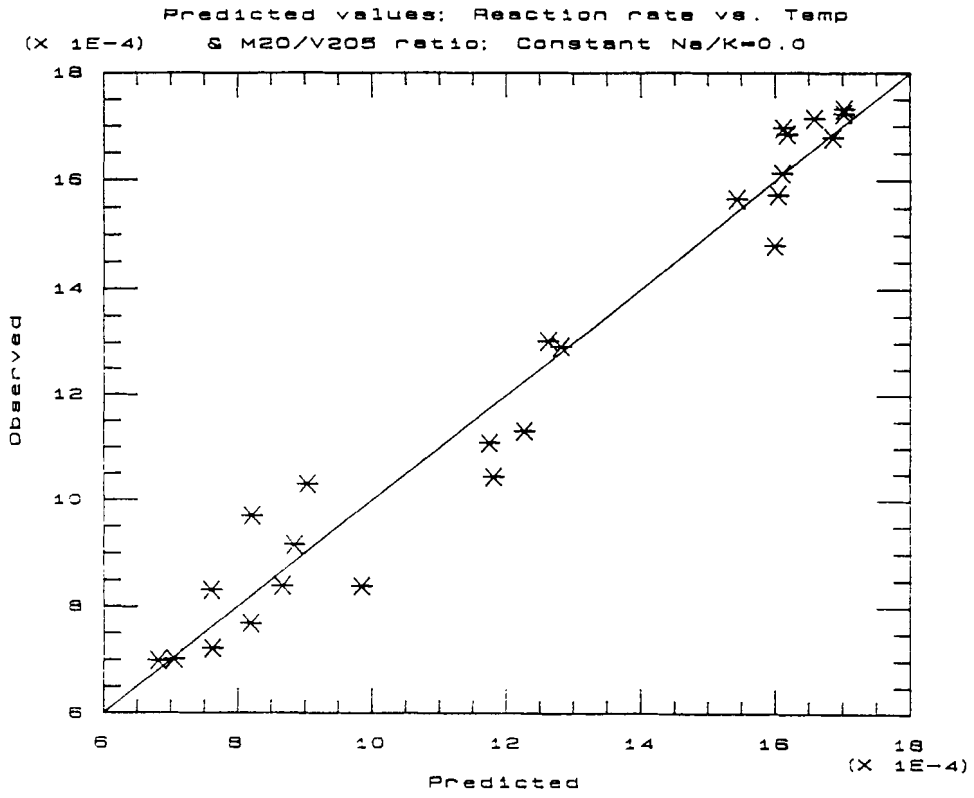

APPENDIX C2.1:
Statistics for different Na/K ratios

Model fitting results for: r32

Independent variable	coefficient	std. error	t-value	sig.level
CONSTANT	0.264098	0.036165	7.3027	0.0000
t32	-0.001037	0.000141	-7.3290	0.0000
nk32	0.001584	0.001231	1.2864	0.2166
t32*t32	1.350132E-6	1.837443E-7	7.3479	0.0000
nk32*nk32	0.000042	0.000045	0.9361	0.3631
t32*nk32	-4.348596E-6	3.205049E-6	-1.3568	0.1937
t32*t32*t32	-5.80422E-10	7.91992E-11	-7.3286	0.0000
t32*nk32*nk32	-4.258269E-8	5.766589E-8	-0.7384	0.4709
t32*t32*nk32	2.88496E-9	2.07117E-9	1.3929	0.1827

R-SQ. (ADJ.) = 0.9504 SE= 0.000084 MAE= 0.000059 DurbWat= 2.451
Previously: 0.0000 0.000000 0.000000 0.000
25 observations fitted, forecast(s) computed for 0 missing val. of dep. var.

Analysis of Variance for the Full Regression

Source	Sum of Squares	DF	Mean Square	F-Ratio	P-value
Model	0.00000330364	8	0.000000412955	58.5206	.0000
Error	0.000000112905	16	7.05658E-9		
Total (Corr.)	0.00000341655	24			

R-squared = 0.966953 Stnd. error of est. = 8.40035E-5
R-squared (Adj. for d.f.) = 0.95043 Durbin-Watson statistic = 2.45067

Residual Summary

Number of observations = 25 (0 missing values excluded)
Residual average = -4.90753E-17
Residual variance = 7.05658E-9
Residual standard error = 8.40035E-5

Coeff. of skewness = 0.248454 standardized value = 0.507155
Coeff. of kurtosis = -1.05815 standardized value = -1.07997

Durbin-Watson statistic = 2.45067

APPENDIX C2.2

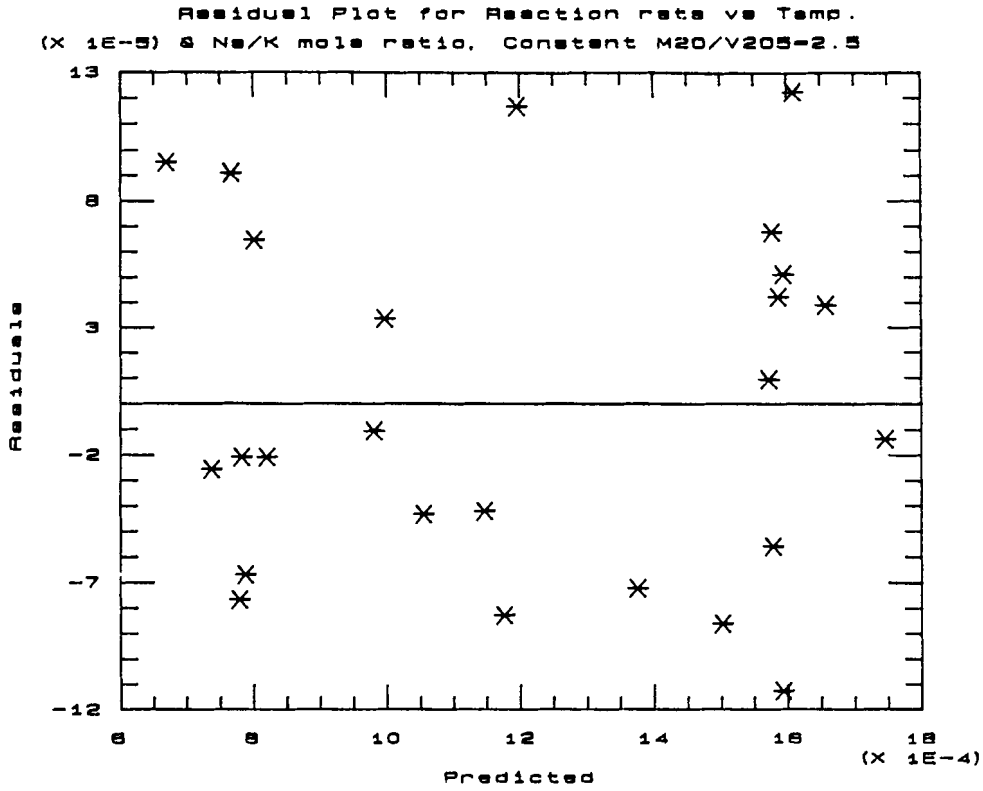

APPENDIX C2.3

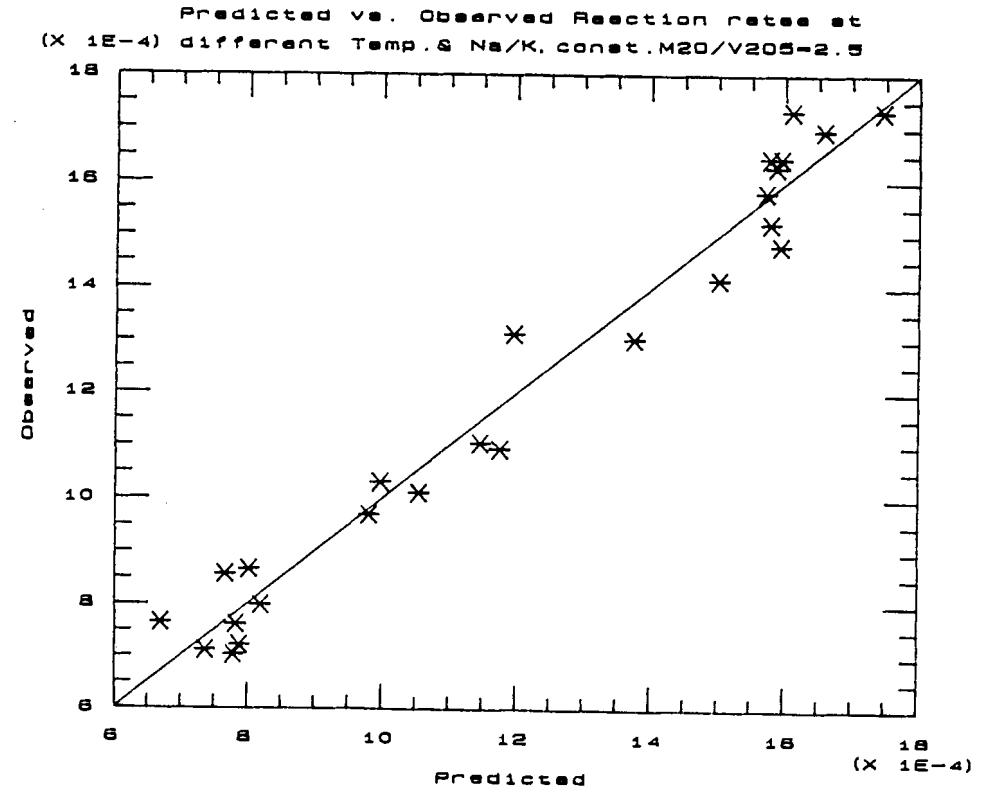

APPENDIX C3.1:
Statistics for different M_2O/V_2O_5 and Na/K mole ratios

Model fitting results for: r3

Independent variable	coefficient	std. error	t-value	sig.level
CONSTANT	0.284652	0.023454	12.1367	0.0000
t3	-0.001128	0.000092	-12.3247	0.0000
mv3	0.002112	0.000927	2.2785	0.0262
nk3	0.001108	0.000976	1.1349	0.2608
t3*t3	1.474788E-6	1.188295E-7	12.4110	0.0000
mv3*mv3	-0.00028	0.000132	-2.1166	0.0383
nk3*nk3	0.00003	0.000032	0.9373	0.3522
t3*nk3	-3.012635E-6	2.539462E-6	-1.1863	0.2400
t3*mv3	-2.278861E-6	1.193862E-6	-1.9088	0.0609
t3*t3*t3	-6.34516E-10	5.12127E-11	-12.3898	0.0000
t3*mv3*mv3	3.004085E-7	1.704752E-7	1.7622	0.0830
t3*nk3*nk3	-2.771267E-8	4.174663E-8	-0.6638	0.5093
t3*t3*nk3	1.987973E-9	1.640717E-9	1.2116	0.2302

R-SQ. (ADJ.) = 0.9427 SE= 0.000094 MAE= 0.000070 DurbWat= 1.211
Previously: 0.9419 0.000095 0.000070 1.213
75 observations fitted, forecast(s) computed for 0 missing val. of dep. var.

Analysis of Variance for the Full Regression

Source	Sum of Squares	DF	Mean Square	F-Ratio	P-value
Model	0.0000108864	12	0.000000907198	102.488	.0000
Error	0.000000548808	62	8.85174E-9		
Total (Corr.)	0.0000114352	74			

R-squared = 0.952007 Stnd. error of est. = 9.40837E-5
R-squared (Adj. for d.f.) = 0.942718 Durbin-Watson statistic = 1.21081

Residual Summary

Number of observations = 75 (0 missing values excluded)
Residual average = 3.56085E-16
Residual variance = 8.85174E-9
Residual standard error = 9.40837E-5

Coeff. of skewness = -0.131954 standardized value = -0.466526
Coeff. of kurtosis = -0.509872 standardized value = -0.901335

Durbin-Watson statistic = 1.21081

APPENDIX C3.1

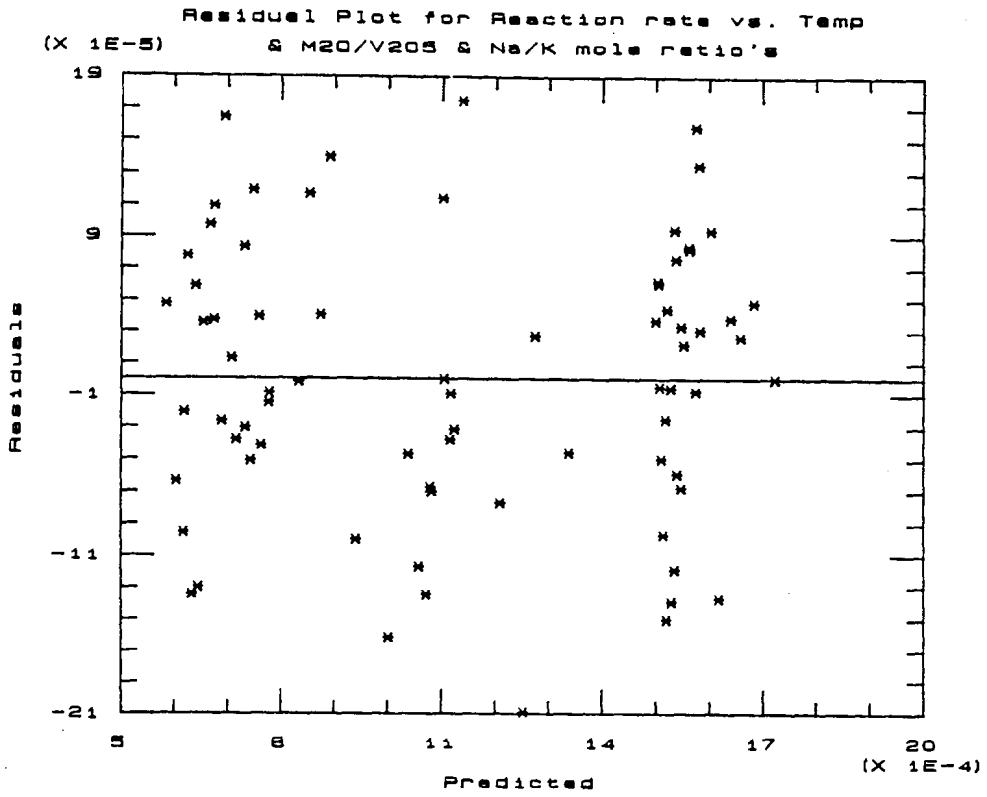

APPENDIX C3.2

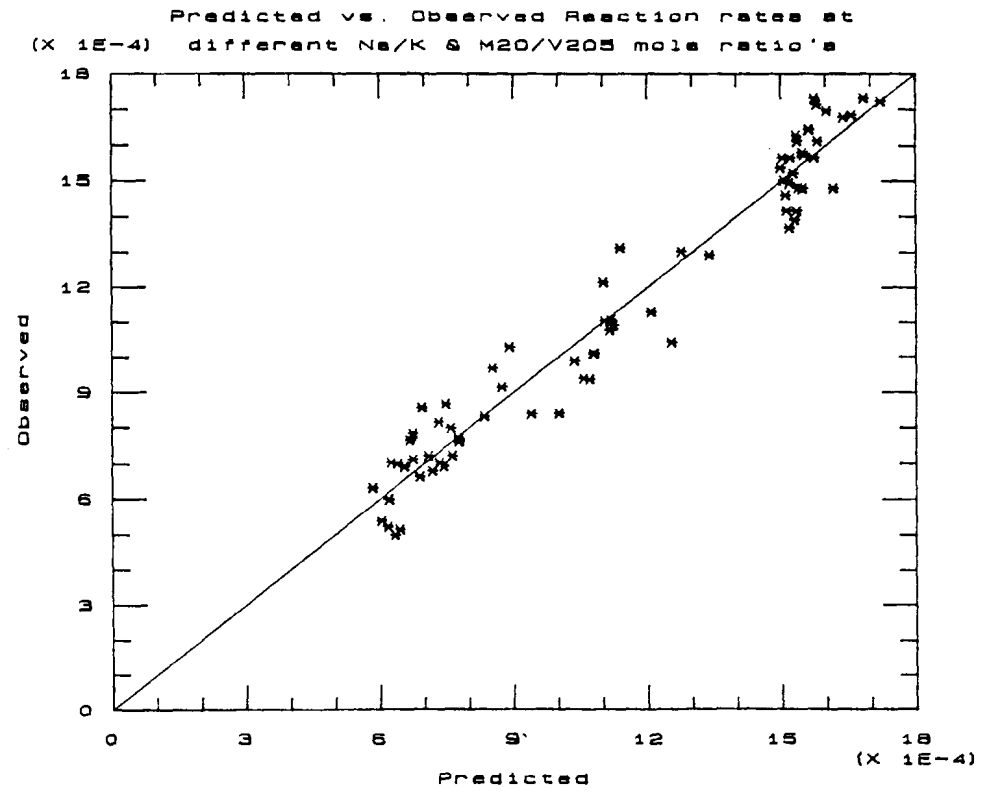

APPENDIX C4.1:
Statistics for activation energy versus Na/K and M_2O/V_2O_5 ratios

Tue Jan 26 1988 11:44:33 AM

Model fitting results for: E

Independent variable	coefficient	std. error	t-value	sig.level
CONSTANT	47803.235664	4.770514E4	1.0021	0.3730
M2OV2O5	92906.60595	5.832174E4	1.5930	0.1864
NaK	-1.58929E4	5.529412E4	-0.2874	0.7881
M2OV2O5^2	-3.946167E4	2.179985E4	-1.8102	0.1445
NaK^2	-1.527155E4	4.324723E4	-0.3531	0.7418
NaK*M2OV2O5	11224.308454	3.220314E4	0.3485	0.7450
NaK^3	-60.634113	185.505523	-0.3269	0.7602
M2OV2O5^3	4644.036428	2410.740689	1.9264	0.1263
(NaK^2)*M2OV2O5	8534.40445	1.258418E4	0.6782	0.5349
(M2OV2O5^2)*NaK	-1955.429394	4346.604036	-0.4499	0.6761

R-SQ. (ADJ.) = 0.7106 SE= 1885.925567 MAE= 628.361275 DurbWat= 3.240
Previously: 0.0000 0.000000 0.000000 .0.000
14 observations fitted, forecast(s) computed for 0 missing val. of dep. var.

Analysis of Variance for the Full Regression

Source	Sum of Squares	DF	Mean Square	F-Ratio	P-value
Model	145523633.	9	16169293.	4.54613	.0794
Error	14226861.	4	3556715.		
Total (Corr.)	159750494.	13			

R-squared = 0.910943 Stnd. error of est. = 1885.93
R-squared (Adj. for d.f.) = 0.710566 Durbin-Watson statistic = 3.23982

Residual Summary

Number of observations = 14 (0 missing values excluded)
Residual average = 1.27017E-9
Residual variance = 3.55672E6
Residual standard error = 1885.93

Coeff. of skewness = -0.732916 standardized value = -1.11955
Coeff. of kurtosis = 1.88463 standardized value = 1.43941

Durbin-Watson statistic = 3.23982

APPENDIX C4.2

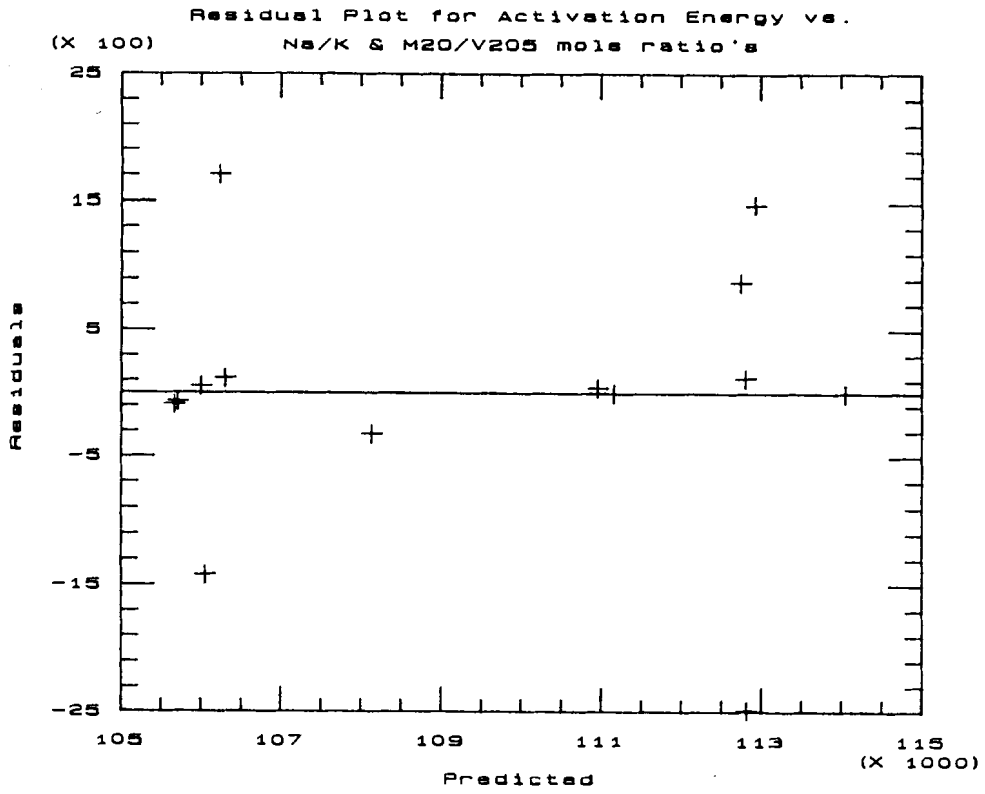

APPENDIX C4.3

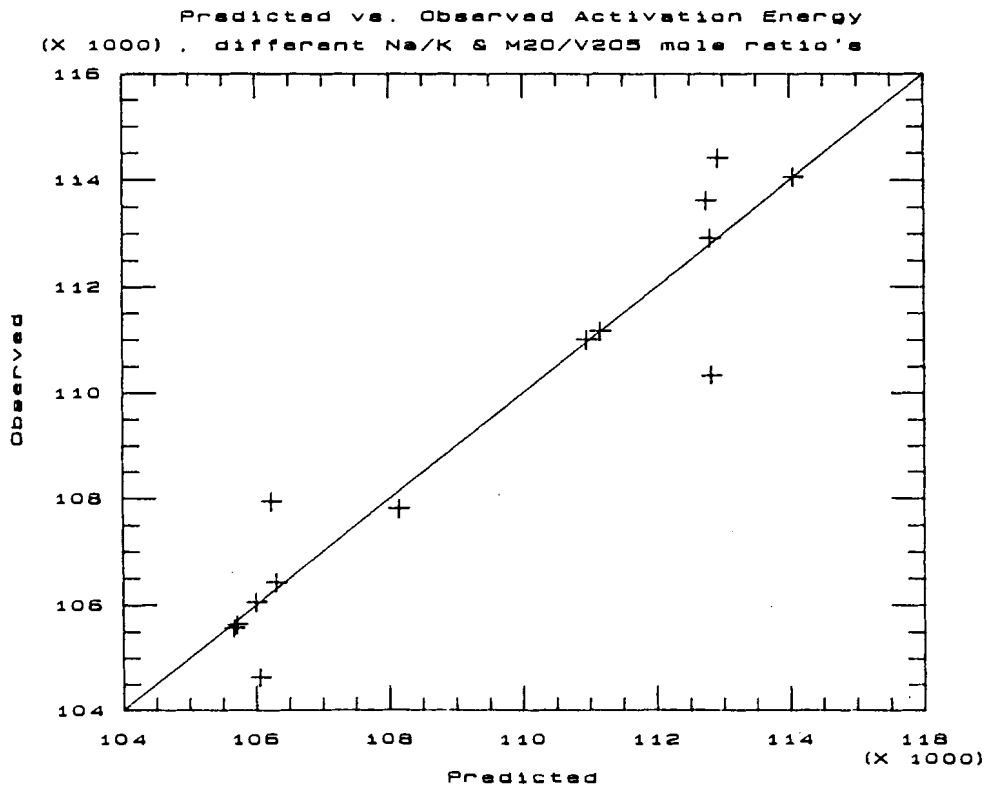

APPENDIX A5.1:
Statistics for different M_2SO_4/MOH mole ratios

Mon Jan 25 1988 09:04:58 PM

Model fitting results for: r4

Independent variable	coefficient	std. error	t-value	sig.level
CONSTANT	0.21993	0.026992	8.1480	0.0000
t4	-0.000872	0.000106	-8.2566	0.0000
sh4	-0.001182	0.001251	-0.9445	0.3635
t4*t4	1.148434E-6	1.371506E-7	8.3735	0.0000
sh4*sh4	-0.000027	6.408656E-6	-4.1955	0.0012
t4*sh4	3.458082E-6	3.256057E-6	1.0620	0.3091
t4*t4*t4	-4.99601E-10	5.91165E-11	-8.4511	0.0000
t4*t4*sh4	-2.448958E-9	2.104169E-9	-1.1639	0.2671

R-SQ. (ADJ.) = 0.9658 SE= 0.000056 MAE= 0.000037 DurbWat= 2.760
Previously: 0.9627 0.000059 0.000037 2.760
20 observations fitted, forecast(s) computed for 0 missing val. of dep. var.

Analysis of Variance for the Full Regression

Source	Sum of Squares	DF	Mean Square	F-Ratio	P-value
Model	0.00000170778	7	0.000000243968	77.5665	.0000
Error	3.77434E-8	12	3.14528E-9		
Total (Corr.)	0.00000174552	19			

R-squared = 0.978377 Stnd. error of est. = 5.60828E-5
R-squared (Adj. for d.f.) = 0.965764 Durbin-Watson statistic = 2.75998

Residual Summary

Number of observations = 20 (0 missing values excluded)
Residual average = 2.34811E-16
Residual variance = 3.14528E-9
Residual standard error = 5.60828E-5

Coeff. of skewness = -0.280741 standardized value = -0.51256
Coeff. of kurtosis = -1.22418 standardized value = -1.11752

Durbin-Watson statistic = 2.75998

APPENDIX C5.2

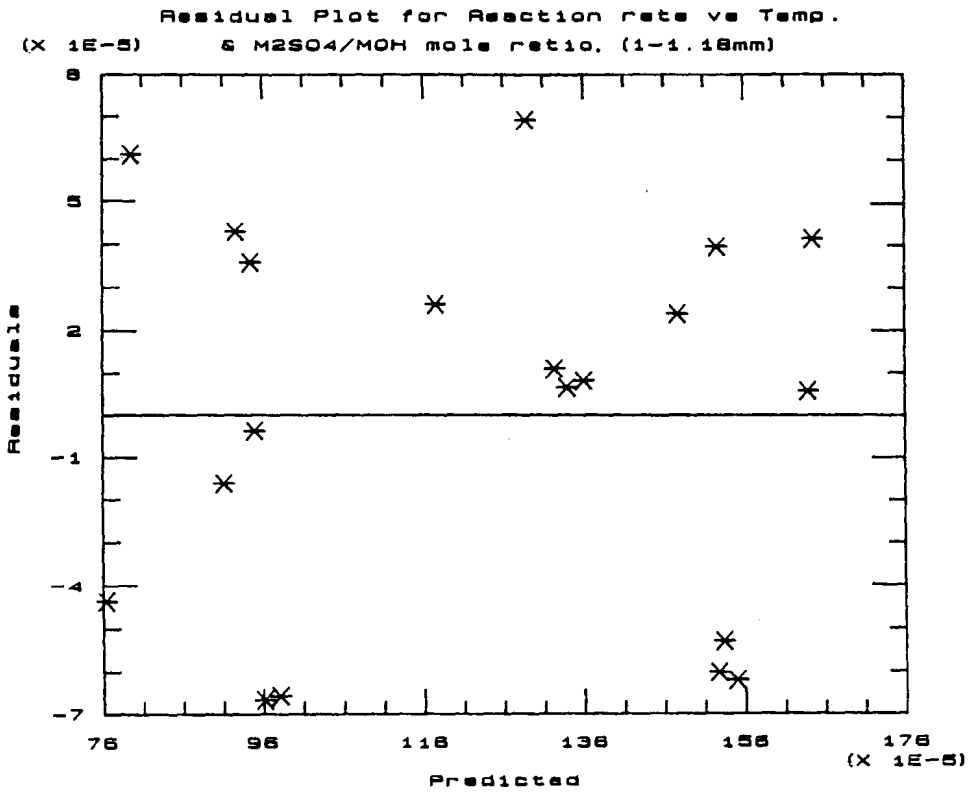

APPENDIX C5.3

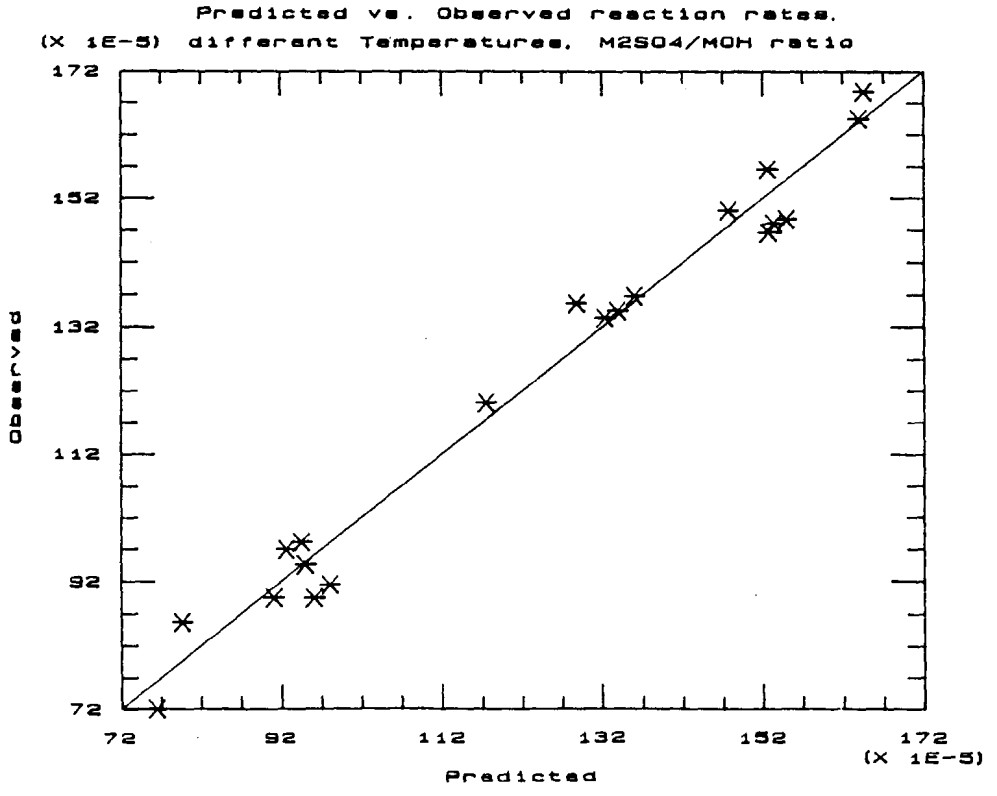

APPENDIX C6.1: Statistics for liquid loading

Model fitting results for: rl

Independent variable	coefficient	std. error	t-value	sig.level
CONSTANT	0.031201	0.007159	4.3586	0.0002
tk	-0.000123	0.000028	-4.4099	0.0001
1/lf	0.000209	0.000066	3.1525	0.0038
tk*tk	1.618041E-7	3.629416E-8	4.4581	0.0001
tk/lf	-5.70932E-7	1.725455E-7	-3.3089	0.0026
tk*tk/lf	4.088154E-10	1.11504E-10	3.6664	0.0010
tk*tk*tk	-7.02838E-11	1.56398E-11	-4.4939	0.0001

R-SQ. (ADJ.) = 0.9730 SE= 0.000020 MAE= 0.000014 DurbWat= 1.626
Previously: 0.0000 0.000000 0.000000 0.000
35 observations fitted, forecast(s) computed for 0 missing val. of dep. var.

Analysis of Variance for the Full Regression

Source	Sum of Squares	DF	Mean Square	F-Ratio	P-value
Model	0.000000474837	6	7.91395E-8	205.425	.0000
Error	1.07869E-8	28	3.85248E-10		
Total (Corr.)	0.000000485624	34			

R-squared = 0.977787 Stnd. error of est. = 1.96277E-5
R-squared (Adj. for d.f.) = 0.973038 Durbin-Watson statistic = 1.62592

Residual Summary

Number of observations = 35 (0 missing values excluded)
Residual average = 1.90645E-18
Residual variance = 3.85248E-10
Residual standard error = 1.96277E-5

Coeff. of skewness = -0.0201043 standardized value = -0.0485564
Coeff. of kurtosis = 0.643151 standardized value = 0.776679

Durbin-Watson statistic = 1.62592

APPENDIX C6.2

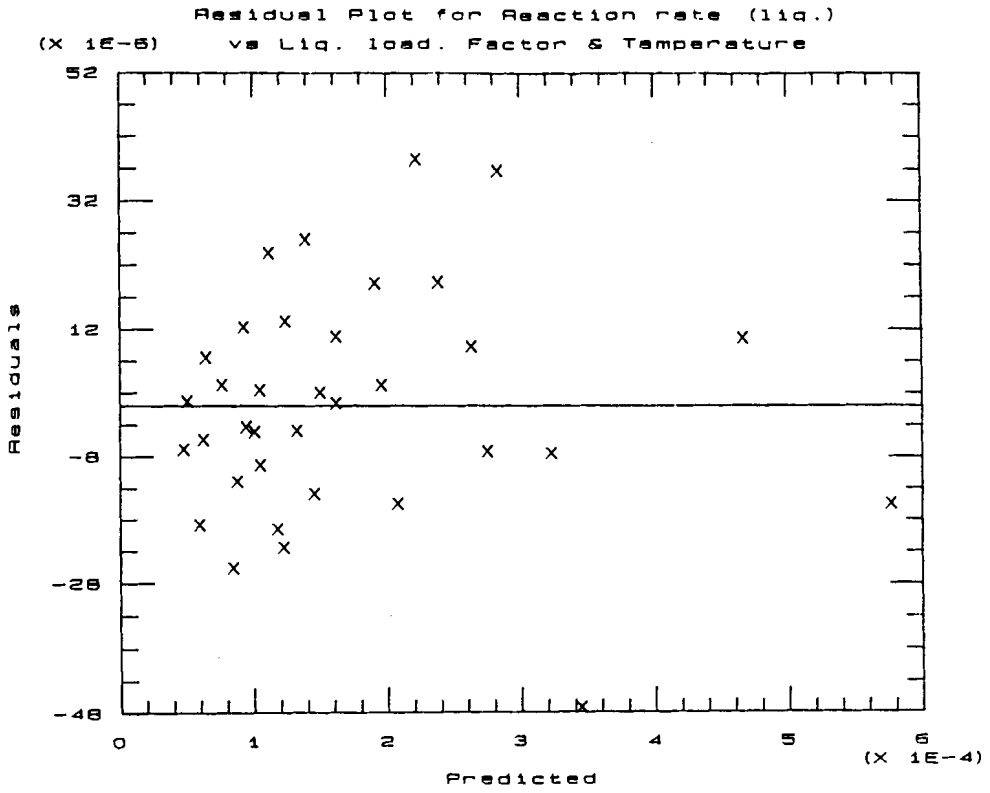

APPENDIX C6.3

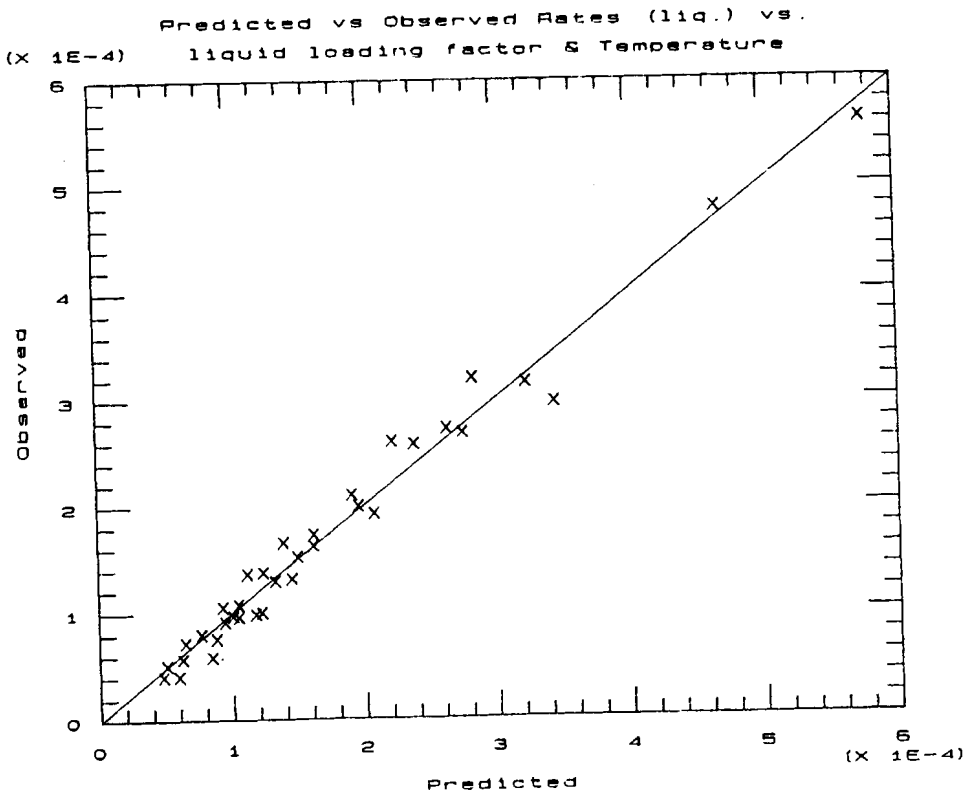

APPENDIX C7.1:
Statistics for liquid effectiveness

Sat Jul 30 1988 12:07:21 AM

Model fitting results for: nl

Independent variable	coefficient	std. error	t-value	sig.level
CONSTANT	-0.386778	0.173332	-2.2314	0.0328
1/(lf^0.4)	0.312727	0.019059	16.4082	0.0000
tk	0.000356	0.000218	1.6368	0.1115

R-SQ. (ADJ.) = 0.8881 SE= 0.091060 MAE= 0.066849 DurbWat= 1.937
Previously: 0.8848 0.092405 0.066356 1.960
35 observations fitted, forecast(s) computed for 0 missing val. of dep. var.

Residual Summary

Number of observations = 35 (0 missing values excluded)
Residual average = -6.02692E-16
Residual variance = 8.29197E-3
Residual standard error = 0.0910603

Coeff. of skewness = 0.633654 standardized value = 1.53042
Coeff. of kurtosis = 0.878446 standardized value = 1.06082

Durbin-Watson statistic = 1.93666

Analysis of Variance for the Full Regression

Source	Sum of Squares	DF	Mean Square	F-Ratio	P-value
Model	2.25466	2	1.12733	135.954	.0000
Error	0.265343	32	0.00829197		
Total (Corr.)	2.52000	34			

R-squared = 0.894705 Stnd. error of est. = 0.0910603
R-squared (Adj. for d.f.) = 0.888124 Durbin-Watson statistic = 1.93666

APPENDIX C7.2

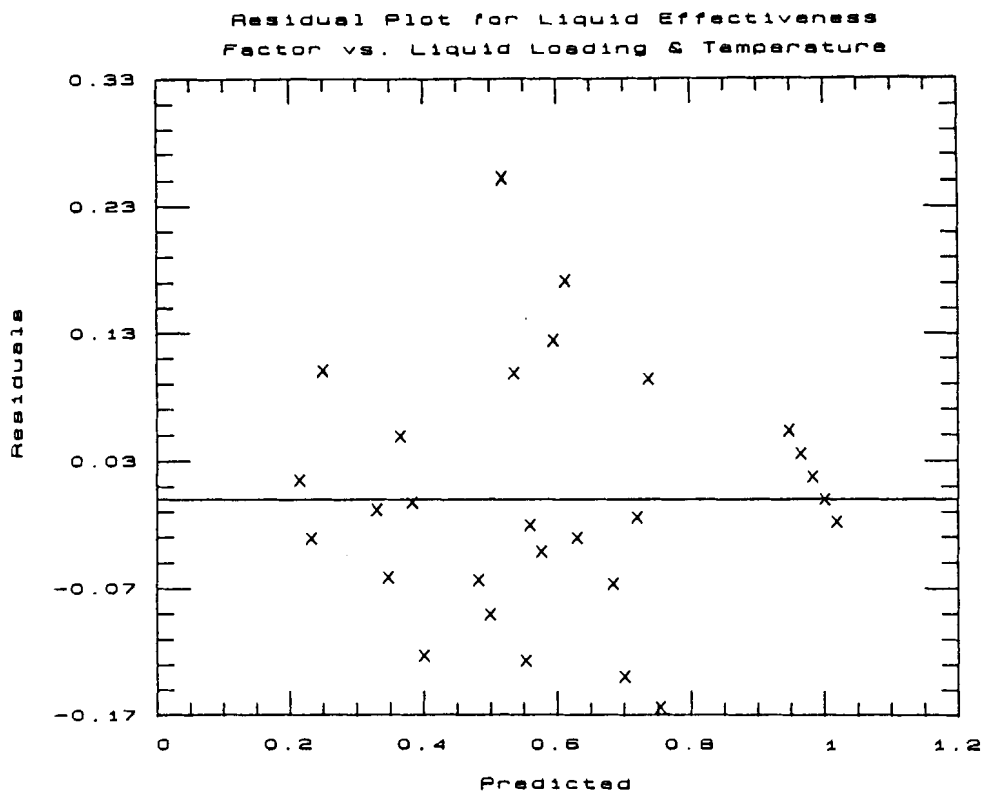

APPENDIX C7.3